Experimental Studies on the Cracking Behaviour of Geofiber Reinforced Expansive Soils

Submitted in partial fulfilment of the requirements

of the degree of

Doctor of Philosophy

of the
Indian Institute of Technology Bombay, India
and
Monash University, Australia

by

Uma Chaduvula

[IITB Roll No.144044003]
[Monash ID: 26414694]

Supervisors:

Prof. B. V. S. Viswanadham (IIT Bombay)

Prof. Jayantha Kodikara (Monash University)

(January 2019)

LEFT BLANK INTENTIONALLY

DECLARATION

I declare that this written submission represents my ideas in my own words and where others' ideas or words have been included, I have adequately cited and referenced the original sources. I also declare that I have adhered to all principles of academic honesty and integrity and have not misrepresented or fabricated or falsified any idea/data/fact/source in my submission. I understand that any violation of the above will be cause for disciplinary action by the Institute and can also evoke penal action from the sources which have thus not been properly cited or from whom proper permission has not been taken when needed.

Notice 1

Under the Copyright Act 1968, this thesis must be used only under the normal conditions of scholarly fair dealing. In particular no results or conclusions should be extracted from it, nor should it be copied or closely paraphrased in whole or in part without the written consent of the author. Proper written acknowledgement should be made for any assistance obtained from this thesis.

Notice 2

I certify that I have made all reasonable efforts to secure copyright permissions for third-party content included in this thesis and have not knowingly added copyright content to my work without the owner's permission.

Student Name: Uma Chaduvula

IITB ID: 144044003

Monash ID: 26414694

LEFT BLANK INTENTIONALLY

ACCEPTANCE CERTIFICATE

IITB-Monash Research Academy

The thesis titled **"Experimental Studies on the Cracking Behaviour of Geofiber Reinforced Expansive Soils"** submitted by **Uma Chaduvula (IITB Roll No. 144044003, Monash ID: 26414694)** may be accepted for evaluation.

Date:

[Prof. B. V. S. Viswanadham,
Professor, Department of Civil Engineering,
IIT Bombay, Powai, Mumbai, India]

 [Prof. Jayantha Kodikara
Professor, Department of Civil Engineering
Monash University, Clayton, Victoria, Australia]

LEFT BLANK INTENTIONALLY

ABSTRACT

Expansive soils are widespread in major parts of India and Australia. These swell in presence of water and shrink in absence of water, leading to development of desiccation cracks. They influence the overall engineering behaviour like seepage, consolidation, compressibility and shear strength characteristics of the soil and thereby cause problems in many different field applications. The objective of the current study is to assess the desiccation cracking behaviour of unreinforced and fiber-reinforced expansive clay using physical model testing at laboratory scale and small-scale physical model testing using centrifuge modelling technique. Thereafter to examine: (i) influence of fiber length, (ii) influence of fiber content, (iii) influence of specimen thickness and (iv) influence of fiber type on crack feature measurements such as crack width, crack spacing, crack depth, crack intensity factor, tensile strength and shrinkage strain.

Laboratory tests on the desiccation of soil reinforced without and with geofibers was carried out. It was observed that fiber inclusion increases the crack reduction in soil. A significant change in the crack morphology visually depicts the significant effect of fiber reinforcement in soil. A series of direct tensile tests were performed to measure the tensile strength-strain characteristics of unreinforced and geofiber reinforced expansive soil. The unreinforced soil attained a peak tensile stress and then rapidly decreased as the specimen cracked. But the soil specimens reinforced with fibers reached higher peak tensile stress and then gradually lost strength as the fibers were pulled out of the soil with an increase in strain, showing a ductile behaviour. Further, the effect of moulding water content on the tensile strength-strain characteristics is presented to understand the influence of fiber content and fiber length. The complete performance of fiber reinforced clay against tensile stresses and desiccation is discussed. Laboratory tests were conducted to investigate the effect of drying-wetting (DW) cycles on the initiation and evolution of cracks in clay layer reinforced with and without fibers. The water evaporation, surface cracks evolution and structure evolution during the DW cycles were monitored through physical model tests in the laboratory at normal gravity. The effect of DW cycles on the geometric characteristics of crack patterns was analysed by image processing and image analysis.

In a novel experimental setup (performed at Monash University, Australia), understanding of desiccation cracking of unreinforced and polypropylene fiber-reinforced soil using distributed

optical fiber sensing (DOFS) was attempted in this study. As the specimen desiccated, a change in the strain conditions in specimen were recorded through data acquisition system. The strain measured from the DOFS was analysed to study the crack initiation and crack propagation in unreinforced and fiber reinforced specimens. The compressive strain that is developed in unreinforced soil specimen increases with loss of moisture, and the soil specimen experiences a progressive reduction in compressive strain with formation and progression of cracking. However, the cracking appears to take place since tensile stresses develop within soil due to mobilized compressive strain and is less than the free shrinkage strain due to partial restraints.

The effect of fiber reinforcement on the desiccation cracking of clay, influence of clay layer thickness, influence of fiber length and fiber type was investigated by using centrifuge modelling technique. Centrifuge modelling of the phenomenon of desiccation cracking was presented by performing tests on a 0.52 m radius small balanced beam centrifuge facility available at Indian Institute of Technology Bombay, India. Digital image analysis and particle image velocimetry technique was employed to arrive at displacement vectors of soil undergoing shrinkage and desiccation cracking. The analysis and interpretation of test results with geofibers indicate the significant potential for geofiber reinforcement to decrease and to restrain desiccation cracking of clay. The displacement vectors after particle image velocimetry (PIV) analysis show that the crack widens in unreinforced soil specimens after the initiation of the crack, whereas in fiber-reinforced soil specimens, the widening of the crack is restrained and controlled. The displacement vectors after crack formation in fiber reinforced specimens indicate that the fibers do not allow the micro cracks to widen, thereby maintaining the integrity of soil specimen. Centrifuge model tests prove that the specimen thickness significantly influences the crack feature measurement of a clay layer. The crack width, crack depth and time of crack initiation increases with increase in clay layer thickness.

Keywords: Desiccation cracking, expansive soil, fiber reinforced soil, geofibers; laboratory tests, drying-wetting cycles, centrifuge modelling, distributed optical fiber sensing

CONTENTS

LIST OF FIGURES

LIST OF TABLES

26

NOTATIONS AND ABBREVIATIONS

Symbol/ Abbreviation	Description
f	Fiber content (%)
l	Fiber length (mm)
l_e	Embedded length of fiber
w	Water content (%)
p	Pressure (kN/m^2)
G_s	Specific gravity
e	Void ratio
ε	Strain (%)
σ	Tensile strength (kN/m^2)
c_e	Evaporation rate (mm/min)
D_w	Soil moisture diffusivity (mm^2/min)
P	Ultimate load (kN)
A	Cross sectional area (m^2)
s_c	Crack spacing (mm)
s_{avg}	Average crack spacing (mm)
A_{avg}	Average cracked cell area (mm^2)
$c_{w, avg}$	Average crack width (mm)
t_i	Time of crack initiation
d_c	Depth of crack (mm
θ	Ambient temperature
d	Clay layer thickness
σ_{ur}	Tensile strength of unreinforced soil

σ_{fr}	Tensile strength of fiber-reinforced soil
$\Delta\sigma_f$	Increment in tensile strength due to fiber reinforcement
τ_{fi}	Interfacial shear strength between fiber and clay
k	Permeability of the corresponding clay layer
k_{ur}	Permeability of the unreinforced clay layer
k_{fr}	Permeability of the fiber-reinforced clay layer
Υ	Unit weight of soil
Υ_{ur}	Unit weight of unreinforced soil
Υ_{fr}	Unit weight of fiber-reinforced clay
α	Fiber orientation
R_e	Effective radius
Ω	Angular velocity of the centrifuge
g	Acceleration due to gravity
a_c	Centrifugal acceleration
υ	Frequency of light source
K_T	Temperature calibration constants
$K\varepsilon$	Strain calibration constants
N	Scale factor
PP	Polypropylene
PET	Polyester
PP-T	Polypropylene tape
CH	Clay of High Plasticity
USCS	Unified Soil Classification System
LL	Liquid limit (%)

PL	Plastic limit (%)
SL	Shrinkage limit (%)
RPM	Revolutions per minute
DIA	Digital image analysis
CIF	Crack intensity factor
CRR	Crack reduction ratio
SWCC	Soil water characteristic curve
CMOS	Complementary metal-oxide-semiconductor
FPS	Frames per second
MP	Megapixel
XRD	X-ray diffraction
XRF	X-ray fluorescence
PIV	Particle image velocimetry
OFS	Optical fiber sensors
DOFS	Distributed optical fiber sensors
ODiSi	Optical Distributed Sensor Interrogator-B

LEFT BLANK INTENTIONALLY

Chapter 1

INTRODUCTION

1.1   General

Desiccation crack patterns are encountered in everyday life. These are visible in drying soil, concrete, bitumen, wood, paint, cement, human skin, etc. Although these cracks exhibit patterns unique to a given material, similarities exist even with entirely different material constitutive behaviour. For example, crack patterns on an old painting or stove tiles are similar in some respects to those which emerge on heated ceramic slab after quenching it. The common cause of cracks in these materials, including human skin is the development of tensile stress due to shrinkage within a limited region of the material (Boeck et al. 1999).

Shrinkage is caused by many factors including desiccation, quenching, cooling, relocation processes and chemical reactions. Out of the many factors responsible for shrinkage of soils, desiccation is the most common, which is basically, loss of water due to evaporation. Because

of the varying climate throughout our planet, large portions of the Earth's land are under the influence of desiccation cracking. Basically, wherever surface of the soil is not permanently flooded, the phenomenon of desiccation takes place. Majority of soils are saturated when placed geologically. Lacustrine deposits, for example are deposited at water contents above liquid limit and are then consolidated by the weight of the overlying sediments. Desiccation of the soil takes place from the exposed surface in downward direction when exposed to air or heat by the sun and thus, cracking takes place. Cracking, which is generally observed in fine-grained soils, creates zones of weakness in the soil mass and reduces its overall strength and stability. The phenomenon is dependent on many environmental factors and thus the problem of desiccation cracking of fine-grained soils has been a difficult problem to tackle despite being very common.

1.2 Expansive soil

1.2.1 Distribution of expansive soils in India and Australia

Expansive soil is widespread throughout the world. The areas include U.S.A., China, France, Spain, Denmark, South Africa, Australia, Romania, Saudi Arabia, Zimbabwe, the U.K and India (Chen 1988). Expansive soils are commonly known as black cotton soils in India, because of their colour and their suitability for growing cotton. The colour of black cotton soil is black because of the presence of high organic content in the soil, which also makes it suitable for agricultural purposes (Ramachandran et al. 1959). Black cotton soil is one of the major regional soil deposits in India, covering an area of about 3.0 lakhs sq.km (Subbarao et al. 2011). In India, the area covered by expansive soils is nearly 22.2% of the total land area. They are predominantly found in the states of Maharashtra, Madhya Pradesh, Gujarat, Andhra Pradesh, Telangana, Karnataka, Tamil Nadu, Rajasthan, Bihar, Orissa and Uttar Pradesh of India (Figure 1.1). These are derived from the basaltic traps and ferrogenous gneisses and schists of central and South-central India. The presence of montmorillonite mineral imparts high shrink-swell potentials (Chen 1988). Figure 1.2 shows the distribution of expansive soil in Australia.
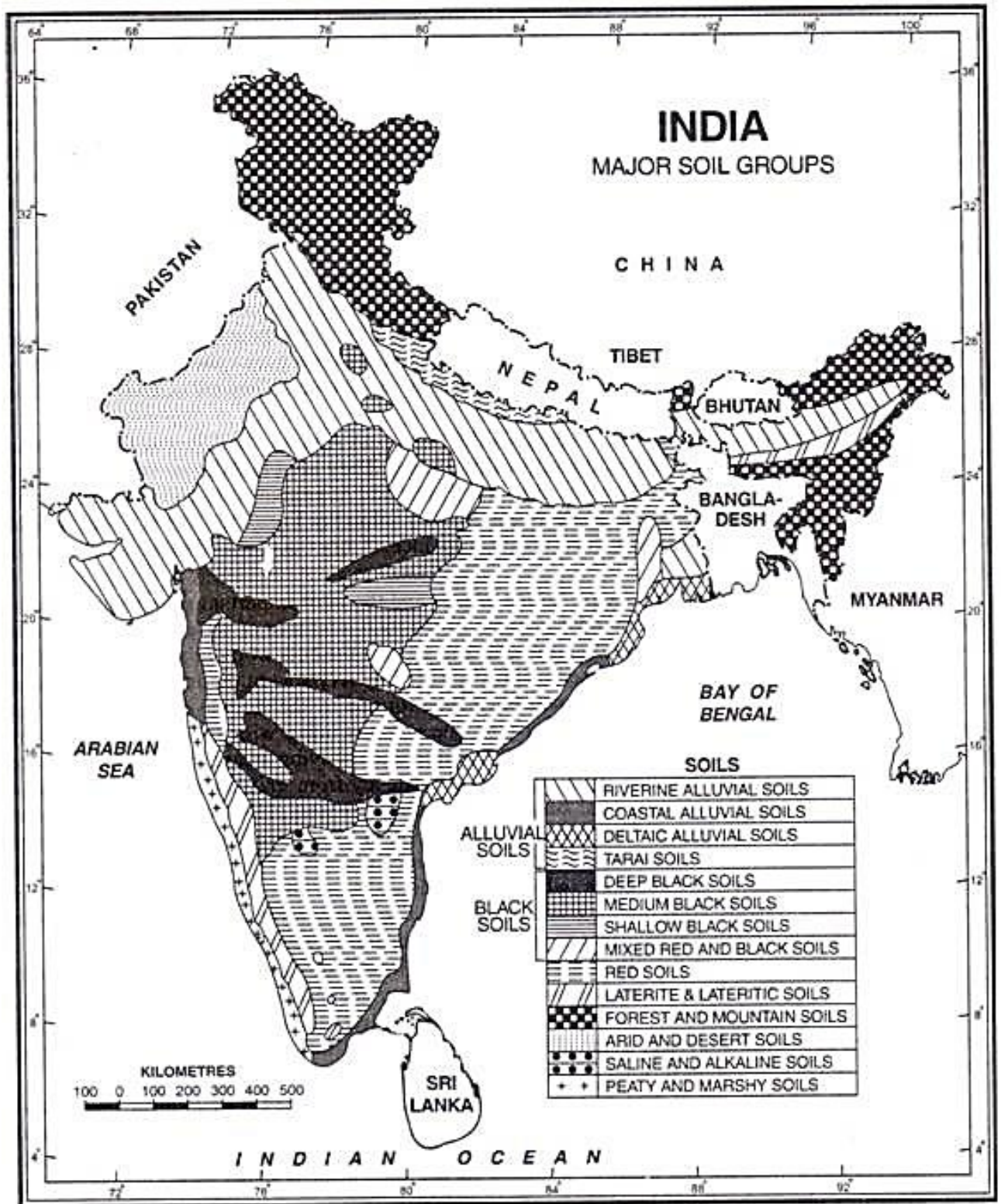
Figure 1.1Distribution of soil types in India (After, Indian Council of Agricultural Research, 1998)
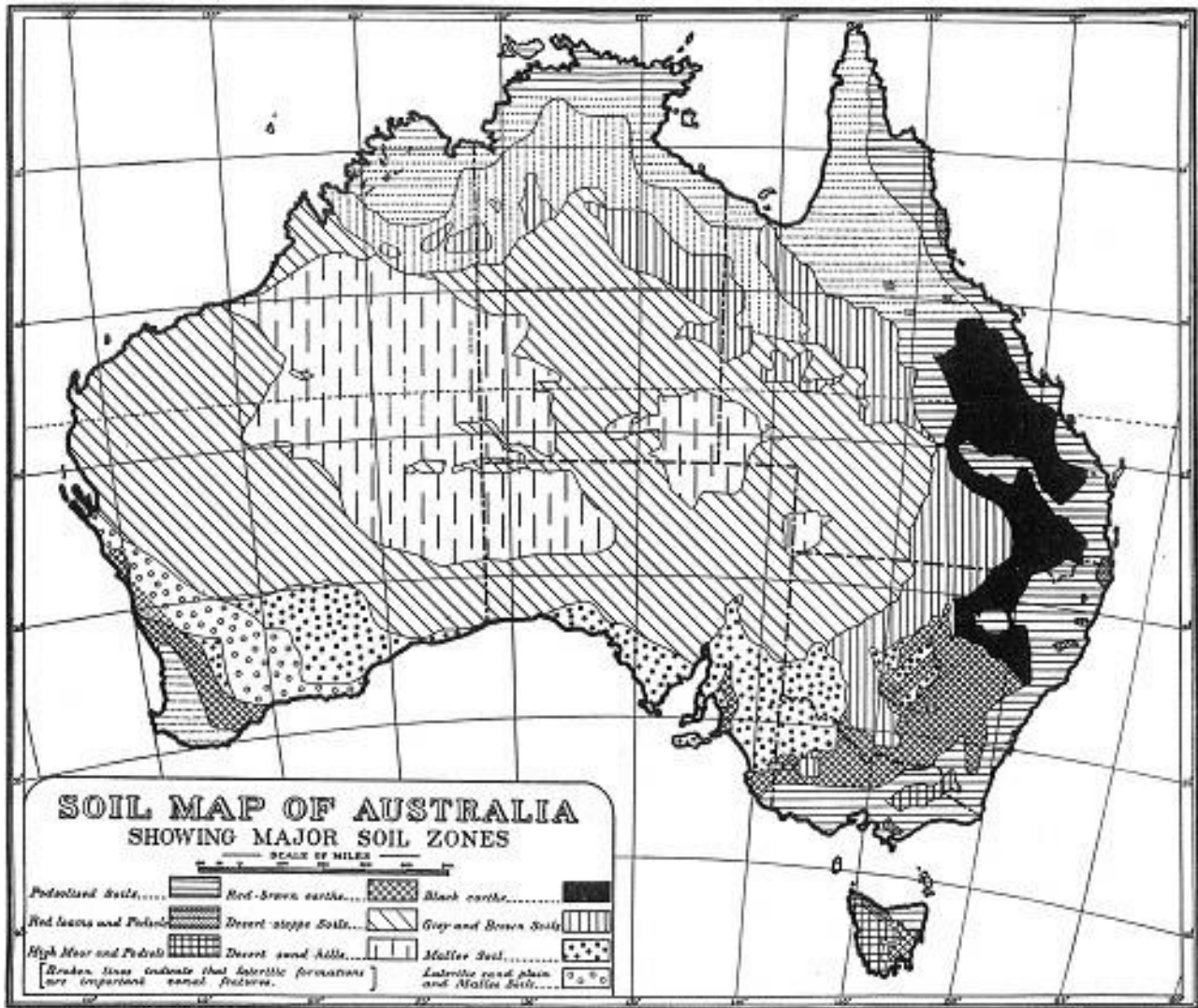
Figure 1.2 Distribution of expansive soil in Australia (Isbell 1992)

Expansive soils are widespread throughout Australia. The distribution of the major areas of expansive soils in Australia are shown in Figure 1.2. The expansive soils include around 7 lakhs sq.km of grey and brown soils and 3.3 lakh Sq.km of black cotton soil. The montmorillonite mineral is formed due to alkaline environment and insufficient leaching of clay particles in semi-arid tropical and temperate regions (Abduljauwad 1993). The black cotton soils have liquid limit values ranging from 50 to 100%, plasticity index ranging from 20 to 65% and shrinkage limit from 9 to 14%. Since expansive soil is widespread in India and Australia, it formulates an interesting and useful research topic. India and Australia both suffer extensively from expansive soil induced distress to vital infrastructure that underpins respective economies, and hence this research will help improve the construction industry of these places. Through

34

this research parts of Maharashtra, Gujarat, Andhra Pradesh and Karnataka states of India and parts of Victoria, New South Wales and Queensland states of Australia will get benefited.

1.2.2 Problems associated with expansive soils

Changes in the environmental conditions will cause expansive soils to experience volumetric changes that might be problematic to the infrastructure. The differential movements in the soil mass as well as the pressure exerted by the soil to the structures generally generate distresses that may induce damages of various degrees to the structures built on swelling soils.

Pavement distresses: Buckling as well as distortion and cracking in all directions generate bumps which increase the roughness of pavements resulting in poor riding comfort. These problems usually occur due to the shrink-swell nature of the subgrade with predominantly black cotton soil type (Nelson and Miller 1992).

Floor slab cracking and retaining and building walls cracking: These types of damages are tensile in nature and generally result in hogging/ convex or sagging/ concave side like deformation due to differential movements occurred in the structure in both lateral and vertical directions.

Buried pipes- differential movement and cracking: Buried pipes may get disjointed or even break when buried in swelling soils especially when water content changes in the expansive soil. Usually, movements are relatively small however the moisture fluctuation may generate considerable differential displacements between two adjacent points in the soil mass, which adversely affect the pipe performance (Kunert et al. 2016).

Slope failures: Stability of slopes is affected when the seasonal drying-wetting process generates desiccation cracks during dry season. These cracks get filled with water during rainfall leading to the reduction of the soil shear strength, thus triggering the failure (Cho and Lee 2001).

1.2.3 Swelling and shrinkage behaviour of expansive soil

Swelling soils, which are clayey soils, are also called expansive soils. The expansive nature is due to the presence of mineral called montmorillonite. The schematic diagram of the montmorillonite structure is shown in Figure 1.3.
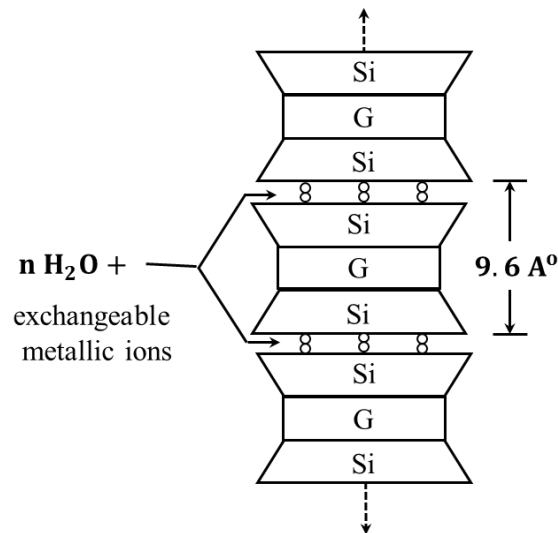
Figure 1.3 Schematic diagram of structure of mineral montmorillonite

The clay mineral montmorillonite, part of the smectite family, can absorb very large amounts of water molecules between its clay sheets, and therefore has a large shrink–swell potential. When expansive soils become saturated, water molecules are absorbed between the clay sheets, causing the bulk volume of the soil to increase, or swell. This same process weakens the inter-clay bonds and causes a reduction in the strength of the soil. When water is removed, by evaporation or gravitational forces, the water molecules between the clay sheets are removed, causing the overall volume of the soil to decrease, or shrink. As this occurs, structural changes, such as creation of macro voids or desiccation cracks, occur. The amount of swell generally increases with an increase in the plasticity index. The swelling potential depends on the type of clay mineral, crystal lattice structure, and cation exchange capacity, ability of water absorption, density and water content.

1.3   Desiccation cracking in soils

Desiccation cracking is caused by pore water evaporation which develops negative pore water pressures in the soil. The effective stress increases due to the negative pore water pressures. This reduces the volume of soil. As the pore water pressure acts in all directions or isotropically, the soil tends to shrink in all directions (Kleppe and Olson 1985).

1.3.1 Soil cracking mechanism

Haines (1923) showed that there are two stages of drying in soils: primary and residual drying. Based on this, Kodikara et al. (1999) recognized three phases in shrinkage of soils. The three phases of drying of soils can be represented by a plot of void ratio (e) against the volumetric water content (w). In primary drying, water is removed from the soil without significant entry of air. The soil particles move closer together when the water leaves the soil, hence the change in the volume of specimen (de) is equal to the change in the volume of water (. In residual drying, air enters the sample whilst water is still removed, i.e., change in volume of water is greater than the soil volume decrease (. In zero shrinkage zone, the particles are in contact each other and cannot further reduce the volume of the sample.

Cracking moisture content, defined as the moisture content at which first desiccation crack is observed, can vary, depending on a number of factors including the thickness of the layer, drying speed and boundary conditions. Nahlawi and Kodikara (2006) discussed that the cracking moisture content should be independent of the desiccation rate based upon unsaturated soil mechanics, as cracking is initiated by tensile stress development from the matric suction (a direct function of the water content of the soil given by the soil water characteristic curve for drying) and cracking occurs when the tensile stress developed exceeds the tensile strength. Therefore, for a given soil, provided the soil is fully restrained, cracking occurs at the same moisture content regardless of the thickness of the soil layer as long as the drying is uniform. The desiccation rate is defined as the rate at which the moisture is lost from the soil in a given

amount of time. However, there is experimental evidence to show that cracking water content decreases with increasing desiccation rate (Corte and Higashi 1964).

Mechanism behind one-dimensional desiccation can be understood in steps proposed in the model shown in Figure 1.5. The steps involved in desiccation of a horizontal soil layer are discussed (Konrad and Ayad 1997),(a) At time $t = 0$, the evaporation initiates, (b) At time $t = t_1$, the soil being cohesive, develops suction pressures, thereby causing capillary consolidation. Since the lateral deformations are restrained, vertical deformations are observed.
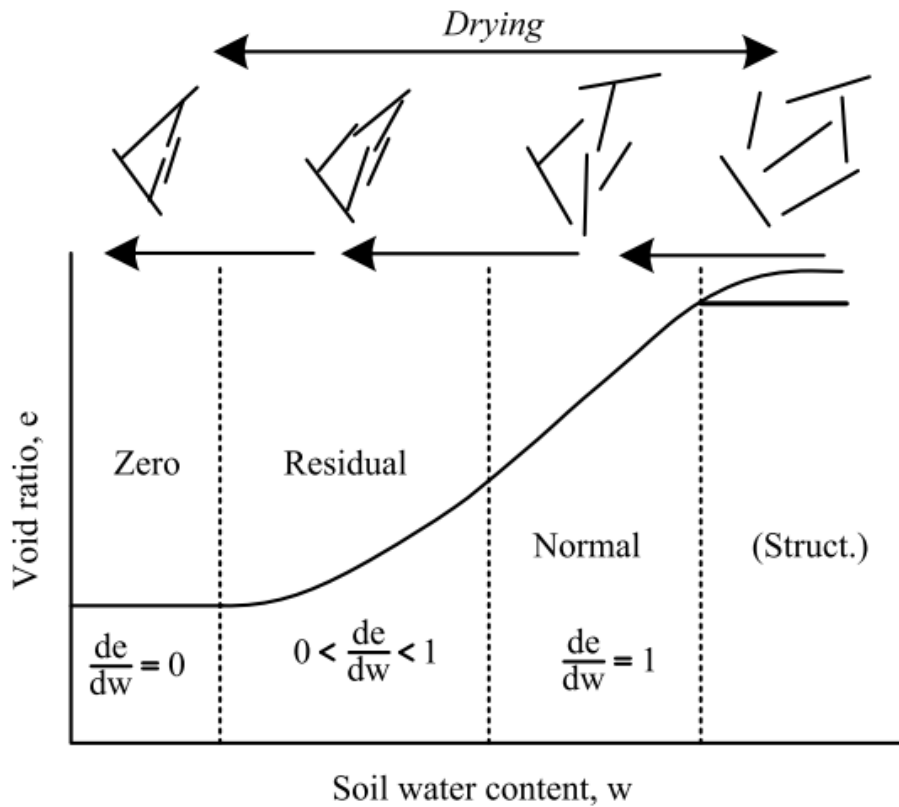
Figure 1.4 The three shrinkage phases of clay aggregates upon drying. (After Kodikara et al. 1999)

For a soil element at the ground surface, since there are no strains in lateral directions, the element undergoes a continuous increase in the total horizontal stress while the total vertical stress remains zero, (c) When the total horizontal stress acting on the soil surface reaches the tensile strength of the soil (σ_t), crack initiates. At this point, the negative pore-water pressure acting on the soil element adjacent to the surface just reaches a critical value, $\psi_{cr,}$ (d) As the soil crack propagates, it reaches to a depth A and certain distance between them as D (Figure 1.5d). Here, σ is the tensile stress, is the total lateral stress $\sigma_v = \sigma_1$ is total vertical stress, and ξ is the evaporated water at a particular time from the soil due to desiccation.

Established desiccation crack initiation theories in soils are summarised in Table 1.1. These theories are applicable only to fine grained soils like clay.
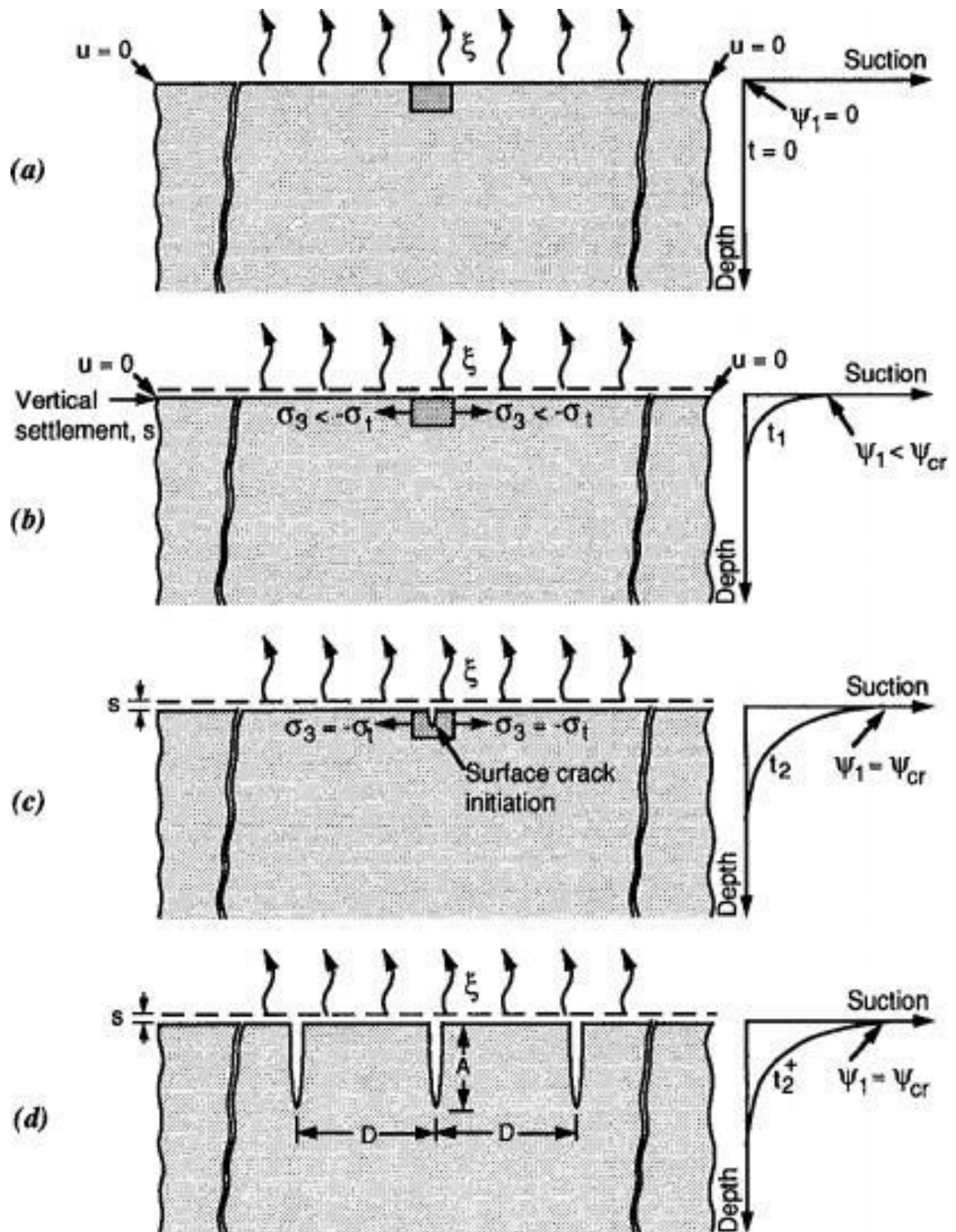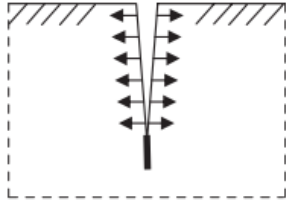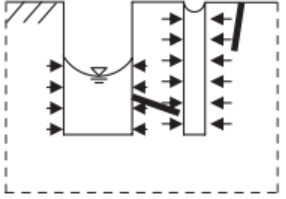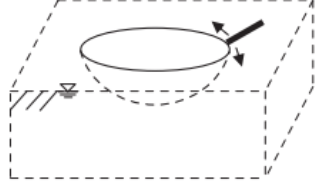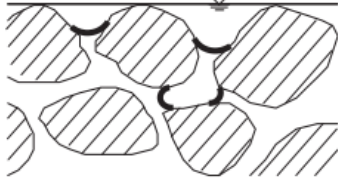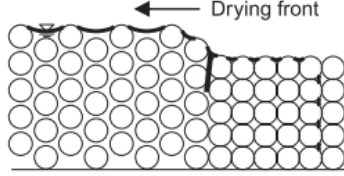
Figure 1.5 Schematic illustration of desiccation cracking, (a) Evaporation, (b) Tension development, (c) Crack initiation, (d) Crack propagation (After Konrad and Ayad, 1997)

Table 1.1 Previous theories for crack initiation in fine grained soils

Theory	References	Mechanism	Illustration	Remarks
Tensile failure	Lachenbruch, 1962; Allen, 1982; Morris et al. 1992; Abu-Hejleh, A. and Znidarcic, 1995; Konrad and Ayad, 1997	Tensile stresses in material increases than its tensile strength		Most commonly assumed model
Irregular drying front	Zarzycki et al. 1982	Difference in capillary pressures and subsequent failure of pore walls		Conceptual – no verification
Circumferential tension	Scherer 1990	Growth of radial crack due to hoop tension		Conceptual – no verification
Air entry	Herrera et al. 2007	Menisci invasion due to increasing capillary tension		Conceptual – no verification
Packing collapse	Holmes et al. 2006	Collapse of particle layers by capillary suction	Drying front	Concept used to explain desiccation cracks in a drying strip

1.3.2 Problems due to desiccation cracking

Desiccation cracking of the soil is known to create problems to engineering structures, especially geotechnical structures. Desiccation cracking of soil is responsible for building failures as shown in Figure 1.6 . They are normally found in various geotechnical applications such as dams, slopes (Tang et al. 2008), foundations, landfill liners (Peron et al. 2009) and pavements (Nahlawi and Kodikara 2006). They are commonly seen in pavements (Figure 1. 7), hydraulic barriers, cricket pitches and turfs, and agricultural land (shown in Figure 1.8).
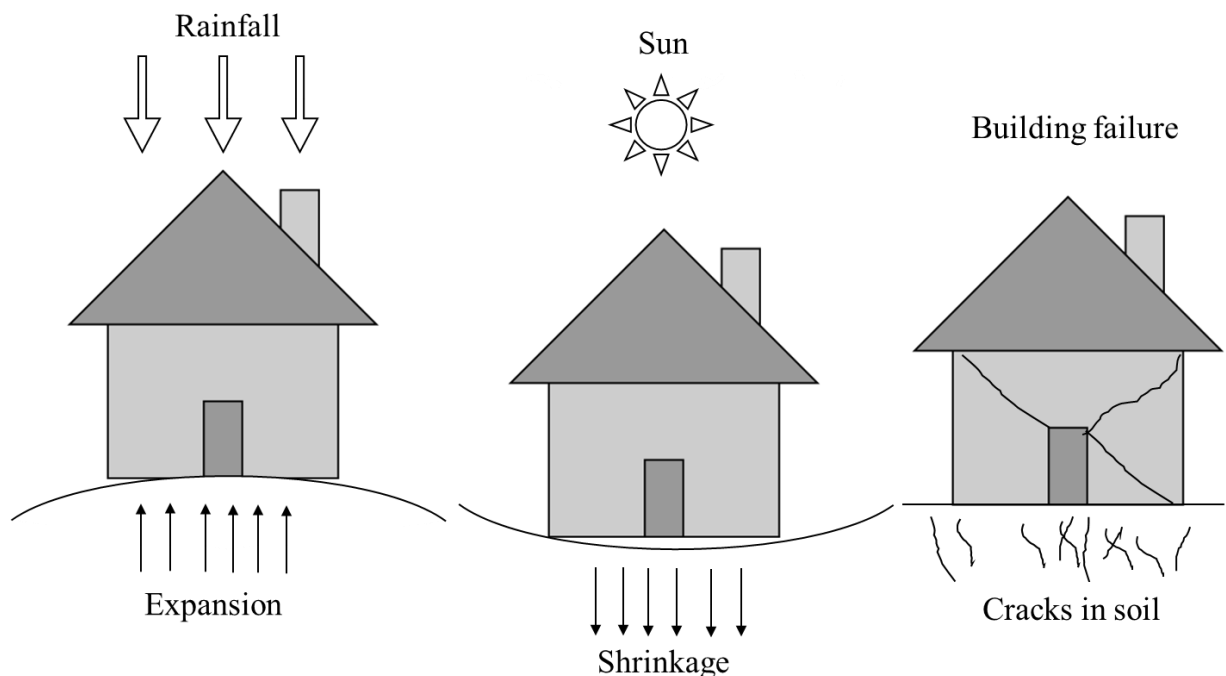
Figure 1.6 Building failure due to desiccation cracking of soil

There can by varying scale of desiccation cracks from few centimetres to kilometres. Figure 1.9 shows the various scales of desiccation cracks. Photos A, B and C are ordinary mud cracks. Photo D shows what is referred to as large soil cracks. Photo E is an aerial view of a giant desiccation cracks near Rodeo, USA. Photo F is a giant desiccation crack in a road in the Aravaipa Valley, Arizona, USA that is part of a large polygonal network of cracks (Harris 2004).
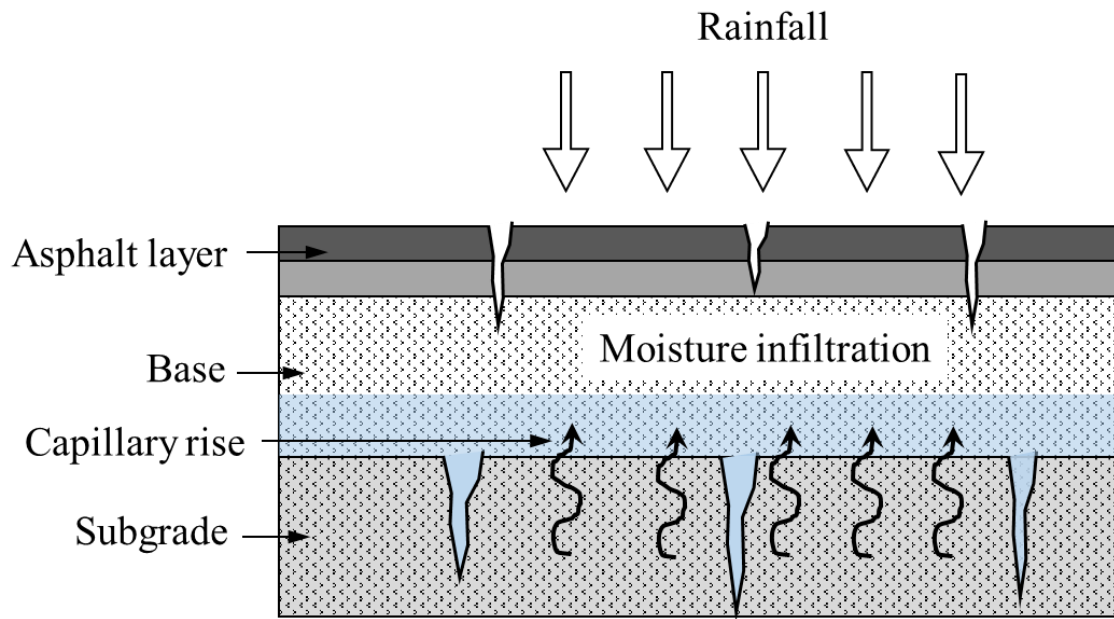
Figure 1. 7 Failure in pavements due to cracking of subgrade

Figure 1.8 Desiccation cracking in soils in drought affected Vidarbha, India (Source:
https://indianexpress.com/article/india/india-news-india/marathwada-dams-to-be-
interlinked-water-grid-proposed-for-effective-management-2855513/)

The phenomenon of desiccation occurs primarily due to loss of moisture content of the soil.
The loss of moisture content in the soil is attributed to prevailing severe environmental
conditions like temperature and wind. To deal with this geo-environmental issue, researchers
have studied and established experimentally and numerically various cracking characteristics,
such as crack intensity factor, crack width and crack depth, cracking moisture content, tensile
strength of the soil, initiation and geometry of primary, secondary and tertiary cracks.
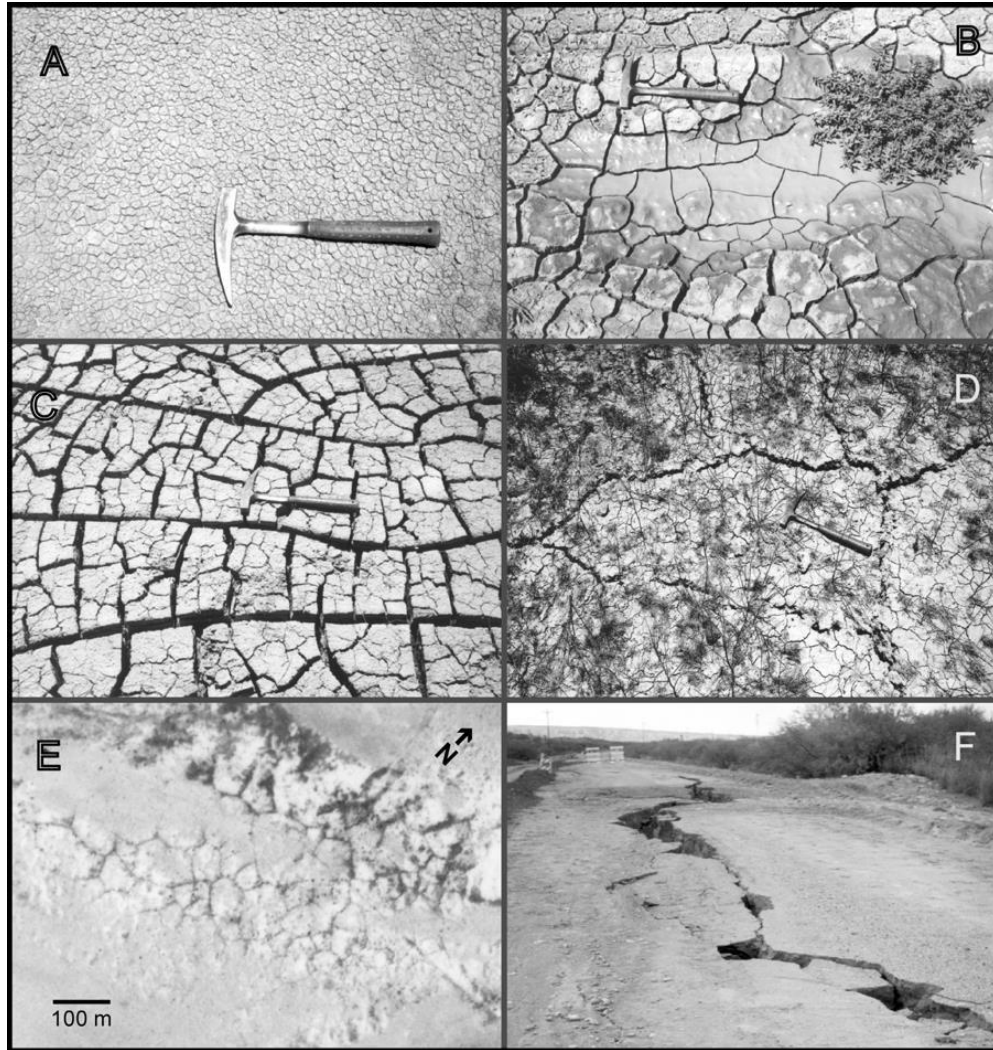
Figure 1.9 Various scales of desiccation cracks. Photos A, B and C: ordinary mud cracks. Photo D: large cracks. Photo E &F: giant desiccation cracks (After Harris, 2004)

Desiccation cracking intrinsically influences the overall engineering behaviour like seepage, consolidation, compressibility and shear strength characteristics of soil and thereby can create problems in different field applications (Morris et al. 1992). Figure 1. 10 represents the failure of landfill lining system due to desiccation cracking of top capping and bottom lining system.
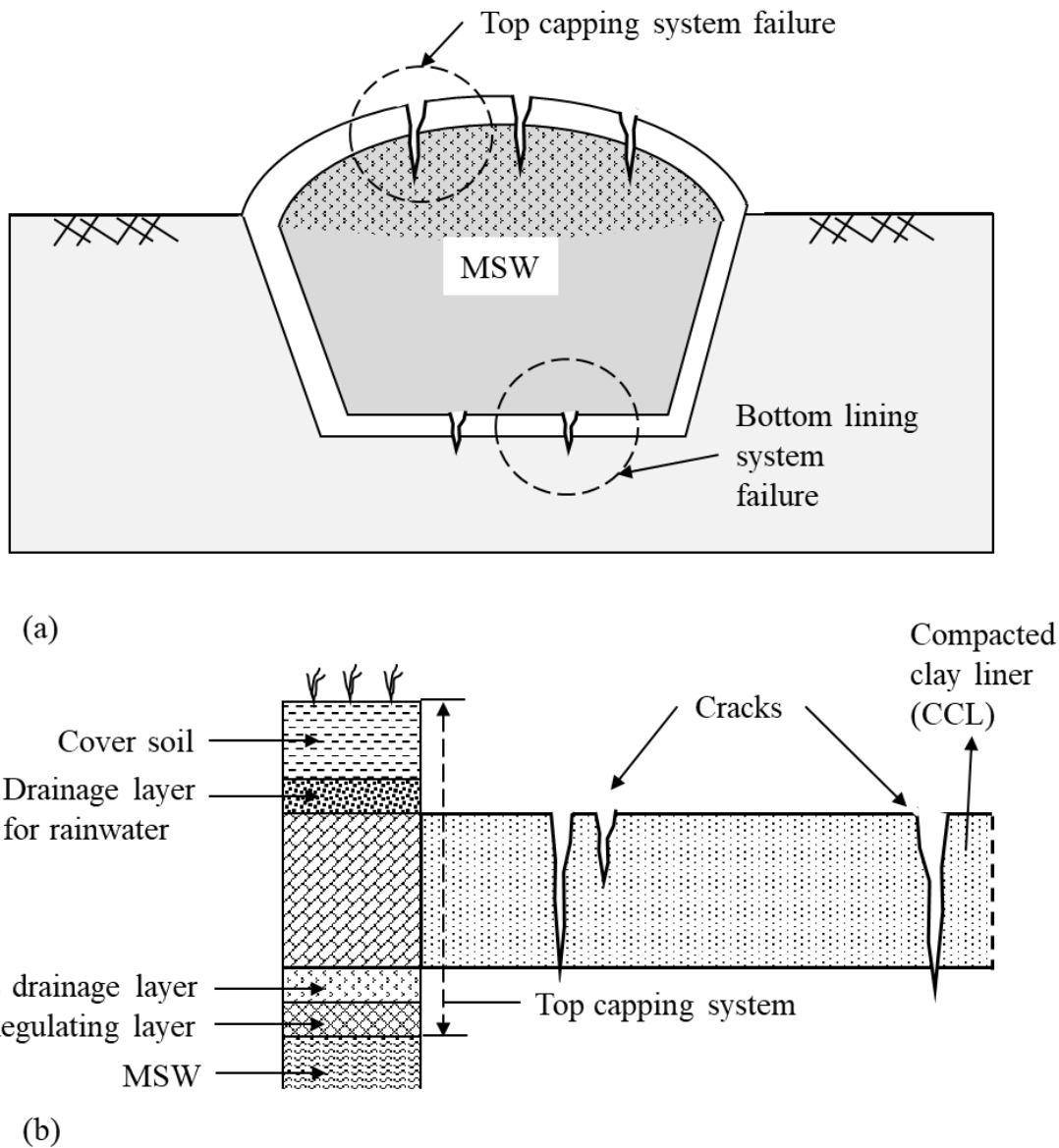
Figure 1. 10 Schematic respresentation of failure of (a) landfill lining system, (b) Top capping system due to desiccation cracking

For instance, cracks increase the hydraulic conductivity and thereby provide speedy pathways for water and contaminant migration through clay liners of landfills. Desiccation cracking of landfill cap covers can aggravate gas leakages through landfills. Cracks also reduce the intact strength of the soil mass and increase the risk of the erosion of the soil in earthen structures like dam cores. Owing to these adverse problems, desiccation cracking has become one of the main concerns in geotechnical and geo-environmental engineering, especially while designing and constructing top covers and bottom liners of landfills in arid regions with expansive soil.

1.3.2.1 Avenues for mitigating desiccation cracking

Researchers attempted several methods to overcome the negative effects of desiccation cracking noted above. Methods for stabilizing expansive soils include the use of chemical additives/admixtures, rewetting of the soil, soil replacement, compaction control, moisture control/dewatering, surcharge loading, and thermal methods.

Replacement of the Expansive Soil by Cushions

In this technique, the expansive soil is replaced either in part or full of a material that doesn't undergo swell. The load of the cushion provides the load necessary to counter heave.

Sand Cushion Method

In this method the entire depth of the expansive soil stratum or a part there-of is removed and replaced with a sand cushion, compacted to the desired density and thickness. The basic advantage of the sand cushion method is its ability to adapt itself to volume changes in the soil (Satyanarayana 1966). However, the sand cushion method has several practical limitations particularly when it is adopted in deep strata.

CNS Layer Method

Replacement by soils with relatively impervious material may, to a great extent offset the disadvantages of sand cushion method. Katti (1978) has developed a technique where by removal of about 1m of expansive soil and replacement by cohesive non-swelling (CNS) soils.

Fly Ash Cushion

Developments of cohesive bonds in a lime-stabilized fly ash cushion, when stabilized with lime, is expected to produce a structural stabilisation effect environment like the one obtained in CNS material following saturation arresting potential heave.

Deep Foundation Techniques

In this method, the foundation is made to rest at depth bypassing the soil in the active zone, i.e. the zone within which volume changes in the soil occur due to seasonal moisture changes. Foundations like as Under-Reamed Piles and Granular Pile-Anchor Foundation (GPAF) System are be used (Nelson et al. 2015).

Chemical Stabilization

In this method, the soil strength is increased by using additives such as lime, cement and sand. Leung and Vipulanandan (1995) investigated the effects of soil additives like lime and cement on clays against volumetric change and permeability. It is opined that the addition lime decreases the amount of desiccation cracking, but the hydraulic conductivity increases in some cases. The plasticity of soil is also decreases significantly, thereby decreasing the potential of compacted clay soil to crack due to shear forces. But in some cases, it was observed that usage of additives increases the hydraulic conductivity of the soil. The soil plasticity was also observed to decrease due to interaction between clay and additive particles. Cement is another stabilizing agent that is widely used, mostly in combination with lime, for soil improvement after lime. Addition of cement in fine-grained soils reduces the shrinkage cracks in the soil. The reactivity of cement increases with decrease in grain size.

According to Daniel and Wu (1993), the desiccation cracking problem can be mitigated by (1) use of clayey sands, which have low permeability and low shrinkage upon drying; (2) adapting suitable range of compaction water content and dry unit weight that ensures both low permeability and low shrinkage potential; (3) relying on large compressive stress, to close pre-existing desiccation cracks and prevent the development of new ones; and (4) protecting the soil from drying by placing a thick layer of topsoil or placement of geomembranes above,

below, or both above and below the soil barrier to minimize drying and (5) using geofiber reinforcement inclusions.

Stabilization by Industrial Wastes

Utilization of industrial wastes like fly ash, quarry dust, silica fume, copper slag, tannery sludge, etc. in the geotechnical engineering field helps to solve the problem of disposal of these wastes. Extensive research is being carried out by geotechnical investigators to reduce the swelling of expansive soils by using industrial wastes. For example, fly ash is added to soils treated with lime to increase the pozzolanic reaction and improve the gradation of granular soils. The pozzolanic activity of silt soils has been improved by using a mixture of lime-fly ash in ratios such as 1:2. Liquid limit decreases and plastic limit increases with increase in the percentage of fly ash.

Horizontal Moisture Barriers

Horizontal moisture barriers can be installed around buildings in the form of membranes, both flexible and rigid. Horizontal barriers are meant to prevent excessive intake of moisture. Asphalt membranes can be used to cover the surface of expansive soils so that non-expansive fill can be placed on top of the membranes. This minimizes infiltration of surface water into the under-slab soils.

Vertical Moisture Barriers

Vertical moisture barriers using concrete, ferrocement or any other impervious material like geomembrane/ geosynthetic clay liner, around the perimeter of the building, to cut off the source of water, can be very useful in minimizing seasonal drying and shrinkage of the perimeter foundation soils and in maintaining long term uniform moisture conditions beneath covered areas. Vertical moisture barriers should be provided to a depth greater than the depth of seasonal moisture changes.

Geofiber reinforcement

In recent times, the concept of reinforcing the soil by including randomly distributed fibers is being investigated. One of the main advantages of randomly distributed fibers over conventional geosynthetic reinforcement is the absence of potential plane of weakness (Maher and Gray 1990). However, more recently there has been an increasing interest in studying the behaviour of fiber reinforced soil to increase the desiccation cracking resistance (Harianto et al. 2008; Miller et al. 2004; Wahab and El-Kedrah 1995; Ziegler et al. 1998). It is found that geofibers reduce the soil cracking.

1.4   Motivation behind the present study

Desiccation cracking is a common problem found in fine grained soils especially expansive soils. Quantification of cracking properties like crack intensity, crack dimensions, crack initiation, and crack pattern is an important aspect to study behaviour of cracked soil. Desiccation alters the properties of soil adversely viz. the seepage, consolidation, and compressibility and shear strength characteristics of the soil. Cracking increases the hydraulic conductivity of the clay liner systems and thereby provides speedy pathways for water and contaminant migration. Therefore, to utilize expansive soils as a barrier soil layer in liner systems, mitigation of desiccation cracking becomes vital.

1.5   Aim and objectives of the present study

The aim of the present study is to understand the influence of discrete and randomly distributed geofiber inclusions in restraining desiccation cracking. The improvement in tensile strength of the barrier material is the most essential factor in the liner system for protecting the environment from pollution. Desiccation cracking is very common in compacted fine-grained soil layers; and these tensile cracks can compromise the sealing efficiency of barriers made with fine

grained soils. This necessitates the inclusion reinforcement elements for improving the performance of fine-grained soil barriers. Therefore, it is important to study the usage of discrete fibers for restraining desiccation cracking.

The tensile strength of a compacted clay barrier material in a liner system is very important. Keeping in view the importance of tensile strength-strain characteristics of the barrier material, this work will evaluate the desiccation cracking and tensile strength-strain characteristics of clay barrier material with and without geofiber inclusions.

As, the knowledge pertaining to the modelling considerations of tensile cracking of the soil caused by heating due to radiation is limited, centrifuge modelling of desiccation cracking of the expansive clay with and without geofiber inclusions will also be presented. Thus the objectives of the present study are:

a) To evaluate and understand the effect of fiber content and fiber length on desiccation cracking of expansive clay with and without geofiber inclusions,

b) To investigate the influence of cyclic drying and wetting on the desiccation cracking behaviour of geofiber reinforced expansive clay compared to unreinforced expansive clay,

c) To investigate the influence of fiber content, fiber length and water content on the tensile strength-strain characteristics of geofiber reinforced expansive clay,

d) To understand the desiccation cracking behaviour of unreinforced and geofiber reinforced expansive clay using distributed optical fiber sensing (DOFS),

e) To model the phenomenon of desiccation cracking in a geotechnical centrifuge and evaluate desiccation cracking of expansive clay with and without geofiber inclusions.

The aims are completed by four main types of tests: laboratory desiccation cracking tests, direct tensile strength test, optical fiber sensing and centrifuge model tests. The tests will be compared to determine whether effect of geofiber inclusions mitigate desiccation cracking of expansive clay. The factors influencing the desiccation cracking of the clay such as cyclic drying and wetting and specimen thickness will be studied. The desiccation crack measurements will be established and measured for expansive clay with and without geofibers. The results obtained from the laboratory scale tests will be compared with the findings from centrifuge model tests.

1.6   Structure of the thesis

Chapter 2 details a critical review of the existing literature, commending various techniques, methodologies and investigations proposed by several researchers related to the studies on understanding the suction, tensile strength, their relationship with the cracking characteristics, methods of quantifying the cracking patterns and the proposed models from the outcome of these studies. Studies on the usage of sensors for understanding desiccation cracking of soil are discussed. Also, studies on centrifuge modelling of desiccation cracking of soil are reviewed, following with a critical appraisal highlighting the research gaps.

Chapter 3 presents the modelling considerations of desiccation cracking of unreinforced and fiber reinforced soil in the study. The chapter also deals with the modelling of fibers and scaling of their properties inside a small centrifuge. The details of the small centrifuge used in the study are discussed. Various errors pertaining to centrifuge modelling were addressed for the given centrifuge.

Chapter 4 presents the experimental investigation carried out to evaluate the geotechnical, mechanical, mineralogical, and chemical properties of the expansive clay used in the present study. The mechanical and chemical properties of various reinforcing fibers are also presented. The consolidation properties and consistency limits of soil and fiber mix was also studied in this chapter.

Chapter 5 presents the laboratory investigation of effect of fibers on the desiccation cracking of expansive clay. A laboratory desiccation cracking setup was designed to subject soil slurry sample to desiccation cracking in considerably controlled environment. The crack feature measurements of expansive soil with and without fibers are compared to study the influence of fiber content and fiber length. The direct tensile test to measure the tensile strength behaviour of unreinforced and fiber reinforced expansive soil was discussed. Further, effect of water content on the tensile strength is presented to understand the influence of fiber content and fiber length. The complete performance of fiber reinforced clay against tensile stresses and desiccation is discussed.

Chapter 6 deals with the influence of cyclic drying and wetting on the desiccation cracking behaviour of expansive clay reinforced with and without fiber reinforcement. This chapter highlights the healing property of expansive clay due to the presence of fibers. The unreinforced and fiber reinforced expansive clay specimens were subjected to cyclic drying and wetting cycles and digital image analysis was used to evaluate the results.

Chapter 7 presents the study of understanding the desiccation cracking behaviour of unreinforced and fiber reinforced expansive clay using distributed optical fiber sensing (DOFS). The test setup including DOFS, digital image acquisition system and moisture content monitoring was developed at Monash University, Australia. This novel experimental setup helps us to understand the strain behaviour of soil undergoing shrinkage and desiccation cracking with the help of optical fiber sensing. Particle image velocimetry technique was also employed to get interesting information about the soil movement during drying and cracking.

Chapter 8 presents the desiccation cracking in a clay layer inside a geotechnical centrifuge. It presents the centrifuge model test package for drying of soil at high gravities, test program, model preparation of unreinforced and fiber reinforced expansive clay and testing procedure. The influence of fiber reinforcement, specimen thickness, fiber length and fiber type on desiccation cracking was also studied. Particle image velocimetry technique was employed to study the effect of fiber reinforcement on the desiccation cracking of soil.

Chapter 9 deals with the summary and conclusions evolved from the present study. Before presenting the scope for the future work, an attempt was made to summarise major research contributions evolved in the present study.

LEFT BLANK INTENTIONALLY

Chapter 2

LITERATURE REVIEW

2.1   General

Cracking in soils is a complex phenomenon and a problem which has occurred throughout the ages and is likely to always occur. Soils, specifically fine-grained soils/clays, can undergo cracking by: mechanical loading-induced cracks, desiccation, and thermal or chemically-induced cracking. As cracking due to desiccation is most common, exhaustive research is being carried out around the world to study the desiccation cracking behaviour of expansive soils. A review of the available literature pertaining to the desiccation cracking of soils, their characteristics and fiber reinforced expansive soil is presented in this chapter. For the sake of better understanding, the literature has been divided into different heads, presented in the following sections which are directly associated with the topic of study, as summarized below in the subsequent sections.

2.2 Studies on the use of expansive soils as construction material

Wiggins et al.(1978) listed six major natural hazards; earthquake, landslide, expansive soils, hurricane, tornado, and flood. The study pointed out that the expansive soil tie with hurricane wind/storm surge for second place among most destructive natural hazards that occur in terms of losses to structures. The annual cost of damage due to expansive soils is estimated at £150 million in the UK, $1000 million in the USA and many billions of pounds worldwide (Viswanadham and Phanikumar 2009). The damage to buildings, roads, and other structures built on expansive soils exceeds $10 billion annually in United States alone (Steinberg 1998).

2.2.1 Building Foundation Failures

Many authors have conducted studies on the building foundation failures. Tree growth can also be another factor responsible for damage to foundation in expansive soils. This can cause both the physical disturbance as well as shrinkage of ground by removal of water. The failure of foundation occurs, when volume of soil beneath the foundation is unevenly distributed. Al-Rawas (2006) conducted a study on the potential problems associated with expansive soils on foundations in the Arabian Gulf.

2.2.2 Pavement Failures

The shrinkage of expansive soils is the reason for the failure of pavements. The drying of the soil causes the shrinkage of the soil which propagates through the pavement system causing longitudinal, transverse and fatigue cracking and rutting in the pavement surface. In addition to this, bumps caused due to heave can increase the roughness of pavement and result in poor riding comfort. Differential soil movements may induce large changes in moments and shear forces in the pavement structures. All these factors if not accounted in the original design, both

rigid concrete and asphaltic pavements may experience severe distress in the forms of high roughness and cracking in both the longitudinal and transverse directions, as shown in Figure 2.2.
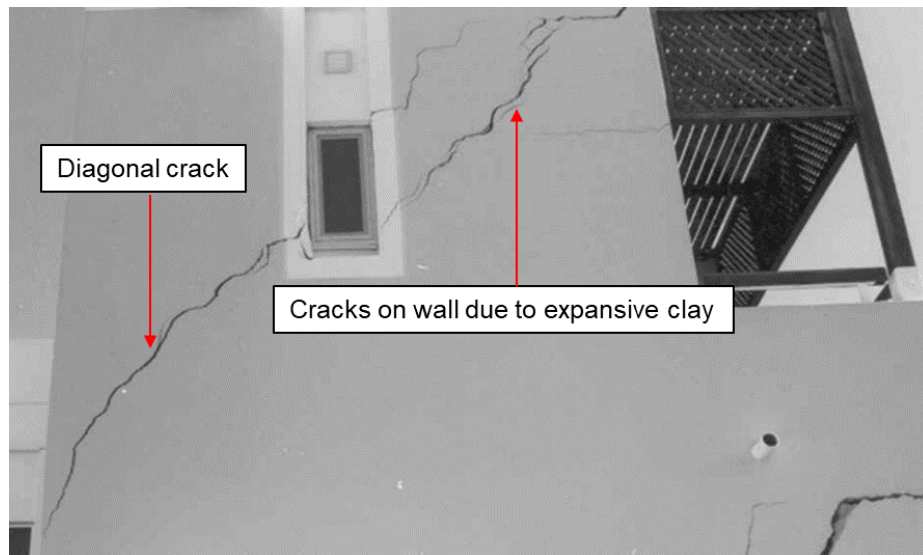
Figure 2.1Structural damage due to foundation failure (After Al-Rawas, 2006)

Puppala et al. (2011) conducted studies on pavements constructed on expansive soils. Lime stabilization techniques were utilized to mitigate the expansive behaviour of these soils and found to be successful. Figure 2.3 is a pavement distress caused by swell-shrink characteristic of expansive soils.
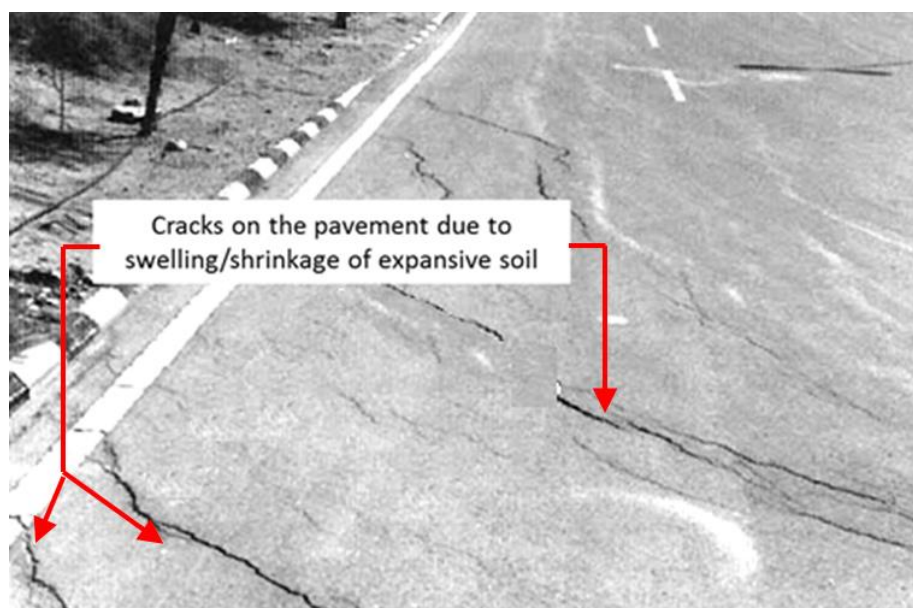
Figure 2.2 Pavement failure (After Al-Rawas, 2006)

Figure 2.3 Pavement distress caused by swell shrink soil (After Puppala et al. 2011)

2.2.3 Slope Failure

Slope failure occurred at Grapevine Dam in the State of Texas, USA was reported by (McCleskey et al. 2008)). This dam is built on expansive soil and is subjected to desiccation cracks during seasonal changes. During a rainfall event, water infiltrated into the soil through the desiccation cracks which increased pore water pressure which leading to reduction of shear strength triggering failure (Fredlund and Rahardjo, 1993; Cho and Lee, 2001).

During dry season, the shrinkage cracks are formed, and the water exerts hydrostatic pressure resulting in sliding of slope from the crack which is responsible for an increase of width of shrinkage crack. Figure 2.4 shows the slope failures associated with expansive soils. These failures are quite detrimental and clearly showed the extent of damage.

2.2.4 Landfill liners

Figure 2.5 shows the images of desiccation cracks developed on the mud soil layer on The Pekin Landfill project, Illinois, USA. The landfill needed to be covered. Around 10,000 MT mud from sediments of a lake were used for using as final cover topsoil on this old landfill. The rehabilitation of desiccation was done by covering the area with vegetation. But, if the land is to be utilized for construction purpose, vegetation will not solve the problem of surface failures caused by desiccation.

Figure 2.4 Slope failure triggered by desiccation cracks of expansive soils (After McCleskey et al. 2008)

Figure 2.5 Desiccation cracks on mud used as landfill top cover at Pekin Landfill Illinois (Source: https://www.istc.illinois.edu/research/resource_recovery/mud_to_parks_il_ river_project/photos/pekin_landfill/)

Rowe (2012) reported that desiccation results from drying of the clay from its compacted state and may be especially severe for CCLs compacted near or above the plastic limit. Desiccation may occur after construction of the clay liner and before placing the Geomembrane. Figure 2.6 shows image of a compacted clay liner having desiccation cracks before the geomembrane is placed.

Figure 2.6 Compacted clay liner (forming part of a composite liner) that has desiccated (After Rowe, 2012)

The desiccation cracks in landfill covers may act as potential pathways for permeation of water into the landfill during substantial infiltration. Also, this may lead to serious hazards, such as

permeation of leachate into the groundwater system. Differential settlement of the clay liner may also take place due to reduction in the tensile strength of the soil due to desiccation Cracks and uneven settlements can affect the structural integrity of the liner system and the landfill as a whole.

2.3 Studies on desiccation cracking in soils

This section presents field, laboratory an analytical or numerical study on desiccation cracking in soils. Various methodologies and parameters during the studies are summarized in Table 2. 1- Table 2. 5.

2.3.1 Field studies

Researchers have been trying to solve the puzzle of desiccation since the early twentieth century and the history of study of desiccation cracks in geo engineering dates back to the same period.

Kindle (1917, 1923) produced one of the initial works on desiccation cracking found in the literature. Experimental studies in the formation of erratic lines known as mud- cracks, sun-cracks and shrinkage cracks were investigated. The relative effects of rate of desiccation on the same mixture, effect of composition of mud on cracks, possibility of parallel mud-cracks and difference between the saline and freshwater mud-cracks was established.

Chico (1964) reported that the topography at microscopic level of a desiccated soil is composed of cracks and blocks or cell polygonal in shape. The length, depth, width, shape, and number of cracks vary greatly. Crack pattern can be determined by observation of soil cracks and thus many morphometric properties of cracks be computed.

Idso et al. (1974) studied different stages in drying of a field soil during all seasons of the year. Three stages of soil drying have been classified depending on the intensive measurement of evaporation, soil heat flux, soil-water content, soil temperature, albedo, and net radiation. The

first stage being the evaporation of water; the second stage involves drying of the soil surface at relatively lesser evaporation rate, whereas the third drying stage initiates at a surface water content that corresponds to the retaining of two molecular layers of water around the soil particles. Nevertheless, the third stage includes evaporation till the volumetric water content reaches a value of 6%. The evolution from the second to the third drying stage is predicted assuming that the physical adsorption occurs in the first two molecular layers of water surrounding the soil particles. It is concluded that the rewetting of the surface soil may re-establish wetting and drying cycles.

Velde (1999) has validated the utility of image analysis of photographs to study the surface crack structure in cultivated soils (Andosol, Vertisol, Mollisols) and mud deposits as a function of soil type. Surface crack (viz., crack segment and intersection frequency) photographs obtained from the field soil were employed for this purpose. The results show that there is no major difference between the cracks networks developed in a variety of cultivated soils and mud deposits. Based on the results, authors have developed crack network models using fractal analysis, which considers the distribution of pores in a 2-D plane. Authors have also opined that the area-fractal dimension relations could be used to identify shrinkage processes. It has been concluded that irregularity of the structures is the greatest in the soils at low porosity and for the same porosity the irregularity decreases as one goes from soils to mud at deep locations.

Ringrose-Voase and Sanidad(1996) have developed a technique to measure insitu surface cracks. A mathematical model to measure the volume of cracks was also formulated. Crack width and depth was measured using a flexible plastic ruler of 300mm length. The volume of cracks was estimated by assuming different shapes of cracks (viz., rectangular, triangular and square root shape model). The results computed from the mathematical model were validated by measured crack volumes that were obtained by filling the field cracks with very fine sand of known densities. It has been concluded that for the soil which are still undergoing shrinking, triangular shape can be considered.

Elias et al.(2001) have investigated the Vertisol field soil cracking at three sites in Northern, central and Southern Gezira, Sudan. Blocks of area 4 sq. m were selected. Various parameters like crack dimensions such as depth, width (measured using a meter tape) and crack volume (which is equal to the volume of very fine sand required to fill the cracks formed in the area selected) were measured. As the aridity of area increased the crack intensity and depth increases. However, it was concluded that the crack dimension and volume measurements by

probe and very fine sand are not very accurate and vary far more than the actual depth and dimensions.

2.3.2 Laboratory studies

Abedine and Robinson (1971) have established an apparatus to measure and study the crack geometry and their pattern. This technique could be used to measure the crack depth, width, spacing and total volume of the crack. The setup consists of plate cut into bilateral section with base of 120 mm long and head angle of 22°30'. The sides of bilateral are graduated and scaled to measure the width of crack and graduated metal probes to measure depth. Before conducting experiments, influence of environmental parameters like soil type, drying period, soil history, rainfall and vegetation were studied on the Vertisols in four areas of Sudan. It has been concluded that the crack intensity is a function of the clay content of the soil. Whereas, the depth of crack and width of crack are a function of drying period, type of soil and clay content.

O'Callaghan and Loveday (1973) introduced the method of obtaining the crack patterns in soil sample from surface photographs using a computer program. Effect of addition of gypsum to the soil was studied. The program was used to identify the clods (which is the area within cracks) to produce a crack skeleton and which was then used to measure the length and width of cracks. It was observed that the presence of gypsum decreased the measured width of major cracks that are visible externally and considerably larger in size. However, the presence of gypsum does not show any effect on the internal or minor cracks.

Towner (1987) experimentally studied the tensile forces generated in clayey soils due to shrinkage at different moisture contents. Initial water content, cracking moisture content, and tensile strength at different water contents were measured. Cracking water content was observed to be same and practically independent of the moulding initial water content, under the same drying conditions. A relationship between the measured tensile strength during drying of the clay and water content was established. It has been observed that when clays are prevented from shrinkage during drying in one direction, they do not crack until the stress developed in that direction is equal to or greater than the corresponding tensile strength. It has been opined that the induced stress is equal to that of the change in the soil-water suction for

isotropic shrinkage. However, it should be noted that the initial saturation of these samples was high.

Miller et al. (1998) performed laboratory experiments on scaled models of a landfill clay liner. The experimental setup included a soil tank, rainfall simulation system (for wetting cycle), drying system (drying cycle), drainage system, surface crack recording system, and water potential measuring system. To simulate the wind action and desiccation on soil surface, blowers were fixed on the wall and psychrometers were used to measure the water potential. The clay bed was compacted to 160 mm thickness, which is within the range of recommended thickness and wetting drying cycle of this clay bed was studied for three periods i.e. Compaction-dry, dry-wet and wet-dry period. They concluded that a clay layer with low PI and compacted dry of optimum also experiences desiccation cracking. The desiccation cracking of soil was highly dependent on the cycle of desiccation and was very intense in the period of desiccation. The Crack intensity factor (CIF), which was defined as the ratio of area of cracks to the total area of soil under consideration, changed significantly at the beginning of drying cycle but stabilizes with further increase in soil suction (at 168 hours). They observed that large intensity of rainfalls widened the cracks with erosion of soil.

On the basis of published data, Kodikara et al. (2000) presented modes and mechanisms of desiccation of soils. The cracking in soils has been divided into orthogonal and non-orthogonal. It has been established that the morphology of these cracks depends on the desiccation rate, thickness of the sample, its density and the initial water content. The base adhesion characteristics play an important role in crack formation. The base adhesion characteristics were studied using different base materials like plain wood, greased wood, sheet of glass and sand layer. It has been reported that a glass base induces smaller crack cells and the cracking pattern has been compared with that obtained for the wooden base. No cracking was observed when the sand base has been used. It has been demonstrated that the water content at the time of cracking significantly decreases with an increase in desiccation rate. The concept of mean cell area, which is defined as the total cell area divided by the number of cells when the soil is dry, has been used to differentiate between the cracking patterns (viz., triangular, rectangular and hexagonal). It has been opined that the total length of the cracks is inversely related to the layer thickness.

Yesiller et al.(2000) experimentally investigated the soil samples collected from three landfill sites from South Michigan against desiccation and cracking, subjected to series of wetting and

drying cycles simulating field conditions. Image analysis was used to quantify the number of surficial cracks in the form of CIF. The main factors that influence formation of cracks on soil mass are the type, amount of clay content, negative pressures or suction moisture, density of the soil, overburden and wetting/drying environmental conditions. The samples were first dried after compaction and then subjected to wet/dry cycles. The CIF for wet–dry cycles were significantly greater than the CIF for compaction–dry cycles. Generally, soils with high fines content have high suctions demonstrate rapid increases in suctions and high amount of cracking. Moreover, it was observed that amount of cracking increased significantly with addition of moisture to soils.

Albrecht and Benson (2001) have studied the response of 8 different naturally available soils, which were used for the construction of liners and covers. Soils were subjected to seasonal environmental conditions, compacted to different energies (standard, modified and reduced Proctor compactions) and specimens were prepared to conduct hydraulic conductivity tests using flexible wall permeameter. The samples were initially saturated and tested during which the volumetric shrinkage stresses and strains were measured as samples dried. The volumetric shrinkage strain decreased with increased compactive effort. Minerals (like Smectite or Illite/ Smectite layer) that help swelling also play a role in formation of shrinkage cracks. Shrinkage is found to be less in the presence of minerals like Illite, Kaolinite, and Quartz. It has been opined that the hydraulic conductivity of these specimens varies with drying and wetting cycles and the resulting changes were observed to be much higher after the first wetting and drying cycle.

Tay et al.(2001) have investigated the behaviour of Bentonite Enhanced Sand mixtures (BES) when subjected to air-drying. BES mixtures containing 10% and 20% Bentonite by dry weight and compacted at moisture contents ranging from 8% to 32 %, moulded into beds of size 800 $\times$ 800 mm^2, each were tested for desiccation cracking, shrinkage and hydraulic conductivity. Upon air-drying all the samples underwent volumetric shrinkage and this shrinkage was found proportional to the decrease in moisture content. However, this shrinkage was not found to be dependent on the compactive effort used in preparation of the samples. It has also been observed that no desiccation cracking occurred on compacted beds of BES containing 10 % and 20 % Bentonite, if the initial moisture content is 15 % - 14 %. For the range of mixtures tested, it appears that cracking only occurs when BES undergoes more than about 4 % volumetric shrinkage when air-dried from 10 % – 15% moulding moisture content.

Tarafdar et al.(2006) have studied the desiccation crack behaviour of natural and synthetic clays. The samples were tested in petri-dishes of 120 mm diameter with 2.5 gm of Laponite (synthetic clay) mixed with 50 mL of distilled water. To induce desiccation cracking, two electrodes were inserted inside the sample to complete the circuit. Two types of tests were conducted, one with and one without constant voltage applied. The Nano-sized disc like units carrying quadruple moment with the field gradient in non-uniform field of radial symmetry were observed to be responsible for developing the crack pattern. The cracks first generate at the centre and then propagate radially towards the negative electrode. When no voltage was applied no characteristic crack, pattern was observed for same geometry. It has been observed that the pattern of cracks formed is strongly affected by the geometry and the direction of the applied electric field.

Nahlawi and Kodikara (2006) studied the desiccation cracking on thin layers of clay samples prepared in samples of varying sizes (length to width ratio = 10 to 24) and used Perspex and metal moulds. The natural clay used in the study is highly reactive soil present in Victoria. Two types of samples having high water content (127 %) and compacted soil (32.5 %) were subjected to desiccation cracking tests in a humidity chamber. A constant temperature of 23°C and 50% relative humidity was maintained. The crack patterns in the rectangular moulds were categorized as primary, secondary, and tertiary cracks. Number of cracks, crack propagation, number of cells, water content measurements were observed. They concluded that with the increase in layer thickness, the cracking water content increases, whereas ratio of crack spacing to depth and desiccation coefficient decreases. The mean area of cells increases with increasing clay layer thickness and is found more for compacted soil samples than for clay slurry samples.

Tang et al.(2008) have investigated the effect of temperature, thickness of the soil layer, wetting and drying cycles and soil types on the crack pattern of desiccating clay layers. A Crack Image Analysis System (CIAS) was developed for analysing the shrinkage crack patterns. These parameters were then employed to evaluate the crack segments, intersection, average crack length, width and aggregate area, Crack Intensity Factor (CIF), and the corresponding Probability Density Functions (PDFs). The values computed from the software were validated by comparing the results of tests conducted on eight different soil samples. It is observed that the crack parameters are related to the PDF of the soil, which increases with increase in temperature. It has been found that the average crack length, width, aggregate area and CIF increase with the thickness of the sample (Corte and Higashi 1964; Kenney et al. 1984; Nahlawi

and Kodikara 2006). It is observed that as the number of wetting-drying cycles are increased, the soil surface generates more irregular and sparsely formed cracks and CIF decreases. The extent of cracking is a function of the amount of fines and plasticity index and this finding is consistent with that by Corte and Higashi(1964) and Yesiller et al. (2000).

Birle et al. (2008) investigated the behaviour of compacted clays for the effect of initial water content and dry density on the soil water characteristic curve (SWCC). The soil was compacted at three different compactive energies with the water content being constant in all cases. Shrinkage tests were conducted on cylindrical samples and suction of each sample was measured using potentiometers. The primary drying process is strongly influenced by the initial water content. In contrast, the rate of the volume change of the residual drying process is unaffected by the initial water content.

Kalkan (2009) studied the influence of waste silica fumes on the desiccation cracks of compacted clayey soils. The investigation of the suitability of silica fumes as a stabilization material to reduce the development of desiccation cracks in the compacted clay liners and cover systems was carried out. Interesting observations were made when silica fume content decreased the development of desiccation cracks on the surface of clayey soil-silica mixtures. In addition, silica fume showed the ability to decrease the compressibility and swelling behaviour of clayey soil-silica mixtures. This highlights the importance of clay mineralogy on soil reactivity and associated desiccation and cracking. It should be noted, however, that there can be significant health hazards in using silica fume in large scale in open spaces.

Tang et al.(2010a) investigated the temperature dependence of desiccation cracking behaviour of clayey soils. Desiccation cracking was observed in saturated clay slurry samples at three temperatures (22°, 60° and 105 °C). Over-saturated slurry specimens were prepared by mixing soil powder with distilled water at a water content of about 170%. The slurry was hand-mixed; and then desired slurry quantity was poured into glass cups (117 mm in diameter). The crack pattern was studied by mounting digital camera on top of specimens during drying. Quantitative analysis of cracks by digital image processing technique was used calculate surface crack ratio. They claimed that water content corresponding to initiation of desiccation crack and surface crack ratio increases with increase in temperature. Surface crack ratio (RSC), which is the ratio of the surface cracks area to the total surface area of a specimen, was determined at different water contents to quantify the cracking extent on the soil surface. The cracking curve (RSC vs

water content), to some extent, reflects the shrinkage properties of soil: the larger the soil shrinkage, the larger the value of RSC.

Tang et al. (2011a) investigated the desiccation cracking behaviour of an initially saturated (90 %) clay layer of approximately 8 mm in thickness (160 mm x 160 mm glass plates). Three identical specimens were placed in oven at 40º C and 32±1% relative humidity. The processes of soil water evaporation, development of capillary suction (radius of menisci R_s), drying shrinkage, crack initiation when the tensile stress T_s developed exceeds the tensile strength and propagation were monitored and studied, as shown in Figure 2.7. An image processing technique with the help of a digital camera was applied to study the geometric and kinematic characteristics of the surface crack pattern are described quantitatively. The developed suction during drying, was considered to act as the mechanical initiator of the desiccation cracks. After crack initiation the surface-crack ratio increases with further decrease in water content, which can be related with lateral and vertical strains computing the volumetric strain.
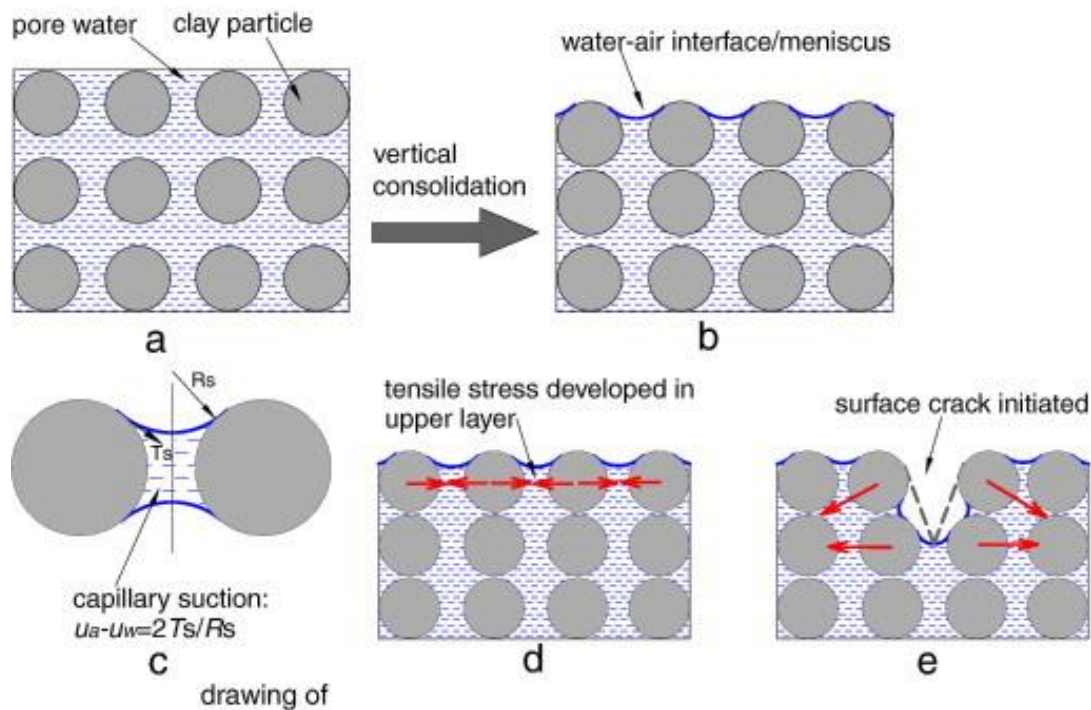
Figure 2.7 Schematic drawing of desiccation crack initiation process, (a) Development of capillary suction, (b) Increase in tensile stress during drying, (c) Surface crack initiation (After Tang et al. 2011a)

Analysis of desiccation crack depth in three compacted clay liners exposed to annual cycle of atmospheric conditions with and without a geotextile cover was carried out by Safari et al. (2014). Three soils in pairs were subjected to real atmospheric conditions for a full annual cycle.

The pairs included one set of compacted soils with the bare surface exposed to atmospheric conditions and one set covered with a separator geotextile. The hydraulic conductivity of the soils at the end of the experiment increased substantially in both bare and covered soils. However, the magnitude of increase in hydraulic conductivity was considerably lower in soils covered with the white geotextile. The depth of cracks increased as a result of evaporation from the surface of the soils, which came to a relatively constant value after a few months from the beginning of the experiment.

Tollenaar et al. (2017a) discussed the observations on the desiccation and cracking of clay layers. A series of tests were carried out to try to separately evaluate the role of material properties and that of boundary conditions on the initiation and development of cracks in drying clay. This included varying the initial layer thickness, the initial water content, the surface area of the set-up and the container material type. Emphasis was given to the conditions of fracture initiation and propagation, particularly looking at what occurs vertically across the soil layer.

Tollenaar et al. (2017b) carried out small-scale evaporation tests on clay and studied the influence of drying rate on clayey soil layer. The study was carried out by assessing the drying behaviour of a clay from two different starting conditions (high and low water contents), under fast and slow evaporation. At the same time, the influence of the different evaporative regimes on the development of suction in the soil was explored. Some aspects of the rate-dependent process were highlighted and tentatively discussed.

Julina and Thyagaraj (2018) carried out the quantification of desiccation cracks using X-ray tomography (XCT) for tracing shrinkage path of compacted expansive soil. Digital camera surface images and XCT images were captured during the intermediate stages of drying to understand the development of volume change pertaining to annular gap and cracks on the surface of soil specimen. XCT images were analysed using ImageJ software for quantification of crack volumes (Figure 2.8). This demonstrates that the XCT imaging technique in conjunction with the image analysis technique can serve as an alternative non-destructive method for the accurate determination of volume of desiccated soil specimens.
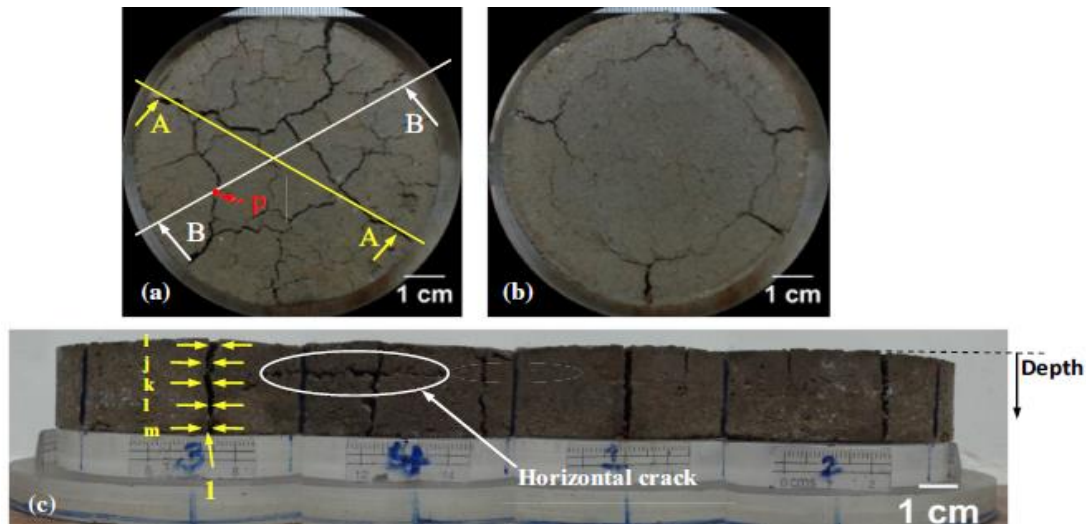
Figure 2.8(a) Top view, (b) bottom view, (c) lateral view of surface images of soil specimen (at water content of 38.5% (After Julina and Thyagaraj, 2018)

Wang et al.(2018) studied the nucleation and propagation mechanisms of soil desiccation cracks by continuous full-strain measurements on soil sample surfaces using digital image correlation techniques. The mode I variety of cracks are tensile in nature. The results show that desiccation cracking was of the mode I variety, i.e. tensile cracking and can be reliably predicted through strain field analyses: the observed cracking was restricted mostly to high stretching domains. The observed high stretching stems from either external restraints or internal flaws of the shrinking soil. The cracks redistribute the stress in their vicinity and lead neighbouring cracks to intersect them mostly orthogonally.

2.3.3 Analytical/ Numerical Studies

Corte and Higashi (1964) were the earliest researchers to study and quantify the desiccation cracking and the crack pattern. They observed that the crack initiates from the centre and reaches the surface or bottom at different time periods. The parameters such as shape, size, porosity, and depth of scattered stones were found to affect the initiation of cracks but did not relate to the geometry and the mean area of the crack cells. It was highlighted that the wide spaced cracks were due to slow desiccation and more cracking was due to the slower desiccation. The initiation of the cracks was reported as mainly due to the coalescence of micro-

cracks during desiccation. This crack coalescence was found to be proportional to the tensile stress caused by desiccation at a point of drying time.

Morris et al. (1992) proposed a theory of cracking in drying soils based on their investigations in Australia and Canada. After a critical synthesis of unsaturated soils, models and theory have been developed based on (a) elasticity theory, (b) the transition between tensile and shear failure and (c) linear elastic fracture mechanics (LEFM). The validity of the relationships was undertaken by comparing the measured and observed crack depths in the field. It has been found that the cracking of the soil depends upon the properties such as compression modulus, Poisson's ratio, shear strength, tensile strength and the specific surface energy. It has been opined that the proposed relationships would be useful for predicting the onset of secondary cracking and for determining the depth of the cracks. However, no quantitative analysis was proposed for this.

Kodikara et al. (2004) introduced the modelling of curling in desiccating thin clay layers. Curling is a common deformation pattern which occurs during desiccation of thin layers. The curling was reported to occur in two forms i.e., lifting off from the edges and lifting off from the middle. The curling was primarily attributed to differential shrinkage strain increments that occur down the soil profile and their variation with the progression of desiccation. The modelling of shrinkage and curling deformations of soft clay strips has been developed using FLAC software. This model was validated vis-à-vis with that obtained from the laboratory experiments conducted on very high swelling clays in controlled temperatures of 16°C and 18°C and Rh 40%-50%.

Kodikara and Choi (2006) presented a simplified analytical model to explain desiccation cracking of clay layers in laboratory cracking tests. This model can predict the sequential cracks based on the maximum tensile stress concept. A schematic diagram of the analytical model is shown in Figure 2.9. The first crack will occur at the middle and subsequent cracks will subdivide the soil layer, thereafter, as shown in Figure 2.9a. It was highlighted that the free shrinkage strain was linearly correlated to moisture content reduction. Figure 2.9b shows the tensile stresses at the interface between clay layer and the base. They used empirical correlations to represent non-linear material properties of clay and the basal interface, which was found to have a significant influence following the work of Corte and Higashi (1964).
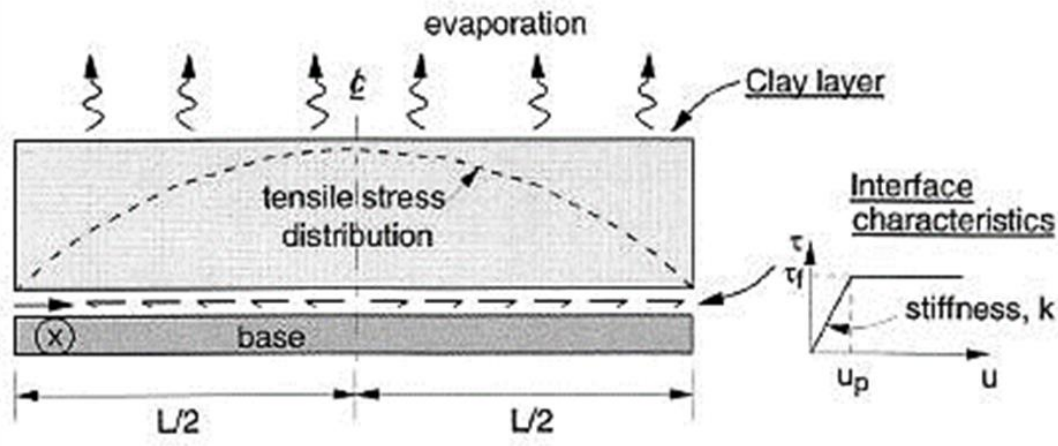
(a) Tensile stress distribution in clay layer   (b) Interface characteristics

Figure 2.9 Schematic representation of the model proposed by Kodikara and Choi (2006) to explain desiccation cracking of clay layers

Costa et al. (2018) presented theoretical analysis of desiccation crack spacing of a thin, long soil layer. They predicted the approximate spacing-to-depth ratio of parallel cracks that form in long desiccating soil layers subjected to uniform tensile stress (or suction profile) while resting on a hard base by two approaches, namely stress relief and energy balance. The theoretical developments have examined the formation of simultaneous and sequential crack patterns and have identified an important relationship between the stress relief and energy approaches. In agreement with experimental observations, it was shown that the spacing to- depth ratio decreases with layer depth, and crack spacing generally increases with layer depth.

2.4 Studies on restraining desiccation cracking of soils

In this section various experimental studies on desiccation cracking of soil at laboratory and field level with setups have been discussed. Figure 2.10 gives various types of synthetic and natural geofibers used by the researchers.

Synthetic fibers	Natural fibers

Polyester fibers · PP Tape fibers

Polypropylene fibers

Sisal fibers · Palm fibers

Coir fibers
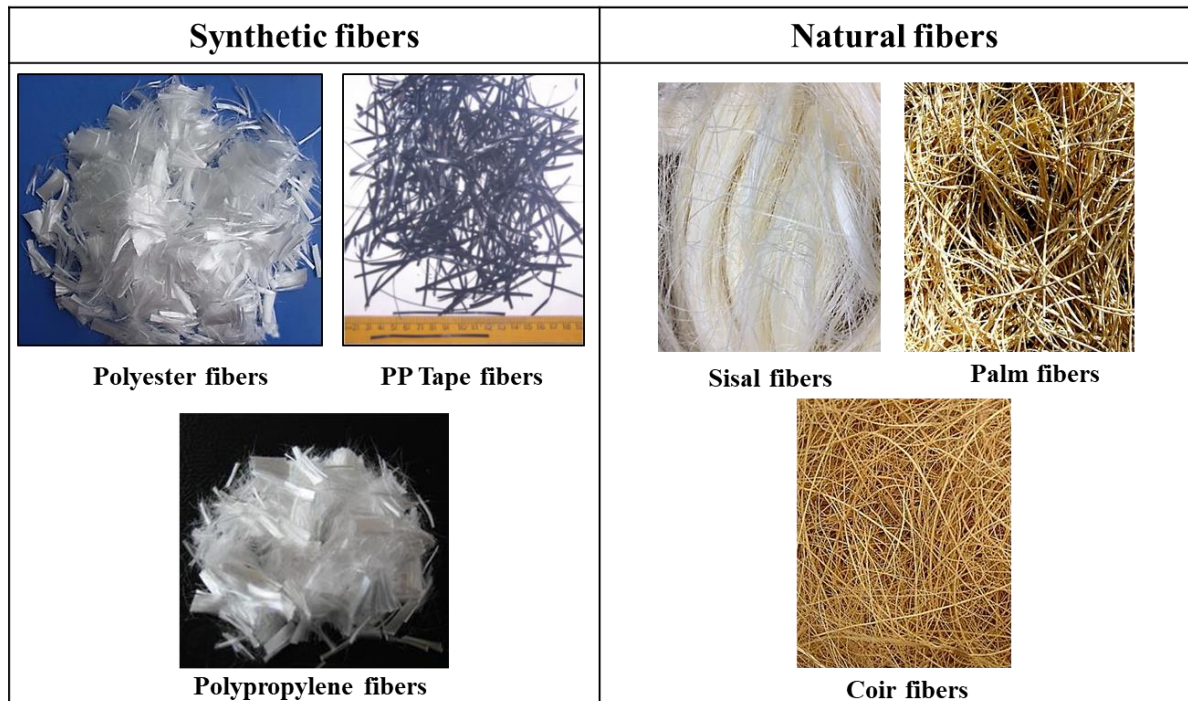
Figure 2.10 Various types of synthetic and natural geofibers used by researchers

Allan and Kukacka (1995) studied the mechanical behaviour and durability of inclusion of 19mm long fibrillated polypropylene fibers in cementitious grouts (composed of cement, water, sand, bentonite, and super plasticizer). The grouts were investigated for suitability as waste containment landfill liners. The fiber reinforced cementitious grouts were subjected to strength, wet-dry and freeze-thaw durability and shrinkage crack control tests. It was observed that though the compressive and flexural strengths of the grout material was not observed to increase, the crack widths showed significant reduction, by virtue of bridging action.

Ziegler et al. (1998) experimentally studied the effect of inclusion of randomly distributed discrete, fibrillated polypropylene fibers on clay. Samples were prepared by mixing synthetic soil with fiber (content levels of 0%, 0.1% and 0.3%) in a mechanical mixer at a moisture content of 3.5% above optimum and cured. The specimens were prepared in standard Proctor mould and subjected to different number of drying (oven at 48°C and period of 24 hours) and wetting (Submerged in water for 24 hours) and thereby, Cracking/volume changes were recorded. A tension test was conducted on the soil mix on a direct shear test apparatus at a displacement rate of 0.4 mm per minute. It was concluded that the fibers are effective in reducing the desiccation cracking. However, when subjected to wet-dry cycles, the effectiveness of fibers was not that evident.

71

Miller et al. (2004) investigated the inclusion of polypropylene fibers on clay samples against desiccation cracking of waste containment soil liners. They studied the impact of fiber reinforcement on soil workability, compaction characteristics and hydraulic conductivity of clay liner. They also reported that polypropylene fibers being hydrophobic and chemically inert material, does not absorb or react with soil moisture or leachate. First, the crack intensity factor (CIF) for cracked samples was found by preparing compacted samples of soil and fiber content as 0.0%, 0.2%, 0.4%, 0.6% and 0.8%, and dried for a period of at least 3 days. Hydraulic conductivity tests of the cracked sample were also done to evaluate the effect of fiber inclusion in clay liners. The hydraulic conductivity test was performed on samples using fiber contents of 0.0%, 0.2%, 1.0%, 1.5% and 2.0%. The optimum fiber content with acceptable hydraulic content to achieve maximum dry density and optimum moisture content were found to be 0.4% and 0.5%. The maximum crack reduction was observed to be approximately 90%, for a fiber content of 0.8%, in comparison to unreinforced samples. However, it was opined that the even though crack reduction is observed for fiber reinforced sample, the hydraulic conductivity increased significantly, and the practical limits of usage were exceeded.

Diambra et al. (2007) analytically determined the fiber orientation distribution in fiber reinforced sands. A sphere of fiber reinforced sand is assumed. The volume of fibers intersecting the vertical and horizontal planes of the spheres are determined and divided by the total volume of the sphere. The determined volume of fibers in a plane is then integrated through the remaining potential points through which the fibers could pass in the sphere. The established theoretical model was applied on cylindrical models of moist fiber reinforced sand, prepared by tamping technique.

Tang et al. (2007) reported studies on discrete and random short polypropylene fiber reinforced clayey cemented (i.e. 5% and 8% by weight) and uncemented soil. The strength and mechanical behaviour of reinforced soil was evaluated for three different fiber contents i.e. 0.05, 0.15, 0.25% by weight of soil by conducting UCS and direct shear tests after 7-, 14- and 28-day curing periods. They observed that the inclusion of fibers increase UCS, shear strength and failure axial strain value for both cemented and uncemented samples. Whereas, the stiffness of sample decreased, and cemented sample showed ductile behaviour rather than brittle. Scanning electron microscopy images of the fiber-soil interface, supported the presence of good bond behaviour and thus better mechanical behaviour, though is influenced by components mix, normal stresses around fiber body, area of contact between fiber and soil and roughness of fiber.

Harianto et al.(2008) investigated the effect of inclusion of polypropylene fibers (10 mm in length and 50 μm in diameter) on cracking characteristics of the highly plastic silty soil. The fiber content in the soil sample was in various proportions, viz.,0.0%,0.2%,0.4%, 0.6%, 0.8%, 1.0% and 1.2% by dry weight of the sample and compacted, at room temperature (25±2°C, 50±1% relative humidity). Samples of 300mm diameter and 100 mm length were subjected to drying and CIF (ratio of area of crack to total area) was computed, which was then employed to estimate the magnitude of desiccation cracks developed in the soil as the ratio of desiccation crack area and final effective area of the sample. The compaction characteristics, crack intensity and the volumetric shrinkage have been reported to decrease with the amount of fibers added to the soil. This has been attributed to the interaction of fibers and soil particles.

Nag et al. (2010) investigated the crack patterns of clay-polymer mixture undergoing desiccation cracking. A synthetic clay Laponite was used for experiments. The polymer used was polyethylene oxide mixed with a fraction of solute and methanol. The suspension was poured into petri dishes and allowed to dry under ambient conditions. The images were taken to observe the propagation of cracks and the sample was dosed with dye for high clarity images. For the cracked samples, crack morphology, crack area, and fractal dimensions were studied. The cracks having broad widths, that separate solid soil pieces were termed as 'peds', which were observed to get jagged as the polymer was added. Particle image velocimetry technique was utilized, and the photographed images were analysed using Image Pro Plus software during drying and sequencing of crack propagation was established. It is opined that such clay-polymer composites help in reduction of desiccation cracks as the polymers offer a tortuous path for the crack to propagate in the disordered lattice. The electrical fields are also found to affect crack formation.

Tang et al.(2012) studied the improvement of clayey soils by short polypropylene fiber reinforcement. A total of 19 tests were performed with six fiber contents (0.05%, 0.1%, 0.2%, 0.4%, 0.6%, and 0.8% of the dry soil mass) and three fiber lengths (6 mm, 12 mm, 19 mm). The samples were kept in room conditions of 25±1°C and relative humidity of 50% ± 5%. The crack pattern was studied by mounting a digital camera on the top of specimens during drying. Quantitative analysis of cracks by digital image processing technique was used to characterize the crack initiation, crack-resistance of fiber reinforced soil and crack length, width. They found out that with increase in fiber content decreases the crack network, surface crack ratio, number of clods, average length, and width of cracks, as shown in Figure 2.11. Two types of nodes were

considered: intersection nodes between crack segments and end nodes of a single crack that does not intersect another crack. The average area of clods, number of nodes per unit area, number of crack segments per unit area, and crack density increased with increase in fiber content. The surface-crack ratio increased with decreasing water content and then reached stabilization.
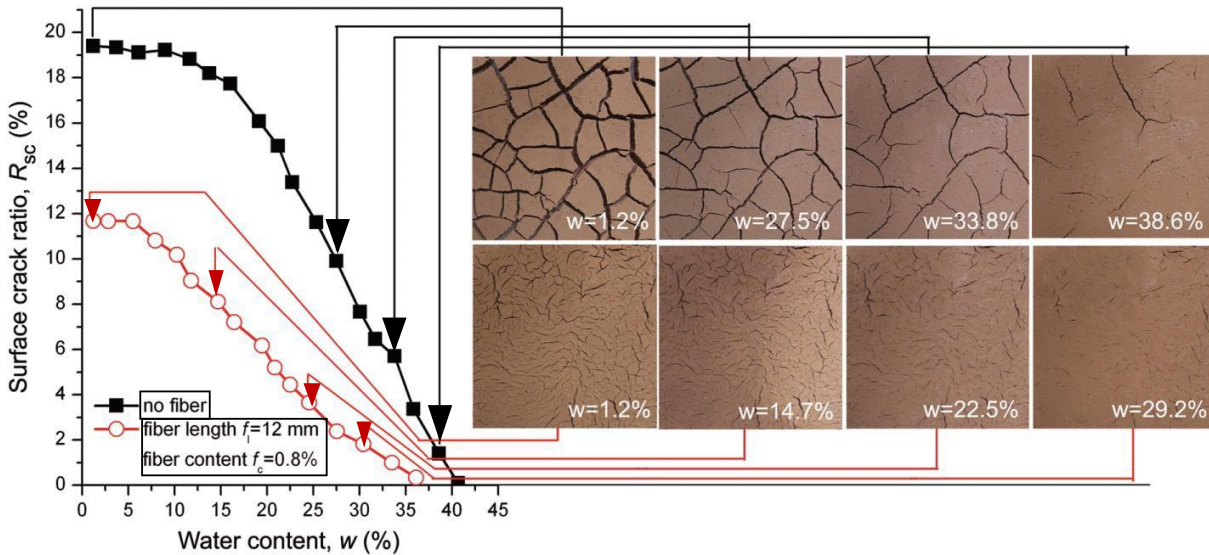
Figure 2.11 Variation of surface crack ratio with water content for natural and fiber-reinforced soil specimens (after Tang et al. 2012)

Qiang et al. (2014) studied the cracking resistance performance, permeability, and strength and deformation characteristics of improved clay reinforced with straw-fiber. The samples prepared were systematically evaluated by cracking test, water permeability test, unconfined compression test and shear test, respectively. The sample reinforced with straw-fibers demonstrated high resistance against cracking. Although with increase in fiber content the Crack Intensity Factor was observed to increase, the effect of fiber on surface shrinkage was not significant. The samples were subjected to wetting-drying cycles. The result of water permeability test for cracked clay samples show that a traditional landfill cover system that is constructed with only compacted clay will not act as an effective barrier against water percolation. The unconfined compressive strength and the shear strength were also reported to increase with increase in fiber content up to optimum level. The improved clay with straw fiber additive could be used in landfill cover system to enhance the anti-seepage ability and strength of landfill liners.

74

El-Halim (2017) utilized image processing technique to assess the use of sugarcane pith to mitigate clayey soil cracks. Experiment was carried out to investigate the effects of sugarcane pith additive on mitigating desiccation cracks, the volumetric shrinkage strain, the total porosity, and water retention at field capacity of clay soils. The clay soil was treated with the sugarcane pith at dosages of 1, 2, 3, 4 and 5% on dry weight basis. Various experimental methods were used to determine the variations in volumetric shrinkage, total porosity and water retention at field capacity. The characteristics of crack patterns were studied using an image processing technique. Compared with the untreated soil, the results showed that the sugarcane pith can increase the total porosity and water content at field capacity, while reducing volumetric shrinkage strain, and consequently, mitigating the development of desiccation cracks.

Table 2. 1 Summary of test setups for inducing desiccation cracking in the laboratory using oven drying method

Reference	Type of materials used	Methodology	Model specifications	Parameter studied
Ziegler et al. 1998	Synthetic clay Mixture of Kaolinite, calcium/sodium bentonite PP fibers	Oven drying at 48°C 3 wetting drying cycles	Standard Proctor mould	Crack pattern Tensile strength
Bhadriraju et al. 2005	Expansive soil CH type soil Carbon, Nylon, PP fibers (0.4%, 0.6%, 1%)	Oven drying at 110°C	Dimensions of specimens: 58 mm diameter and 125 mm height	Crack pattern Volumetric shrinkage using image processing
Rayhani et al. 2007	Landfill liner cover soils Three CL type and One CH	Oven drying at 50°C for 24 hours	Standard Proctor mould	Crack formation and pattern Volumetric shrinkage Hydraulic conductivity
Tang et al. 2008	Local clayey soils Type CL	Oven drying at 30, 40, 50°C	Glass plates	Average crack length, width, area, Crack Intensity Factor
Mijares and Khire 2010	Silty clay Type CL	To simulate annual temp cycle, dried at 21°C to 22°C and then elevated at 45°C (summers)	PVC columns equipped with sensors to measure w%	Soil Water Characteristic Curves (SWCC)

Tang et al. 2010b	Type CH clay	Three temperatures (Room at 22 °C, Oven at 60 °C and 105 °C)	Glass cups	Crack propagation and pattern Surface crack ratio
Tang et al. 2011	Type CL clay	Oven drying	160 mm X 160 mm Glass plates	Crack patterns Surface crack initiation and propagation using image analysis

Table 2. 2 Summary of test setups for inducing desiccation cracking in the laboratory using Drying/Blowing air

Reference	Type of materials used	Methodology	Test setup container	Parameter studied
Miller et al. 1998	Silty Clay Type CL-ML	Drying system (blower fixed on wall for drying and desiccation cycle), drainage system	Steel reinforced Plexiglas tank of 1.5 m (width), 1.0 m (length) and 0.5 m (depth)	Water potential CIF
Tay et al. 2001	Bentonite and sand	Evaporative drying by passing warm air at 30°C	80 cm X 80 cm by 25 cm Deep wooden box for liner desiccation test	Shrinkage, Hydraulic conductivity
Qi et al. 2003	Soil-cement mixture 19 and 50 mm PP fibers	Environment chamber with heater and blower	Cylindrical samples	Crack width crack pattern
Hu et al. 2006	Bioley Silt with 27% clay fraction	Slow cracking in room conditions and rapid cracking in oven at elevated temperatures	Thin rectangular Teflon moulds (10 cm long)	Shrinkage tests

Harianto et al. 2008	Type CH Fibers- PP fibers of 10 mm length	Fan at room conditions for 30 days	Standard Proctor mould	Volumetric shrinkage CIF
Qiang et al. 2014	Clay Straw fibers (3-5 cm)	Dryer at 50°C	Sample prepared in circular dishes	Surface shrinkage
Safari et al. 2014	Clay, Type CH and CLGeotextile cover (GM-400)	Direct exposure to atmospheric conditions (one year)	Large containers (1000 mm X 1000 mm) to avoid size effect	CIF

Table 2. 3 Summary of test setups for inducing desiccation cracking in the laboratory using Controlled environment Room Conditions

Reference	Type of materials used	Methodology	Test setup container	Parameter studied
Allan and Kukacka (1995)	19mm long fibrillated PP fiber in cementitious grouts	Room conditions to test ongoing crack opening and role of fibers.	Cylindrical specimen	Shrinkage Wetting drying Freeze thaw
Albretch et al. (2001)	Eight soils Two CH & six CL type	Room conditions for 2 weeks	Standard Proctor mould	Volumetric shrinkage, Hydraulic conductivity
Miller and Rafai (2004)	Medium plasticity soil Type CL PP fibers	Room conditions for 3 days	Steel cylindrical moulds	Crack reduction
Nahlawi and Kodikara (2005)	Type Highly reactive clay	Room conditions	Rectangular cross section Perspex and metal moulds	Cracking test

Rodriguez et al. (2007)	Mining waste and tailings	Open plates and closed hermetic conditions at 22°C	Open plates	Desiccation tests Hydraulic properties
Kalkan (2008)	Highly plastic Clay Silica fume	Kept in room conditions for 28 days to undergo desiccation.	Cylindrical metal mould	Compaction, cracking, oedometer, swelling, cracking tests
Peron et al. (2009)	Two types of silts	Room conditions at 19°C	295 mm X 15 mm X 15 mm square Aluminium and Teflon moulds	Free desiccation tests Constrained desiccation tests Crack pattern tests
Vallejo (2009)	Bentonite clay	Constant air temperature of 25°C	Plexiglas container, 37 cm long, 29.5 cm wide, 2.5 cm deep	Crack pattern and dimensions
Azad et al. (2011)	A silty-sand typical of GCL composite liner	heating the water reservoir (to keep thermal gradients low)	PVC container 549 mm high, with an internal diameter of 160 mm.	Desiccation Hydraulic conductivity tests
Lakshmikantha et al. (2011)	Silty clay Type CL	Environment controlled room conditions at 21°C	Sample of surface area of 1, 0.5, 0.25, 0.125, and 0.0625 m^2 thickness: 10 and 20 mm.	Tensile tests
Eberemu et al. (2011)	Type CL clay Rice husk ash	Air dried at 24°C	Standard Proctor moulds	Compaction tests Volumetric shrinkage tests

Shin and Santamarina (2011)	Ca-montmorillonite	Room conditions at 25°C	Square samples	Crack initiation using microscope and image analysis
Tang et al. (2012)	Clayey soil Type CL PP fibers	Room conditions	16 cm X 16 cm glass plates	Surface crack ratio, Number of clods, Crack width, length
Amarasiri and Kodikara (2013)	Type Highly reactive clay	Controlled conditions and 18 and 20°C	Rectangular cross section Perspex and metal moulds	Cracking test
Sanchez et al. (2013)	Highly plastic Organic silt	Allowed to dry at 19.5°C	Sample in petridish A 2D/3D laser scanner Scan Control 2700-100 from Micro-Epsilon	Digital model of cracking soil generated
Varsei et al. (2014)	Lean and fat clay	Air dry at 24°C	Desiccation box (25 cm X 35 cm)	Cracking using image analysis SWCC

Table 2. 4 Summary of test setups for inducing desiccation cracking in the laboratory using Suction induced desiccation

Reference	Type of materials used	Methodology	Test setup container	Parameter studied
Hejleh et al. (1995)	Soft cohesive soils	Suction test	Oedometer ring	Desiccation compressibility Suction tests
Witt and Zeh (2005)	Soil CL-ML type	Suction by applying air pressures on sample	Cohesive clay liners	Crack formation

Table 2. 5 Summary of test setups for inducing desiccation cracking in the laboratory using Heating source induced desiccation

Reference	Type of materials used	Methodology	Test setup container	Parameter studied
Vogel et al. (2005)	Different mixtures of sand (S) and bentonite (B), 1:1 and 5:1	Oblique incident Heat induced on samples by four halogen lamps	glass plates with a size of 24X30 cm.	Crack patterns and image processing
Sentenac and Zeilinski (2009)	Galston clay high plastic clay	1.2 kW infrared heater was placed 0.9 m above	1.5 m length, 0.25 m wide and 0.4 m high Perspex tank	Clay fissuring network
Costa et al. (2013)	Thick black clay soil Highly reactive clay potato starch milled quartz sand	Four flood lamps- 500 W capacity. Lamp distances (350 mm, 500 mm and 750 mm)	140 mm diameter, Glass container (80 mm X 80 mm)	Crack pattern quantification

Table 2.6 Summary of test setups for inducing desiccation cracking in the laboratory using Electrodes

Reference	Type of materials used	Methodology	Test setup container	Parameter studied
Sujata et al. (2006)	Synthetic clay (Laponite RD)	Electrodes made of aluminium foil	Glass Petridish	Crack pattern

2.5   Tensile Strength-Strain Characteristics of Soil

The direct tensile test is considered to be the most fundamental and possibly the only test that satisfies the condition of true uniaxial tension. In principle, uniaxial tensile test should subject a specimen to stresses that are uniform throughout the specimen. This implies that there should be no bending or torsional stresses, or stress concentration resulting from any geometrical irregularities of the specimen. Ideally, the end restraints should not cause any disturbance of the intermediate stress field. In this test, as the name applies, the tensile force is directly applied to the specimen along its longitudinal axis until failure occurs. The shape of the specimen is usually simple, cylinder, prism or briquette. The tensile strength (σ_t) can be calculated from the ultimate load (P) sustained by the specimen and the cross-sectional area (A) upon which it acts

The direct tension test can be grouped into two types based on the load direction acting on the test pieces, these being vertical and horizontal. Although some limitations such as frictional resistance are encountered in the moving and guiding parts, the horizontal type apparatus is reported to be more suitable for soils (Hasegawa and Ikeuti 1966).The advantages of the direct tensile test over indirect tensile tests can be summarised as follows:

- In principle, all induced stresses and strains are homogeneous, and they can be directly computed from test measurement.

- It is a uniaxial total stress test. Therefore, it can measure true stress-strain relationship under tension with no confinement.

- No assumptions or adjustments of test results are needed to obtain useful results. It is the only test that satisfies the condition of true uniaxial tension.

However, the shortcomings of the direct tensile test are: It is difficult in practice to design an apparatus that is capable of applying a uniform stress distribution to the entire specimen due to the end restraints. The influence of stress concentration and eccentric loading cannot be avoided. Complete elimination of misalignment is relatively impossible. Problems associated with effective shape of the specimen, clamping or holding the end of the specimen are relatively more difficult compared to other tests.

Towner (1987) used samples that were initially dried from a high-water content (80% or 64%) and tested by hand loading using a dog-bone shaped mould and spring balance. The tensile strength was determined by initially drying the sample to known moisture content then tested under load-induced cracking. The samples which were dried from higher water content gave very similar tensile strengths to those dried from lower water content.

Nahlawi et al.(2004) proposed a direct tensile strength test for unsaturated geomaterials based on Hannant et al.(1999) using a dog-bone like shape. The sample was compacted or in a slurry state form for a high range of moisture contents. Tensile strength was found to decrease with increasing moisture content beyond 20% (Figure 2.12).
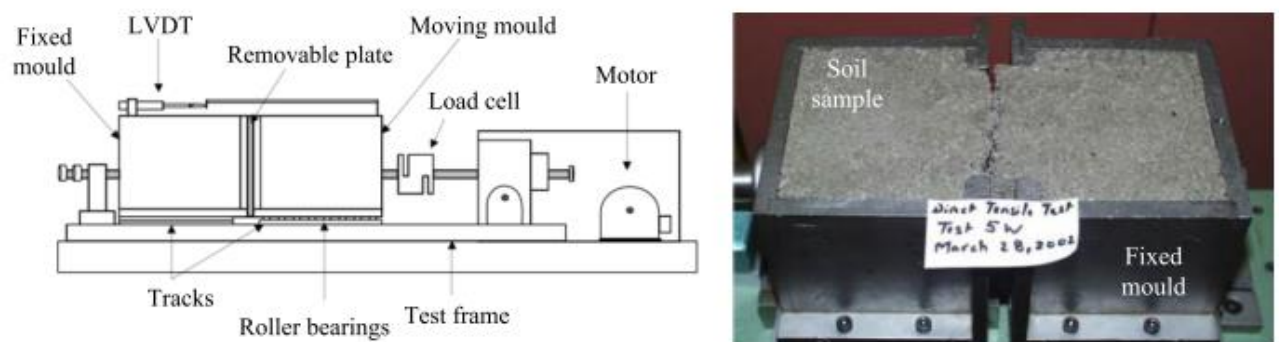
Figure 2.12 Schematic drawing of direct tensile mould apparatus, (b) cracking of Werribee clay in a direct tensile mould (After Nahlawi et al. 2004)

Mesbah et al.(2004) developed a direct tensile test for measurement of tensile strength of earth blocks reinforced with natural fibers. Direct tensile tests were conducted on the earth blocks, to examine the tensile reinforcing effects of randomly distributed sisal fibers. The test specimens were prepared by pressing the fiber reinforced earth blocks in standard dimensions. The anchorage problems were overcome by sawing the block at mid-section where failure is expected to occur. The tensile stress was measured by a simple assumption that the applied tensile stress is given by the tensile load applied to the cross-sectional area long the plane. However, this method does not account with the variable cross section during the test due to necking at the mid-section.

Win (2006) conducted direct tension tests (dog-bone shape) at a variety of compaction efforts with four different soil types. The test apparatus was based upon Leavell and Peters (1987). Samples were compacted to 76 mm high, 51 mm wide and 229 mm long from 95–100% compaction effort of standard Proctor compaction. A central 50 mm section was trimmed to 38

mm wide and 64 mm high. A load controlled direct method was used. Samples were either wetted or dried using a humidity chamber or controlled drying. Samples compacted wet of optimum had a decrease in strength and increase in failure strain compared to samples compacted dry of optimum.

Plé and Lê (2012) used direct tensile tests on unreinforced and polypropylene reinforced silty clay to study the effect of the polypropylene fiber reinforcement for improved the ductility of silty clay. A series of direct tensile strength tests and axi-symmetric triaxial compression strength tests were performed. The ability of fibers to increase the ductility of silty clay was evaluated by estimating the strength and brittleness index for unreinforced and fiber reinforced specimens.

Divya et al. (2014) conducted a series of direct tensile tests on unreinforced and fiber-reinforced soil. The fiber content and fiber length were varied as 0.25%, 0.5% and 0.75% and 30 mm, 60 mm and 90 mm respectively. The effect of fiber inclusions on the tensile strength-strain characteristics and crack formation was studied. During tensile tests, unreinforced soil showed a brittle behaviour compared with the ductile behaviour of fiber-reinforced soil. The tensile strength increased due to the fiber addition.

Tang et al.(2014) assessed the direct tensile strength of clay reinforced with fibers with varying fiber length and fiber content. The mixing water content was also varied. The tensile test results showed that fiber inclusion significantly increased the soil peak strength, reduced the post peak strength, and changed the brittle tensile failure behaviour to a more ductile one. Soil tensile strength increased with the increase in fiber content. The tensile strength of both reinforced and unreinforced specimens decreased with increasing water content and increased with increasing dry density.

Araki et al. (2016) evaluated the tensile properties of soils by performing direct tensile strength tests and split tensile strength tests on the prepared specimens. The specimen was prepared to the shape of a cylinder and dog-bone to ensure uniform stress throughout the specimen during the tensile test. The direct tensile strength test was found to be more effective than split tensile test in finding out interface frictional properties.

2.6   Measurement of strain development in soils using DOFS

In the early 1970s, some of the first experiments had successfully used low cost optical fibers for sensor purposes. Optical fiber sensing is utilization of an optical fiber connected to a light source to allow for strain detection in applications with tight spaces or where a small profile is beneficial. Optical Fiber Sensors (OFS) technologies have developed rapidly since that time, and several types of OFS have been proven to accomplish practical applications in the field of civil and aerospace engineering now (Grattan and Sun, 2000). Currently, assessment of buildings, bridges, dams, tunnels, and other vital civil engineering infrastructures are carried out by engineers trained in visual inspection, which sometimes can be inaccurate due to differences in their background for safety condition assessment. Figure **2.13** shows the basic principles and types of optical fiber sensors used. This nomenclature is derived, from the frequency of signal that is analysed and the discrete peaks within the electromagnetic spectrum.
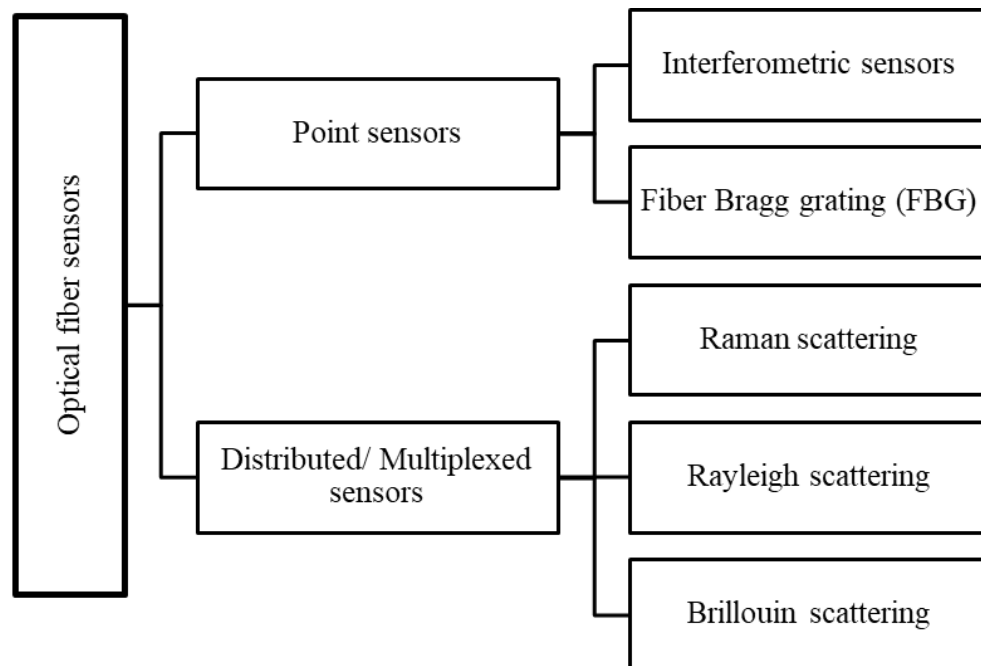
Figure 2.13 Overview of basic principles and types of optical fiber sensors

More specifically, the light scattering in a fiber optic cable contains three spectral parts: (1) Rayleigh scattering which is directly correlated with the wavelength of the laser source used, (2) Stokes line components which are from photons shifted to longer wavelengths (lower

frequency) than the Rayleigh and (3) anti-Stokes line components which are from photons shifted to shorter wavelengths (higher frequency) than the Rayleigh.

To improve the inspection accuracy and efficiency, optical fiber sensors (OFS) are one of the fastest growing and most promising researched areas, due to their features of durability, stability, small size and insensitivity to external electromagnetic perturbations, which makes them ideal for the long-term health assessment of built environment.

For Optical Fiber Sensor, the sensing element can cover the entire strand of an optical fiber (globalised), or the sensing element can be just a point or section of the optical fiber (localised). Depending on the length of the sensing element, the optical fiber sensors can be configured into a 'point' sensor which performing measurement at a point or an 'integrated' sensor obtaining the averaged information over a particular region. Table 2.6 and

Table **2.7** summarize the advantages and limitations of DOFS, FBG and strain gauges, respectively.

Table 2.6 Advantages of DOFS, Fiber Bragg Grating (FBG), and Strain Gauges

DOFS	Fiber Bragg Grating	Strain gauges
• Cost effective	• Real-time monitoring	• Low cost
• Ease of installation	• Small size and Wireless monitoring	• Flexibility
• Distributed strain measurement in continuous space	• Large measurement range	• Large measurement range
• Small size, Light weight	• Highly resistant to Electromagnetic Interference (EMI)	
• Highly resistant to Electromagnetic Interference (EMI)	• Single end	
• Long distance monitoring		
• Simple connection and handling		
• High robustness and elasticity.		

Table 2.7 Limitations of DOFS, Fiber Bragg Grating (FBG), and Strain Gauges

DOFS	Fiber Bragg Grating	Strain gauges
• Limited measurement resolution • Limited measurement frequency • Pretension required in measurement • Loop optical fiber measurement • Limited bending diameter	• Point strain measurement • Complicated encapsulation method • High cost • Pretension required in measurement	• Point sensors • Sensitivity to temperature and humidity • Low strain resolution • Limited measurement range • Less reliability in highly explosive monitoring atmospheres • Not suitable for long-term monitoring • Low measurement frequency

Optical fiber sensors have long been employed in diverse domains for various applications in geotechnical engineering such as monitoring of slopes, dams, and tunnels. One of the most common and important geological problems is the slope stability (Habel and Krebber 2011) encountered during and after building road in mountainous areas.

Stability monitoring and health diagnosis are imperative to the natural slope and slope engineering with potential sliding. Commonly the slope monitoring includes two aspects: one is the deformation monitoring of the rock and soil mass, and of the retaining wall, anchor cable and frame beam; the other one is the stress and pressure monitoring of the rock and soil mass and retaining wall. Conventional monitoring methods include the inclinometer, crack detector, reinforcement detector and displacement meter. Obviously, these monitoring methods are of point- mode and cannot meet the monitoring requirement for the whole slope stability, especially for large- scale slopes. In addition, the conventional measuring instruments are often incompatible with rock- soil mass deformation, and the installation difficulties and erratic readings due to unforeseen circumstances.

Distributed optical fiber sensors (DOFS) have been a popular geotechnical structural health monitoring technology for a decade (Leung et al. 2015). A sensor point is formed by first measuring and storing the Rayleigh backscatter signature of the optical fiber at an ambient state (called the baseline condition). A change in strain from the baseline condition results in a shift in the spectrum of light scattered in the fiber. These changes can be measured and calibrated to determine the local strain and/or temperature in the fiber. A digital acquisition system linked to the optical fiber sensors records the behaviour of the structure. With technological advancements, the DOFS have been used for maintenance and monitoring of structures like soil nails, soil anchors, pavements, geotextiles, pipelines, piles, retaining walls, tunnels, slopes, and embankments(Zhu et al. 2015; Wong et al. 2016).

2.7 Centrifuge modelling of desiccation cracking of soils

Centrifuge modelling is recognized as a powerful tool for solving problems where the weight force is a determining force or where the field stress conditions are to be duplicated. The basic principle of centrifuge modelling is that when a soil sample model (N times smaller than its prototype) is subjected to N times the acceleration due to Earth's gravity (Ng) by centrifugation, it results in identical self-weight stresses at homologous points in the model and the prototype. These characteristics are especially interesting to investigate with a material such as soil, which has many geotechnical properties, such as compressibility permeability, and strength, to mention some, depending on stress level.

For better understanding of desiccation cracking behaviour of fiber reinforced expansive clay, robust physical modelling is needed. Considering the practical difficulties and time delay in performing full-scale model tests and also the limitations of reduced scale model tests for simulating stress dependant phenomenon, centrifuge model tests are necessary for the study of desiccation cracking of clays. Till now no literature is available on determination on scale factors for desiccation cracking in centrifuge models. So, this creates a motivating research avenue for studying the desiccation cracking at prototype and model dimensions.

2.8 Critical appraisal of the reviewed literature

a) The reviewed literature designates that several factors (viz., type of soil, clay content, mineral composition, tensile strength, suction characteristics, temperature and humidity, pore fluid characteristics, chemical composition, fiber addition, density and moisture conditions, initial moisture, confining pressures, wetting and drying cycles etc.) strongly influence the desiccation cracking of soils

b) In addition, researchers have critically evaluated various techniques of inducing desiccation cracking to laboratory setups and thus study the parameters of desiccation cracking by resorting to various techniques (viz., image analysis, fracture mechanics, PIV) and several analytical and numerical models have been developed to study desiccation cracking, crack development, egress of water from the soil, suction development, depth of the crack(s) and its propagation in the soil mass.

c) Literature indicates that problem of desiccation cracking can be reduced by replacement of soil, chemical stabilization, mechanical stabilization, isolation of problematic area, increase of overburden etc. With an advent in study of discrete Fibers reinforcement in the soil for restraining desiccation cracking, quite a few researchers have studied this technique at laboratory level.

d) For offering better tensile strength characteristics, the cross section of fiber plays an important role. But the effect of different cross section of fibers on restraining desiccation cracking is absent in the literature.

e) The chemical composition of fibers affect the micro-mechanical behaviour of fiber soil matrix, attributing to the soil-fiber adhesive properties. Literature does not indicate the best suited synthetic fiber composition pertaining to different environmental conditions.

f) In addition to this, a detailed study on the optimum cross section of fibers for best performance of fiber reinforced soil in clay liners is needed.

g) For supporting the technique of fiber reinforcement, much more robust physical modelling of fibers reinforcement is needed to validate its application in actual site

conditions. Centrifuge modelling technique provides an excellent tool for the authorisation, particularly in terms of confirming the crack-formation mechanism. Short of an actual well-controlled field case, it is probably the only technique available to study crack development, since the field stress conditions that control crack propagation are properly simulated in the centrifuge models. Till now no literature is available on determination on scale factors for desiccation cracking in centrifuge models.

2.9   Methodology adopted in the present study

Depending on the literature, number of methods for inducing desiccation cracking were reviewed. A laboratory desiccation test was proposed and performed on the model expansive soil procured from nearby region. Model fibers were procured as per the requirement. The main objective of this study was to evaluate the influence of fiber inclusion on desiccation cracking of soil. Effect of length of fiber and fiber content was investigated.

A laboratory test setup was designed based on the requirements. After performing the tests, results and discussions on desiccation cracking test on unreinforced and reinforced expansive soil were described in detail. Analysis of results, digital image analysis and their interpretation was carried out. Effect of fiber length and fiber content on desiccation cracking was studied and discussed. The influence of cyclic drying and wetting on the desiccation cracking behaviour of expansive clay reinforced with and without fiber reinforcement was studied. The healing property of expansive clay due to the presence of fibers was also studied.

The direct tensile strength test to measure the tensile strength behaviour of unreinforced and fiber reinforced expansive soil. Further, effect of water content on the tensile strength is presented to understand the influence of fiber content and fiber length. The complete performance of fiber reinforced clay against tensile stresses and desiccation is evaluated.

Distributed optical fiber sensors were utilized in the study and understanding of the desiccation cracking behaviour of unreinforced and polypropylene-fiber-reinforced expansive soil. The strain measured from the DOFS is analysed to study the crack initiation and crack propagation in the soil specimens. The strain that is measured in the fiber-reinforced soil specimens is

compared to that of the unreinforced specimens and has been discussed in the subsequent sections. Additionally, the particle image velocimetry (PIV) technique was used to measure the strains that developed on the top surface of the specimen during drying, which aided in the extracting of meaningful information about the movement of soil particles in unreinforced and fiber-reinforced soil. The desiccation cracking in a clay layer inside a geotechnical centrifuge was studied. The centrifuge model test package was developed, which included heating system, image acquisition system, illumination assembly during desiccation cracking. The influence of fiber reinforcement, specimen thickness, fiber length and fiber type was studied.

LEFT BLANK INTENTIONALLY

Chapter 3

MODELLING CONSIDERATIONS ON THE DESICCATION CRACKING BEHAVIOUR OF FIBER REINFORCED CLAY

3.1   Introduction

Physical modelling is concerned with replicating an event comparable to what may exist in the prototype. The two events should be similar, and that similarity needs to be related by appropriate scaling laws. Geotechnical centrifuge modelling is a useful tool available in the profession to replicate in situ stresses. Soil models placed at the end of a centrifuge arm can be accelerated so that they are subjected to an inertial radial acceleration field which, as far as the model is concerned, seems like a gravitational acceleration field but many times stronger than acceleration due to gravity (Taylor 1995). Centrifuge modelling allows the increase of self-

weight by the increase of gravitational acceleration, which is equal to the reduction of the model scale, as well as the reduction of time for model tests as the scale is reduced (Schofield 1980).

3.2   Scaling considerations

Physical modelling is performed in order to study aspects of the behaviour of prototype. But if the material behaviour is non-linear like the soil, the derivation of scaling factors becomes vital. It is important to understand the nature of the expected behaviour so that details of the model can be correctly established, and the scale factors be applied for the extrapolation of the model observations to the prototype scale.

3.2.1 Dimensional analysis of desiccation cracking phenomenon

Desiccation cracking is a complex phenomenon that affects the overall behaviour of clay layers. Various researchers have identified the influence of several factors on the desiccation cracking of clay layers. For example, Tang et al.(2008); Kodikara et al.(1999); Lakshmikantha et al. (2012); Costa et al. (2013) discussed the salient factors influencing the desiccation cracking initiation and subsequent propagation. The effect of specimen thickness, tensile strength, drying rate, clay type and boundary conditions are the primary factors influencing desiccation cracking.

Dimensional analysis is a mathematical technique for deducing elements in the form of a theoretical relationship from consideration of the variable and parameters that make up that relationship (Langhaar 1951). Each physical phenomenon can be expressed by an equation, composed of variable (or physical quantities) which may be dimensional and non-dimensional quantities. Dimensional analysis helps in determining a systematic arrangement of variables in that physical relationship and combining dimensional variables to form non-dimensional parameters. Reasonably, the derivation of a dimensional analysis to account for all the factors governing the desiccation cracking of clay layer is a challenging task. In this study, a

94

dimensional analysis is performed for desiccation cracking of an unreinforced and fiber reinforced clay layer.

In this analysis the crack feature measurements considered for analysis are crack width (c_w), crack spacing (s_c), crack depth (d_c) and time of crack initiation (t_i). A clay layer of thickness d and water content $w\%$ is subjected to an ambient temperature (θ). The crack feature measurements depend invariably on tensile strength of unreinforced soil (σ_{ur}), tensile strength of fiber-reinforced soil (σ_{fr}) and permeability of the corresponding clay layer (k). The considered variables for unreinforced and fiber reinforced clay layers are in Figure 3.1 and Figure 3.2.

Clay layer thickness (d)

It is the thickness of the clay layer undergoing desiccation cracking. The crack morphology and crack feature measurements differ for different clay layer thicknesses of same material (Lakshmikantha et al. 2012; Uday and Singh 2013; Tollenaar et al. 2017a). The thickness affects evaporation rate and suction profile throughout the thickness of clay layer. Thinner clay layers tend to desiccate faster than thicker clay layers.

Water content (w%)

It is the water content of the clay layer, expressed as percent ratio of the weight of water (W_w) to the dry weight of soil solids (W_s). The initial water content does not directly affect the evaporation rate, however, the intensity of desiccation cracking is dependent on the initial water content (Birle et al. 2008).

Ambient temperature (θ)

The amount of water content lost from the clay layer depends on the atmospheric conditions like temperature and humidity (Tang et al. 2010a).

Rate of evaporation (c_e)

It is the rate at which moisture is lost from the clay layer. The evaporation rate remains unaltered with change in initial moisture content (w), and increases with increase in ambient temperature and clay layer thickness (Uday and Singh 2013).
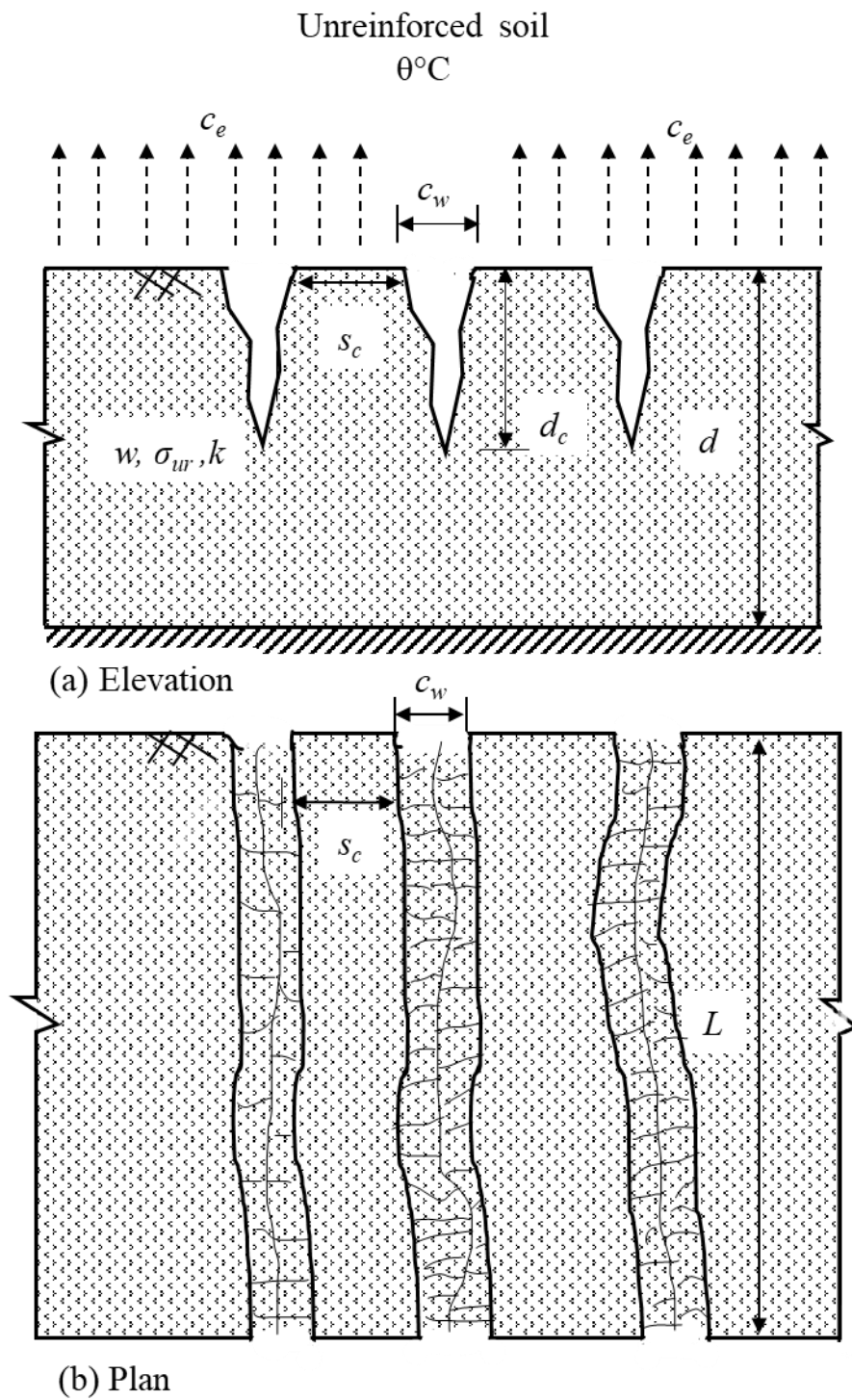
Figure 3.1 Schematic representation of factors affecting desiccation cracking phenomenon for unreinforced soil
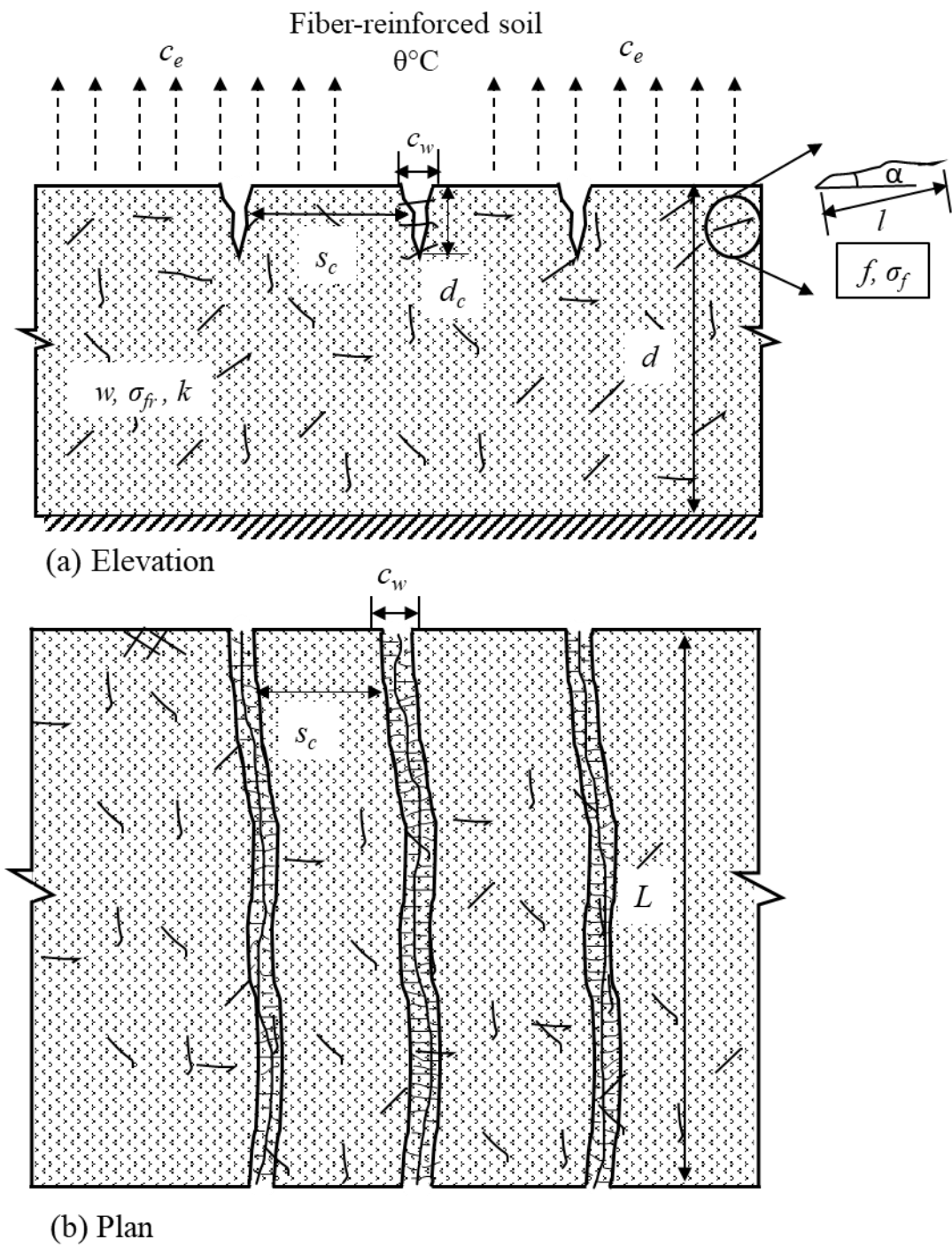
Figure 3.2 Schematic representation of factors affecting desiccation cracking phenomenon for fiber reinforced soil

Crack width (c_w)

It is the shortest distance between edges of two separated soil masses formed due to cracking of soil. The crack width is dependent on the tensile stresses (σ_t) in the soil produced due to boundary conditions at the clay layer interface.

Crack spacing (s_c)

It is the shortest distance between one point on the boundary of a cell and the point on opposite boundary of the same cell. The crack spacing depends on the thickness of the clay layer, rate of desiccation, and the boundary restraints (Corte and Higashi 1964).

Tensile strength of unreinforced soil (σ_{ur})

Desiccation cracking is a type of tensile failure of clay layer and the crack feature measurements depend on the tensile strength of the clay. Theoretically, as the soil dries up, the shrinkage strains developed in the soil experience restraints from the base of the layer, thereby producing tensile stresses (Kodikara and Choi 2006). The tensile stresses (σ_t), developed in the clay layer are a function of suction and the reduction in the water content. When the maximum tensile stress ($\sigma_{t,max}$) exceeds the tensile strength of the clay (σ_{ur}), it is assumed that a crack would develop in the layer.

Fiber content (f)

The fiber content is ratio of dry weight of fibers to the dry weight of the soil. It is expressed in percentage.

Fiber length (l)

The fiber length is the cut-length of fibers used for reinforcing the soil.

Fiber orientation (α)

The orientation of fibers at the cracks plays important role in the extent of desiccation crack. It is the angle between the fiber length and failure plane at crack, as shown in Figure 3.2. Fibers are most effective when oriented in the same direction as tensile loading. The contribution of

the fibers are enhanced by anisotropic distribution of their orientation in the direction of tensile strains, particularly for reducing the desiccation cracking (Diambra et al. 2007).

Tensile strength of fiber-reinforced soil (σ_{fr})

Fiber-reinforcement increases the tensile strength of clay layer mainly due to interfacial mechanical interactions between fibers and clay matrix (Tang et al. 2014). Theoretically, the tensile strength of fiber-reinforced clay (σ_{fr}) is composed of tensile strength of unreinforced clay (σ_{ur}) and increment in tensile strength due to fiber reinforcement ($\Delta\tau_f$).

$$\sigma_{fr} = \sigma_{ur} + \Delta\sigma_f \qquad (3.1)$$

Figure 3.3 schematically represents the bridging action of fibers at the crack and pulling out of fibers during cracking. The increment in tensile strength due to fiber reinforcement (is proportional to the interfacial shear strength of the fibers and embedded length of fiber (l_e). It is assumed that the fibers are straight and align themselves perpendicular to the crack (α = 90.

(a) Plan

(b) Magnified view at the crack
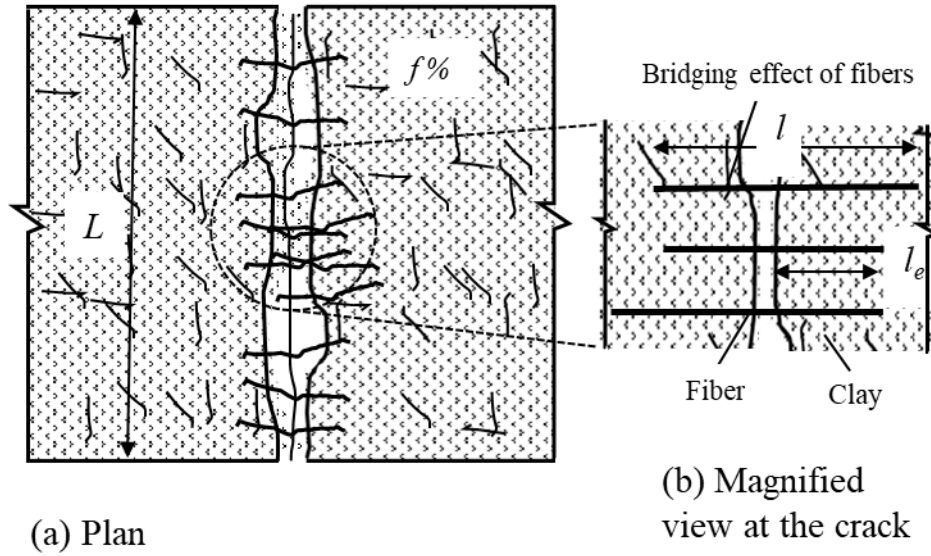
Figure 3.3 Schematic representation of pulling out of fibers during cracking

Therefore,

$$\Delta\sigma_f = \frac{\pi d \sum_{i=1}^{i=n_f} \tau_{fi} l_i}{A} \qquad (3.2)$$

Where, n_f is the number of fibers crossing the crack, σ_f is the interfacial shear strength between fiber and clay, τ_{fi} is the individual pull-out length of fibers, f is the fiber diameter, A is the

99

cross-sectional area at the crack. It is assumed that all the fibers are of same tensile strength. Assuming a homogeneous mixture, l_i varies between 0 and $l/2$. Effective embedded length of fiber (l_e) is

$$l_e = \frac{\frac{l}{2} + 0}{2} \tag{3.3}$$

Therefore eq.3.2 can be written as,

$$\sigma_f = \frac{\pi d l n_f}{4A} \tau_f \tag{3.4}$$

As τ_f is proportional to f, and k_c being the proportionality constant, eq. 3.4 can be written as,

$$\Delta\sigma_f = \frac{\pi d l k_c f}{4A} \tau_f \tag{3.5}$$

Hence, increase in tensile strength of a clay due to fiber reinforcement is a function of f and l.

Permeability of the unreinforced clay layer (k_{ur})

The rate of evaporation of clay is a function of its permeability and water retention capacity. Permeability of the unreinforced clay layer (k_{ur}) is the amount of water that seeps through the unreinforced clay layer in a given duration of time. A clay layer with low permeability and high-water retention will experience lower rate of evaporation.

Permeability of the fiber-reinforced clay layer (k_{fr})

Permeability of the fiber-reinforced clay layer (k_{fr}) is the amount of water that seeps through the fiber-reinforced clay layer with time. Due to the presence of fibers, the permeability of the clay layer gets altered and is generally increased with increase in fiber content.

Unit weight of soil (γ)

The specific weight (also known as the unit weight) is the weight per unit volume of soil. As the fibers are almost weightless, assuming unit weight of unreinforced and fiber-reinforced clay to be equal, $\gamma_{ur} = \gamma_{fr}$.

Based on the above expressions, the functional equation for desiccation cracking phenomenon can be expressed involving crack width (c_w), crack spacing (s_c), time of crack initiation (t_i), clay

layer thickness (, water content , tensile strength of unreinforced clay , tensile strength of fiber-reinforced clay , fiber length (*l*), fiber content (*f*), permeability of unreinforced clay (k_{ur}) and permeability of fiber-reinforced clay (k_{fr}), unit weight of soil (γ) and ambient temperature (θ) as follows,

$$\phi\left(c_w, s_c, d_c, t_i, w, f, l, \sigma_{ur}, \sigma_{fr}, k_{ur}, k_{fr}, \theta, d, \gamma\right)= \text{Constant} \qquad (3.6)$$

Thus, there are 13 variables involved in the fundamental relationship which are expressible in terms of 4 fundamental dimensions. Table 3. 1 shows the dimensions of the variables used in the analysis.

Table 3. 1 Variables used in the analysis and their dimensions

Sr. No.	Variables	Symbol	Dimensions
1.	Crack width	c_w	$[L]$
2.	Crack spacing	s_c	$[L]$
3.	Time of crack initiation	t_i	$[T]$
4.	Clay layer thickness	d	$[L]$
5.	Water content	w	$[M^0 L^0 T^0 \theta^0]$
6.	Tensile strength of unreinforced clay	σ_{ur}	$[M^1 L^{-1} T^{-2}]$
7.	Tensile strength of fiber-reinforced clay	σ_{fr}	$[M^1 L^{-1} T^{-2}]$
8.	Fiber length	l	$[L]$
9.	Fiber content	f	$[M^0 L^0 T^0 \theta^0]$
10.	Permeability of unreinforced clay	k_{ur}	$[LT^{-1}]$
11.	Permeability of fiber-reinforced clay	k_{fr}	$[LT^{-1}]$
12.	Ambient temperature	θ	$[\theta]$
13.	Unit weight of clay layer	γ	$[M^1 L^{-2} T^{-2}]$

M – Mass*; L*- Length; *T*- Time; *θ*- Temperature

According to Buckingham's Pi theorem (Buckingham 1914) and (Butterfield 1999), the above fundamental relationship may be replaced by another one involving only (13 − 4) = 9 dimensionless π-terms.

Thus, taking *d*, *t$_i$*, *k*, *θ* as repeating variables, and by inserting fundamental dimensions and equating exponents of *M, L, T* and θ, we obtain,

$$\pi_1 = {^{c_w}}\!/_d \tag{3.7}$$

$$\pi_2 = {^{s_c}}\!/_d \tag{3.8}$$

$$\pi_3 = {^{t_i k_{ur}}}\!/_d \tag{3.9}$$

$$\pi_4 = w \tag{3.10}$$

$$\pi_5 = f \tag{3.11}$$

$$\pi_6 = {^l}\!/_d \tag{3.12}$$

$$\pi_7 = {^{\sigma_{ur}}}\!/_{\gamma d} \tag{3.13}$$

$$\pi_8 = {^{\sigma_{fr}}}\!/_{\gamma d} \tag{3.14}$$

$$\pi_9 = {^{k_{fr}}}\!/_{k_{ur}} \tag{3.15}$$

Therefore,

$$\varphi\left[{^{c_w}}\!/_d, {^{s_c}}\!/_d, {^{d_c}}\!/_d, {^{t_i k_{ur}}}\!/_d, w, f, {^l}\!/_d, {^{\sigma_{ur}}}\!/_{\gamma d}, {^{\sigma_{fr}}}\!/_{\gamma d}, {^{k_{fr}}}\!/_{k_{ur}}\right] = \text{Constant} \tag{3.16}$$

Use of dimensional analysis in presenting experimental data

The final expressions for crack width *(c_w)*, crack spacing *(s_c)*, and time of crack initiation *(t_i)* can be computed by carrying out series of experimental investigation and validate the effects of dimensionless parameters on the phenomenon of desiccation cracking. In this study, experiments are performed to estimate the tensile strength of unreinforced clay(σ_{ur}), tensile strength of fiber-reinforced clay (σ_{fr}), permeability of unreinforced clay (k_{ur}) and permeability of fiber-reinforced clay (k_{fr}). A planned model investigation is carried out to experimentally validate the dependence of phenomenon of desiccation cracking on the dimensionless parameters as discussed below.

Normalized crack width (c_w/d) is the ratio of measured crack width (c_w) and clay layer thickness (d).

Normalized crack spacing (s_c/d) is the ratio of measured crack spacing (s_c) and clay layer thickness (d).

Time of crack initiation factor $\left(t_i k_{ur}/d\right)$ is the factor that can be used to expressed time of crack initiation of a clay layer of depth d.

Tensile strength factor of unreinforced clay layer $\left(\sigma_{ur}/\gamma d\right)$ is the ratio of measured tensile strength of unreinforced clay (σ_{ur}) to the unit weight of the clay (γ) and clay layer thickness (d).

Tensile strength factor of fiber-reinforced clay layer $\left(\sigma_{fr}/\gamma d\right)$ is the ratio of measured tensile strength of fiber-reinforced clay (σ_{fr}) to the unit weight of the clay (γ) and clay layer thickness (d).

Permeability ratio $\left(k_{fr}/k_{ur}\right)$ is the ratio of permeability of fiber-reinforced clay layer to the permeability of unreinforced clay layer.

The results obtained from the model tests may be transferred to the prototype by centrifuge modelling technique and the scaling considerations are discussed in the subsequent sections.

3.2.2 Basic scaling relations

Centrifuge modelling involves scaling laws and scaling errors. The dimensional analysis for various factors involved in the phenomenon can be used to derive the basic scaling laws. If the model is subjected to a similar stress history ensuring that the packing of the soil particles is

replicated, then for the centrifuge model subjected to an inertial acceleration field of N times Earth's gravity, the vertical stress at depth d_m will be identical to that in the corresponding prototype at depth d_p (Taylor 1995). This ensures the stress similarity between model and prototype, as shown in Figure 3.4. Therefore, the scale factor for linear dimensions is 1: N, where N is the scale factor or g-level. The value of N can be calculated by

$$N = \frac{R_e \omega^2}{g}$$

(3.17)
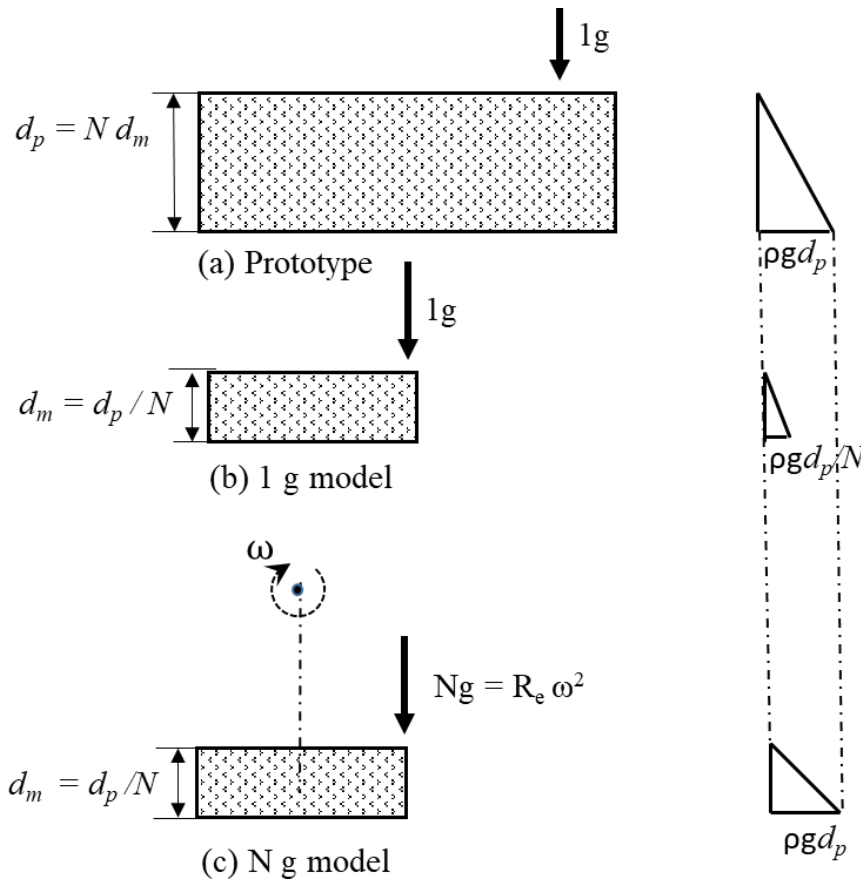
Figure 3.4 Concept of geotechnical centrifuge modelling

Where R_e is the effective radius, ω is the angular velocity of the centrifuge and g is the acceleration due to gravity. Hence, the linear crack feature measurements like crack width (c_w), crack spacing (s_c) have s scale factor if 1: N. Similarly, to maintain identical thickness should be 1: N. The cracked area will scale as 1:N^2. The scaling is done to ensure same stress conditions in the homologous points in model and prototype. The scale factor for the time can be

established by using expression for time of crack initiation derived from dimensional analysis. According to Schofield 1980, the scale factor for the coefficient of permeability, k is N.

Therefore from eq. 3.15,

$$\left(\frac{t_i k_{ur}}{d}\right)_m = \left(\frac{t_i k_{ur}}{d}\right)_p \tag{3.18}$$

$$\frac{(t_i)_m}{(t_i)_p} = \frac{(d)_m}{(d)_p}\frac{(k_{ur})_p}{(k_{ur})_m} = \left(\frac{1}{N^2}\right) \tag{3.19}$$

Therefore, the time scales as $1/N^2$ in a model with respect to the prototype. Table 3. 2 provides a summary of scale factors (model: prototype) for geotechnical centrifuge modelling for desiccation cracking of unreinforced and fiber reinforced clay.

3.2.3 Scaling considerations of modelling fibers in a centrifuge

As the scaling down of length, breadth, and thickness of fibers is impractical, the scaling considerations of the fibers are very important for the modelling of fiber reinforced soil in a centrifuge. The parameters under consideration for modelling of fibers are the tensile strength and bond strength. Viswanadham et al. (2011), presented the scaling considerations for modelling fibers in a geotechnical centrifuge present at IIT Bombay.

In geotechnical centrifuge, as the model and prototype dimensions are N times scaled, the length, breadth, and thickness of fibers are scaled down by 1/N times. As it is difficult to manufacture fibers of dimensions 1/N of the actual fibers, for the testing, the important parameters considered for the fibers are tensile strength and bond strength along the surface. In this study three types of fibers are taken into consideration.

Table 3. 2 Scaling factors for centrifuge modelling of desiccation cracking

Parameter	Scaling factor
*^Length, L (m)	*1/N
^Area, A (m^2)	1/N^2

^Volume, V (m^3)	1/N^3
Force, (kN)	1/N^2
Cohesion, c (kN/m^2)	1
Stress, σ (kN/m^2)	1
Crack width, c_w (mm)[a]	1/N
Crack spacing, s_c (mm)	1/N
Crack depth, d_c (mm)	1/N
Cracked area (mm^2)	1/N^2
Crack intensity factor, CIF (%)	1
Layer depth, d (mm) [a]	1/N
^Coefficient of permeability of clay, k_{ur} (m/s)	1
Tensile strength of unreinforced clay, σ_{ur} (kN/m^2)	1
Tensile strength of fiber-reinforced clay, σ_{fr} (kN/m^2)	1
Tensile strain at cracking (ε_t)	1
Time of first crack, t_i (min, diffusion)	1/N^2

[*] $L_m/L_p = 1/N$; L_m = Length in model dimension, L_p = Length in prototype dimension;

^ Schofield 1980a; Taylor 1995

Polypropylene and polyester fibers with trilobal cross section, with an equivalent diameter ~40 µm and polypropylene tape fibers with a thickness t and breadth b were considered. Divya (2012) discussed the usage of fibers in a geotechnical centrifuge (Figure 3.5). Considering two different fiber cross sections, rectangle (breadth b and thickness t) and triangular cross section (size b), the bond strength may be defined as the stress at the soil and fiber interface, when they start losing their contact. The pull-out force and tensile force obtained is as follows.
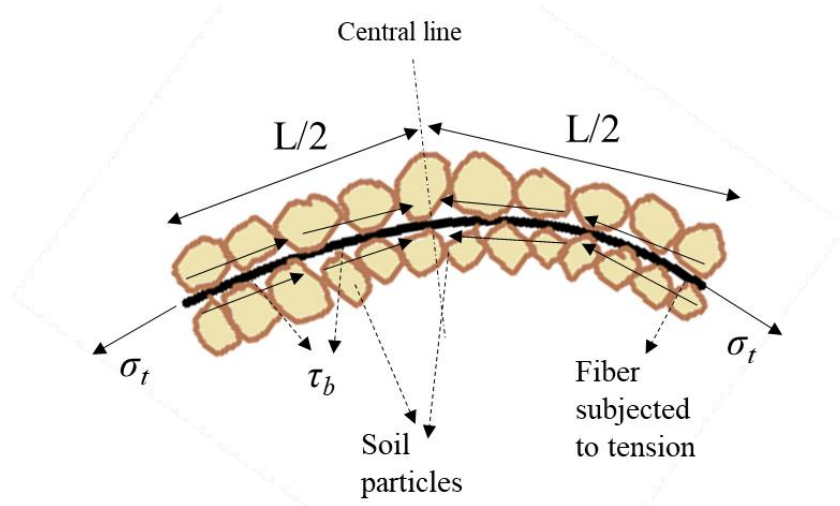
Figure 3.5 Modelling considerations of fiber in a centrifuge (After Divya, 2012)

Adhesive force $= \tau_b A'$, where A' is the circumferential area of the fiber over length L, i.e, [$2L(b + t_f)$] for rectangular cross section and ($3bL$) for equilateral triangular cross section. Tensile force $= \sigma_t A$, where A is the equal to ($b.t_f$) for rectangular cross section and ($\frac{\sqrt{3}}{4} b^2$) for equilateral cross section. Considering the force equilibrium conditions for bond stress and tensile stress, pullout of fiber and breaking or pull-out failure of the fiber and equating the maximum pull-out force and maximum tensile force,

$$\sigma_t A = \tau_b A' \tag{3.20}$$

Equation. 3.8 can be written as, for rectangular fiber cross section

$$\frac{l'}{b} = \frac{\sigma_t t}{\tau_b(b+t)} \tag{3.21}$$

For equilateral triangular cross section

$$\frac{l'}{b} = \frac{1}{2\sqrt{3}} \frac{\sigma_t}{\tau_b} \tag{3.22}$$

Equations (3.21) and (3.22) lead to the scale factor of the aspect ratio as unity. Aspect ratio is defined as the ratio of length to width for fibers with a rectangular cross- section, and to the size of the side for fibers with an equilateral triangular cross-section area. It indicates that identical fibers can be used in the centrifuge model and prototype by maintaining identical aspect ratio. Hence, fibers can be treated as discrete inclusions. Fiber content (f), which is defined as the

ratio of weight of fibers to the weight of dry soil (expressed as a percentage) can be considered as same in model and prototype.

3.3   Details of centrifuge equipment used in the present study

A small beam centrifuge facility at IIT Bombay has been used in the present study. The small beam centrifuge at IIT Bombay is being used for studying simple problems of geotechnical and geo-environmental engineering. The maximum outer radius of the centrifuge is 490 mm. The centrifuge is housed in a steel chamber at the ground level. It is a simple centrifuge with mechanical rotating arrangement and two swing baskets. One swing basket is for the specimen container and the other swing basket is used for counter weight. In the present study appropriate slipring arrangement was made to the small centrifuge to aid power supply at high gravities. The centrifuge has a swing bucket at one end and an adjustable counter weight at the other end. The maximum payload capacity of the centrifuge is 3 kg. The centrifuge reaches the ramping angle of ~90º at ~230 RPM. Summary of major specifications of the small centrifuge is given in Table 3.3. Figure 3.6 shows the elevation and cross-sectional view of the small centrifuge facility at IIT Bombay. The actual photographs of the small centrifuge facility at IIT Bombay are shown in Figure 3.7 and Figure 3.8.

Table 3.3 Summary of major parameters of small centrifuge

Property	Value
Maximum payload	3 kg
Maximum outer radius -[a]	512 mm
Maximum angular velocity	500 RPM
Ramping angle ~90º achieved at	~230 RPM
Dimensions of basket	207.6 mm x 140.4 mm x 171.5 mm

[a]Radius measured from centre of the shaft to the top surface of the basket; RPM- Revolutions per minute
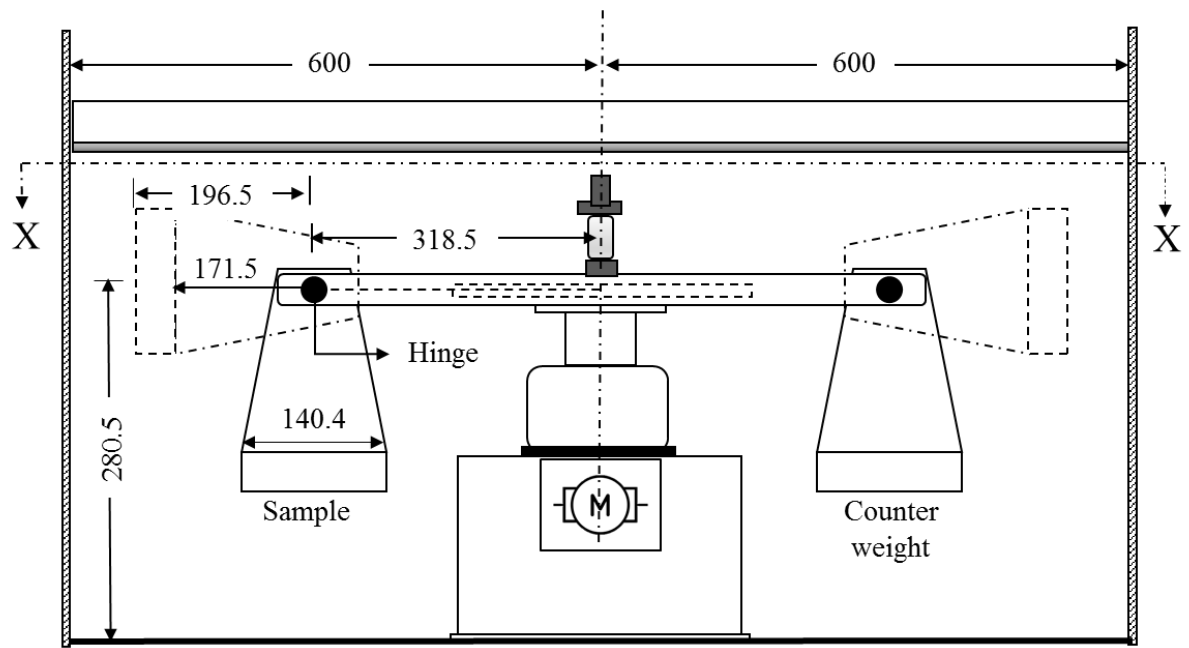
(a) Elevation
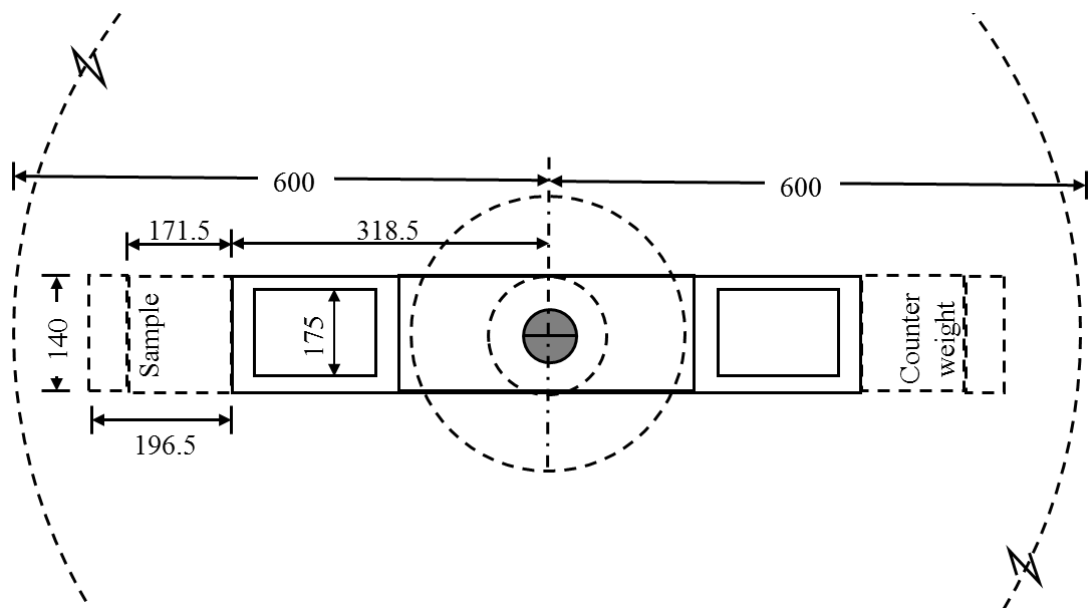
(b) Plan through section XX

Figure 3.6 (a) Elevation and (b) Plan through section of the small centrifuge facility at IIT Bombay (All dimensions are in mm)
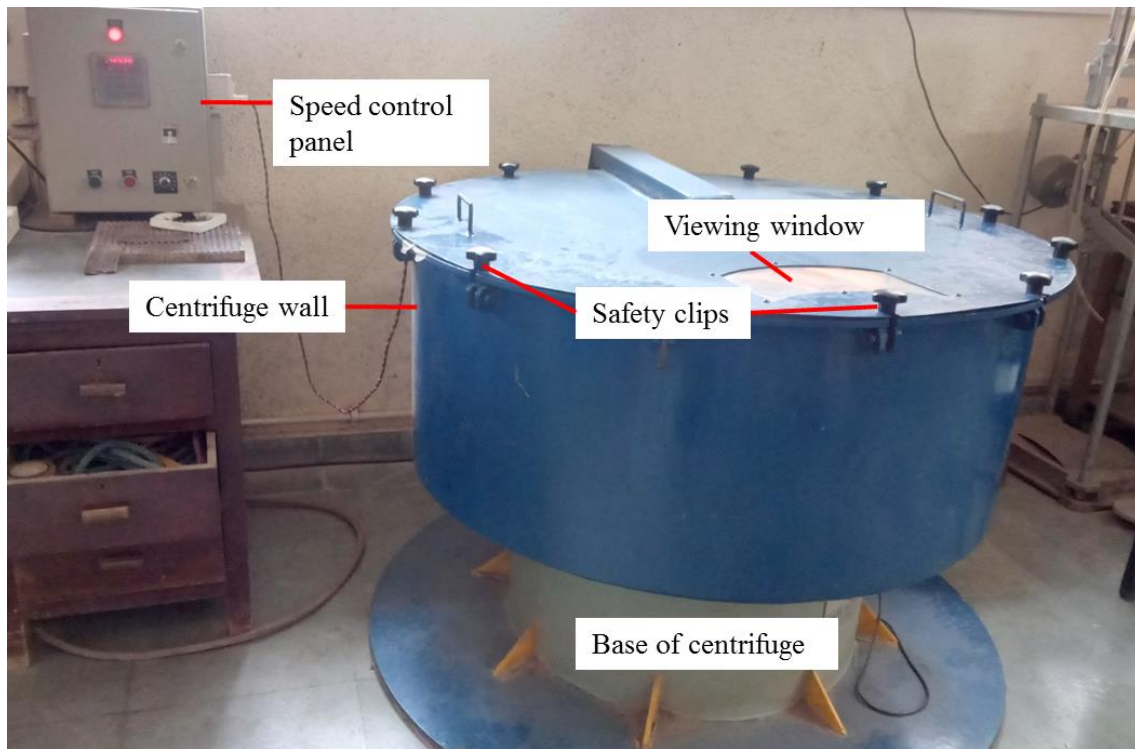
Figure 3.7 Actual photograph of the small balanced beam geotechnical centrifuge facility at IIT Bombay
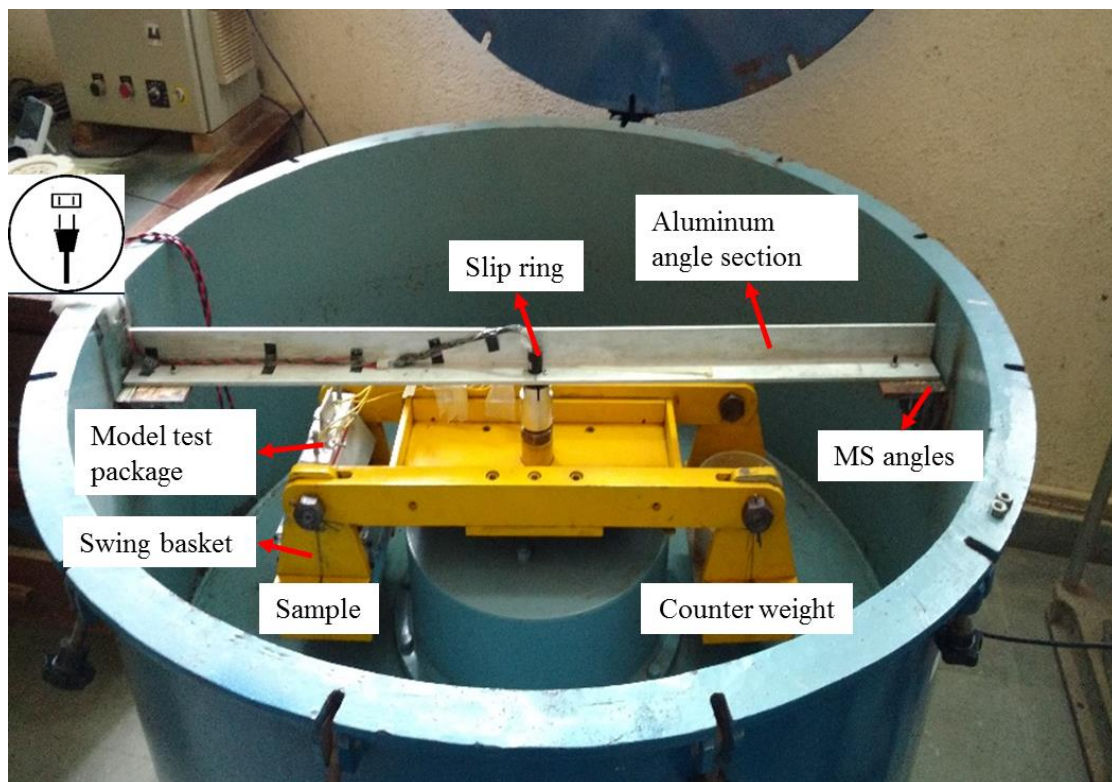
Figure 3.8 Actual photograph of the components inside balanced beam geotechnical centrifuge used in the present study

3.3.1 Swing baskets

The design of the centrifuge rotor arm incorporates a swinging payload platform that accommodates a variety of test specimens, as shown in Figure 3.9. At the opposite end, a fixed counterweight container filled with fine sand balances the net centrifugal tensile forces transmitted to the centrifuge arm. The radial distance from the centre of rotation to the payload platform surface inflight measures 548 mm.
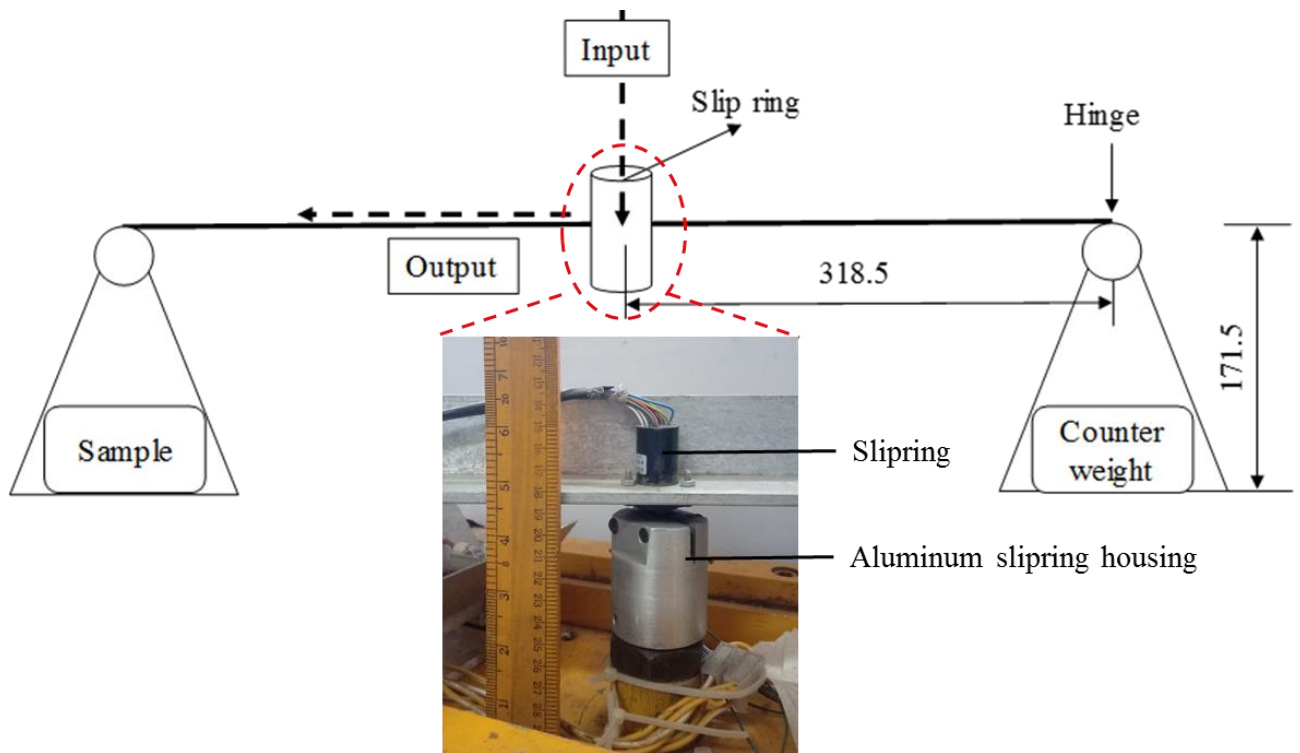
Figure 3.9. Schematic side view of the slipring assembly and swing baskets (All dimensions are in mm)

Centrifugal acceleration, a_c, depends on the radial distance from the model to the centre of rotation, r, and the angular velocity of the centrifuge, ω, defined as:

$$a_c = r\omega^2 \tag{3.23}$$

Depending on the effective centrifuge arm radius, the minimum angular velocity at which the ramping angle of the swing basket becomes as nearest to 90 degrees is calculated and plotted in Figure 3.10.
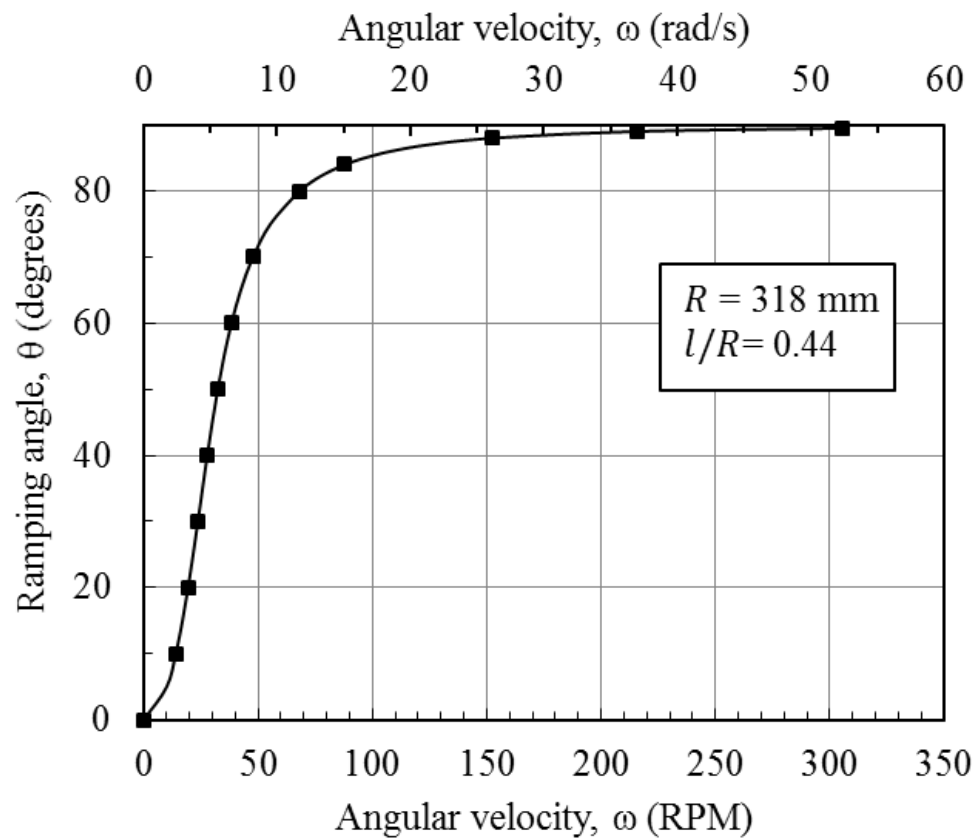
Figure 3.10 Variation of ramping angle of small centrifuge with increasing angular velocity

Therefore, the minimum angular velocity at which the ramping angle of the swing basket became as nearest to 90 degrees was 310 revolutions per minute (RPM). In this study, the minimum angular velocity under consideration is 350 RPM and the maximum is 480 RPM, as per the specification of slipring (i.e. max 500 RPM).

3.3.2 Slipring assembly

In order to simulate desiccation cracking inside a centrifuge, a light source with convection heating was required. For this, a slipring assembly was designed for power supply to existing small centrifuge. A 12 Wires 5Ampere 22 mm diameter, 500 RPM Collector Ring Wind turbine slipring was procured. Figure 3.11 present the schematic view of the slipring assembly in the centrifuge.
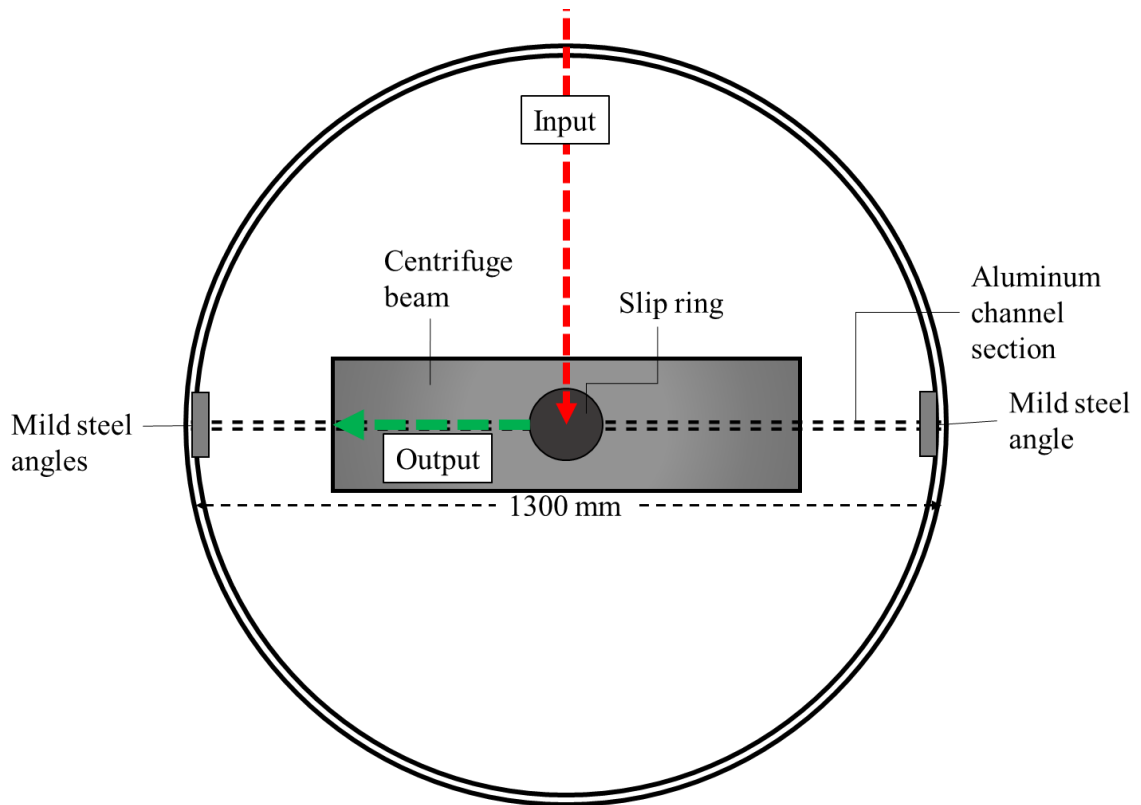
Figure 3.11 Schematic top view of the slipring assembly

Table 3. 4 Specification of the slipring assembly unit

Sr. No.	Specification	Value
1	Speed	maximum 500 RPM
2	Number of channels	12
3	Rated voltage	240V AC / DC
4	Rated current	5 A / Wire
5	Working temperature	-20 ~ 80 °C
6	Contact Material	Gold
7	Insulation resistance	1000MΩ / 500VDC
8	Shell material	plastic or metal can be selected
9	Working life	≥500 million transfer

A 10 mm thick Aluminium angle section was placed on the existing centrifuge for placement of slipring to avoid any rotary or lateral movement of the slipring, which may damage it at high RPM. An aluminium holder was designed for slipring such that the holder sits on the rotating centre of the beam shaft of centrifuge. The centre of slipring was carefully aligned with the centre of the motor shaft, so that no eccentric movement occurs during flight.

113

3.3.3 Illumination assembly

Tungsten halogen lamps serve the best purpose as a heat source, as they reach to the temperature of ~200 degree Celsius within one minute. The lighting assembly of the test setup consisted of two 50W miniature Tungsten halogen lamps, holder for halogen lamps, aluminium light reflector and stand for holding the lighting assembly with adjustable height. The halogen lamps were carefully clamped with the help of ceramic holders. The aluminium light reflectors were designed to guide the heat on the specimen in the container.

3.3.4 Optical data acquisition system

A digital camera (GoPro Hero4, USA) was positioned directly above the specimen. A camera holding arrangement was designed to hold the camera in position during the flight. The camera took photos at every 5 seconds interval. In this study, adventure camera was used as it is compact in size (41 mm x 59 mm x 21 mm), heat resistant and safe to operate at high gravities. Table 3.5 summarizes the specifications of the digital camera used in the present study.

Table 3.5 Specifications of the digital camera used in the present study

Sr. No.	Property	Value
1	Optical Sensor Type	CMOS
2	Effective Photo Resolution	12.0 MP
3	Protection	Shockproof, Waterproof
4	Continuous Shooting Speed	10 FPS*, 3 FPS, 5 FPS
5	Weight	87.88 gm

*CMOS = complementary metal-oxide-semiconductor; MP = Megapixel; FPS = Frames per second.

3.4 Scale effect and errors due to rotational acceleration field

It is usually inevitable that the prototype be exactly and accurately modelled. As the model is subjected to rotational acceleration field unlike earth's constant gravity, it results in errors. These are: (i) variation of gravity level with depth in the model, (ii) variation of gravity level with the horizontal distance in the model, (iii) non-linear variation of vertical stress, and (iv) Coriolis effect.

In addition to these errors, the model tested in a centrifuge can experience scale effects. They are: (i) boundary effects and (ii) grain size effect.

3.4.1 Variation of vertical stress with model depth

Figure 3.12 shows the non-linear variation of vertical stress in the centrifuge model. As the radius of rotation for each element in the model is different, a minor error in the vertical stress within the model is produced.

This error is minimum, when the quantity of the under stress is equal to the quantity of maximum overstress. It has been proved that this situation occurs when the effective radius is taken as $(R_o th/3)$, where h_m is the height of the model (here in Figure. 3.12, $h_m = d =$ thickness of clay layer). This produces a maximum error of $(h_m/6R_e)$, which is generally less than 3% of the prototype stress for most of geotechnical centrifuges (Taylor 1995). In the present study, since the maximum thickness of the model soil layer is $h_m = 30$ mm, and the effective radius, $R_e = 0.458$ m, therefore maximum error due to vertical stress was found to be 1.071%, which is less than 3%, and hence within limits prescribed by (Taylor 1995).
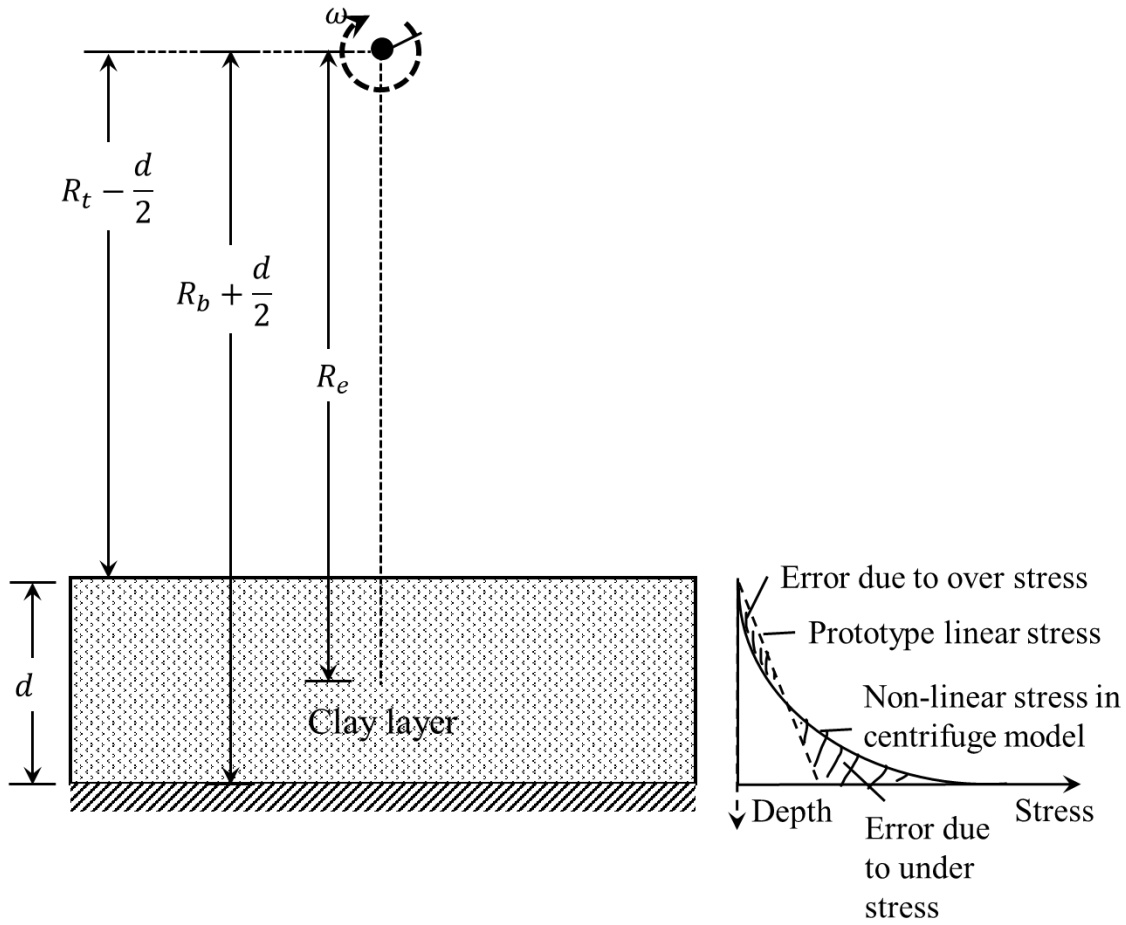
Figure 3.12 Error due to non-linear variation in vertical stress in centrifuge model

3.4.2 Variation of gravity level with model depth

The magnitude of gravity level varies with the model as the centrifuge accelerates radially. Figure 3.13 shows the variation of variation of gravity level with model depth and depicts the fact the magnitude of stress levels at the top of the model are not same as that at the bottom of the model, due to variation in gravity level. In the present study, the maximum error due to variation of gravity level from top to the mid-height of model depth is found to be $(R_e - R_t)/R_e$ = 4.71%. Although it is a limitation for a small beam centrifuge, this error is found to be less and assumed to be negligible in the present study.
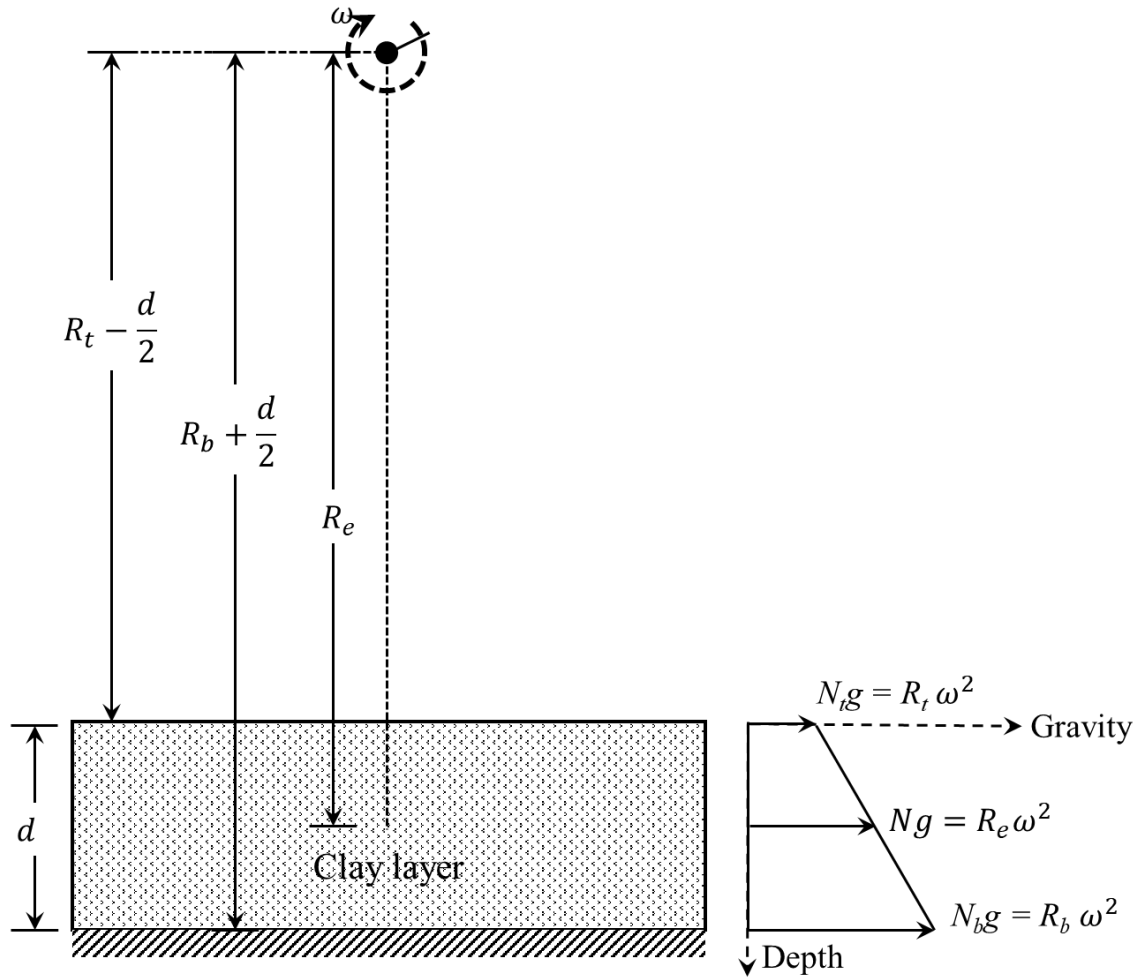
Figure 3.13 Error due to variation of gravity level with model depth

3.4.3 Variation of gravity level with horizontal distance

The magnitude of gravity level varies with the model as the centrifuge accelerates radially. Figure 3.14 shows the variation of gravity level with horizontal distance in centrifuge. If the top surface of the model is horizontal, it produces higher gravity level along the edges of the model (R_h) compared to the g-level at the centre of the model (R_e).
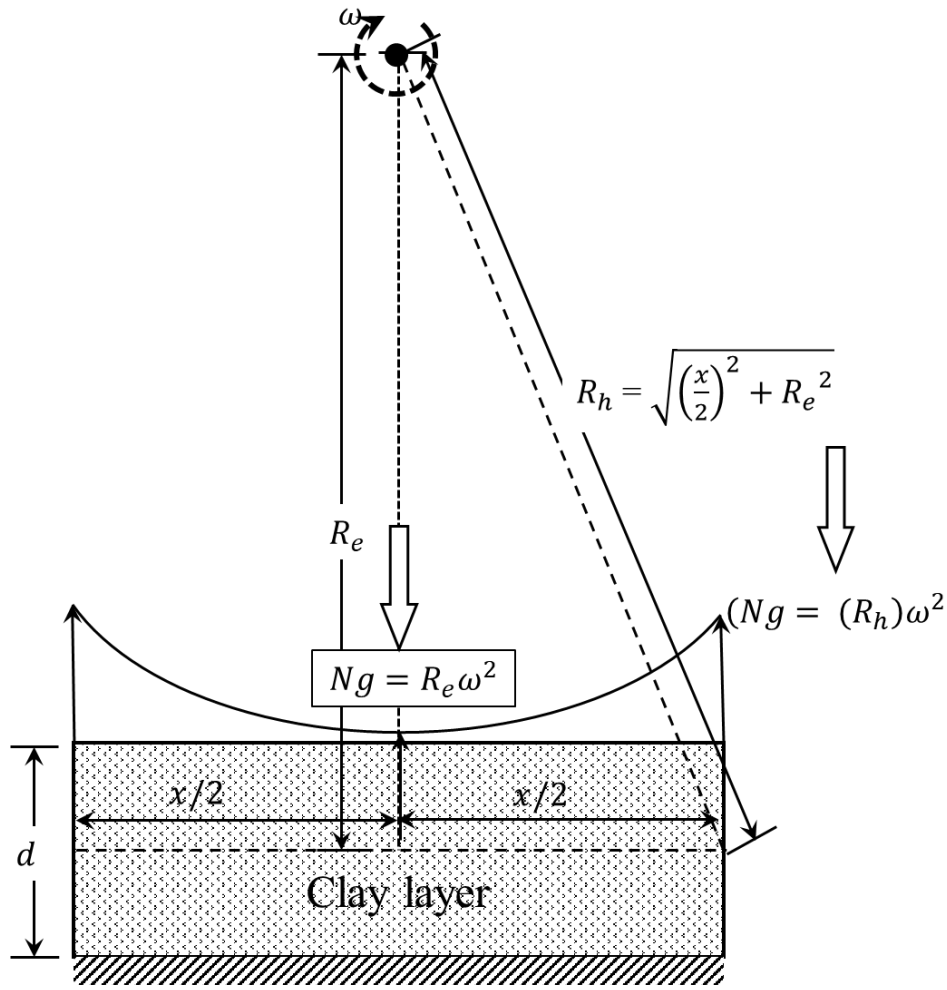
Figure 3.14 Error due to variation of gravity level with horizontal distance

Hence the magnitude of radius at the edge of model is $= R_h = \sqrt{\left(\frac{x}{2}\right)^2 + R_e^2}$, which comes out as, $\sqrt{(0.05^2 + 0.318^2} = 0.3219$ m. Hence the variability due to variation of radius with horizontal distance in this study is $[(R_h - R_e) / R_e] = [(0.3219-0.318)/0.318] = 1.23\%$. As the error is found to be negligible, the error arising due to variation of g-level with horizontal distance of the model is assumed to be insignificant for all practical purposes.

3.4.4 Particle size effect

It is seldom possible to exactly replicate all details of the prototype in physical modelling studies, including centrifuge testing. Thus, it is important to recognize the limitations of the studies and to attempt to evaluate the magnitude of scale effects. The linear dimension scale factor is 1: N. As such, it is logical to expect that soil particle size must also be adjusted between prototype and model dimensions. Thus, fine sand used in a 1:100 scale model might be thought of as representing a gravel. Using the same argument, a clay would then be thought of as representing a fine sand. Taylor (1995) recommends that simple guidelines on the critical ratio between a major dimension in the model to the average grain diameter be developed to avoid problems of particle size effects. It is stressed that in some circumstances particle size effects may be more important and that the model test series include sufficient relevant investigation to assess its significance in the problem being studied. Particle size effect decays with a decrease in the particle size. Since the present study deals with clay, the limitation of the particle size effect can be considered as negligible.

3.4.5 Coriolis Effect

The Coriolis Effect occurs when there is a movement of mass within the plane of rotation. The greatest impact from the Coriolis Effect is when the mass is moving in a plane 90° to the rotation axis. Typically, the acceptable error from this source is 10%. For example, if a seepage velocity of 0.1 m/sec to occur in a soil sample within a centrifuge with an arm radius of 0.5 m, rotating at 400 RPM, then the magnitude of error would approximately 1%. When considering fine grained materials, 0.1 m/sec is a very large velocity, usually the order of 1×10^{-7} m/sec is more appropriate, so Coriolis effects would be nearly negligible when dealing with fine grained soils.

3.4.6 Boundary effects

The effect of friction and adhesion between the walls of the container (bottom and sides) and the soil is called the error due to boundary effects. These errors can influence the shrinkage of the clay specimen and affect the results. In the present study, the boundary effects are minimized by applying white petroleum grease on the sides of the container walls. However, no grease was applied on the bottom surface to provide restraint to shrinkage, thereby aiding cracking of soil.

3.5 Closure

Centrifuge modelling of desiccation cracking phenomenon has not been attempted in the past literature, hence it led to the present study of centrifuge modelling of desiccation cracking. Centrifuge model studies can be performed to predict the desiccation cracking behaviour of soil in prototype conditions. In order to simulate the prototype stress conditions, similarity requirements of model clay layer must be fulfilled. Dimensional analysis for the phenomenon of desiccation cracking of unreinforced and fiber reinforced clay layer was performed to identify the governing parameters and their scaling laws. The basic scaling considerations for soil layer were discussed and the scaling considerations for the geofibers indicate that the same fibers can be used in prototype conditions as in the model conditions, by maintaining identical aspect ratio. The derived scaling considerations indicate that the time of crack initiation in a clay layer in the centrifuge model is $1/N^2$ times the time taken in the field. This chapter elaborated the details of small centrifuge facility available at IIT Bombay, principle of centrifuge modelling technique and scaling relations used in the present study. The errors in measurements due to high gravities were also highlighted in this chapter.

Chapter 4

EVALUATION OF THE PROPERTIES OF MODEL MATERIALS

4.1   Introduction

This chapter deals with the selection criteria of model soil materials and model geofibers used in the present study. The soil was analysed in the laboratory to ascertain its geotechnical properties. The properties of the model geofibers were evaluated for their tensile stress-strain characteristics as per ASTM standards. The results of experimental investigations carried-out on the selected model materials are explained in detail in the following sections. The consistency limits and consolidation characteristics of fiber reinforced expansive clay were also determined and discussed.

4.2 Properties of expansive clay used in the study

The expansive clay was collected from a construction site at a depth of about 1.5 m below the typical root zone, near the city of Nanded in Maharashtra, India. It is widely known as black cotton soil. The clay was characterized for its physical, mineralogical, chemical and geotechnical properties, as discussed below.

4.2.1 Physical properties

Soil was oven dried and sieved through 425 microns sieve to select finer portion of the soil. Basic index tests were carried-out on the selected portion of the soil. Figure 4.1 shows the images of dry soil at laboratory scale and scanning electron micrograph (SEM) at magnification of 5000x. The details of the SEM instrument and stages in SEM analysis are discussed in Annexure A2.
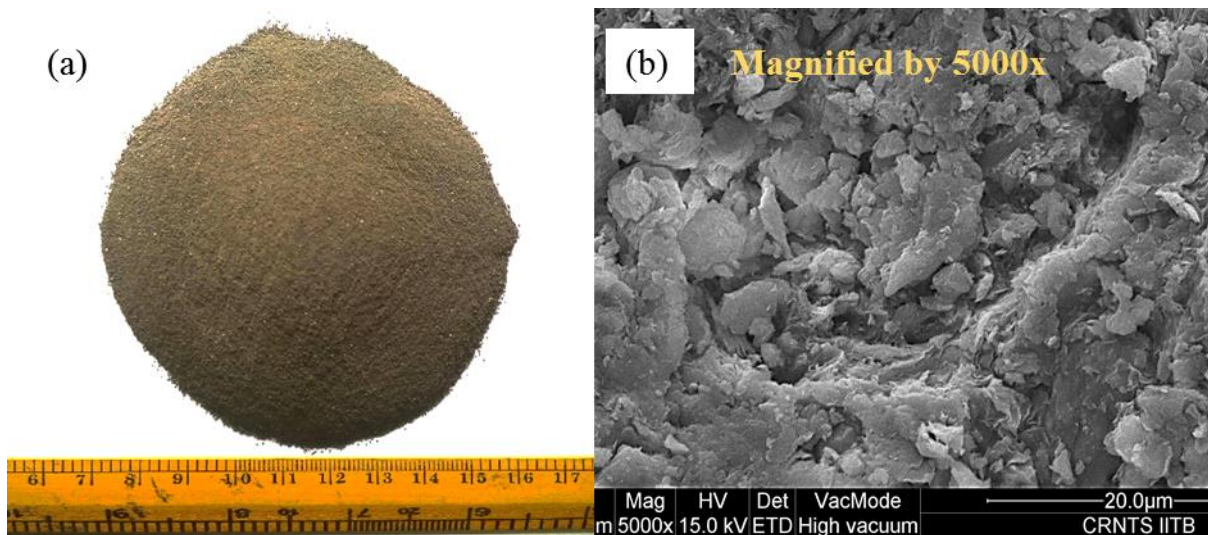
Figure 4.1 Expansive clay used in the present study (a) dry soil; (b) SEM micrograph at a magnification of 5000x

The particle size distribution of the soil is presented in Figure 4.2. Various percentage fractions such as gravel (4.75-20 mm), sand (0.075-2 mm), silt (0.002-0.075 mm) and clay (<0.002 mm) were determined according to ASTM D 422(2007). Standard Proctor tests to obtain maximum

dry density (MDD), γ_{dmax} and optimum moisture content (OMC) were conducted on the expansive clay, as per ASTM D698 (2012). The standard Proctor curve and zero air void ratio for the expansive clay is shown in Figure 4.3. Unconfined compressive strength test was also performed on the expansive clay. The unconfined compressive strength at the MDD and OMC was found to be 200 kN/m^2 and the soil can be defined as a very stiff clay, as shown in Figure 4.4.
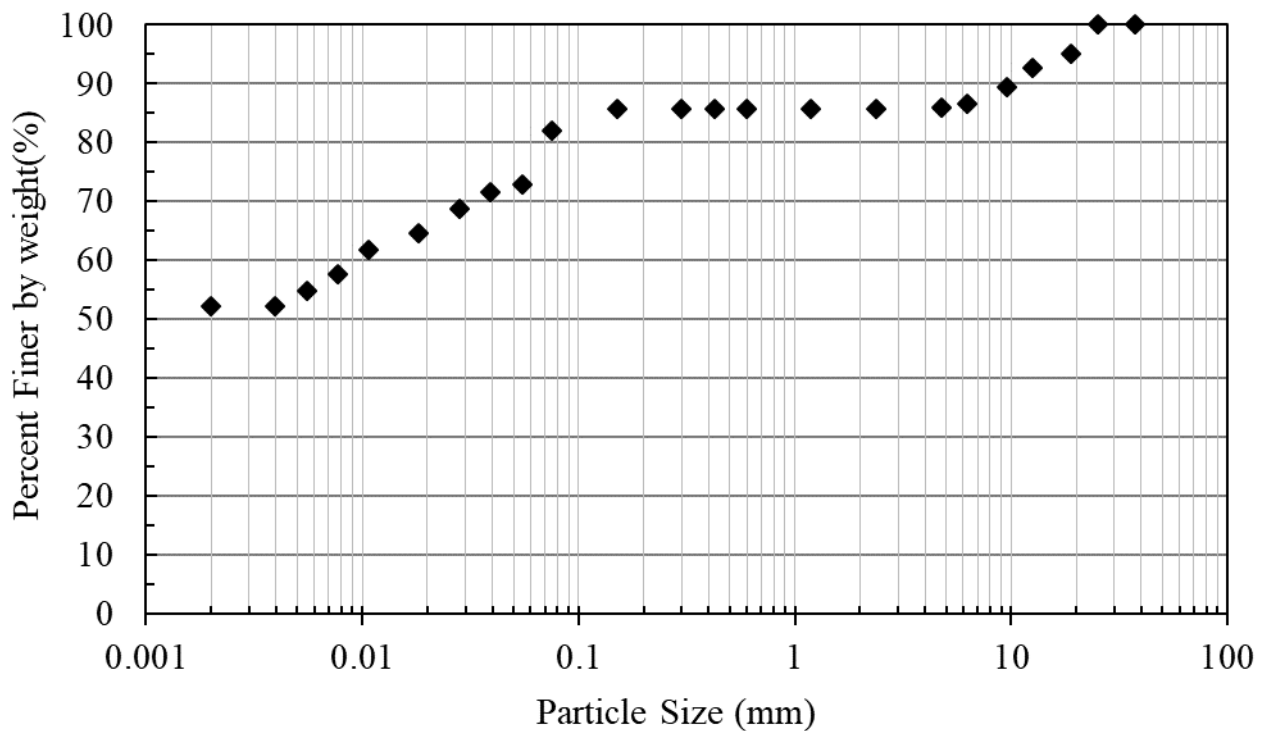
Figure 4.2 Particle size distribution of expansive clay

The specific gravity, G_s, of the clay was determined using Helium Gas Pycnometer (Pycnomatic ATC), according to ASTM D5550 − 14(2014) because it is considered to give reliable and accurate results for expansive clays (Uday and Singh 2013). Details of the pycnometer are provided in Annexure A1. The Atterberg limits were determined according to ASTM D4318, (2017) and ASTM D427 (2004) and the soil was classified as Clay of High Plasticity, CH, according to the Unified Soil Classification System (USCS).The physical properties of the clay are reported in Table 4.1.
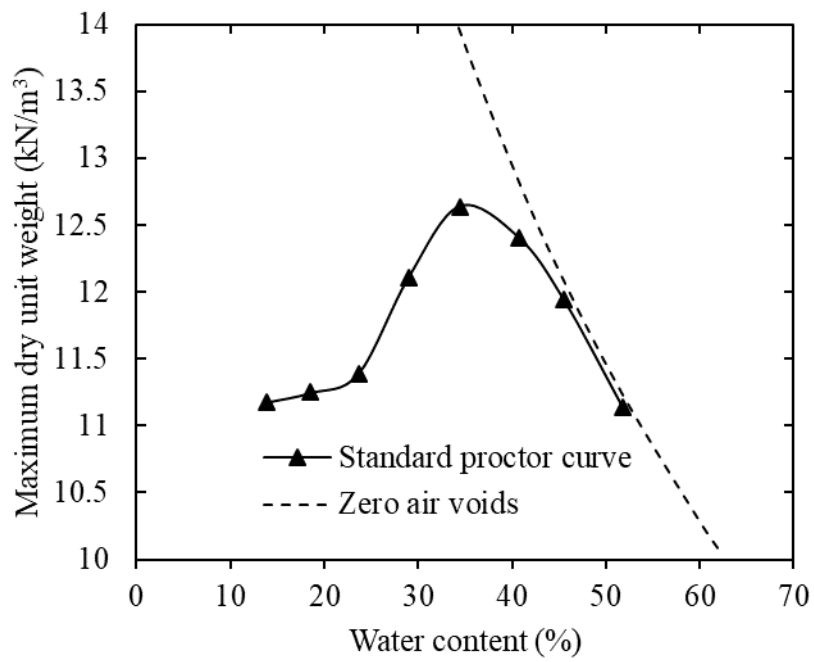
Figure 4.3 Compaction curve for the expansive clay (Standard Proctor compaction)
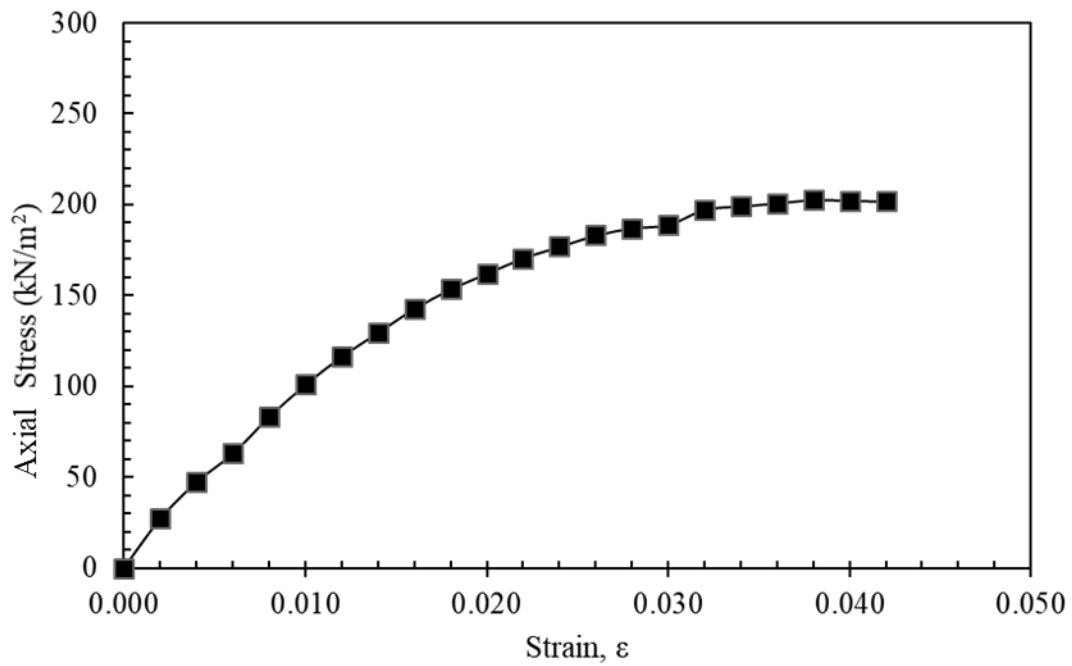
Figure 4.4 Stress versus strain curve for the expansive clay at its maximum dry unit weight and optimum moisture content

Table 4.1 Physical properties of soil used in the study

Properties	Unit	Value
Specific gravity	-	2.58
Gravel	%	1
Sand	%	5
Silty	%	34
Clay	%	60
Liquid limit	%	87
Plastic limit	%	38
Shrinkage limit	%	20
Free swell index	%	120
[a] Soil classification	-	CH
[b] Maximum dry unit weight	kN/m^3	12.5
[b] Optimum moisture content	%	34
[c] Undrained cohesion	kN/m^2	200

[a] according to the Unified Soil Classification System (USCS); [b] according to standard Proctor compaction; [c] at γ_{dmax} and OMC

4.2.2 Mineralogical properties

X-ray diffraction (XRD) spectra yielded the mineralogical composition, which is reported in Table 4. 2. XRD was conducted in XRD apparatus by Panalytical, The Netherlands using a Cu-Kα radiation source (λ= 1·5405 A°) in the range 5–70° (2θ).

The X-ray diffraction spectra reveals that this clay has 49.31% montmorillonite, 41% Anorthite, 5% Calcite, 4.3% Quartz, and 0.4% magnetite. The structural unit of montmorillonite is composed of two silica sheets and one alumina (gibbsite) sheet, a 2:1 mineral. The interlayer bonding between the tops of silica sheets is mainly due to van der Waals forces and is, thus, very weak compared to hydrogen or another ion bonding.

Table 4. 2 Mineralogical and chemical composition of the soil used in the study

[a]Mineralogical	Montmorillonite	Anorthite	Calcite	Quartz	Magnetite
composition (%)	49.3	41	5	4.3	0.4
[b]Chemical	SiO_2	Al_2O_3	CaO		MgO
Composition (%)	47.3	12.5	6.3		8.3

[a]determined by X-ray diffraction (XRD) spectra; [b]determined by X-ray fluorescence (XRF)

Further, as the montmorillonite has a largest specific surface area among major clay minerals, a large amount of water and other exchangeable ions can easily enter between the layers causing the layers to be separated. Because of this affinity for water, clay soils containing montmorillonite mineral are susceptible to substantial volume change. They swell as the water enters the lattice structure and shrink if water is removed. Hence the soil under consideration can be classified as expansive clay.

4.2.3 Chemical properties

Chemical composition

The chemical composition of the clay was determined by X-ray fluorescence (XRF) method and is reported in Table 4. **2**. The x-ray fluorescence spectrometer Model S4 PIONEER BRUKER aXS was used in the study. The details of instrument are explained in Annexure A3.

pH measurement

The pH of the clay was measured using a pH-meter (Toshcon Industries, India). The details of the steps in measurement of pH are shown in Figure 4.5.

(a) Electrode dipped in buffer KCl solution for overnight	(b) Black cotton soil solution	(c) pH measurement in laboratory pH meter
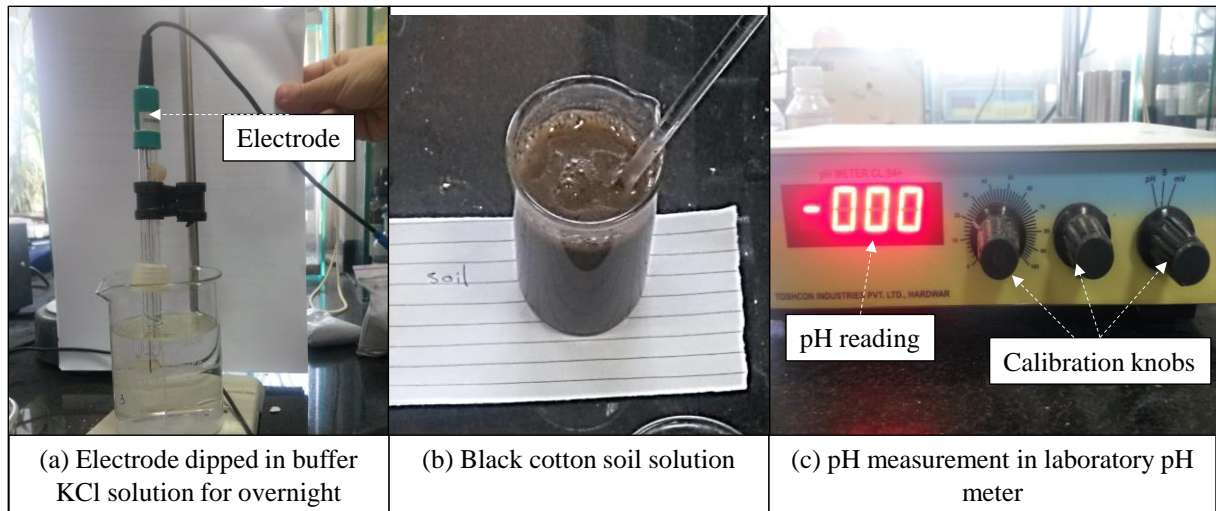
Figure 4.5 Measurement of pH of expansive clay using pH-meter

The setup includes pH meter, buffer solution, and distilled water and ION electrode. The electrode was immersed in a buffer solution of known pH. The display of pH-meter was brought to the known value by means of the asymmetry potential adjustment calibration knobs. The electrode was then removed from the buffer solution and washed with distilled water and immersed in another known buffer (KCl) say 4pH. The display of the pH-meter is brought to the value 4pH by means of calibration knobs. Now, the pH meter is calibrated and ready to be used for soil. The soil slurry at approximately 300% water content was prepared with distilled water. It was ensured that the electrodes are cleaned with distilled water in-between measurements. The pH of the clay used in the present study was found to be about 8, indicating that the clay is slightly alkaline in nature.

4.2.4 Suction properties

To measure low range suction profile and soil water characteristic curve (SWCC) in slurry samples, a suction measurement device called HYPROP system was used (Annexure A6). The UMS HYPROP determines the unsaturated hydraulic conductivity and water retention characteristics of soil samples through laboratory evaporation method (Peters and Durner 2008).

Two high pressure tensiometers (<300 kPa range) are placed at two height levels inside the soil sample from the base. The soil specimen mixed at its liquid limit is placed in the ring. Soil is continuously weighed, and suction readings are taken. Water is evaporated from the top surface under laboratory conditions. Once sensors cavitate (air introduced into the ceramic cup) the test was stopped. From the results and extrapolation software, a water retention curve from each soil sample was plotted. To determine points with higher suction and lower moisture content, a WP4C chilled mirror dewpoint potentiometer device was utilised, the details of the instrument are discussed in Annexure A5.

The WP4C can measure suctions greater than 0.3 MPa and over the air dried theoretical maximum suction of 100 MPa. Samples were left to dry at constant room temperature (22°C) until a predefined moisture content was reached. Samples were tested in the dewpoint potentiometer device at a temperature of 22°C. The results are shown in Figure 4.6. This includes shrinkage during drying or increase of suction. In order to find the true air entry value, the degree of saturation versus suction curve can be drawn.
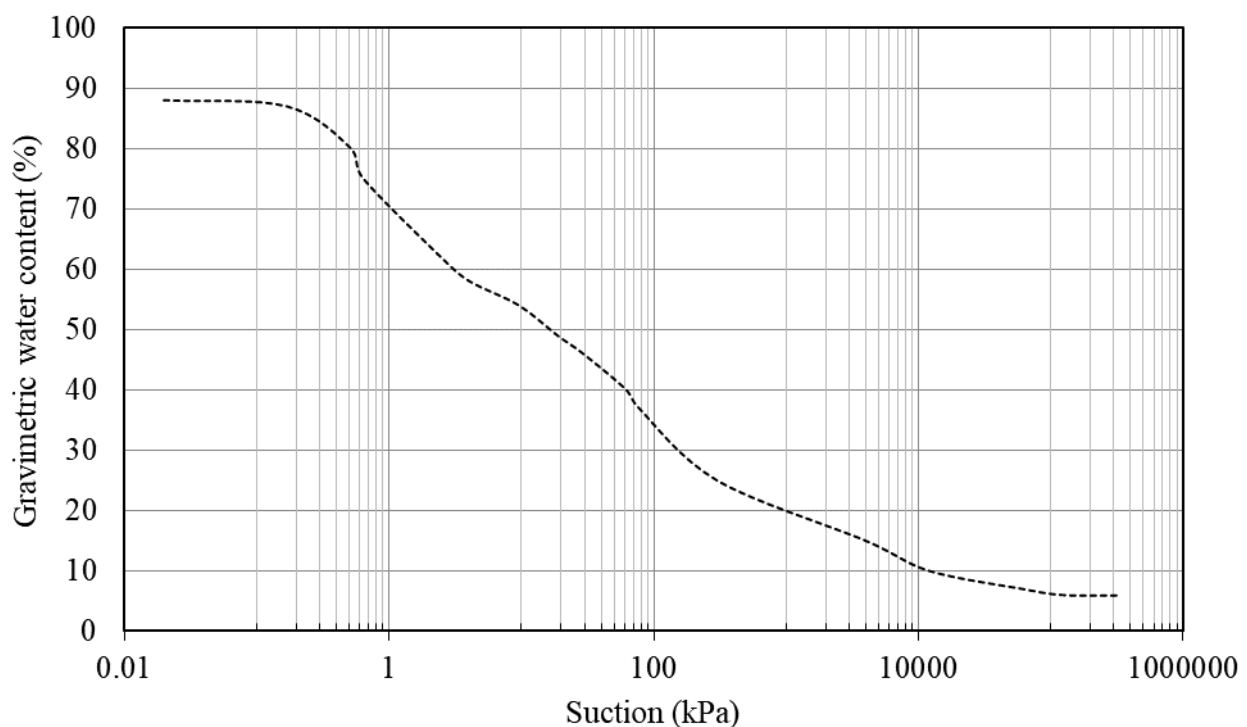
Figure 4.6 Soil water characteristic curve for expansive clay

4.3 Properties of model geofibers

Geofibers (flexible polymeric fibers) are available in different materials such as polypropylene, polyester and poly vinyl alcohol, etc. They are available in different types such as monofilament, fibrillated, tape, etc. In the present study, polypropylene tape fibers (PP-T) of width 2 mm and thickness of 0.02 mm, polypropylene fibers (PP-F) and polyester fibers (PET) having equivalent diameter 40 microns were used. Figure 4.7 shows the types of geofibers used in the present study.

(a) Polyester fibers   (b) Polypropylene fibers   (c) Polypropylene tape fibers
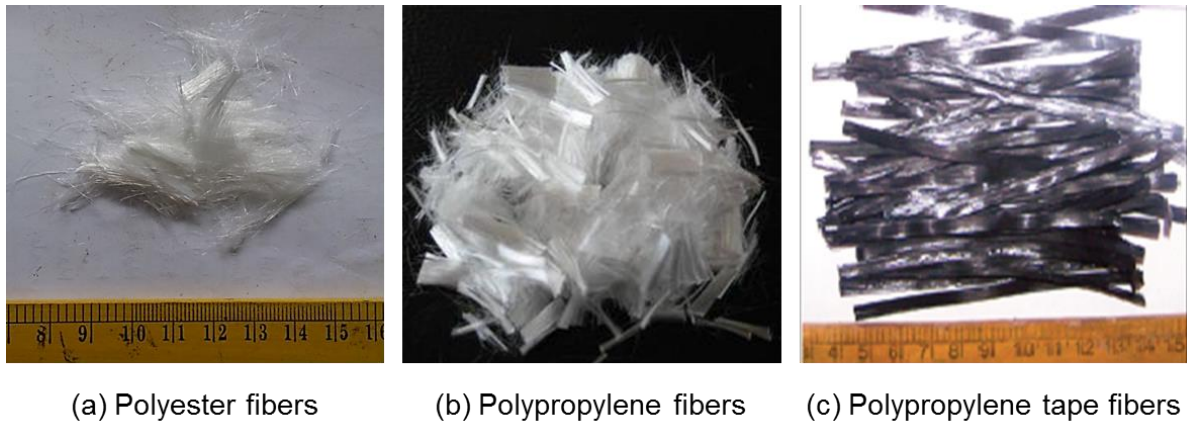
Figure 4.7 Geofibers used in the present study (a) Polyester fibers, (b) Polypropylene fibers, (c) Polypropylene tape fibers

Physical properties of the geofibers were determined and summarised in the subsequent sections. The polyester fibers were checked for their alkaline stability, as the soil under consideration is slightly alkaline in nature. However, polypropylene is found to be highly resistant to alkaline conditions.

4.3.1 Polyester fibers

The polyester fibers that had a special trilobal cross section with an effective diameter of 40 µm were used as shown in Figure 4.8. The amount of adhesion force and fiber sliding resistance between the fiber and the soil is proportional to the contact surface area and the fiber surface

roughness (Frost and Han 1999; Tagnit-Hamou et al. 2005). The irregular trilobal shape offers better surface roughness than the conventional circular cross section.
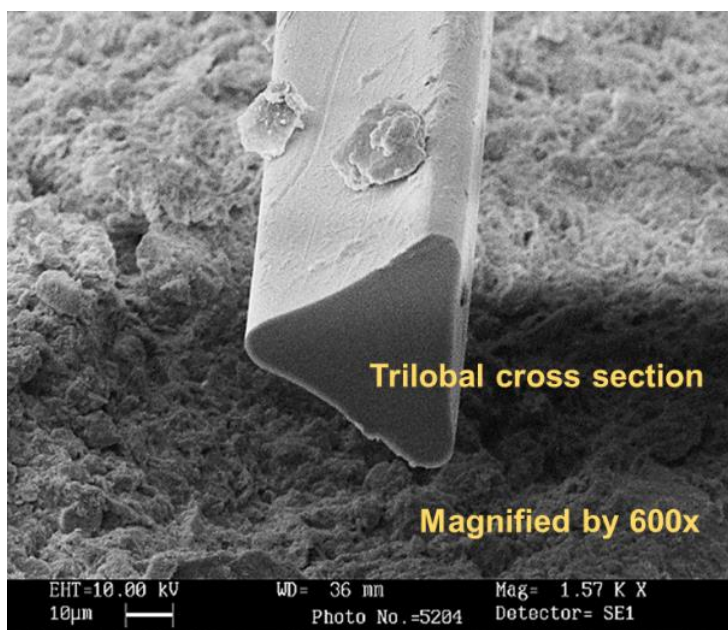
Figure 4.8 SEM photomicrograph of polyester fiber used in the study (magnified by 600x)

Mechanical properties of a single filament of polyester fiber (M/s Pragati Enterprise, India) were determined according to ASTM D1577-07(2018) and ASTM D3822-14 (2014) by using specialized single fiber tensile test equipment (Textechno Fafegraph ME, Germany) at the Bombay Textile Research Association (BTRA), Mumbai, India, as reported in Table 4.3 and Table 4.4. The force-strain curve of a single fiber is presented in Figure 4.9.

The linear density of a fiber is measured as the weight (in grams) of 1000 m of filament of fiber (SI unit: tex). The mechanical strength of a fiber is given by tenacity, which is defined as the breaking force divided by the linear density of the fiber (SI unit: mN/tex). Generally, barrier systems are exposed to aggressive underground environmental conditions. Therefore, fibers must have resistance to various forms of environmental degradations (Netravali et al. 1993).
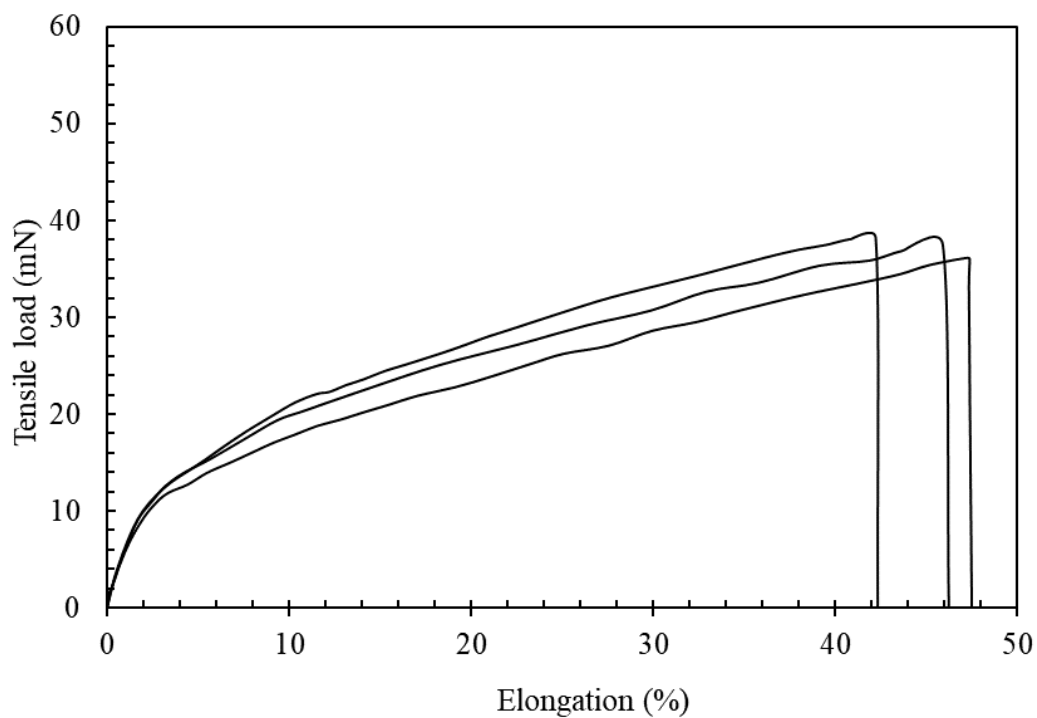
Figure 4.9 Typical force-elongation curve of Polyester fibers used in the study

Table 4.3 Mechanical properties of a single filament of polyester fiber

Properties	Unit	Value
Specific gravity	-	1.35
Effective diameter	µm	40
Linear density	tex	0.331
Breaking force for single filament	mN	112.72
Tenacity	mN/tex	340.56
Strain at break	%	45.53
Fusion point	℃	165

Table 4.4 Properties of untreated and alkali treated polyester fibers used in the study

Status of Polyester fiber	[a]Linear density (tex)	Breaking force (mN)	Strain (%)
Untreated	0.331	112.6	45.18
Alkali treated	0.321	107.6	44.46
[a] SI unit of linear density (mN/tex)			

131

Since the soil under consideration was slightly alkaline in nature, the polyester fibers were tested for their mechanical strength before and after immersion in Calcium Hydroxide, $Ca(OH)_2$ solution (pH=13) for three days at a temperature of 60°C. The fibers showed very good alkaline stability, as reported in

Table 4.4. Almost no strength degradation of fibers was observed even after exposure to a harsh alkaline environment.

4.3.2 Polypropylene fibers

The polypropylene fibers were procured from M/s. Reliance industries. The mechanical properties of a single filament of polyester fiber was determined according to ASTM D1577-07 (2018) and ASTM D3822-14 (2014) by using specialized single fiber tensile test equipment (Textechno Fafegraph ME, Germany) at the Bombay Textile Research Association (BTRA), Mumbai, India, as summarised in Table 4.5.

Table 4.5 Properties of polypropylene fiber used in the study

Properties	Unit	Value
Specific gravity	-	0.90-0.91
Linear density	tex	0.4
Melting point	℃	160-165
Tenacity	gram per denier	4 - 6
Elongation	%	60-90
Alkaline stability	-	Very good
[a] Denier is a unit of measure for the linear mass density of fibers		

4.3.3 Polypropylene tape fibers

Polypropylene tape fibers used in the present study are having a flat surface with rectangular cross-section. The mechanical properties of the fibers are summarized in Table 4.6. Denier is defined as the mass in grams per 9,000 m. The stress at which fiber breaks, expressed in grams per denier (gpd), and known as tenacity of the fiber. The PP fibers are having lower specific gravity compared than the polyester fibers. As the specific gravity of polypropylene fibers is low, larger volume of fibers are present in a given weight of fibers and hence the number of fibers will be more for the same fiber content.

Table 4.6 Mechanical properties of a single filament of polypropylene-tape fiber

Properties	Unit	Value
[a]Linear density	Denier	0.91
Specific gravity	-	0.331
Breaking force	N	48.4
Tenacity	gram per denier	5.45
Strain at break	%	18

[a] Denier is a unit of measure for the linear mass density of fibers

4.4 Properties of fiber-reinforced clay

4.4.1 Liquid limit and plastic limit

In this study, a series of liquid limit tests were performed on unreinforced and fiber-reinforced locally available expansive soil. Table 4.7 summarizes the consistency limit tests performed on the expansive clay with and without fiber inclusions.

The fiber content and fiber length were varied in the test series. The plasticity index and shrinkage limit of fiber-reinforced soil was also determined. The liquid limit of the fiber-reinforced soil was determined by Casagrande method as well as fall cone method (ASTM D4318 and ASTM 2017). Nevertheless, it was observed that the Casagrande method was inappropriate for fiber-reinforced soil as it was difficult to cut an ideal groove due to the pulling out of fibers along with soil owing to erroneous results.

Figure 4.10 shows the difficulty faced while cutting the groove leading to inappropriate groove formation, especially in case of longer fiber lengths. Also, Casagrande method is a highly operator sensitive method, hence, the fall cone method was ideal choice for estimating the liquid limit of fiber-reinforced soils. The specimen paste was carefully placed in the cylindrical metal cup, flattened at the rim to prepare a smooth surface. The cone was lowered to the specimen surface and released for the prescribed period of 5 seconds and its depth of penetration into the soil was recorded. The entire testing procedure was carried out from dry to wet side, by adding required amount of water to the specimen. The depth of penetration versus water content is plotted (referred to as flow curve), and the water content corresponding to a cone penetration of 20 mm is considered as the liquid limit. Figure 4.11 shows the schematic representation of fall cone method for testing liquid limit of soil. Liquid limit values obtained from the fall cone tests for unreinforced and fiber-reinforced soil specimens are shown in Figure 4.12.

It could be observed that there is a steep increase in the liquid limit of soil due to inclusion of fibers. This may be attributed to increased shear strength of the soil specimen due to improved bonding of soil particles with fibers.
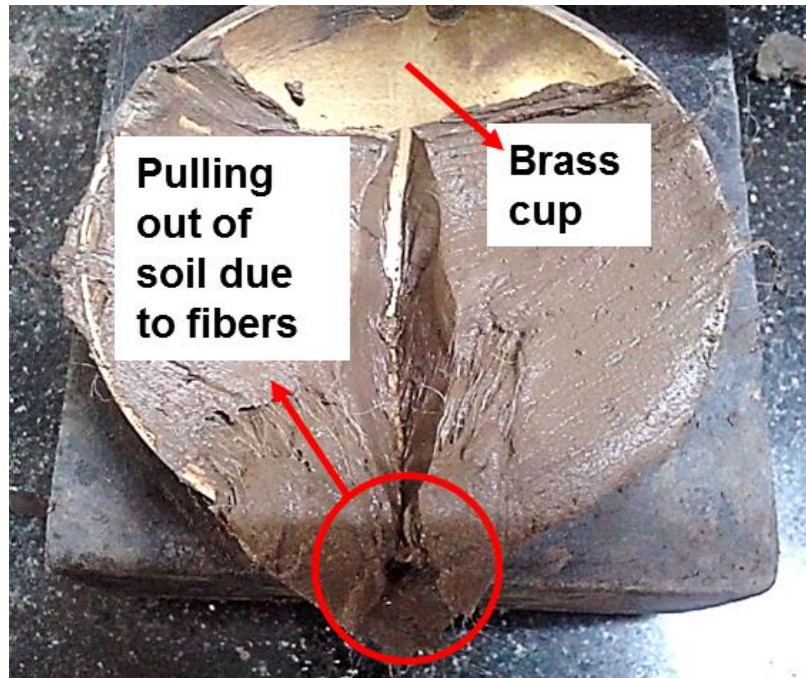
Figure 4.10 Inappropriate groove formation for fiber-reinforced clay in Casagrande apparatus
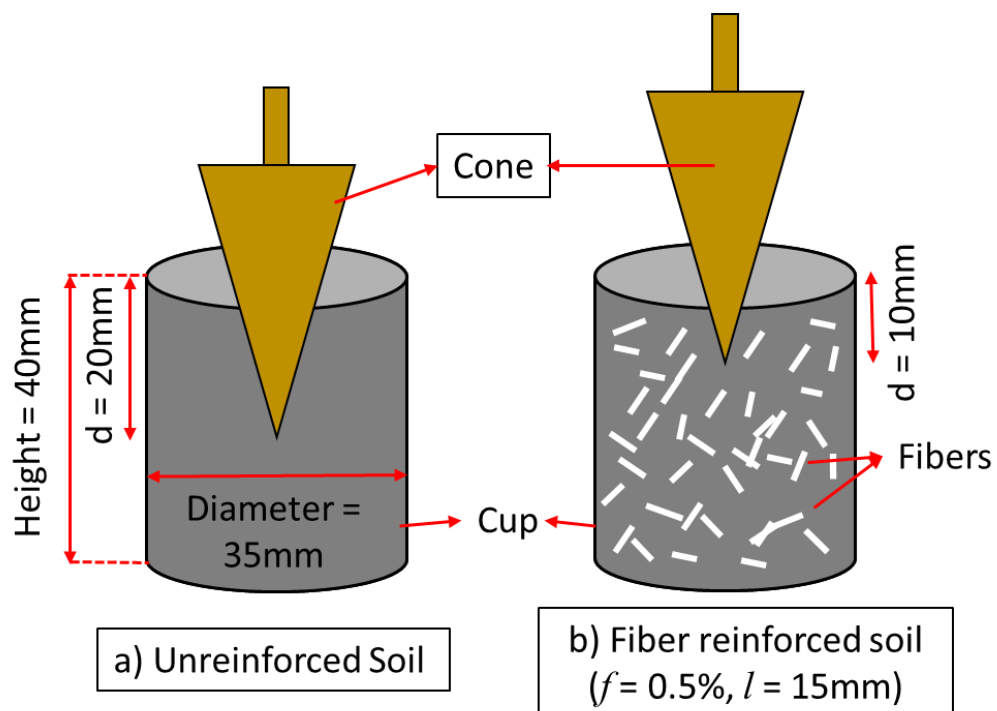
Figure 4.11 Difference in depth of penetration for unreinforced and fiber-reinforced soil specimens during fall cone test

Table 4.7 Liquid limit, plastic limit, shrinkage limit tests performed in study

Test No	Test legend	Tests performed	Specimen type	f (%)	l (mm)
1	UR	LL, PL, SL	UR	_[a]	_[a]
2	FR1	LL	FR	0.25	3
3	FR2	LL	FR	0.5	3
4	FR3	LL	FR	0.75	3
5	FR4	LL	FR	1	3
6	FR5	LL	FR	0.25	6
7	FR6	LL	FR	0.5	6
8	FR7	LL	FR	0.75	6
9	FR8	LL	FR	1	6
10	FR9	LL, PL, SL	FR	0.25	15
11	FR10	LL, PL, SL	FR	0.5	15
12	FR11	LL	FR	0.75	15
13	FR12	LL	FR	1	15
14	FR13	LL, PL, SL	FR	0.25	30
15	FR14	LL, PL, SL	FR	0.5	30
16	FR15	LL, PL, SL	FR	0.75	30
17	FR16	LL, PL, SL	FR	1	30
18	FR17	LL, PL, SL	FR	0.25	50
19	FR18	LL, PL, SL	FR	0.5	50

UR- Unreinforced; FR- Fiber reinforced; LL- Liquid limit, PL- plastic limit, SL- shrinkage limit f- fiber content; l- fiber length; [a] not relevant/not used
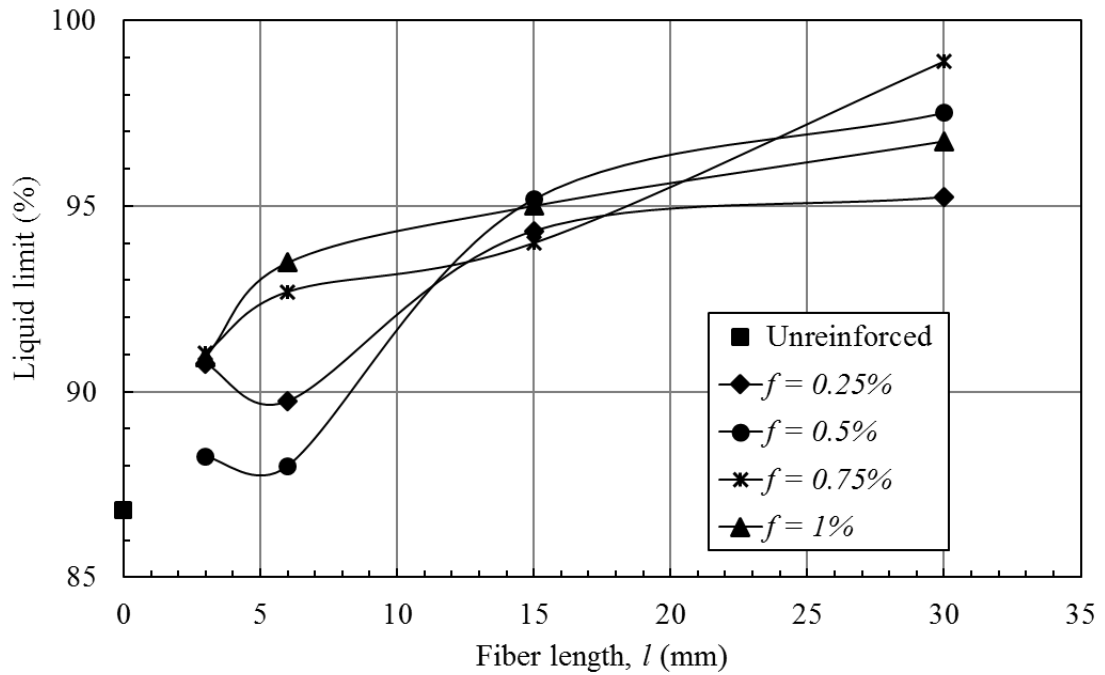
Figure 4.12 Variation of liquid limit with varying fiber content and fiber length obtained using Fall cone method

Due to increased tensile strength of soil, the fibers tend to hold the soil even at lower water contents without crumbling. Figure 4.13 shows the variation of plasticity index of unreinforced and fiber-reinforced soil.

No significant variation of plasticity index is observed with an increasing fiber content. A minor decrease in plasticity index is observed at lower water contents due to uniform distribution of fibers in the specimen. However, the plasticity index of fiber-reinforced soil at higher fiber contents is almost similar at higher fiber contents. This behavior may be attributed to the non-uniform distribution of fibers at higher fiber contents.

Figure 4.14 shows the variation of shrinkage limit of unreinforced and fiber-reinforced soil specimen with varying fiber content and fiber length. It is overserved that there is no significant change in the shrinkage limit due to presence of fibers. This means that fiber-reinforcement does not alter the entrance of soil into unsaturated state.
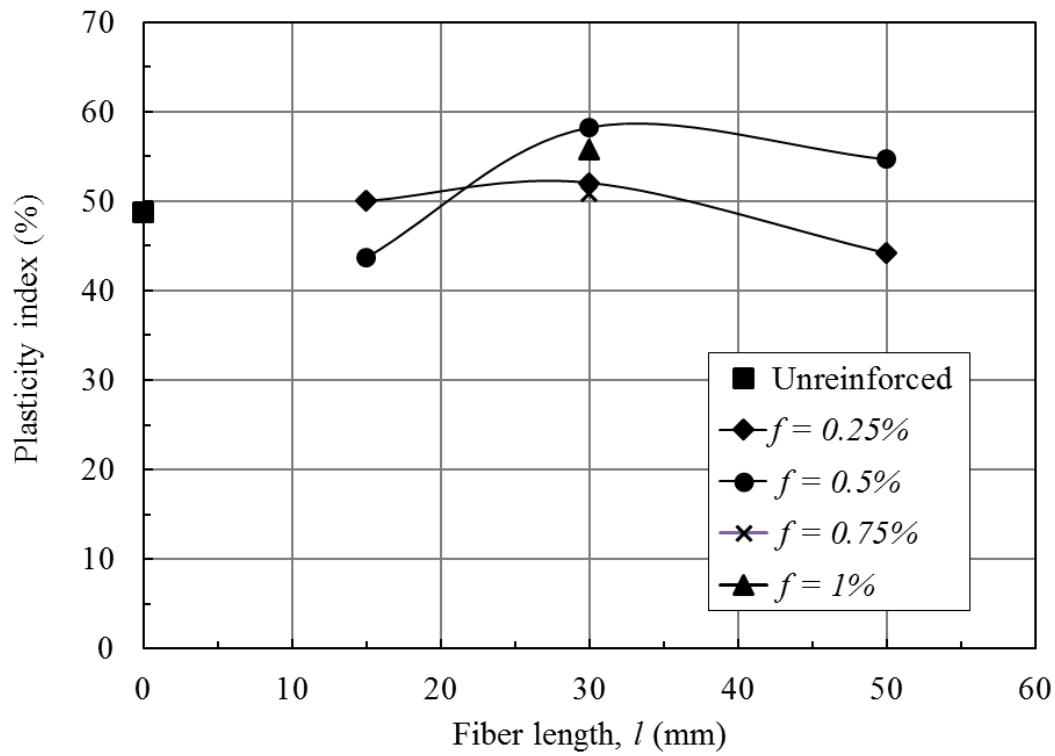
Figure 4.13 Variation of plasticity index of unreinforced and fiber reinforced soil with varying fiber length and fiber content obtained using Falling cone method
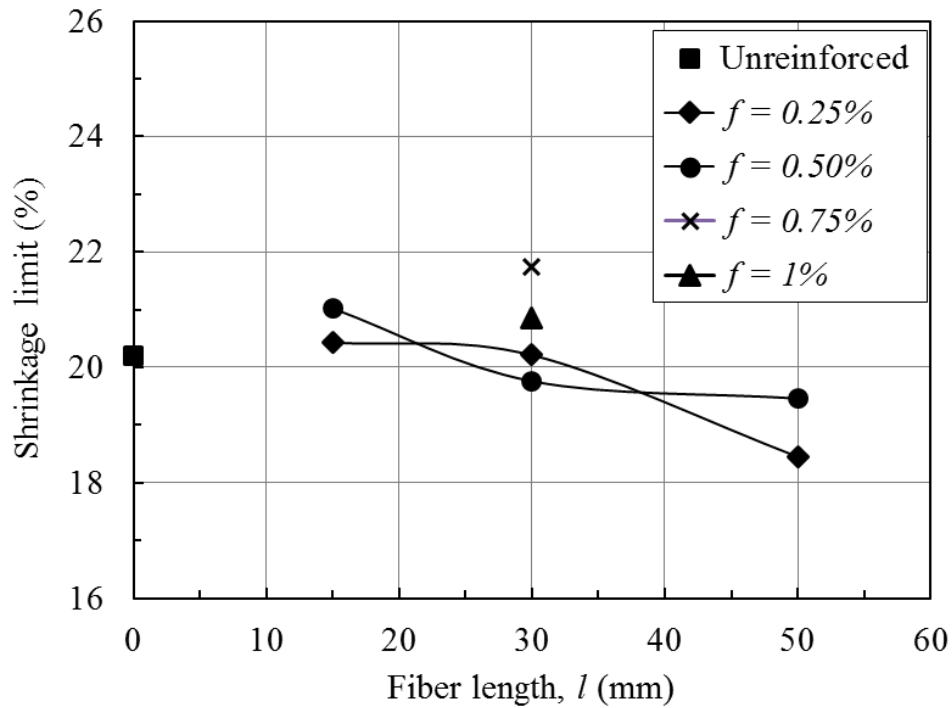
Figure 4.14 Variation of shrinkage limit of unreinforced and fiber reinforced soil with varying fiber content and fiber length obtained using Falling cone method

4.4.2 Consolidation characteristics of expansive soil with and without fibers

The soil samples were tested in LoadTrac III (Geomech Corp., Australia make) which is an automated consolidation oedometer rig (Figure 4.15). A linear variable differential transformer (LDVT) measures the consolidation displacement of the sample. An S shape load cell measures the force by the differential movement in the cell. The force is then converted into a stress by the equivalent area the force is applied to (the top plate of the oedometer cell).

The LoadTrac is load controlled where load will oscillate close to the predetermined stress as the base moves up or down to keep load steady. The LoadTrac can be set to consolidate a soil sample in steps until the t_{100} value is approximated or for a predetermined duration (such as 24 hours). The load is increased once the sample reaches the calculated 100% consolidation displacement for that given stress. Consolidation tests were performed on unreinforced and fiber reinforced expansive clay, so that the consolidation properties could be used for specimen preparation for centrifuge tests.
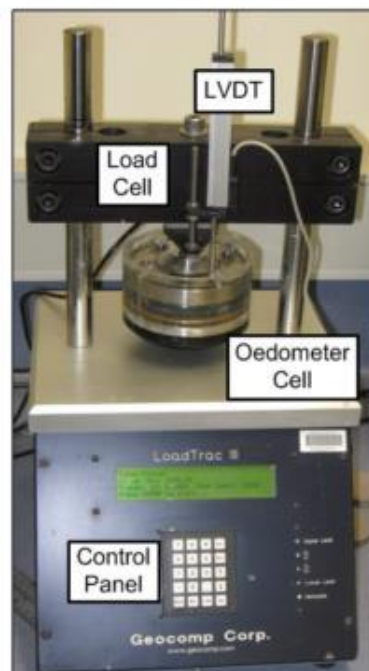
Figure 4.15 LoadTrac III automatic consolidator machine available at Monash University

This was used to determine consolidation properties of the unreinforced and fiber reinforced expansive clay passing through 425µ sieve reinforced with required amount of fibers. The prepared slurry was poured inside the oedometer cylinder. The test program of consolidation test is summarized in Table 4.8. The pressure versus time plot is shown in Figure 4.16.

Table 4.8 Test program for consolidation test on unreinforced and fiber reinforced clay

Test No	Test legend	Fiber content (%)	Fiber length (mm)
1	UR	-a	-a
2	FR1	6	0.25
3	FR2	6	0.5
4	FR3	6	0.75
5	FR4	12	0.25
6	FR5	12	0.5
7	FR6	12	0.75
8	FR7	30	0.25
9	FR8	30	0.5
10	FR9	30	0.75

UR- Unreinforced; FR- Fiber reinforced; [a] not relevant/not used
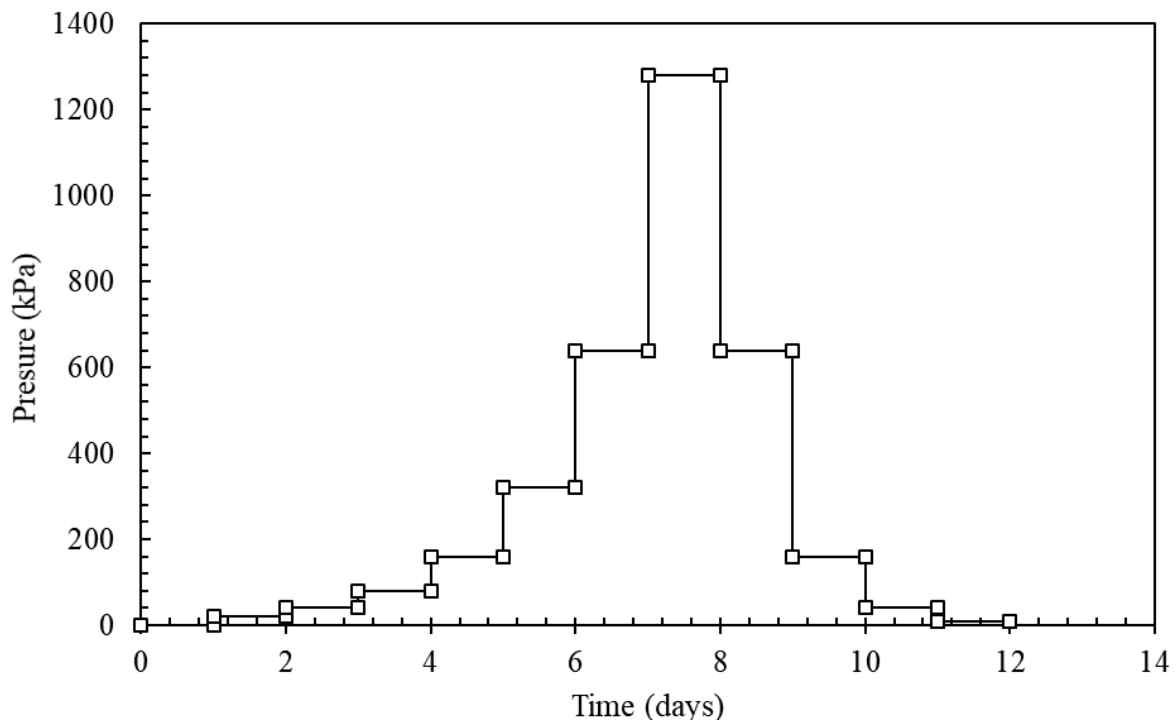
Figure 4.16 Pressure applied versus time of consolidation

Void ratio vs. pressure and water content vs. pressure are plotted for unreinforced and fiber reinforced soil specimens with varying fiber content and fiber length. The plots are shown in Figure 4.17, Figure 4.18, Figure 4.19 and Figure 4.20.
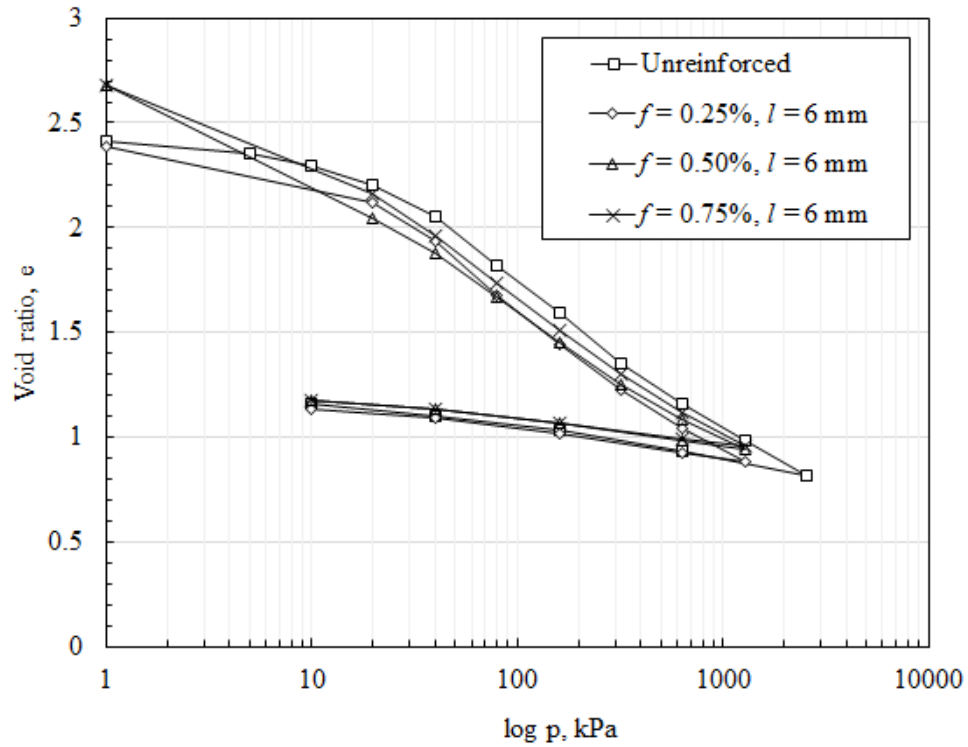
Figure 4.17 Void ratio versus pressure applied curve for unreinforced and fiber reinforced specimens of fiber length l = 6 mm
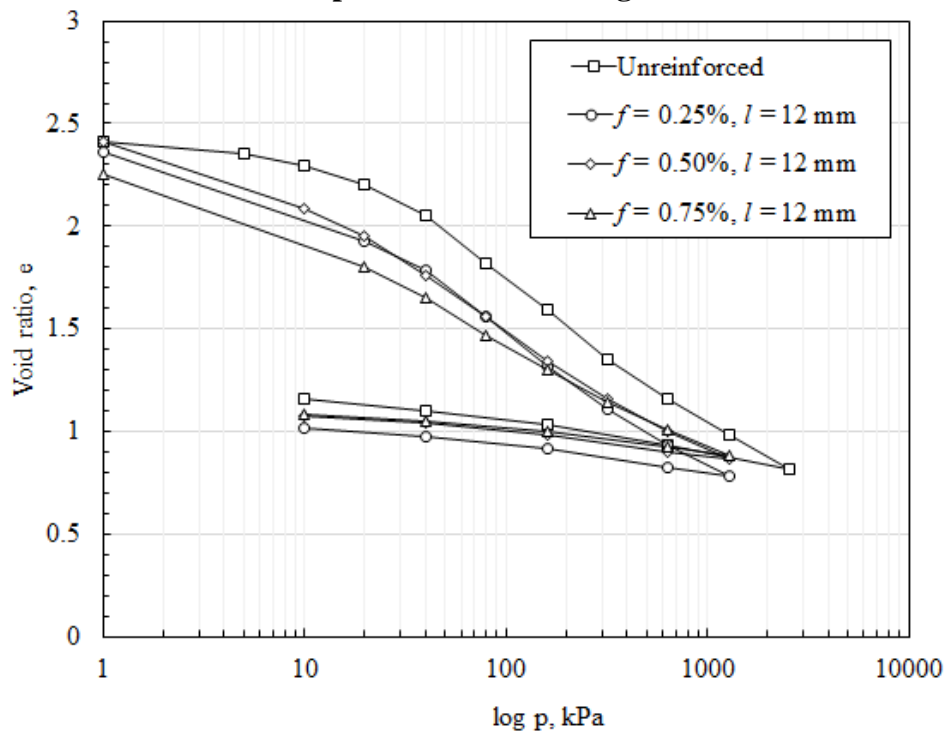
Figure 4.18 Void ratio versus pressure applied curve for unreinforced and fiber reinforced specimens of fiber length l = 12 mm
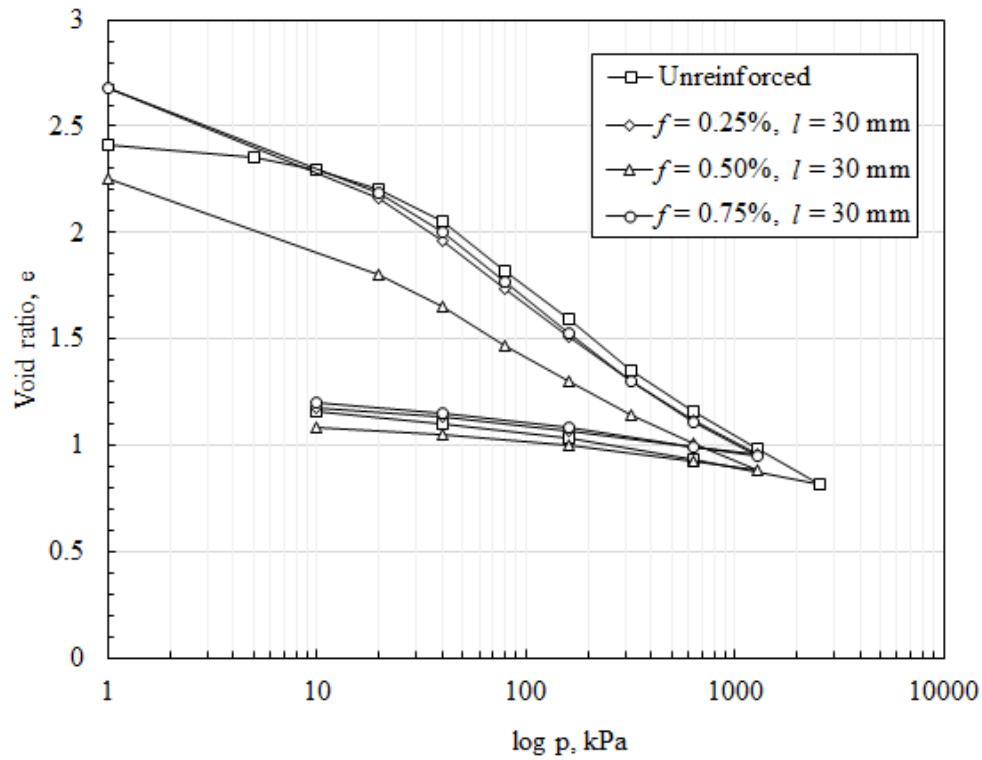
Figure 4.19 Void ratio versus pressure applied curve for unreinforced and fiber reinforced specimens of fiber length *l* = 30 mm
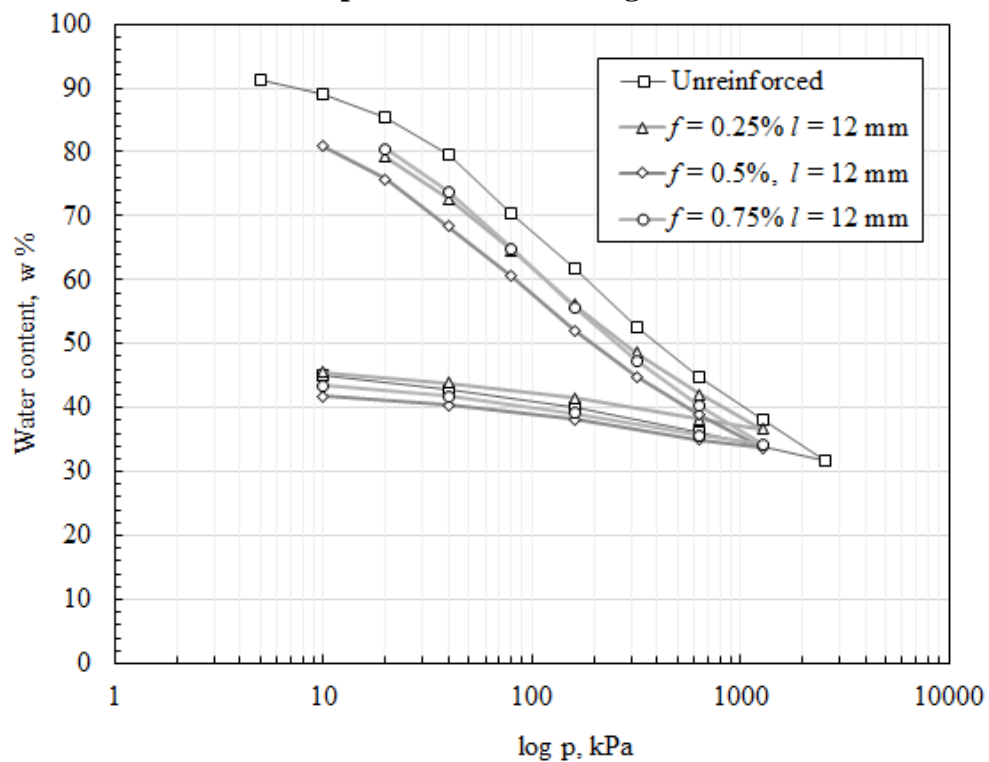
Figure 4.20 Water content versus pressure applied curve for unreinforced and fiber reinforced specimens of fiber length *l* = 12 mm
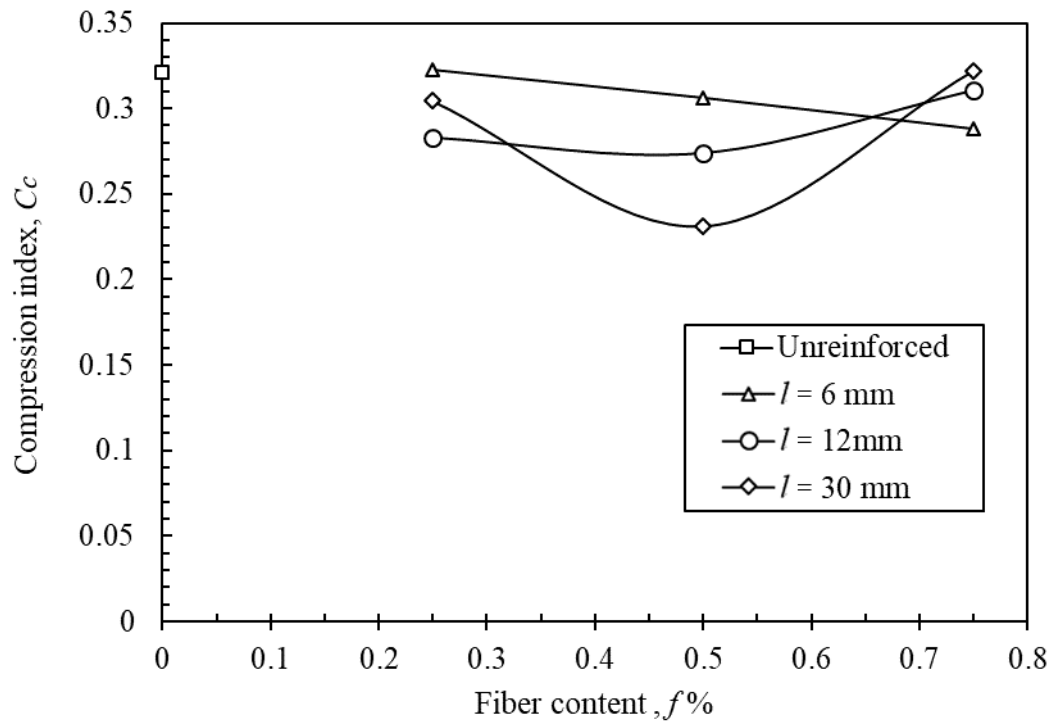
Figure 4.21 Variation of compression index with varying fiber content for unreinforced and fiber reinforced clay

For a normally consolidated clay, it is possible to express the compressibility property of the soil by noting the slope of the straight-line portion of the void ratio versus pressure curve. Figure 4.21 shows the variation of compression index of expansive clay with and without fiber inclusions. The compression index, C_c for all fiber reinforced soil specimens are found to be lesser than unreinforced soil specimens, indicating that higher settlements will be experienced in unreinforced soil specimens.

Evaluation of permeability

The magnitude of soil's permeability is one of the primary characteristics used to judge its acceptability for containment structures (i.e., landfill covers and bottom liners). Therefore, the effect of fiber inclusion on the permeability of the clay soil was evaluated. The coefficient of consolidation was calculated from the time-settlement data obtained from both consolidation oedometer tests and triaxial tests. This value was used to determine the shearing rate for triaxial tests. The coefficient of consolidation, c_v was determined using Equation 4.1, based on the Taylor method (settlement vs. square root time).

$$c_v = \frac{T_{90} H_{dr}^2}{t_{90}}$$

(4.1)

Where, T_{90} is the time factor for 90% consolidation, taken as 0.848. The drainage path length H_{dr} (in this case half the total initial height as two-way drainage was taking place), and t_{90} is the time taken for 90% consolidation to complete. This is determined using Taylor's square root of time method (Taylor 1948). The coefficient of volume change m_v, was calculated for all soils between the increment increases from 20 kPa to 40 kPa using the following formula.

$$M_v = \frac{\Delta e}{(1+e_0)} \frac{1}{\Delta \sigma'}$$

(4.2)

Where Δe is the change in void ratio between the steps, e_o is the initial void ratio for the time step and $\Delta \sigma'$ is the incremental effective stress change between the steps. Finally, the permeability, k

$$k = c_v m_v \rho_w g$$

(4.3)

Where ρ_w is the density of water taken as 1 g/cm^3 and is the acceleration due to gravity (9.81 m/s^2). As the permeability varied with stress, the average permeability was calculated and shown in Figure 4.22 and Figure 4.23 for each fiber content and fiber length combinations and compared with unreinforced soil.

 "The permeability of cracked fiber reinforced soil specimens is greater than the unreinforced specimens. One explanation for this behaviour is the fact that more voids are present in a fiber reinforced soil specimen. Therefore, the fiber strings will have greater opportunity to make pathways for the water to pass through the soil specimen than that of unreinforced soil. The test results indicate an increase in the permeability value as the fiber content is increased from 0.0% to 0.75%. A slight decrease in the permeability value can be seen for fiber content f = 0.5% in Figure 4.22. However, the magnitude of this increase is within the experimental error. The test results show a continuous increase in hydraulic conductivity as the fiber content increases beyond that.
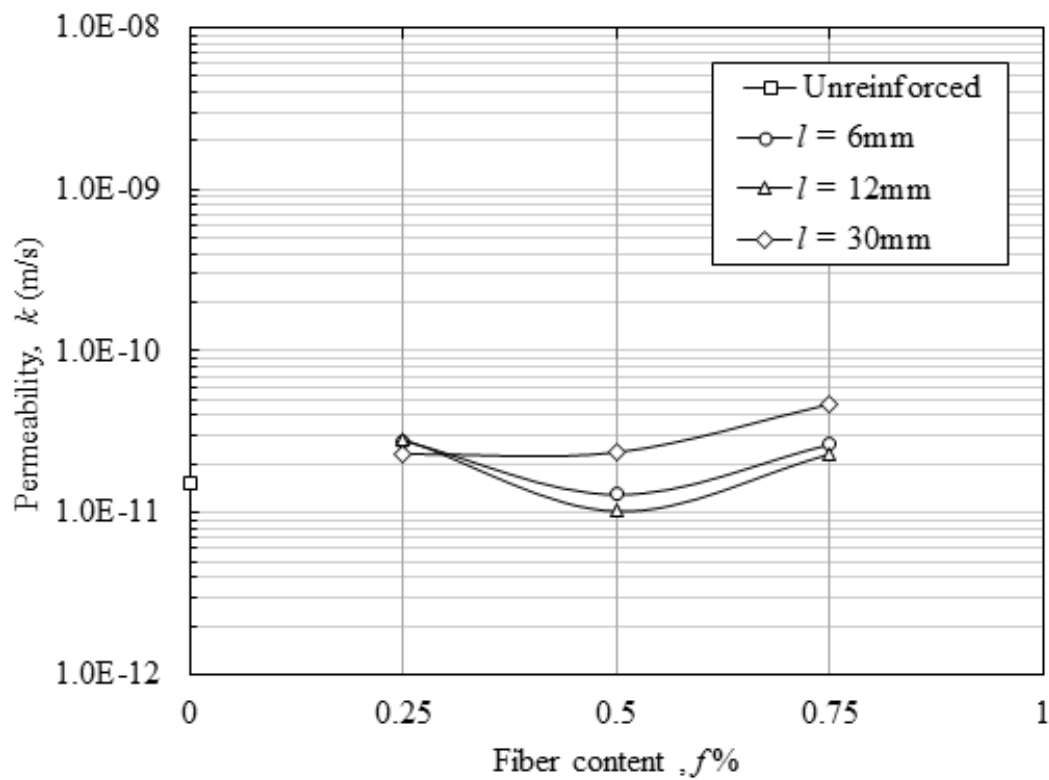
Figure 4.22 Variation of permeability of unreinforced and fiber reinforced soil specimens with varying fiber content for incremental stress, $\Delta\sigma = 20$ kPa
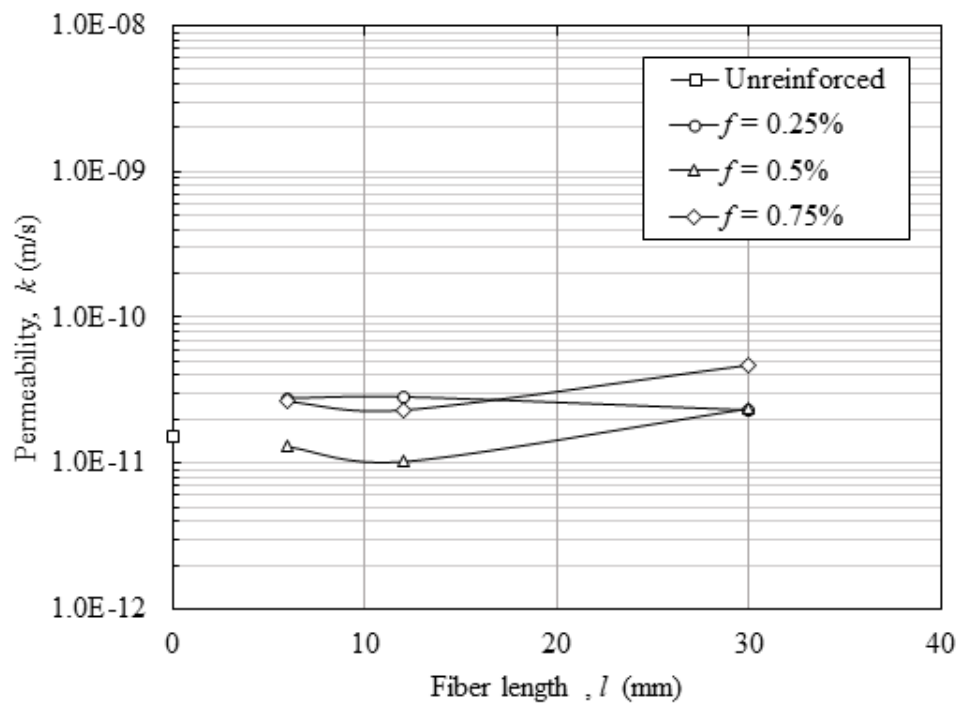
Figure 4.23 Variation of permeability of unreinforced and fiber reinforced soil specimens with varying fiber length for incremental stress, $\Delta\sigma = 20$ kPa

Similarly, Figure 4.23 shows variation of permeability values with an increase in fiber length. The curve for permeability values for f = 0.25% shows that the change in fiber length does not have a strong bearing on permeability values. As the fiber content is percent by dry weight of soil, very few numbers of fibers are present in the specimen causing less number of pathways for passage of water. Nevertheless, for other fiber contents, a considerable increase in permeability is seen for specimens reinforced with longer fibers like l = 30 mm. The longer fiber lengths provide longer pathways for the water to permeate through the specimen than that of in specimens with shorter fibers. Also, longer fibers at higher fiber contents get clustered during mixing that form pockets that allow water passage through the specimen."

4.5 Closure

Geotechnical properties of the selected soil and geofiber materials were presented. Physical, chemical, mineralogical, suction and strength characteristics of the expansive clay were evaluated and discussed. The desiccation characteristics and tensile strength of expansive clay were obtained. Three types of geofibers were used in the present study namely polyester fibers (PET), polypropylene fibers (PP) and polypropylene-tape (PP-T) fibers. The properties and suitability of the fibers used in the study were discussed. The PP and PET fibers have a trilobal cross section with an effective diameter of ~40 μm, which may help in interlocking between the soil particles. The PP-T fibers have a flat surface with rectangular cross-section of width 2 mm and thickness of 0.02 mm. PP-T. Tenacity of PET, PP and PP-T fibers was 3-5 gm/denier, 4-6 gm/denier and 5.45 gm/denier, respectively. Liquid limit, plastic limit and shrinkage limit of unreinforced and fiber reinforced soil was performed. The liquid limit was found to increase with increase in fiber length, l (mm). However, no significant variation in plastic limit and shrinkage limit was found. One-dimensional consolidation tests were performed to determine the consolidation properties of unreinforced and fiber reinforced soil. Permeability of the unreinforced and fiber-reinforced soil blends were computed from the one-dimensional consolidation test results. Permeability values derived from the consolidation tests revealed that the permeability of unreinforced clay increased by 50-200% when reinforced with fibers.

Chapter 5

LABORATORY TESTS ON DESICCATION CRACKING OF UNREINFORCED AND FIBER-REINFORCED EXPANSIVE CLAY

5.1   Introduction

Clay-rich soils having low hydraulic conductivity are used in waste containment systems like landfill liners and covers. Since expansive clays have a high clay content and low hydraulic conductivity (in the order of 1×10^{-9} m/s,) they can potentially be used as an impervious barrier material in landfill lining systems. However, due to their shrink-swell nature, they have a tendency of severe desiccation cracking leading to distress in impervious barriers of landfill lining systems. Even distribution of fibers within the clay mass is paramount in attaining effective fiber reinforcement for improvement in desirable engineering properties of soil. Hence, the primary objective of this work is to develop a methodology for the mixing of soil

and fibers and to assess the potential of the polyester fibers reinforcement in restraining desiccation cracking in expansive soils, so that the influence of the fiber content, *f*, and the fiber length, *l*, can be assessed. The second objective is to understand the desiccation cracking of the expansive clay with and without fiber reinforcement inclusions by using Digital Image Analysis (DIA).

5.2   Experimental test setup

The test setup consisted of illumination assembly, heating assembly and weighing balance. The illumination and heating assembly 500W Tungsten Halogen lamp, as shown in the schematic setup in Figure 5.1. All tests were performed at a constant temperature of 50ºC and relative humidity of 20% Rh, as recorded in the thermo-hygrometer that is located close to the setup.
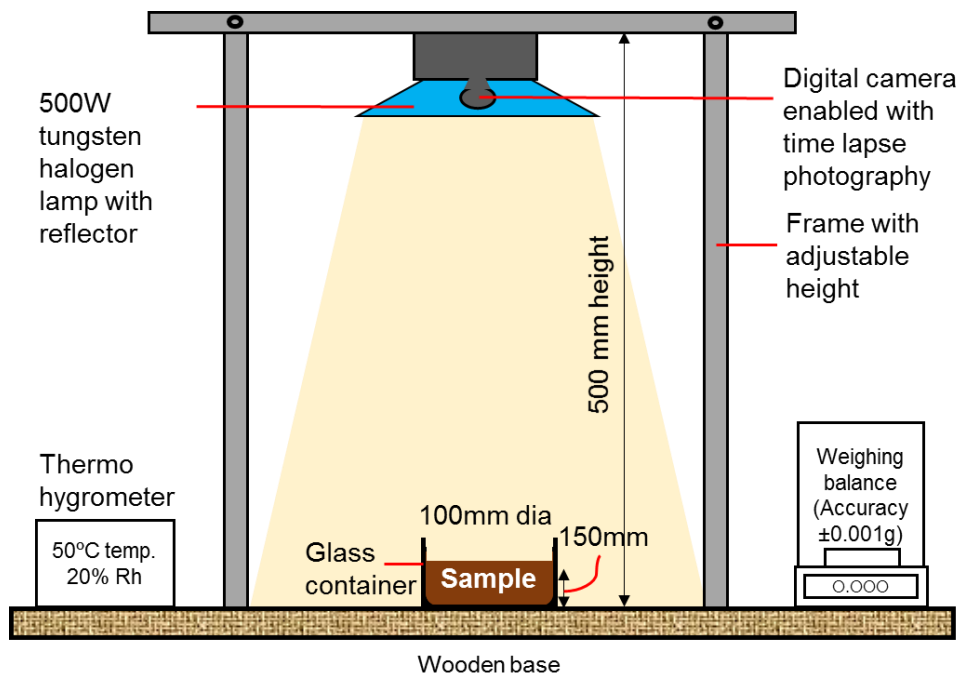
Figure 5.1 Schematic representation of laboratory desiccation cracking test setup

A digital camera, (TG850, Olympus) that was equipped with an interval timer was used to capture images of the drying soil specimen every five minutes. Desiccation cracking tests on expansive soil with and without fibers were carried in a graduated cylindrical Borosilicate Glass

container of 100 mm diameter and 50 mm height. A transparent sheet with markers was attached below the cylinder for scale measurement in image analysis.

5.3 Test procedure and test program

The clay was oven-dried, crushed, and sieved through a 425 µm sieve. Different fiber contents (0%, 0.25%, 0.5%, and 0.75% by dry weight of the soil) were used for fiber lengths of 15 mm, 30 mm, and 50 mm in the preparation of fiber-reinforced clay specimen, as shown in Table 5.1.

Table 5.1 Test program for the desiccation cracking tests

Test No	Test legend	Specimen type	f (%)	l (mm)
1	T1	UR	-[a]	-[a]
2	T2	FR	0.25	15
3	T3	FR	0.50	15
4	T4	FR	0.75	15
5	T5	FR	0.25	30
6	T6	FR	0.50	30
7	T7	FR	0.75	30
8	T8	FR	0.25	50
9	T9	FR	0.50	50
10	T10	FR	0.75	50

UR- Unreinforced; FR- Fiber reinforced; l =Fiber length; f =Fiber content; [a] not relevant/not used

Initially, a mix of dry clay and fibers was prepared, to which water was gradually added to make a slurry. All specimens were prepared close to the liquid limit of the soil. The prepared slurry was poured into a borosilicate glass container (100 mm in diameter) to achieve a specimen thickness of 15 mm, i.e. aspect ratio of 10.33 was maintained.

A specimen height of 15 mm was considered to produce distinguishable crack patterns to compare the effect of fiber content and fiber length. A quantitative analysis suggests existence of minimal aspect ratio of around 5.8, below which no macroscopic cracks occur in the material (Colina and Roux 2000). In the present study, the effect of varying clay layer thicknesses was not considered.

The container with soil slurry was tapped gently on a wooden platform to remove the air bubbles. The inner surface of the glass containers used in the study was free from any scratches, protrusions, and depressions, to provide a uniform drying surface. The prepared specimens were covered with a plastic film and stored inside a desiccator for about 17 hours to allow the soil-fiber mixture to hydrate uniformly.

5.4   Analysis of test results

The desiccation tests were continued till 8 hours for all cases. Moisture content, depth and surficial measurements by digital image acquisition system were analysed. Performance of the setup, image processing, image analysis and results and interpretation of results are discussed in the following sections.

5.4.1 Digital image analysis

Digital image analysis is reliable for surficial crack characterization and has been gaining popularity due to its versatility (Miller et al. 1998; Bhadriraju et al. 2005). An image is a mosaic of very small areas, called pixels, filled with a single grey level or digitally defined colour. Thousands of pixels, touching each other and placed within a grid provides a realistic, smooth image. The basic principle of Digital Image Analysis is sequential storage and transformation of the pixel nature of computerized images to matrices of numbers (Wojnar 1999). Four permanent markers, whose co-ordinates are predefined, are fixed on a transparent sheet, as shown in Figure 5.2, forming a rectangular grid having model dimensions 110 mm in length

and 110 mm in breadth. Since the digital image is a matrix of numbers of pixels, with the help of mathematical functions basic image enhancements such as contrast and brightness control, colour balance and corrections, image blur and anti-aliasing, dust and scratches removal can be performed. In the present study, all images were enhanced using Microsoft PowerPoint 2013.

Digital image analysis was carried out using ImageJ (1.50a) software. ImageJ (Figure 5.2) is a public domain Java based software. It is a popular software among researchers in field of biology and medical imaging. ImageJ software (Abramoff et al. 2014) was extensively used by Lakshmikantha et al.(2012) to characterize the statistical features of crack patterns in drying soils. Following steps were followed for processing each image:

a) Since the software captures image pixels based on its saturation value, very fine cracks cannot be captured by the software during binarization. Therefore, such cracks are highlighted manually using paintbrush on MS Paint.
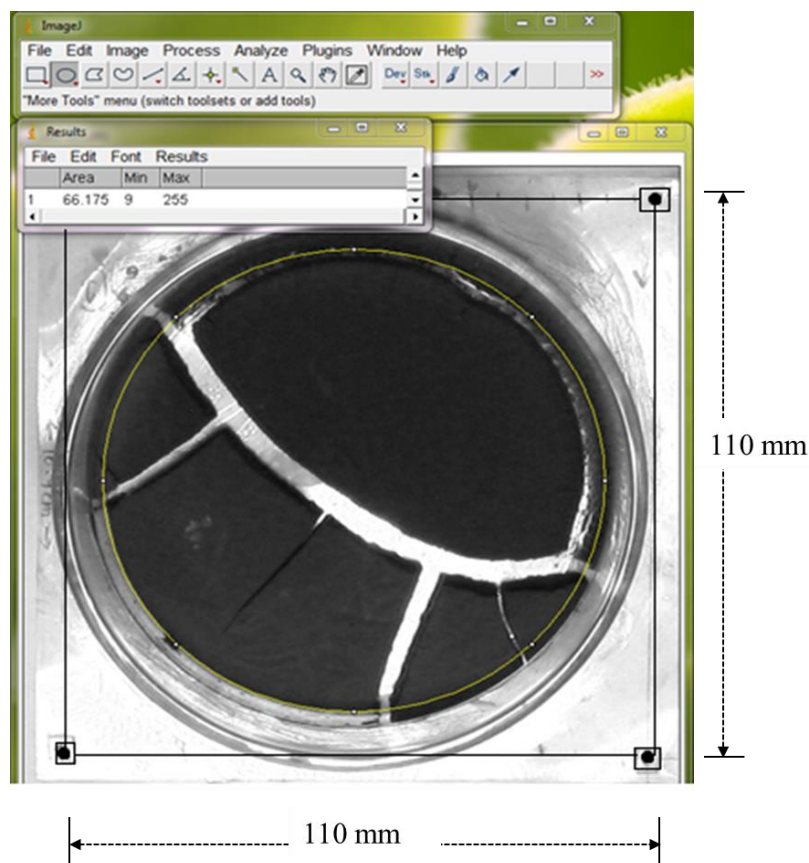
Figure 5.2 Screen shot for crack area measurement in ImageJ estimation during digital image analysis (DIA)

b) The image pixels colours are split from normal RGB into RGB stack image to separate the Red, Green and blue colours.

151

c) The process of conversion of grey scale image to binary image is called binarization. There are several advantages of binary images. Finer features are more distinct in a binary image. The most important application is that, binary image can be employed for counting objects and for measurement of area, perimeter, diameter, deviation moments, location of a centre of gravity, etc. (Wojnar 1999). Therefore, the stack image was converted to binary image by the function tool to capture the cracked portion as black and soil as white. The resultant cracked image looks like the image show in Figure 5.3.

d) The markers set on sample container were measured in software and set as scale. The total cracked area (A_t) is measured using Measure function tool before binarization. After conversion to image to Binary image, the area of black pixels is measured, thus the area of cracks.
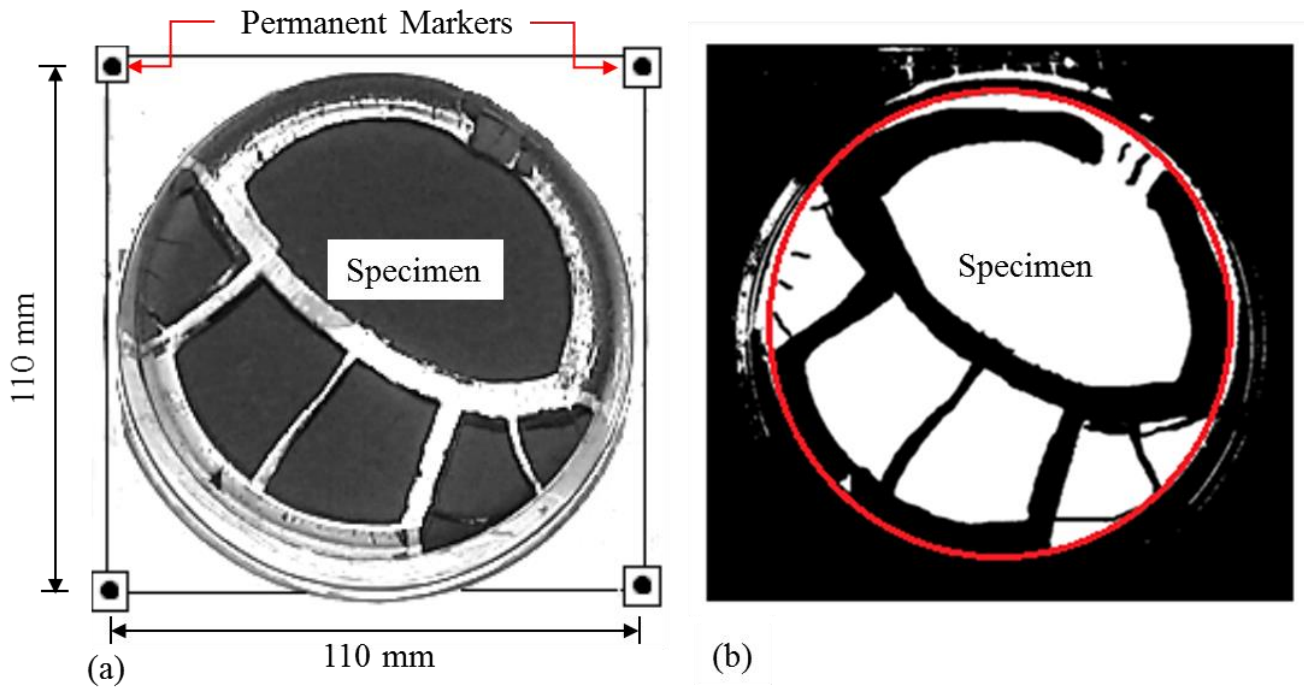
Figure 5.3 (a) Crack formation in unreinforced soil, (b) Binary mage of (a) in ImageJ software

Quantification of geometric features of cracks like length, width and depth is important as they are directly proportional to the hydraulic and mechanical behaviour of soil. Crack intensity factor, CIF (Miller et al. 1998) is a measure of the severity of surficial cracks and is defined as ratio of area of cracks to the total cracked region at a given time.

$$CIF = \frac{A_c}{A_t} \qquad (5.1)$$

Where,

CIF = Crack intensity factor

A_c= Area of cracks in mm^2, excluding uncracked area

A_t= Total cracked area in mm^2, including cracked and uncracked area

The average area of the cells into which the specimen is divided, the average crack opening width, the average spacing between two cracks, and the total cracked area were measured. Linear measurements such as the width of the crack opening and the average spacing were measured in a grayscale image. Area measurements such as the total cracked area and the cell area were measured by converting the grayscale image to a binary image.
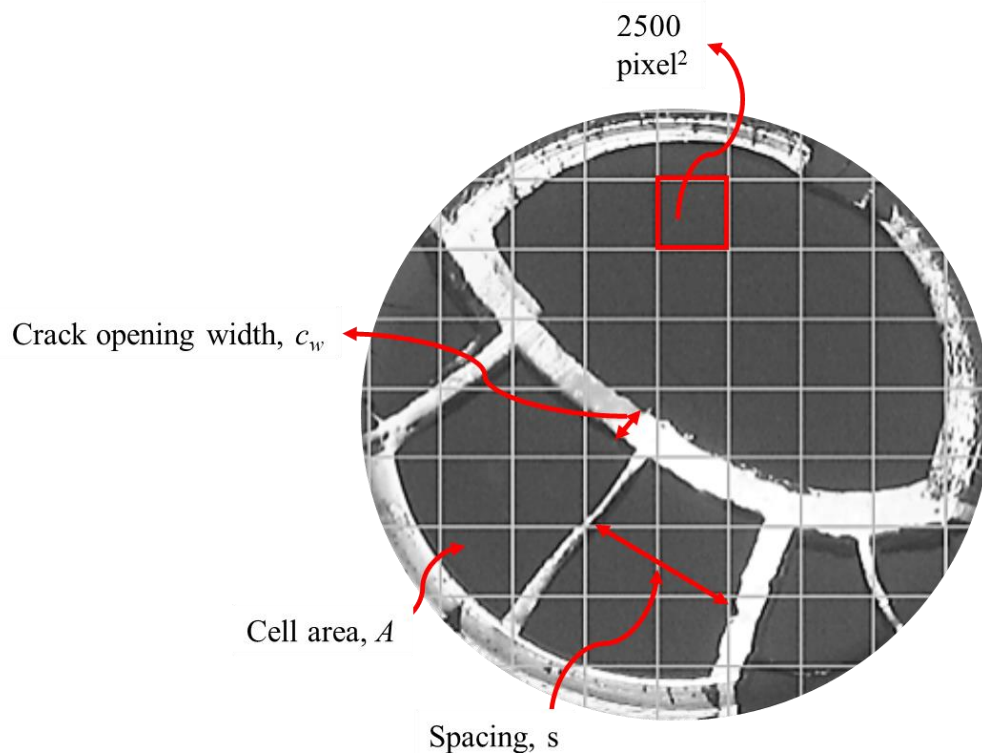
Figure 5.4 Terminology used for crack feature measurements that are used in the present study

A special function in ImageJ was used to measure the quantities from the binary image. The basic crack feature terminology adapted is represented in Figure 5.4. The image was divided into equal parts, such that each grid measured 2500 square pixels. The crack features in each grid were measured in order to obtain an average of the measurements of the crack.
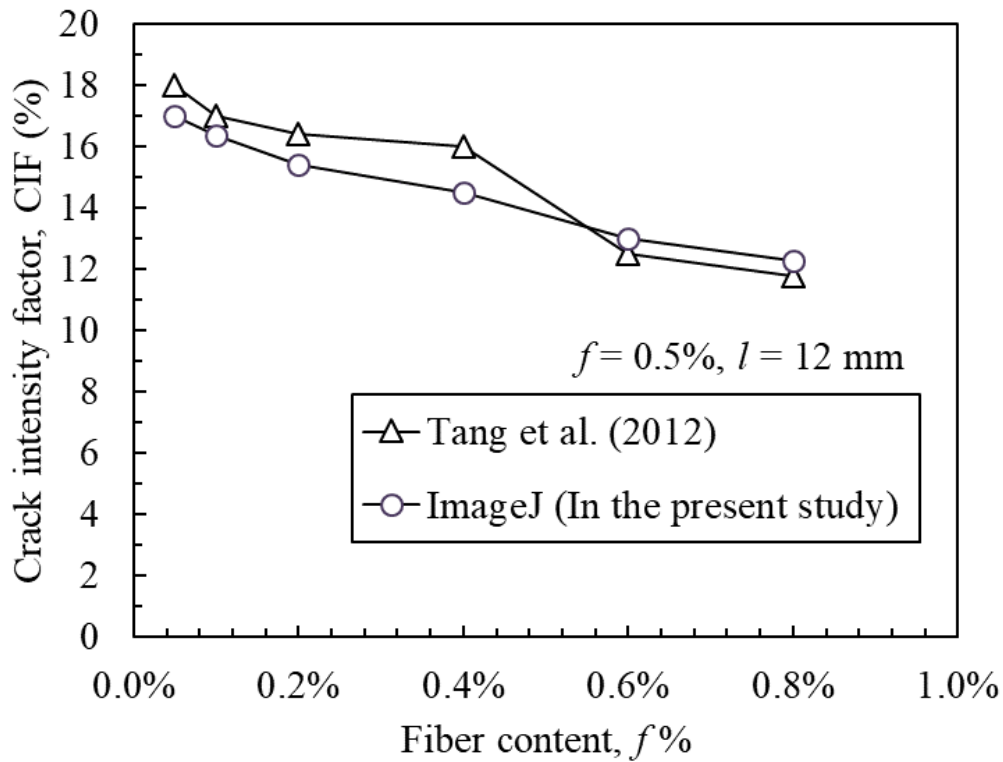
Figure 5.5 Validation of crack measurement in the software ImageJ

The validation of the accuracy of measurement by the software ImageJ was performed. The crack intensity factor from the study of Tang et al. (2012) were measured using ImageJ and compared with the values of CIF reported in their study. Figure 5.5 shows the comparison of CIF values measured in ImageJ and measured in the study by (Tang et al. 2012). The measured values from ImageJ were found to be matching with the results in the study with an error of $\pm$ 6-9%.

5.5   Analysis of results

The results obtained from the laboratory desiccation tests are described in detail in the subsequent section. The results include the crack morphology, moisture content variation during desiccation, time and moisture content during occurrence of first crack, crack intensity factor and degree of saturation. All the results are calculated for unreinforced black cotton soil

and soil reinforced with fiber length 15 mm, 30 mm and 50 mm at 0.25%, 0.5% and 0.75% fiber content.

5.5.1 Crack morphology and cell area

Nahlawi and Kodikara (2006) classified desiccation crack types as primary, secondary, and tertiary. The first set of cracks that is generated within the clay mass is called primary cracks, which subsequently in turn divides to form secondary and tertiary cracks. Figure. 5.6 shows typical appearance and evolution of cracks in unreinforced and fiber-reinforced specimen at three different desiccation times of 150 minutes, 300 minutes, and the time at which time the test was terminated, i.e. 450 minutes. The unreinforced soil specimen forms a characteristic hierarchical cracking pattern, primarily governed by subdivision (Costa et al. 2013).

t_e = 150 min. t_e = 300 min. t_e = 450 min.

a) Unreinforced [Test: T1]

t_e = 150 min. t_e = 300 min. t_e = 450 min.

b) Fiber reinforced [f = 0.50%; l = 15mm; Test: T3]
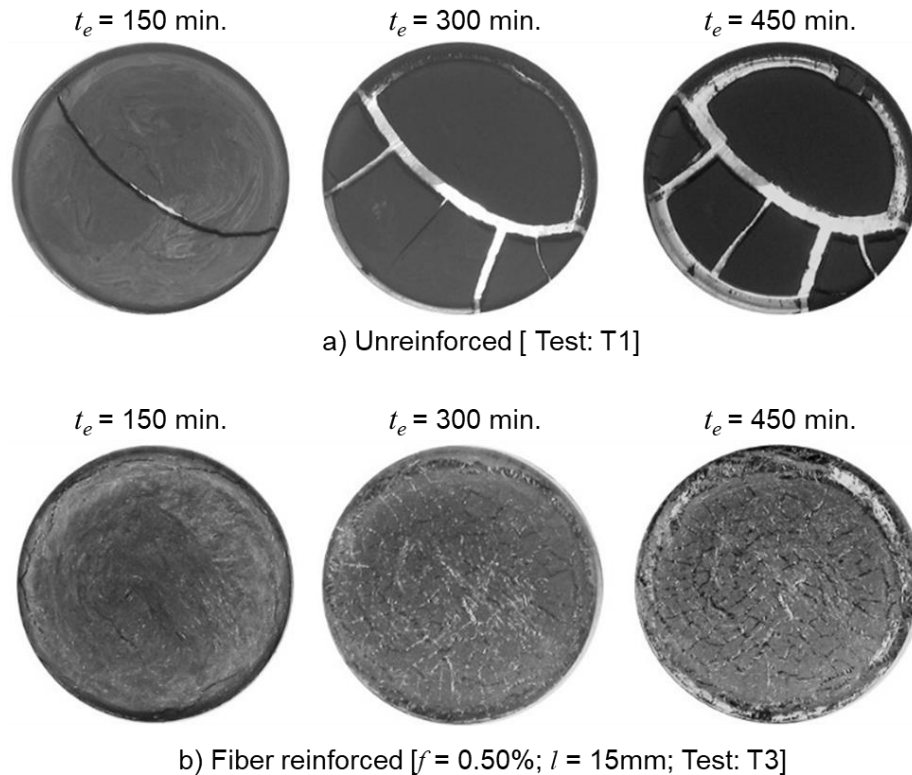
Figure 5.6 Evolution cracks in the soil sample with time for (a) Unreinforced soil, (b) Soil reinforced with 15 mm length fiber at 0.5% fiber content

The primary cracks propagate faster through the entire depth. They are longer, wider, and divide the clay mass into large cells. The cells subsequently shrink upon drying generating large crack widths, as presented in Figure 5.6. However, in specimens with fibers added, the cracks are short and jagged, and the average cell area (A) has reduced drastically along with the crack widths, as shown in the histograms. The average cell area for the unreinforced specimen is 232.65 mm^2; it decreases to 38.6 mm^2 for the fiber-reinforced soil specimen with $f = 0.5\%$ and $l = 15$ mm. It is also worth noting that the crack cell area in reinforced clay is much more uniform than for the unreinforced clay. This helps to keep the crack widths also relatively uniform, which is important from an overall hydraulic conductivity point of view.

5.5.2 Crack propagation

Usually, an internally generated crack tends to propagate from both of its ends till it intersects another crack or in contrast, edge generated cracks would propagate until it meets another existing crack at mostly right angles due to stress relief perpendicular to the existing crack (Morris et al. 1992). The intersection angle between two cracks is almost orthogonal in clays. However, the orthogonality of the cracks changes in the fiber-reinforced soil specimen. The non-orthogonality of cracking pattern occurs due to non-uniform drying, lower thickness of soil layer and variable ground conditions (Kodikara et al. 2002).

The presence of fibers changes the intrinsic propagation and release of the developed tensile stress through the thickness of the soil. An irregular network of cracking pattern consisting of non-orthogonal cracks with intersection angle less or more than 90º is observed. The intersection angle may be considered as a function of the orientation and distribution of fibers in the clay mass during crack initiation. The presence of fibers may cause bifurcation or diversion of single propagating crack. However, more study at micro-structure level during crack propagation is needed for better understanding.

5.5.3 Crack feature measurements

The crack features including the average crack width, spacing, cell area, the final crack intensity factor, and the average shrinkage strain for the unreinforced and fiber-reinforced soils at the end of all tests were measured using digital image analysis, as summarized in Table 5.2.

Crack width

The crack opening width was determined by measuring the shortest distance from one randomly chosen to point on the boundary of one cell to the boundary of the opposite cell. As the soil desiccation progresses further, for all specimen the crack opening width or the crack width, w_{avg}, increases until it becomes generally stable at the end of desiccation for the given environment, as presented in Figure 5.8. The hydraulic conductivity of the desiccated soil is a function of the width of crack. Fluid flow through a single crack is commonly described by parallel plate model. For the theory of laminar flow between parallel plates, the flow rate is proportional to the cube of the spacing between the plates (Witherspoon et al. 1980), which gives an indication of this dependency. Hence, the wider cracks will dominate mass hydraulic conductivity of soil and allow a larger quantity of flow through the cracks, thereby increasing the overall hydraulic conductivity of a clay layer (He et al. 2015). As can be seen from Figure 5.9, the crack widths observed at the point of crack initiation (or initial crack widths) were reduced monotonically as the fiber content increased.

Crack spacing and depth

The crack spacing, s is the shortest distance between one point on the boundary of a cell and the point on opposite boundary of the same cell. The crack spacing or cell area depends on the thickness of the soil layer, the desiccation rate, and the base material (Corte and Higashi 1964). However, some variation is observed in the case of the fiber-reinforced soil specimen, because the cells are irregular, non-uniform and jagged. The average crack spacing (s_{avg}) decreases on inclusion of fibers and keeps on decreasing as the soil shrinks, as presented in Figure 5.10.

Table 5.2 Crack feature measurements at the end of all tests determined using image analysis

Test No	Test legend	f (%)	l (mm)	$c_{w, avg}$ (mm)	s_{avg} (mm)	A_{avg} (mm^2)	CIF (%)	ε_{avg} (%)
1	T1	-[a]	-[a]	6.0±0.21	13.2±2.05	232.6±97.2	37.9	19±1.23
2	T2	0.25	15	1.9±0.15	5.6±1.90	35.7±5.67	25.7	13±1.46
3	T3	0.50	15	1.6±0.18	6.6±1.93	38.7±4.10	12.7	11±1.19
4	T4	0.75	15	2.3±0.18	4.0±1.78	24.8±4.92	23.9	15±1.04
5	T5	0.25	30	2.3±0.17	8.6±1.85	66.3±9.12	19.7	14±1.11
6	T6	0.50	30	1.7±0.15	4.2±1.97	19.7±3.46	15.9	16±0.98
7	T7	0.75	30	2.7±0.19	5.7±1.89	38.7±5.76	27.4	17±1.90
8	T8	0.25	50	2.5±0.19	7.4±1.71	60.3±7.99	19.6	17±1.02
9	T9	0.50	50	2.0±0.20	5.5±1.82	35.6±3.43	23.8	19±1.27
10	T10	0.75	50	3.0±0.19	6.7±1.95	47.7±6.62	27.2	19±1.87

$c_{w, avg}$ = Average crack width; s_{avg} = Average crack spacing; A_{avg} = Average cell area; CIF = Crack Intensity Factor, ε_{avg} = Average shrinkage strain; l = Fiber length; f = Fiber content

The final crack widths (at the end of desiccation), $w_{avg,final}$ of fiber-reinforced soil specimens were generally observed to be always less than the unreinforced soil specimen, as shown in Figure 5.9. Average shrinkage strain was manually computed using ImageJ and is defined as the ratio of change in length of a cell to the original length (Figure 5. 7). It is given by,

$$\varepsilon = \frac{(\delta_1 + \delta_2)}{L} \tag{5.2}$$

Where, L is the length of the cell under consideration. $\delta 1$ and $\delta 2$ are the change in the length of cell due to shrinkage.

$$\varepsilon = \frac{(\delta_1 + \delta_2)}{L}$$
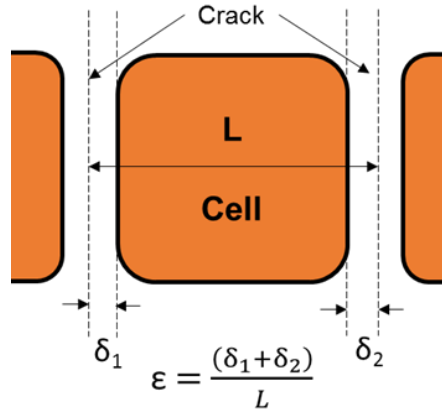
Figure 5. 7 Shrinkage strain of soil

The initial crack spacing is approximately halved with the addition of fibers with similar effects on the final crack spacing. The ratio of average of all final spacing values to the corresponding depth of specimen at the end of the test is defined as $(s_{avg})_{final}/d$. Figure 5.11 shows the variation of $(s_{avg})_{final}/d$ for unreinforced and fiber-reinforced soil specimen for different f and l. The $(s_{avg})_{final}/d$ reduces with addition of fibers, and is found to be minimum for test T3, that is, soil reinforced with fiber, $f = 0.5\%$, $l = 15$ mm.
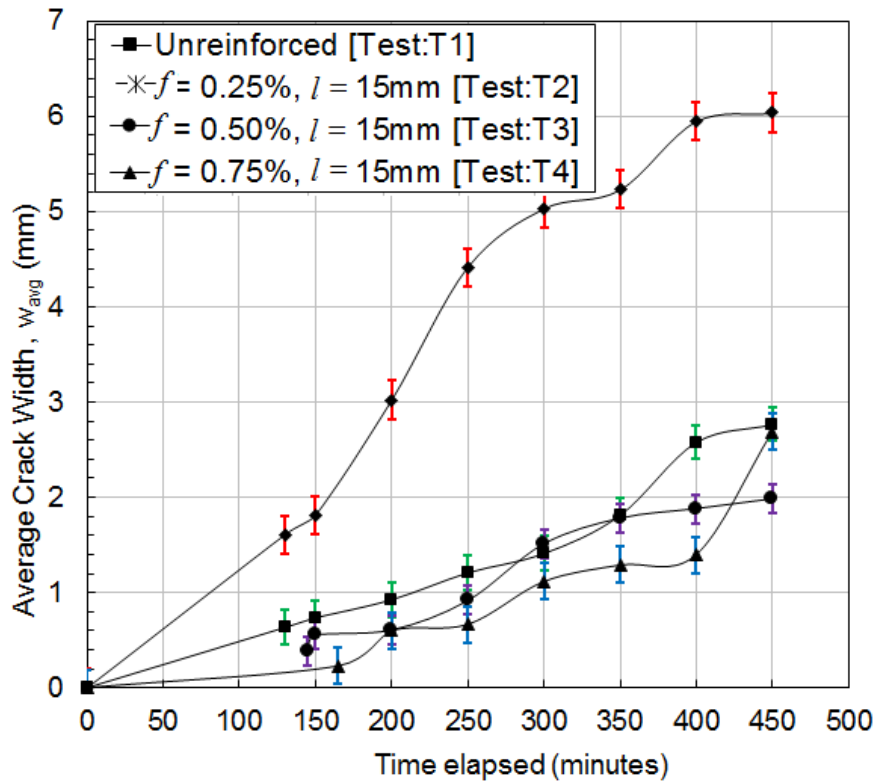
Figure 5.8 Variation of average crack width with elapsed time of test
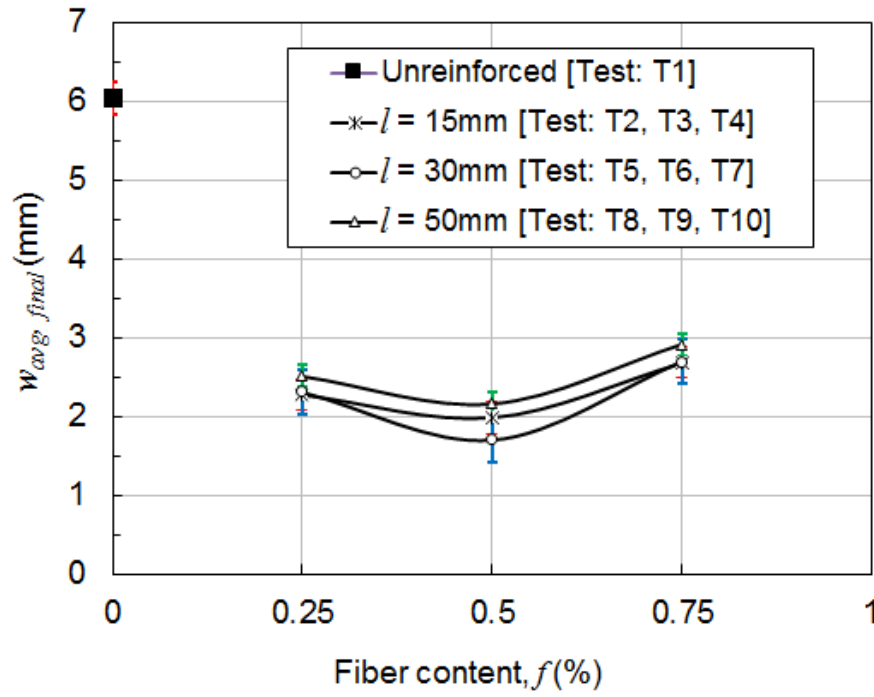
Figure 5.9 Variation of average crack width at the end of test with varying fiber content and fiber lengths
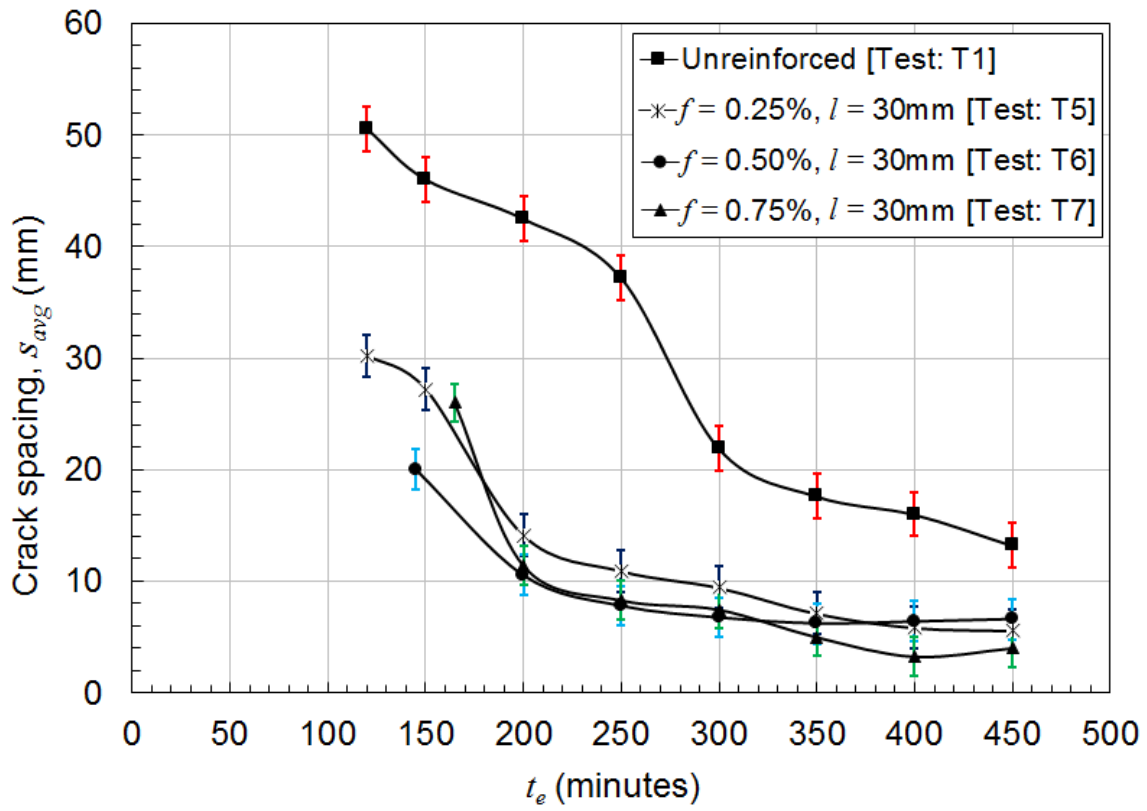
Figure 5.10 Variation of crack spacing, s_{avg} with time elapsed in minutes
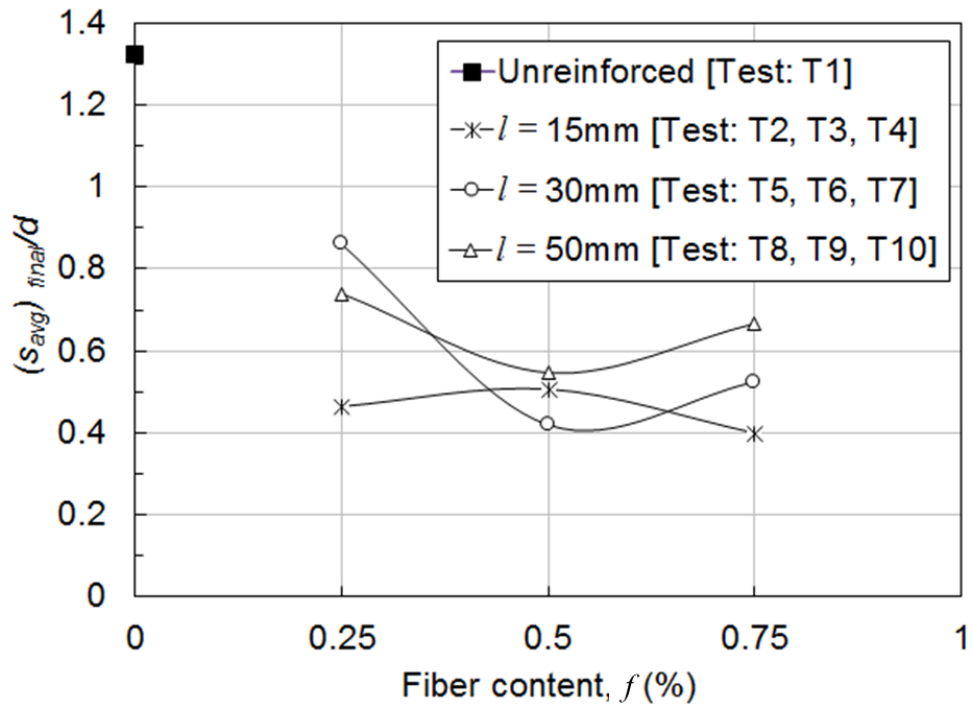
Figure 5.11 Variation of $(s_{avg})_{final}/d$ with fiber content for different fiber lengths

The cracks that formed in the fiber-reinforced soil specimen were relatively narrow, and the crack cells were still connected by the fibers, thereby providing overall stiffness to the clay mass despite cracking. The reduction in crack widths and maintaining certain stiffness within cracked layers were desirable properties for improved performance of a modified barrier system. The influence of different fiber content and length on final crack widths were marginal except that minimum final crack widths were observed for $f = 0.5\%$ and $l = 30$mm.

Crack intensity factor (CIF)

The typical variation of CIF and the water content for unreinforced (Test: T1) and fiber-reinforced soils (Tests: T5, T6, T7) is shown in Figure 5.12. At any water content, the CIF for the unreinforced soil is always higher than the corresponding CIF value of the fiber-reinforced soil. The finer, shorter, and irregular cracks in the fiber-reinforced soil give rise to the lower CIF which results in higher integrity of the soil specimen. The presence of fibers helps in reducing the crack width and the surficial area of cracks, which, in turn, reduces the crack intensity. Similar observations were reported by Miller et al.(2004), Qiang et al.(2014), Harianto et al. (2008) and Harianto (2014).

161
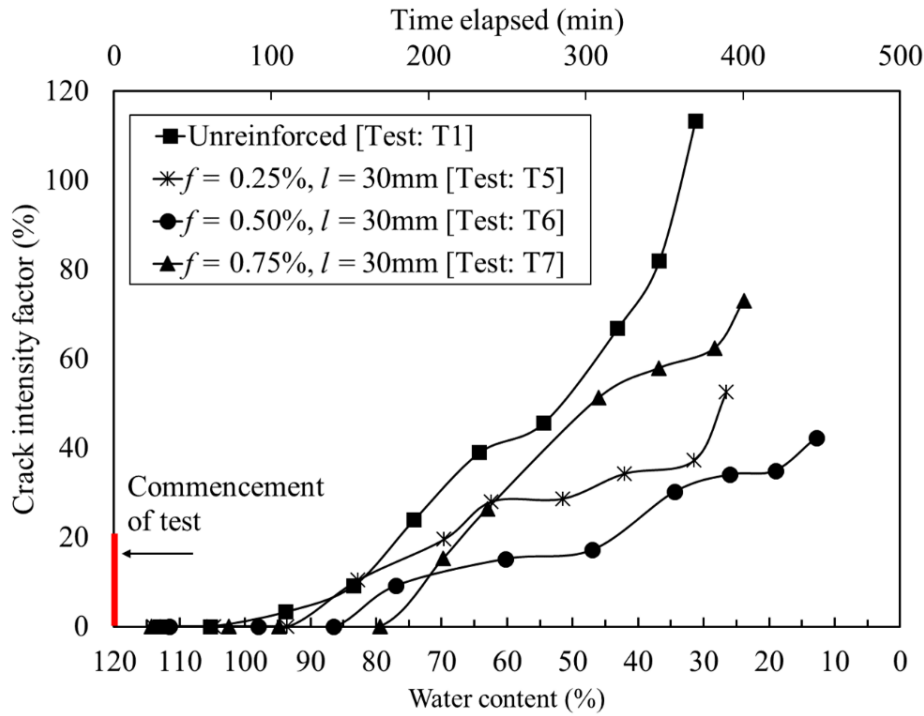
Figure 5.12 Variation of CIF for unreinforced (T1) and fiber-reinforced specimen (T5, T6, T7) with respect to water content

Another important observation is that the water content at which cracking commenced, decreased monotonically as the fiber content increased. As reported by (Costa et al. 2013), the cracks initiate when the tensile stress generated by soil suction reaches prevailing tensile strength of the soil. Therefore, this behaviour can be considered to occur due to the increase in mass tensile strength of clay with the addition of fibers. This effect can also explain the reduction in cell area with the addition of fibers as follows. Because of the increase in tensile strength (or decrease of moisture content at which cracking started) with the increase of fiber content, the strain energy stored in the soil mass increased at the onset of cracking. Since cracks derive energy to propagate from adjacent volume of soil and it needs only to create crack surface areas, this classic mismatch of volume to area leads to smaller cracking spacing when fracture energy is optimized in crack formation.

Shrinkage strain

Digital image-based measurement systems always give better results when compared to manual methods, because the uneven surface cracks are also taken into consideration during analysis.

162

The observed final shrinkage strain was computed for the unreinforced and fiber-reinforced soil specimen as presented in Figure 5.13.
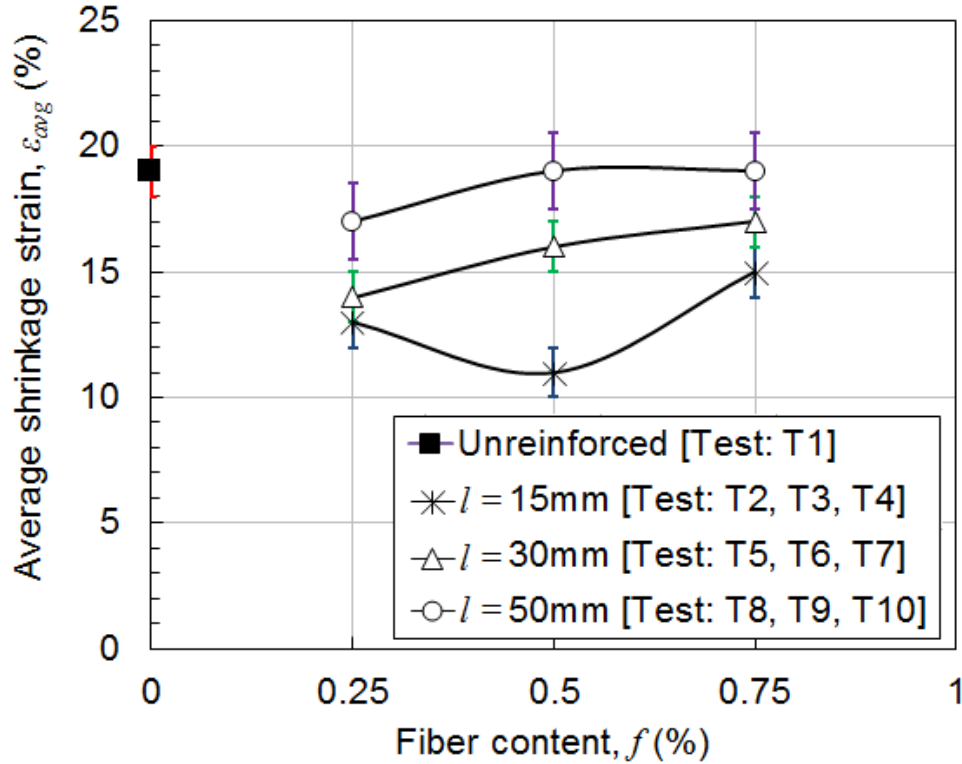
Figure 5.13 Shrinkage strain of expansive soil with and without fibers

Bhadriraju et al. (2005) attempted to measure the volumetric shrinkage strains of the fiber-reinforced expansive soil specimen using digital image analysis. It was found that fiber reinforcement reduces volumetric shrinkage strain by 15-24%. Considering that a cell of original length L shrinks by δ_1 from one side and δ_2 from other side, the shrinkage strain, ε is defined as the ratio of the change in the length of a cell due to shrinkage ($\delta_1 + \delta_2$) to the original length of the cell (L). For regular shapes, the shrinkage strain can be ratio of change in the dimension of crack spacing to the original crack spacing. There is a significant decrease in shrinkage strains for the specimen that are reinforced with 15 mm and 30 mm fiber lengths. Specimen with a fiber length of 50 mm were found to have almost the same shrinkage strain (18-20%) as unreinforced soil.

5.6   Discussion

5.6.1 Uniformity of fibers

The distribution of fibers in the clay mass is very crucial in maintaining the homogeneity of soil specimen, since cracks could occur along paths of least resistance. Therefore, the distribution of fibers in desiccated specimen was examined. The desiccated soil specimen was carefully cut, and soil-fiber mix chunks were selected from five equally placed different locations from each specimen, as shown in Figure 5.14. The initial weight of the chunk was measured for reference. Each chunk was then dissolved in water for 24 hours, dried, and sieved such that the fibers and soil were separated. The fiber content was computed for each case, as presented in the histogram in Figure 5.15. The standard deviation of the measured fiber contents at different locations was found to be 0.04 for l = 15 mm, 0.06 for l = 30 mm, and the maximum, that is, 0.39, for l = 50 mm fibers and f = 0.75 %.
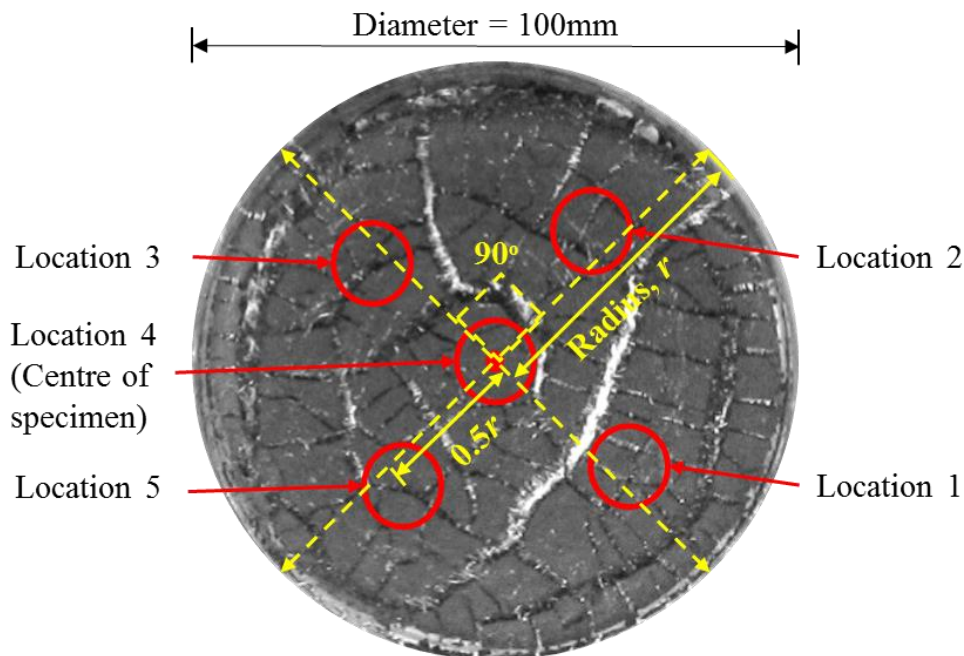
Figure 5.14 Locations for measurement of distribution of fibers on fiber reinforced specimen
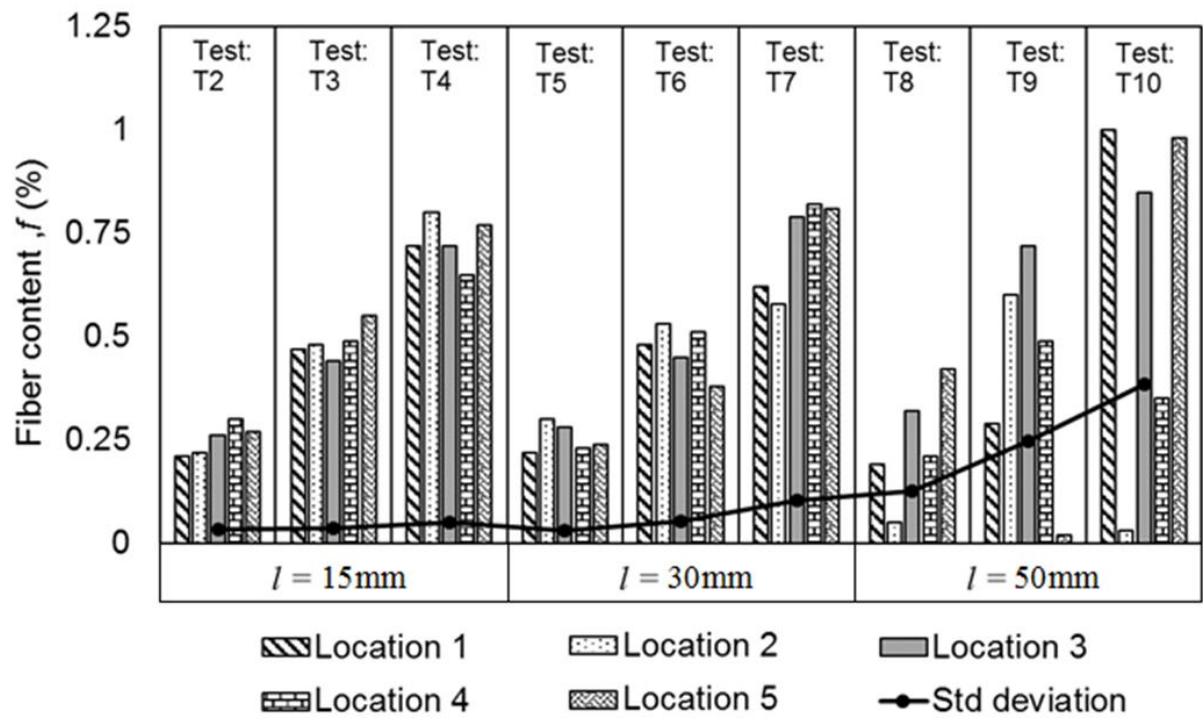
Figure 5.15 Distribution of fibers in reinforced soil specimen with varying fiber content and fiber length

(a) Test: T3
f = 0.5%, l = 15mm

(b) Test: T9
f = 0.5%, l = 50mm
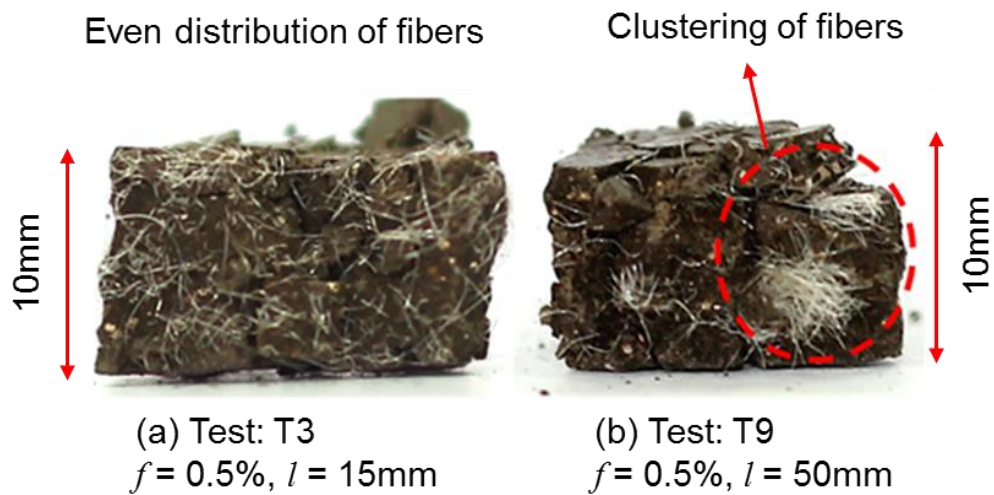
Figure 5.16 Distribution of fibers in reinforced soil specimen

Figure 5.16 shows the typical cross-section of fiber-reinforced soil chunks that were cut out of the desiccated soil specimen. The shorter fibers were noticed to be evenly distributed in the clay mass, as shown in Figure 5.16. The longer fibers undergo clustering and, thus, exhibit a non-uniform distribution of fibers, and this is not favourable for prevention of cracking.

5.6.2 Integrity of fiber-reinforced soil specimen

The performance of the clay barrier in the waste containment system is a function of its intactness or integrity. In these laboratory experiments, the integrity of the clay mass is severely affected due to desiccation cracking. Figure 5.17 illustrates the bridging effect due to fibers.

(a) Unreinforced, Test: T1

(b) Fiber reinforced, Test: T6, f = 0.5%, l = 30mm
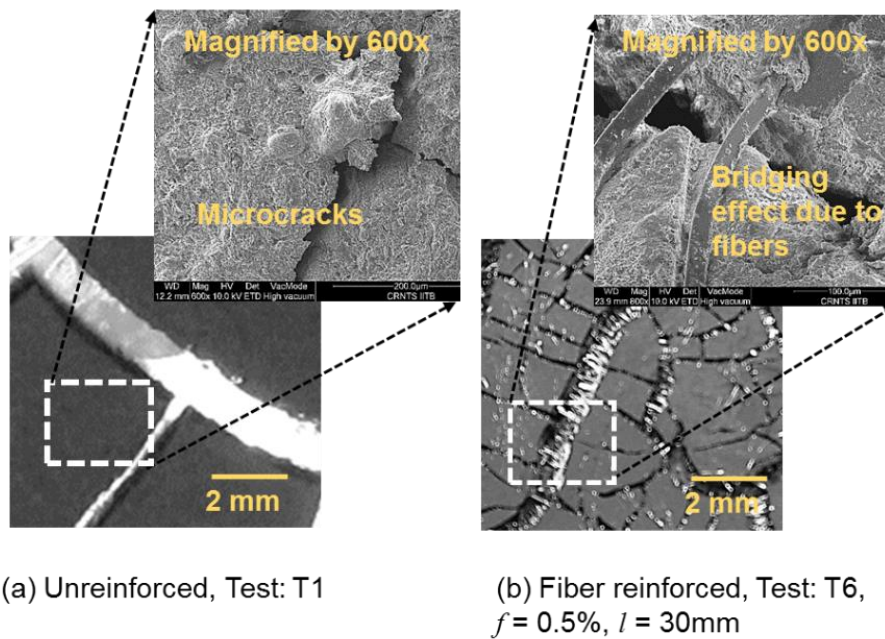
Figure 5.17 Crack formation in unreinforced and bridging effect of fibers in reinforced soil

The effective contact area and the normal stress between the soil and the fibers increases as the soil desiccates due to a decrease in moisture and associated increase in soil suction. This change increases the interfacial strength and helps the fibers to restrain the separating soil mass at crack initiation.

5.6.3 Crack reduction ratio

To cumulatively quantify the effect of fiber reinforcement on all crack measurements, Miller et al. (2004) introduced the Crack reduction ratio (CRR) in order to assess the performance of unreinforced and fiber-reinforced soils, and is given by,

$$CRR = \frac{CIF_n - CIF_f}{CIF_n}\%$$ (5.3)

CIF_n = crack intensity factor for unreinforced soil, and CIF_f= crack intensity factor for fiber-reinforced soil. The CRR was computed for fiber-reinforced soil specimen (Tests: T2, T3, T4, T5, T6, T7, T8, T9, and T10) and is potted in Figure 5.18. There is a 26 to 66% reduction in the cracked area in comparison with the unreinforced soil specimen due to fiber reinforcement. As indicated above, the maximum crack reduction is observed for specimen reinforced with fibers of fiber content f= 0.5% and l = 15 mm. The crack reduction may be attributed to the increased tensile strength of the clay mass due to fiber reinforcement.

5.6.4 Effect of fiber length and fiber content

Effect of fiber length: The crack feature measurements were analysed in order to determine the optimum fiber length for various fiber contents. The crack reduction was found higher for l = 15 mm and l = 30 mm fibers and not for l = 50 mm, as shown in Figure 5.18. The longer fiber length of l = 50mm did not provide the necessary interlocking due to flocculation and non-uniform dispersion. The short fibers get evenly distributed in the clay mass and help in restraining the formation of crack. The longer fibers are longer than necessary and form clusters, leaving a large portion of soil unreinforced. Olgun(2013) reported similar inefficiency of longer length of fibers at l = 20 mm on the strength and volume change characteristics of cement-fly-ash–stabilized clay soil.
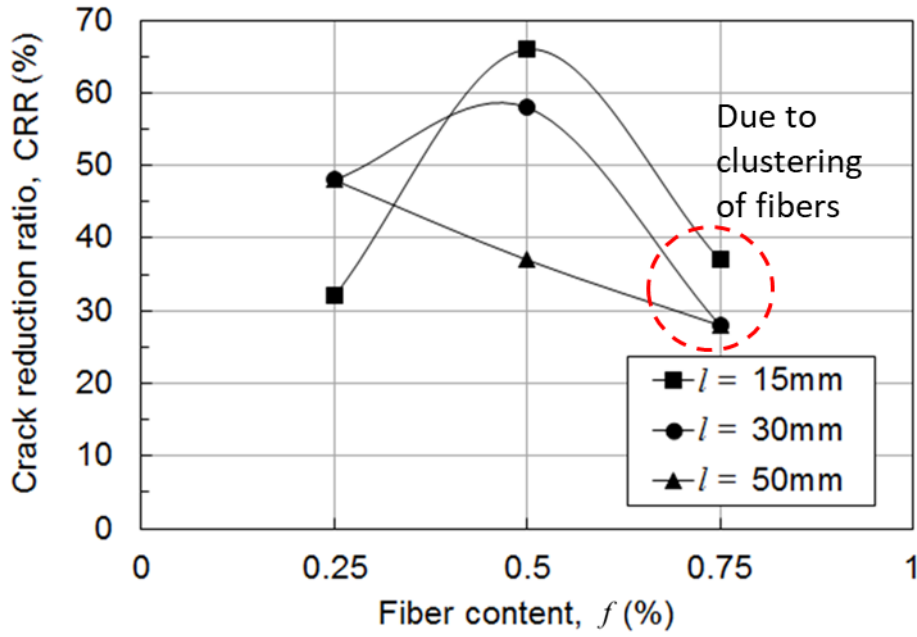
Figure 5.18 Variation of *CRR* withfiber content for different fiber lengths

Tang et al. (2012) reported that crack reduction increased with an increase in fiber content and that no significant effect due to fiber length was observed on the crack reduction of fiber reinforced soil. However, this study substantiates the dependency of crack reduction on the length of fibers. The effect of the length of the fibers is dependent on the range of the stress and strain that is applied to the soil specimen. Whereas, shorter fibers are more effective in mitigating desiccation cracking, longer lengths of fibers play a significant role in large strain problems such as differential settlements and direct shear test. Divya et al.(2014) stated that soil reinforced with very short fibers (30 mm) failed like a brittle material, whereas longer fibers (60 mm and 90 mm) provided a better and prolonged resistance against cracking after crack initiation. Therefore, a more comprehensive study on the combination of fiber lengths is needed in order to restrain desiccation cracking and enhance the tensile properties of the clay layer.

Effect of fiber content: The cracking behaviour of fiber-reinforced soil also depends on the fiber content. This correlates with the fact that the same fiber with same diameter was used in the study. The average effective contact area between the soil and the fiber increases (per unit mass of soil) with an increase in the fiber content. The specimen integrity and crack reduction increased substantially for up to 0.5% of fiber content, but decreased considerably for a fiber content of 0.75%. Estabragh et al.(2012) investigated the mechanical characteristics of a soil-cement-fiber mixture with varying nylon fiber contents and curing time. The increase in the fiber content did not show any significant effect on strength improvement beyond 1%.

168

Olgun(2013) reported a similar observation for fiber-reinforced cement-fly-ash–stabilized clay soil. Therefore, additional fiber content is not required after reaching a certain level.

5.6.5 Effect of fibers on tensile strength-strain characteristics

The crack reduction may be attributed to the increased tensile strength of the clay mass due to fiber reinforcement. The fibers enhance the interfacial shear strength of clay due to adhesion and the surface roughness of the fiber, and hence the clay mass can bear the tensile stresses that develop due to desiccation. The tensile behaviour of fiber reinforced expansive clay and quantifying the fiber contribution to soil tensile strength was done by a series of tensile tests on reinforced and unreinforced soil specimens. Emphasis was put on evaluating the effects of fiber content, water content, and fiber length. The expansive soil was reinforced with polypropylene fibers of cut lengths 12 mm, 30 mm and 50 mm at fiber contents of 0%, 0.25%, 0.35%, 0.5%, 0.65% and 0.75% by weight of dry soil. A direct tensile test setup was used to measure the tensile strength of fiber reinforced soil (Figure 5.19). The test setup consists of a split mould of dimensions 152 x 152 x 152 mm with an open top resting on horizontal platform (Divya et al. 2014).
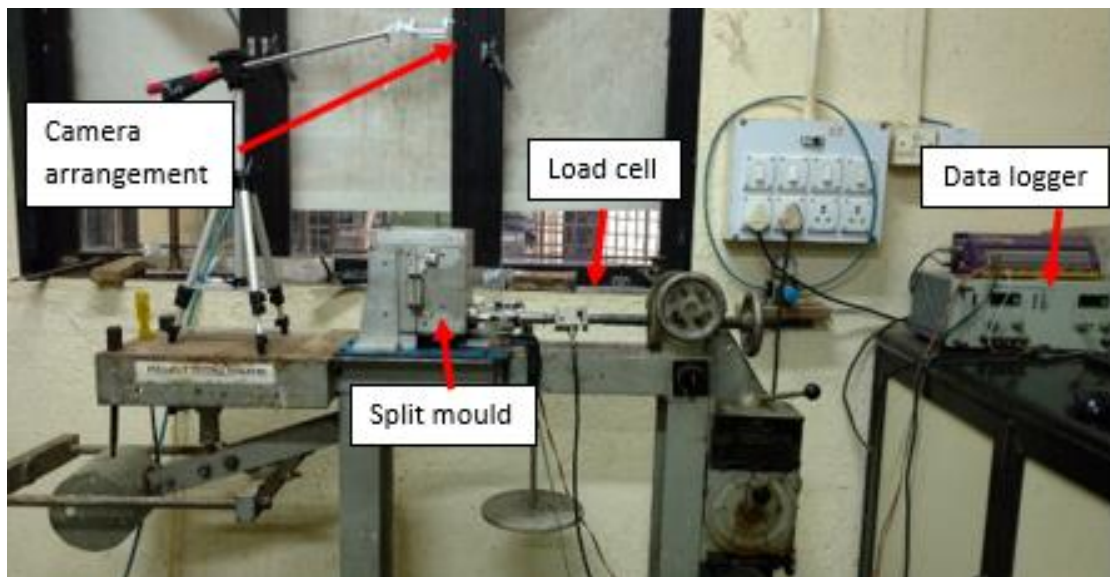
Figure 5.19 Test setup for tensile strength test

Fixed half of the mould is attached at the base, whereas the other half is free to move longitudinally on the polished guide rails. Figure 5.21 and Figure 5.22 present the schematic plan and section view of the tensile test setup.

The water content was varied as OMC-5% to OMC+10% i.e., at 30%, 35%, 40% and 45% to understand the tensile behaviour of fiber reinforced soil mix (Table 5.3). A representative fiber contents of 0.35% and 0.65% were mixed at 30% water content to observe the variation of tensile strength with fiber content. The wet mixes were wrapped in polybags and left to hydrate uniformly for 24 hours before compaction. Tensile tests were conducted at the constant strain rate of 1.25mm/minute till the soil completely separated from the splitting side. The specimen thickness was maintained 100 mm for the tensile tests conducted. The specimen was compacted with the help of special X shaped compacter for uniformity. Table 5.3 summarizes the tensile tests performed in the present study. In total, 16 tests were performed with varying fiber content, fiber length and water content in the fiber reinforced soil specimens.

(a) Dry soil

(b) Dry soil + fiber mix

(c) Mixing of water with soil-fiber mix

(d) Wet soil-fiber mix
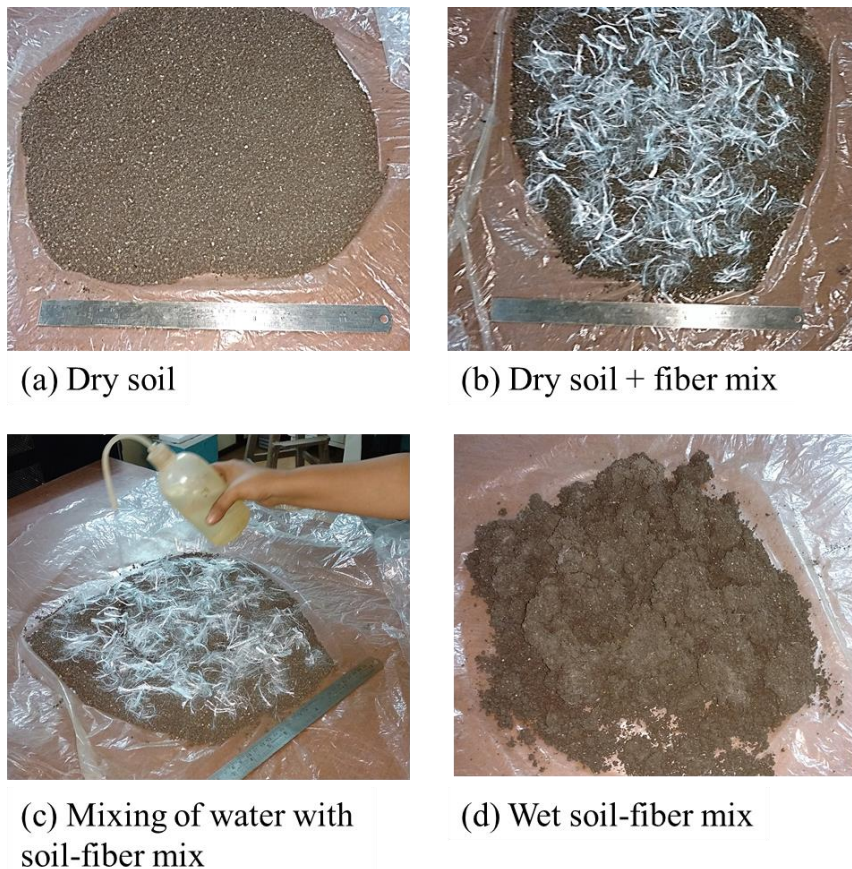
Figure 5.20 Procedure of specimen preparation
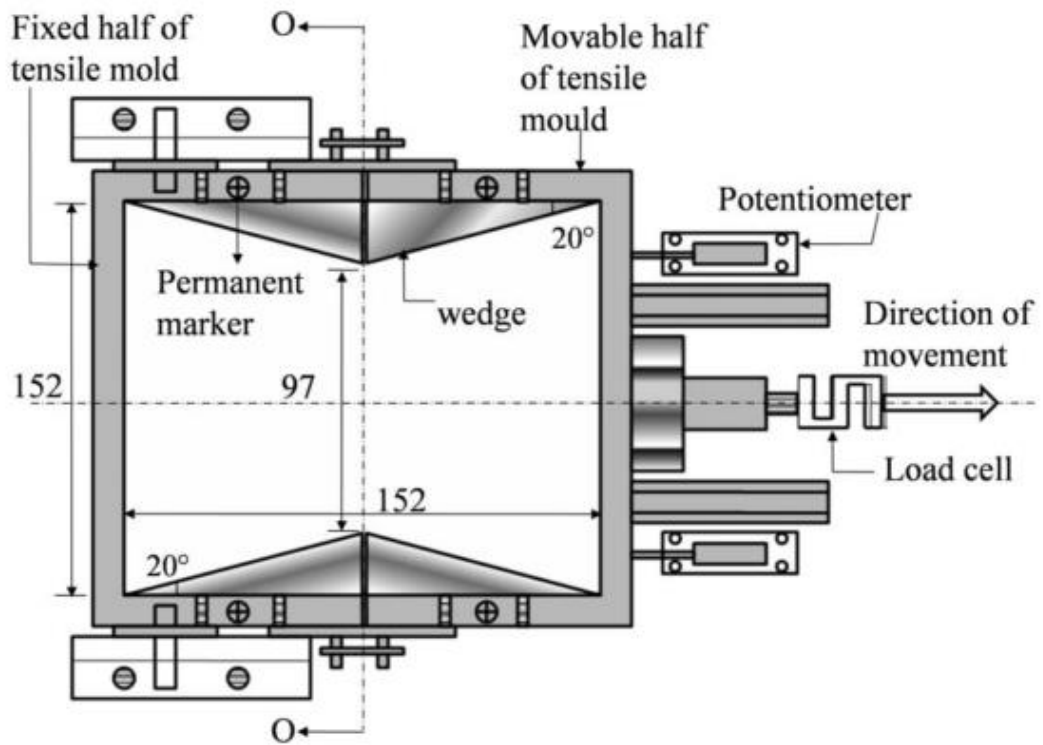
Figure 5.21 Plan view of developed tensile test setup; all dimensions are in mm (After Divya et al. 2014)
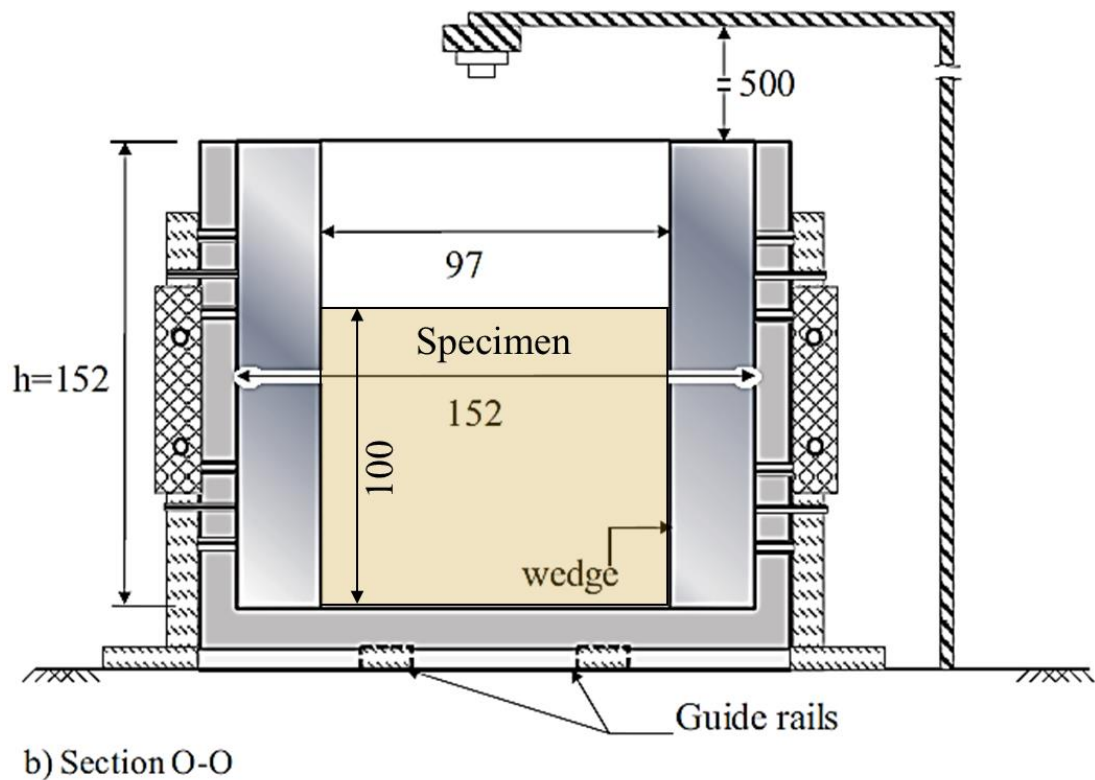
Figure 5.22 Section view of the tensile test setup and specimen thickness; all dimensions are in mm (After Divya, 2012)

Table 5.3 Summary of tensile test program

Test No	Test Legend	Specimen type	f (%)	l (mm)	w (%)
1	UR	UR	-[a]	-[a]	45, 40, 35, 30
2	FR1	FR	0.25	12	45, 40, 35, 30
3	FR2	FR	0.35	12	30
4	FR3	FR	0.5	12	45, 40, 35, 30
5	FR4	FR	0.65	12	30
6	FR5	FR	0.75	12	45, 40, 35, 30
7	FR6	FR	0.25	30	45, 40, 35, 30
8	FR7	FR	0.35	30	30
9	FR8	FR	0.5	30	45, 40, 35, 30
10	FR9	FR	0.65	30	30
11	FR10	FR	0.75	30	45, 40, 35, 30
12	FR11	FR	0.25	50	45, 40, 35, 30
13	FR12	FR	0.35	50	30
14	FR13	FR	0.5	50	45, 40, 35, 30
15	FR14	FR	0.65	50	30
16	FR15	FR	0.75	50	45, 40, 35, 30

UR- Unreinforced; FR- Fiber reinforced l - Fiber length; f - Fiber content; w- Water content; [a] not relevant/not used

The tensile load (P) taken by the soil layer is logged by the S shaped load cell. The tensile stress is given by

$$\sigma_t = \frac{P}{A_c} \tag{5.4}$$

Where, A_c is obtained by multiplying the width of the soil specimen perpendicular to the direction of the movement by the height of the soil specimen. As the tensile stress on the fiber

reinforced soil matrix is increased, the fibers stretch and align themselves in perpendicular direction of the crack to hold the remaining soil mass intact. Figure 5.23 shows the top views of the unreinforced and fiber reinforced soil specimens after the tensile strength test.

Figure 5.24 presents the tensile stress versus displacement curves for the fiber length $l = 50$ mm and w = 30% for varying fiber content of $f = 0.25\%$, 0.5%, and 0.75%. As expected, the tensile stress increased monotonically with the increase of displacement before the tensile strength (peak tensile stress) was reached. After that, the tensile stress decreased suddenly, suggesting that tensile failure occurred at the specimen neck. It was observed that a crack developed quickly throughout the full length of the failure section and the crack surface (failure plane) was quite smooth, indicating that there was an even distribution of tensile force along the failure section during the test. The tensile stress developed in the fiber reinforced soil matrix reached a peak and then gradually drop to reach a strain plateau in case of fiber reinforced soil specimens. The failure is more ductile in case of fiber reinforced soil specimens when compared to the failure of unreinforced soil specimens.

If L(t) is the length of the selected line over time which might become longer as the sample is deforming or subjected to tension, and L_0 be the initial length, the change in length over time t is L(t))-L_0. From the strain profiles at various displacement stages, the maximum value of strain is measured by

$$\varepsilon\,(t) = \frac{dL(t)}{L_0} = \frac{L(t) - L_0}{L_0} \tag{5.5}$$

The tension cracks formed on the failed specimens reveal that the unreinforced soil specimen and fiber reinforced soil specimen with $f = 0.5\%$, $l = 12$ mm undergo brittle failure. The fiber reinforced soil specimens with $f = 0.5\%$, $l = 30$ mm and $f = 0.5\%$, $l = 50$ mm undergo a delayed and ductile failure, as the fibers hold the soil undergoing tension crack.
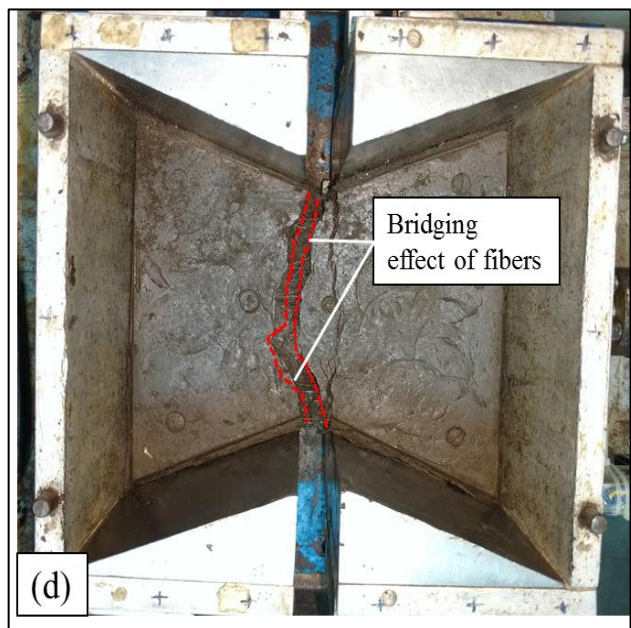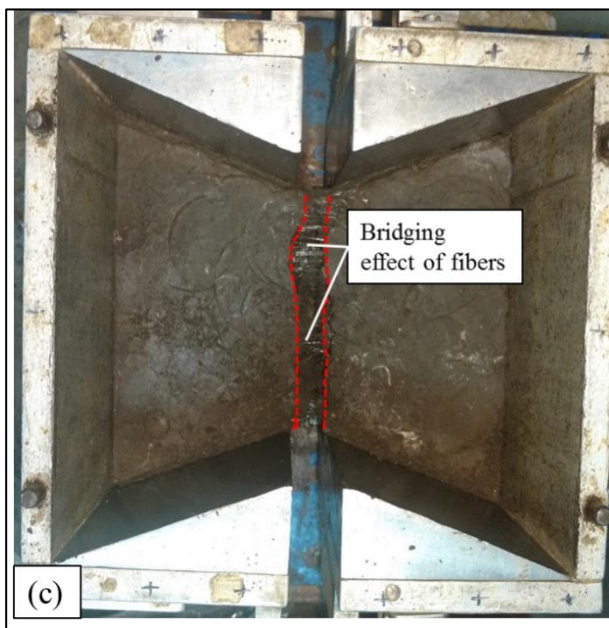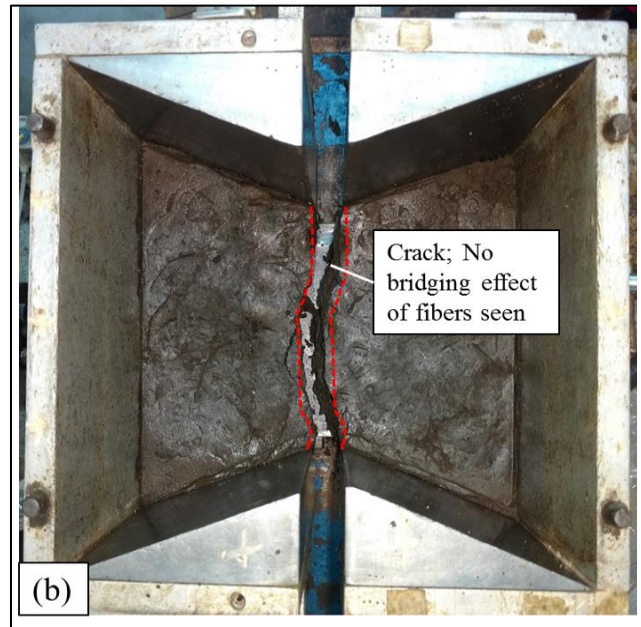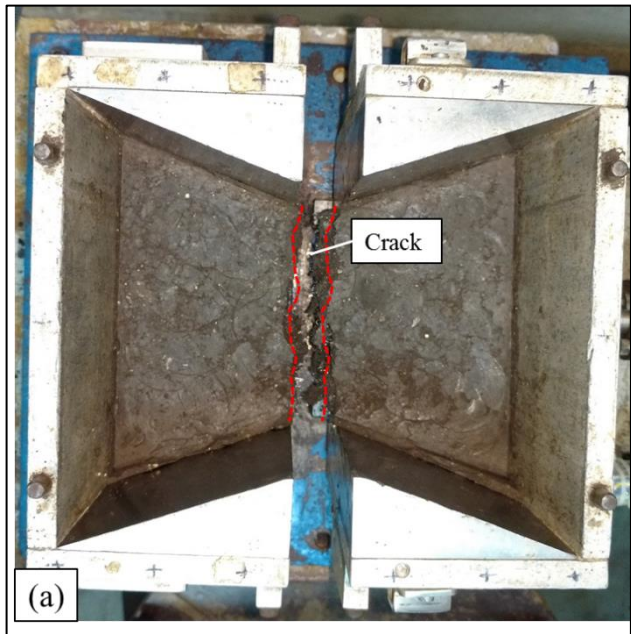
Figure 5.23 Top view of specimens after tension failure (a) Unreinforced, (b) $f = 0.5\%$**,** l **= 12 mm, (c)** $f = 0.5\%$**,** l **= 30 mm, (d)** $f = 0.5\%$**,** l **= 50 mm**
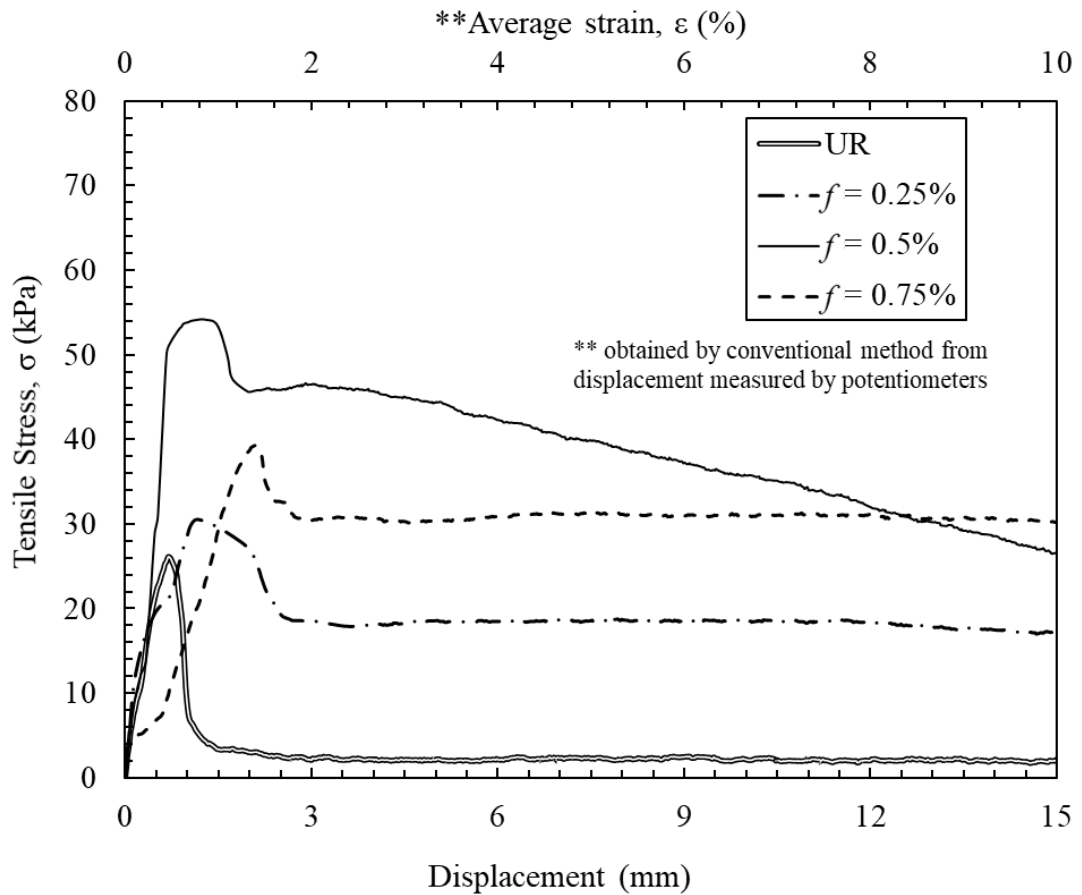
Figure 5.24 Tensile stress versus displacement curve for fiber length, *l* = 50 mm and *w* = 30% for varying fiber content

Figure 5.25 shows the variation of peak tensile strength of fiber content of 0.5% for fiber length, *l* = 12 mm, 30 mm and 50 mm with varying water contents. The beneficial effect of fiber reinforcement on tensile strength can be attributed to the interfacial mechanical interactions between fibers and soil matrix. The reduction in tensile brittleness can be attributed to the so-called bridging effect of fibers.
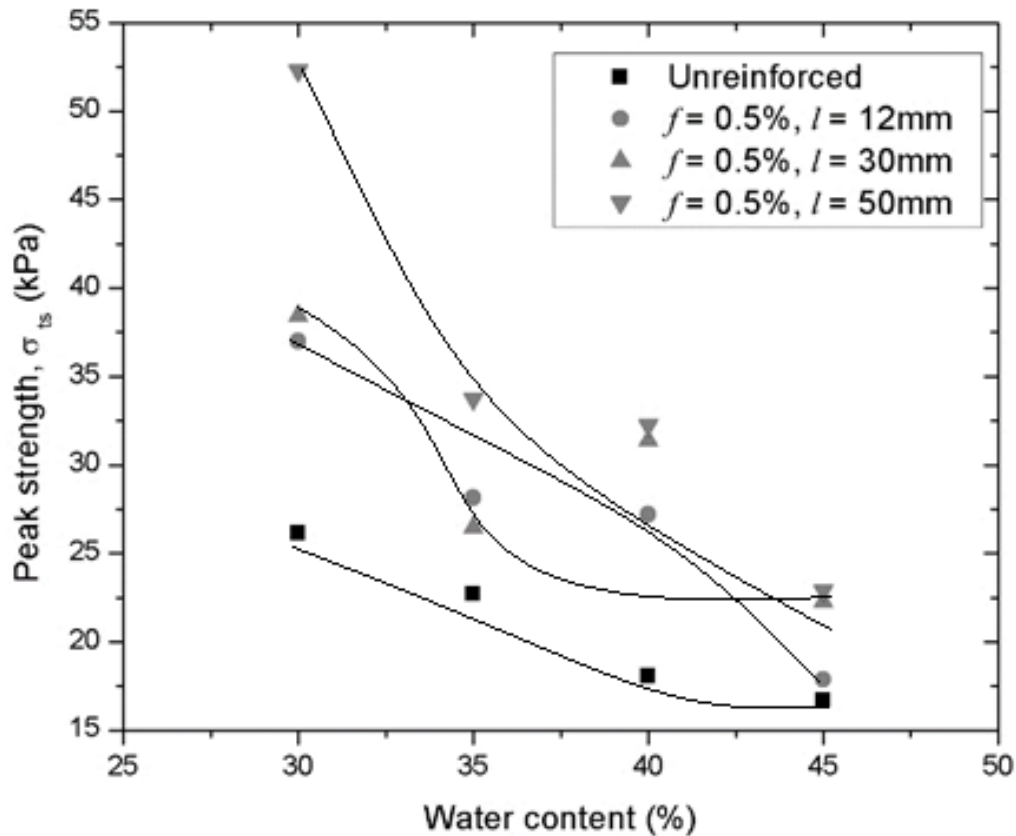
Figure 5.25 Variation of peak tensile strength of fiber content of 0.5% for fiber length 12mm, 30mm and 50mm with varying water contents

For fiber-reinforced soils, limited studies have been carried out to investigate the influence of water content on mechanical behaviour (Miller et al. 2004; Tang et al. 2010b). Moreover, information about the effects of water content on the tensile strength of fiber-reinforced soils has not been studied much yet. At low water content, the soil suction is relatively high and the formed water bridges at particle–particle contact points are strong.

This results in high bonding force between particles, contributing to the soil tensile strength. As the water content increases, the soil suction decreases and the bonding force developed through the bridge system gradually disappears. Upon failure, further overall tensile displacement of the specimen was concentrated on the elastic/plastic extension of the fibers through the opening and the bond slippage of the fiber anchorage on either side of the opening. These fibers somehow served as bridges that bore the entire tensile load. They can therefore efficiently impede the further opening and development of tension cracks, thereby preventing specimens from complete brittle failure.

It is therefore believed that post failure tensile behaviour is conditioned mainly by the interfacial shear strength of the embedded fibers and the tensile strength of fibers. If the applied tensile load exceeds the interfacial shear strength, pull-out failure of fibers can occur. As the fiber length increases the bond length over which the tensile stress is transferred increases. Hence, the peak tensile stress is found highest for fiber length of 50 mm. Figure 5.26 shows the variation of tensile strength improvement with varying fiber lengths for different fiber contents.
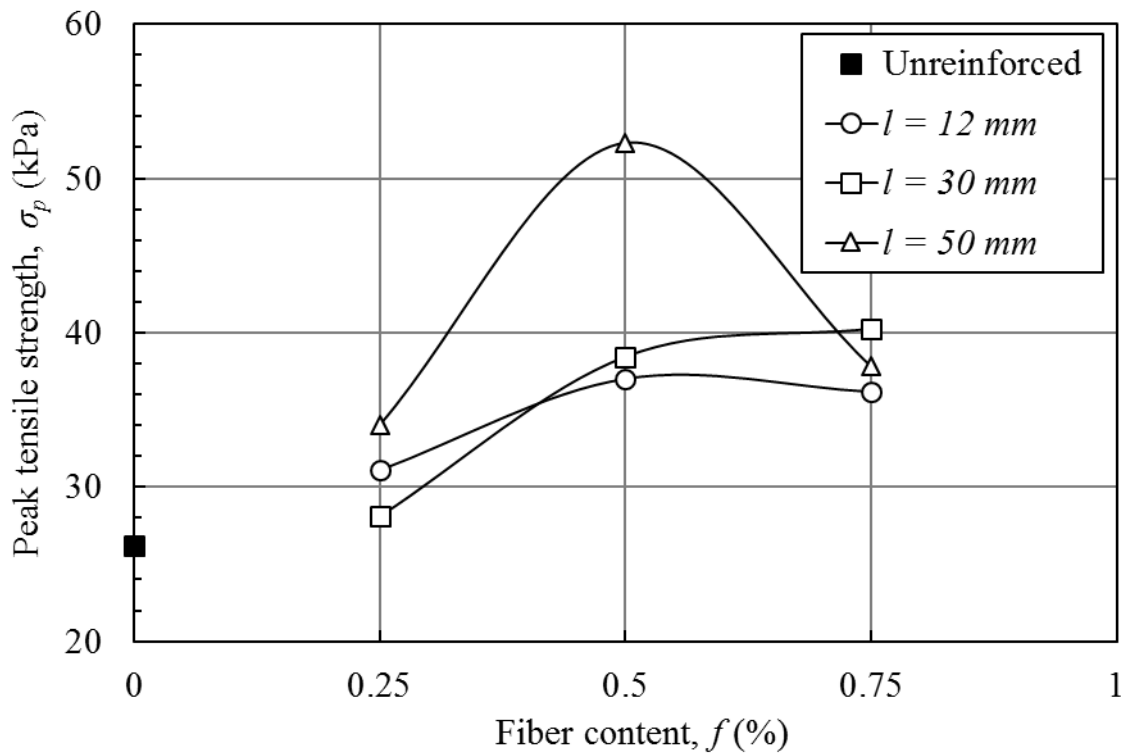
Figure 5.26 Variation of peak tensile strength with varying fiber content for different fiber lengths

Figure 5.27 shows the variation of peak tensile strength with varying fiber lengths for different fiber contents. As observed visually and through the values of tensile strength values, the longer fiber lengths are observed to perform better against large deformations like in the case of direct tensile strength tests. Figure 5.28 schematically represents the importance of fiber length for a fiber reinforced soil specimen undergoing tension. The fiber at the crack takes the entire tensile load during cracking and the fiber gets extended. If the length of fiber on the other side of the crack is enough, the fiber is successful in restraining the cracking, by holding on to the soil. If the fiber is not sufficiently long, the fiber gets pulled out at the crack. Pull-out failure of the fibers occurs when the fibers are strong enough not to break at the crack. Shorter fibers (fiber

length, $l = 12$ mm) get pulled out at the crack, as their pull-out strength is lesser than their tensile strength, as shown in Figure 5.29.
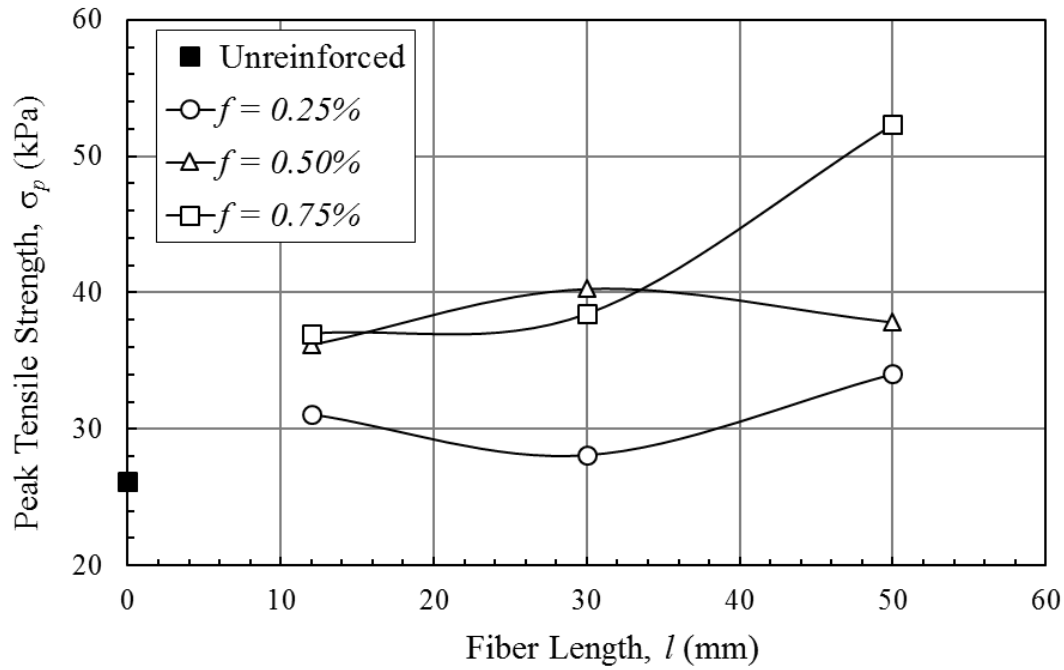
Figure 5.27 Variation of peak tensile strength with varying fiber lengths for different fiber contents
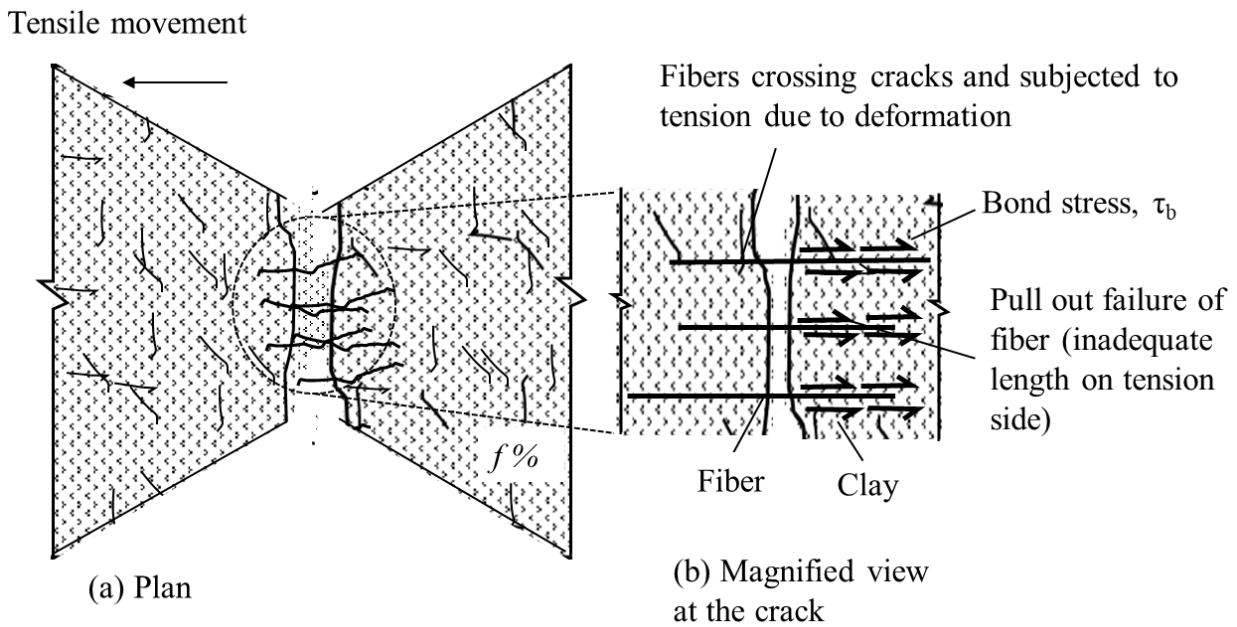
Figure 5.28 Schematic diagram of fibers undergoing tension
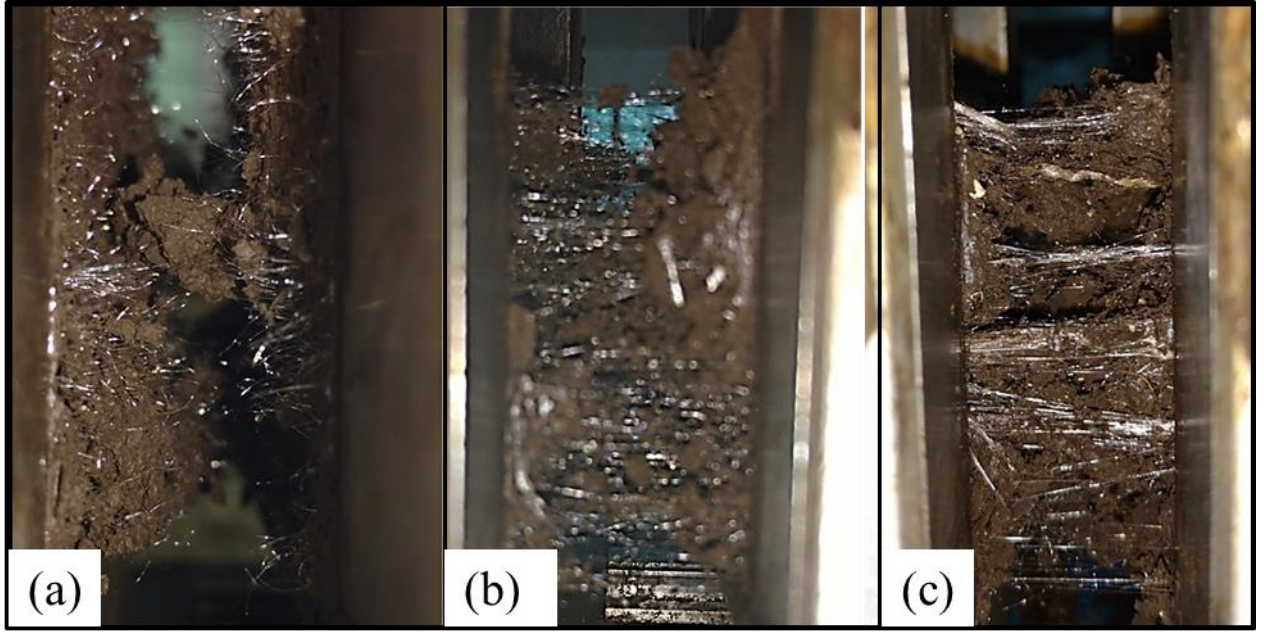
Figure 5.29 Cross-sectional view of fiber-reinforced soil subjected to tension (a) $f =$ 0.5%, l = 12 mm, (b) f = 0.5%, l = 30 mm, (c) f = 0.5%, l = 50 mm

To evaluate the improvement on tensile strength of soil, a factor called tensile strength improvement factor (μ) was computed for the peak tensile strength achieved for respective fiber contents and fiber lengths.

$$\mu = \frac{\sigma_{ptf} - \sigma_{ptu}}{\sigma_{ptu}} \qquad (5.5)$$

μ = Strength improvement index

σ_{ptf} = Peak tensile strength of fiber reinforced soil

σ_{ptu} = Peak tensile strength of unreinforced soil

Figure 5.30 shows the variation of tensile strength improvement with varying fiber content and fiber length. It is interesting to note that the maximum tensile strength is observed for fiber content of 0.5%, not of 0.25% and 0.75%. Which indicates that there lies an optimum fiber content. It was also observed that lumping and balling of fibers was observed in case of higher fiber contents.
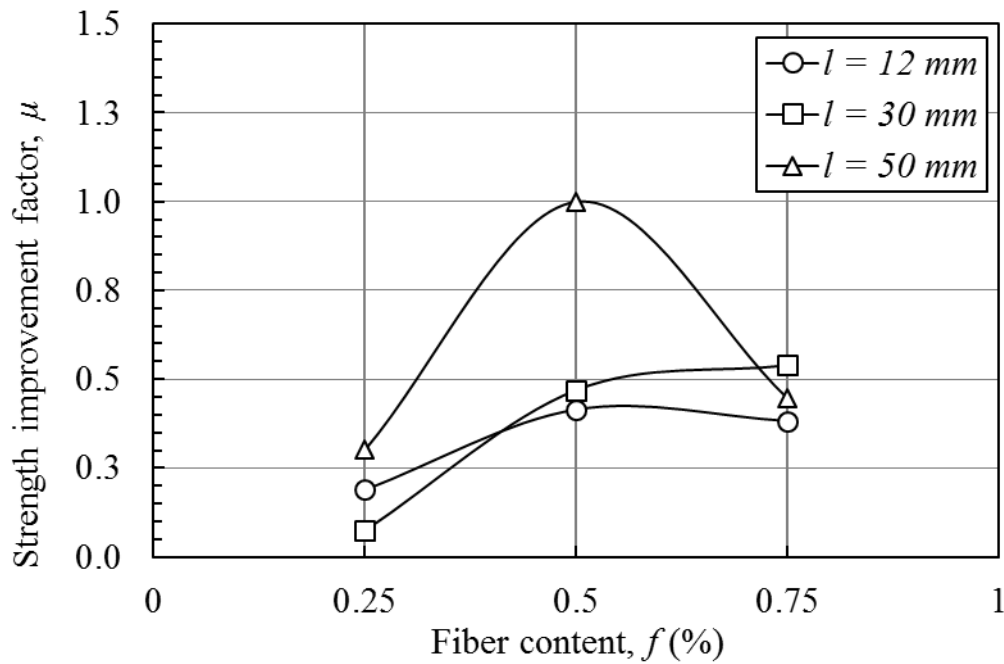
Figure 5.30 Variation of performance index ratio with varying fiber contents
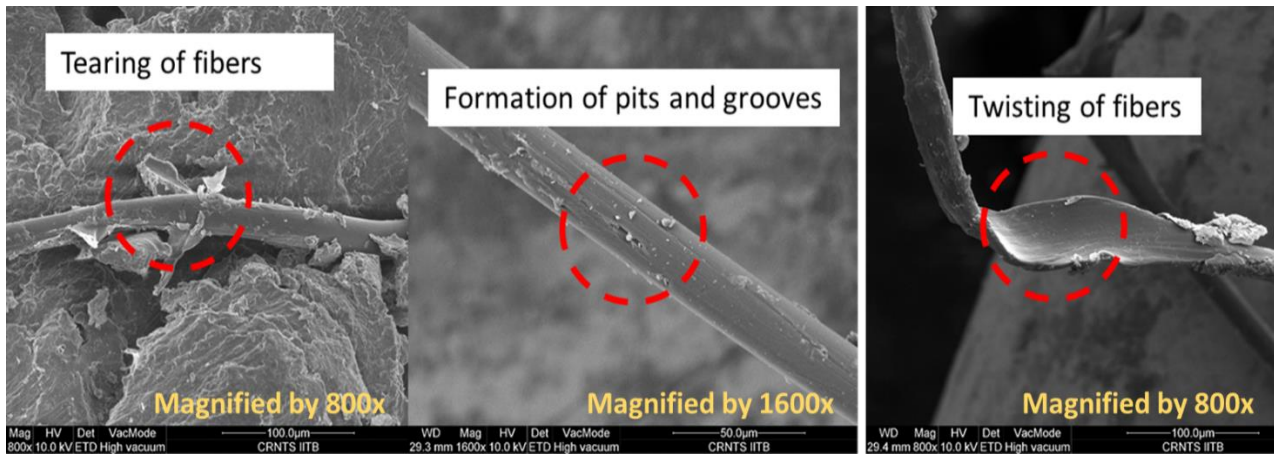
Figure 5. 31 SEM images of fibers extruded from the failure plane after the tensile strength test

As the soil specimen is subjected to tensile stresses, the load is taken by the fibers. This can be seen in the SEM images of the extruded fibers from the failure plane after the tensile strength test (Figure 5. 31). The fibers experience and endure tearing, pits and grooves and twisting, which shows that the fibers participate in bearing the tensile load.

5.7   Closure

Laboratory desiccation tests were performed on unreinforced and fiber-reinforced expansive clay specimens mixed at slurry state. The moisture content variation, temperature and surficial images were captured to study the behaviour of desiccating soil specimens. The crack feature measurements like crack width, crack intensity factor, cell area, spacing and shrinkage strain were evaluated for all the specimens and compared for unreinforced and fiber reinforced specimens. A significant change in the cracking pattern of unreinforced and fiber reinforced expansive clay is observed due to the presence of fibers. While wide crack widths and long cracks are formed in unreinforced soil, the addition of fibers controlled the crack width opening, the cracked area, and the propagation of cracks through the bridging action of fibers. To study the improvement in the tensile strength of the expansive clay with the help of fiber reinforcement, direct tensile strength tests were performed on unreinforced and fiber reinforced soil specimens. The fiber reinforcement inclusions help in decreasing the connectivity of crack networks and maintaining the integrity of clay layer even after being subjected to desiccation cracking.

Chapter 6

EFFECT OF CYCLIC DRYING-WETTING BEHAVIOUR OF EXPANSIVE SOIL WITH & WITHOUT FIBERS

6.1   Introduction

In-situ soil is subjected to consecutive wetting and drying cycles in the form of seasonal rains and dry periods. These cycles significantly affect the properties of soil. Desiccation cracking is a common problem in soils undergoing large moisture variation and alters its strength and hydraulic properties. Recently, application of discrete fiber-reinforcement for restraining desiccation cracking has been studied. Laboratory tests were conducted to investigate the effect of wetting-drying cycles on unreinforced and fiber-reinforced clay. Several studies have been performed in the past to investigate the effect of wetting and drying on soil physical properties (Alonso et al. 2005; Tang et al. 2011). However, the relationship between D-W cycles and

desiccation cracking behaviour is still not clearly understood. In this study, the effect of drying wetting cycles on cracking behaviour of fiber reinforced soil was investigated by subjecting a group of initially saturated clay layers to five D-W cycles. The initiation and evolution of cracks on the specimen surface during the cycles were monitored. The geometric characteristics of surface crack patterns are described and quantified through image processing and the mechanisms involved are discussed.

6.2   Experimental test setup

The schematic experimental set-up used in this study is illustrated in Figure 6.1. The soil specimen was placed in the test setup and allowed to desiccate under two 500W Tungsten Halogen lamps. In order to measure the variation of water content during drying, the specimen was placed on a balance (with an accuracy of 0.01 g) to monitor the weight.
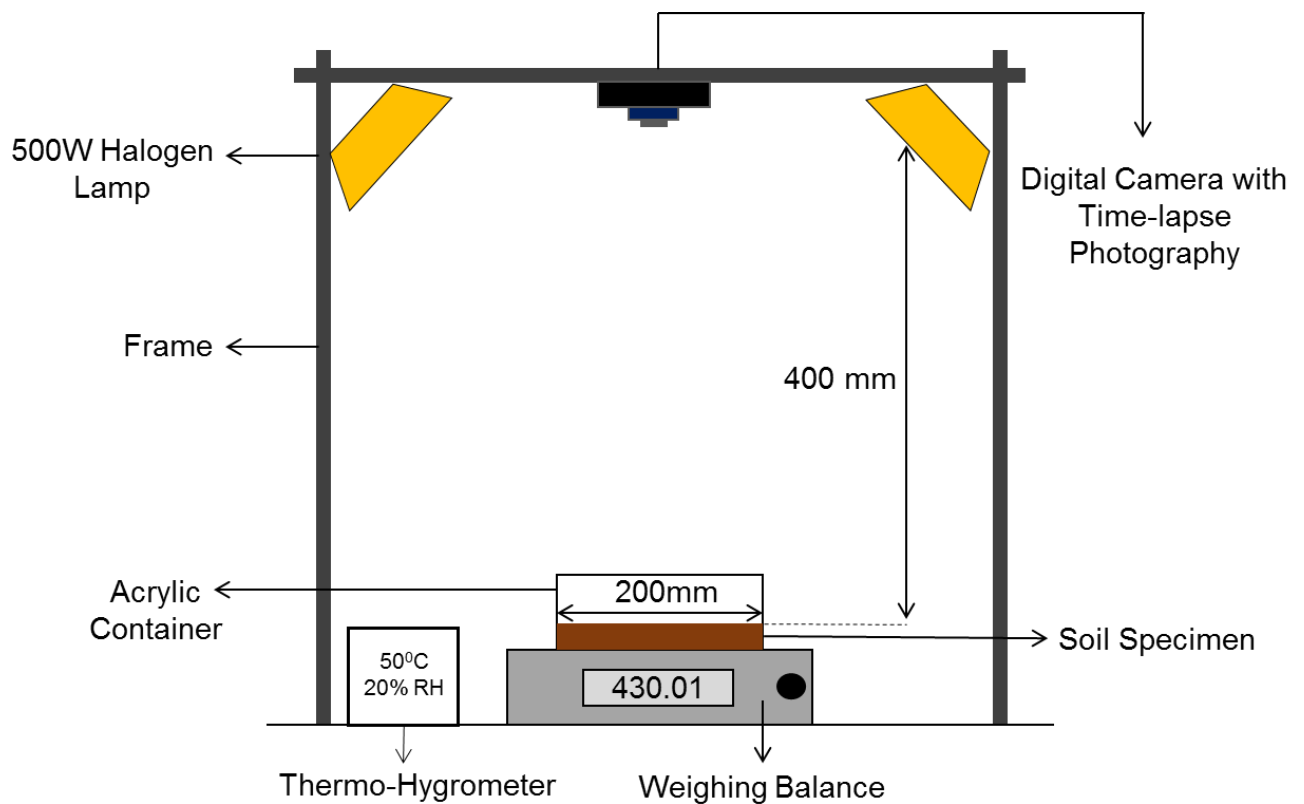
Figure 6.1 Schematic representation of the test setup

183

All tests were performed at a reasonably constant temperature of 50ºC and relative humidity of 20% Rh, as recorded in the thermo-hygrometer that is located close to the setup. Two digital cameras were placed on top and side respectively. Cameras were equipped with an interval timer was used to capture images of the drying soil specimen every five minutes.

Acrylic cylinders of height 80mm and diameter 200mm was used for the tests. The acrylic container was used to reduce heating from the container. A sheet with markers was attached below the cylinder for scale measurement in image analysis. The surficial temperatures of drying specimens were measured using Cetpar Infrared Thermometer, MT-4 at fixed locations.

6.3   Test procedure and test program

The clay was oven-dried, crushed, and sieved through a 425µm sieve. Different fiber lengths of 6 mm, 12 mm, and 18 mm at a fiber content of 0.5% of dry weight of the soil was used in the preparation of fiber-reinforced clay specimen, as shown in Table 6.1. Initially, a mix of dry clay and fibers was prepared, to which water was gradually added to make a slurry.

All specimens were prepared close to the liquid limit of the soil. The prepared slurry was poured into the acrylic containers and was left to hydrate for 24 hours before testing. In the present study, the effect of varying clay layer thicknesses has been considered. Specimen thickness of 5mm, 10mm and 15mm were considered. The dried desiccated samples were inundated with water till they are completely submerged with water and then left for hydration for 24 hours before the next test.

Drying-Wetting (D-W) method. The drying stages were carried out for 10 hours at 50ºC and relative humidity of 20%. For the wetting stages, the desiccated samples were inundated carefully with water close to liquid limit and then left for hydration for 24 hours before the next stage. Figure 6.2 shows the decrease in water content due to desiccation in unreinforced specimens during first, second and third drying-wetting cycle.

Table 6.1 Test Program for the cyclic drying-wetting of unreinforced and fiber-reinforced soil

Test No	Test legend	Specimen type	f (%)	l (mm)	Layer thickness (mm)	Cycles
1	UR1	UR	-[a]	-[a]	5	5
2	UR2	UR	-[a]	-[a]	10	3
3	UR3	UR	-[a]	-[a]	20	3
4	FR1	FR	6	0.5	5	5
5	FR2	FR	6	0.5	10	3
6	FR3	FR	6	0.5	20	3
7	FR4	FR	12	0.5	5	3
8	FR5	FR	12	0.5	10	3
9	FR6	FR	12	0.5	20	3
10	FR7	FR	18	0.5	5	3
11	FR8	FR	18	0.5	10	3
12	FR9	FR	18	0.5	20	3

UR- Unreinforced; FR- Fiber reinforced; f- fiber content; l- fiber length; [a] not relevant/not used
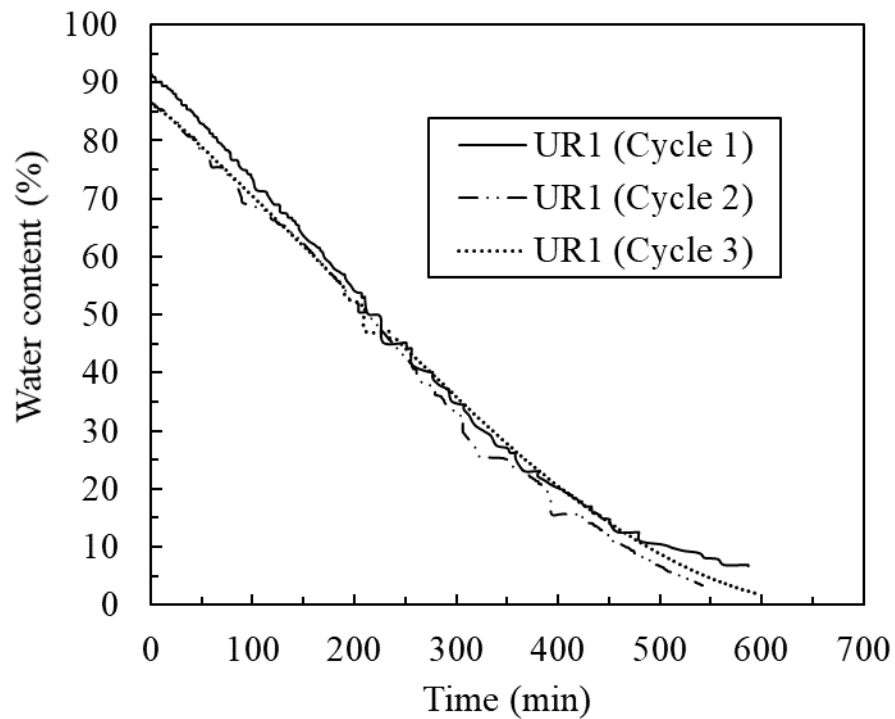
Figure 6.2 Decrease in water content with time for unreiforced specimens during drying-wetting cycles

185

6.4   Analysis of test results

Depending on the initial thickness of the sample, the specimen was desiccated for 480, 600, 720 minutes respectively for 5 mm, 10 mm and 15mm thickness. Moisture content, depth and surficial measurements by digital image acquisition system were analysed.

6.4.1 Digital image analysis

Digital image analysis was employed to measure the surficial crack feature measurements. The methodology adopted for image analysis is explained in Chapter 5, Section 5.4.1. The thickness images were also analysed to study the variation in specimen thickness.

6.5   Results and discussion

The experimental observations and image analysis results were compiled to understand the effect of fiber length and effect of drying-wetting (D-W) cycles on fiber reinforced expansive clay. The average crack opening width ($c_{w, avg}$) and crack intensity factor (CIF) were measured for all the test series. The crack measurements were analysed in an image analysis program, ImageJ (Abràmoff et al. 2014).

6.5.1 Influence of specimen thickness

The effect of specimen thickness on crack patterns has been extensively discussed by many other researchers (Corte and Higashi 1964; Lakshmikantha et al. 2012). It is commonly accepted that thin specimens produce large number of cracks with small cell areas (uncracked

areas) whereas wider and a smaller number of cracks are visible in thick specimens, as shown in Figure 6.3.

For thinner layers, the drying rate may not influence the development of this suction profile to any great extent, except for the time required for cracking. In contrast, thicker soil layers will not develop suction profiles to full depth, and the depth of this zone will depend on the rate of drying. Therefore, these thicker layers will have an 'effective layer thickness' over which the initial cracking takes place, which reduces in thickness as the drying rate increases, thereby influencing the size of the cracked cell areas. The effective layer thickness is the layer depth over which high moisture- content changes and therefore high suction and tensile stresses develop (Costa et al. 2013).

Fine cracks	Medium cracks	Wide cracks
$l = 6$mm, $d = 5$mm	$l = 6$mm, $d = 10$mm	$l = 6$mm, $d = 15$mm
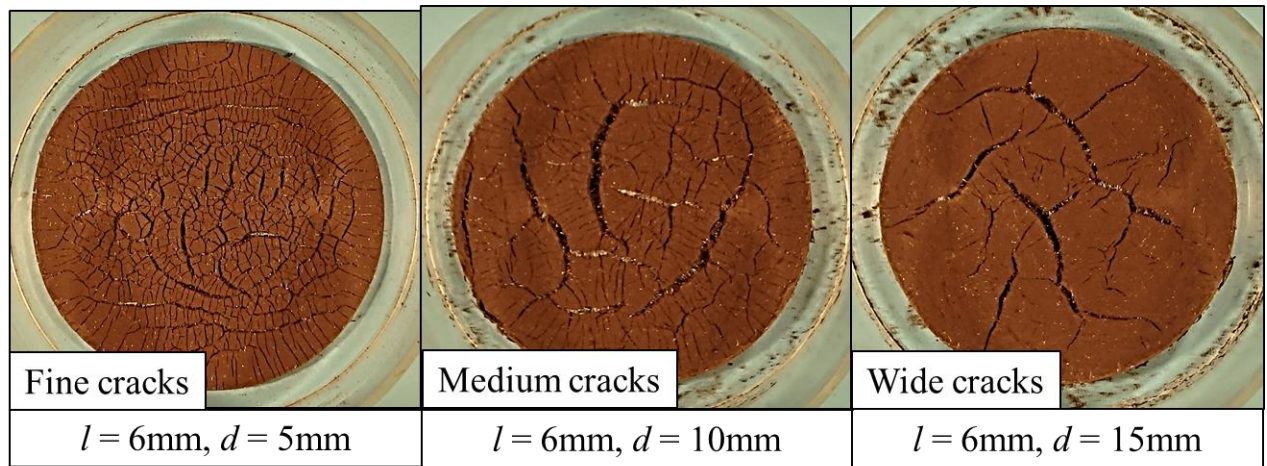
Figure 6.3 Crack patterns for fiber reinforced specimen for different specimen thicknesses

Upon desiccation, the specimens undergo volumetric shrinkage and the clay specimen separates from the sides of the container. Due to shrinkage, the tensile stresses developed because the restraint at the bottom surface restricted soil free shrinkage. When the tensile stress exceeds the tensile strength of specimen, a crack form. In unreinforced clay specimens, the cracks were typically wide, uniform and follow the pattern of subdivision. However, the cracks were more narrow, non-uniform, short and jagged in fiber-reinforced clay specimens. This is consistent with the observations by Tang et al. (2012) and Qiang et al. (2014). During wetting, the formed cracks sealed due to the swelling of soil and breaking of cells formed due to cracking. This phenomenon could be termed as "healing of cracks" and will be discussed in the following section.

6.5.2 Influence of drying-wetting cycles

Effect of drying-wetting (D-W) cycles. This section highlights the effect of cyclic drying-wetting on the behaviour of unreinforced and fiber reinforced clay. The variation of crack opening width and crack intensity factor (CIF) with increasing D-W cycles is addressed.

Crack width

The width of crack is important because wider cracks will allow a larger quantity of flow through the cracks, thus increasing the overall hydraulic conductivity of clay layers (He et al. 2015). Figure 6.4 shows the variation of $c_{w,\,avg}$ for unreinforced specimen of thickness 15 mm after each drying stage of each D-W cycles.
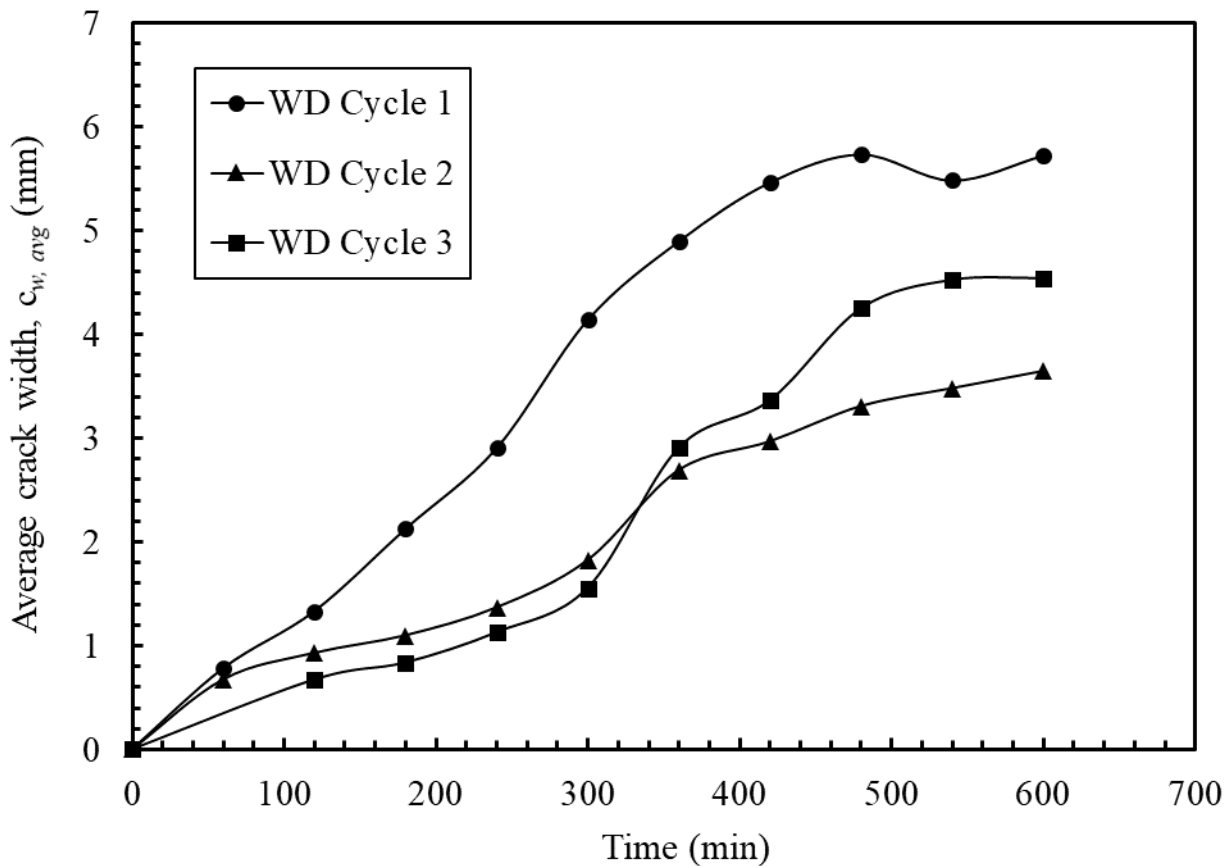
Figure 6.4 Variation of crack width of unreinforced specimens of thickness 15 mm with increasing in drying-wetting cycles

Typically, the crack opening width reduced in clay reduced by 61% due to fiber reinforcement. The results indicate that the D-W cycles severely affect the crack width. In the experiment, the crack width reduced as the number of cracks increase due to formation of minor cracks and voids because of inundation of water. In the case of the unreinforced specimens, the crack width reduced significantly due to the rapid collapse of cells and swelling of clay particles. However, the intensity reduced after third D-W cycle and reached an equilibrium thereafter.

Crack intensity factor

CIF was measured to quantify the intensity of desiccation cracking of unreinforced and fiber-reinforced specimens. The CIF of fiber-reinforced clay specimens was approximately 50% less than that of unreinforced specimens. The cracked area was measured by first converting the greyscale image into the binary image and then a special function in ImageJ was used to measure quantities from the binary image. Figure 6.5 shows the evolution of CIF with cumulative D-W cycles.
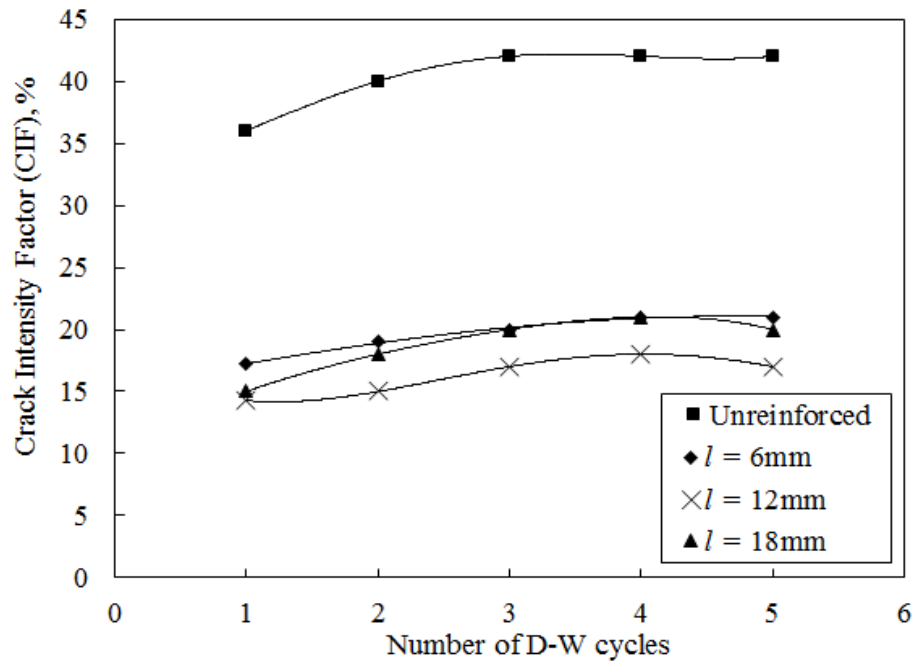
Figure 6.5 Variation of CIF of unreinforced and fiber-reinforced specimens with increasing D-W cycles

The CIF of unreinforced specimen is at no point less than that of the fiber-reinforced specimens. The CIF of unreinforced specimen after the second drying stage was 11% higher than that of the first drying stage. This could be attributed to the increased number of cracks and voids

189

formed due to the infiltration of water during the wetting stage followed by its subsequent drying. It is interesting to note that the increase in CIF of fiber-reinforced specimens is at no point more than that of unreinforced specimens. This observation is consistent with those carried out by Olgun (2013) and Freilich et al. (2008).

Cell Area

The unreinforced soil specimens form a very characteristic hierarchical cracking pattern. The primary cracks propagate faster to the whole depth. They are longer, wider and divide the soil mass into cells. The cells subsequently shrink upon drying. However, when the fibers are added, the cracks patterns are short, jagged and the average cell area (*A*) changes drastically and drops down. The average cell area for $f = 0.5\%$, $l = 12$ mm and specimen thickness $h = 10$ mm for 1, 2 and 3 drying-wetting cycles is plotted in Figure 6.6.
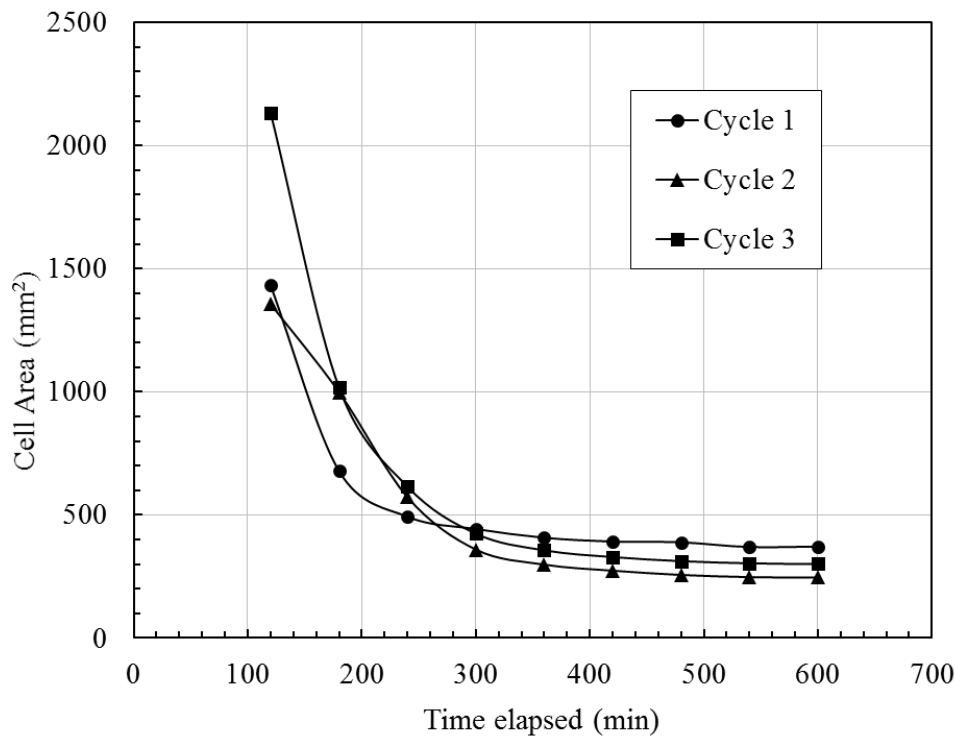
Figure 6.6 Variation of cell area with time for soil reinforced with fiber length 12mm and specimen thickness of 10mm with varying drying-wetting cycles

It is seen that the average cell area is not significantly affected by the drying-wetting cycles. The cracks are observed to heal upon wetting and then follow a similar crack pattern as before.

The typical desiccation crack patterns of unreinforced and fiber reinforced ($f = 0.5\%$, $l = 12$ mm) samples of 10 mm thickness after each drying-wetting cycle can be seen in Figure 6.8.

Pore structure

Kodikara et al. (2002) observed that the soil structure and soil properties stabilized and reached an equilibrium after several wetting and drying cycles and termed this phenomenon as "ripening of soil". From micro-structural point of view such structural stabilization can also be considered as environmental stabilization (Kodikara, 2012). Similar behaviour is observed for the soil under consideration. Figure 6.9 shows that the number pores significantly increase from cycle 1-3, however, not much change is observed from cycle 3-5, thereby justifying the stabilization of pore structure.

6.5.3 Effect of fiber length

The length of fiber offers surface area for bonding with clay. This leads to increased tensile strength of clay and better resistance to desiccation cracking. Uniform distribution of fibers is of paramount importance to maintain homogeneity and is dependent on fiber length and fiber content.
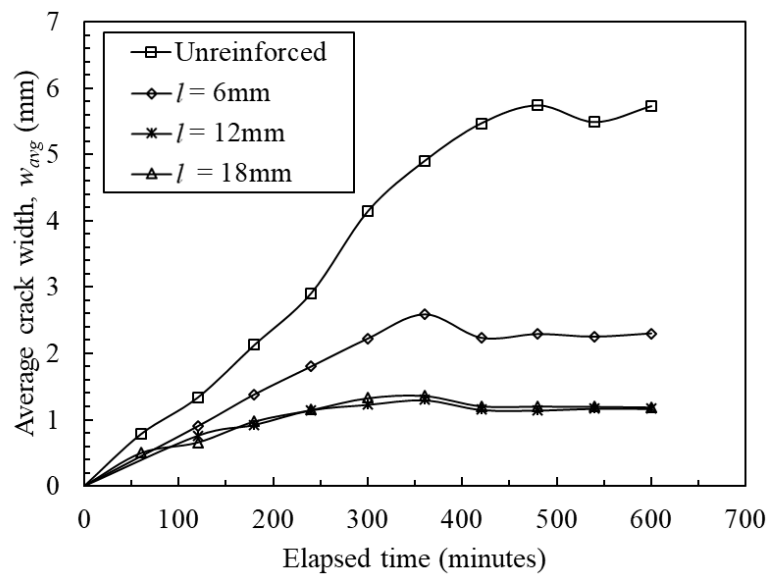
Figure 6.7 Variation of crack width with time for unreinforced expansive soil with varying specimen thickness
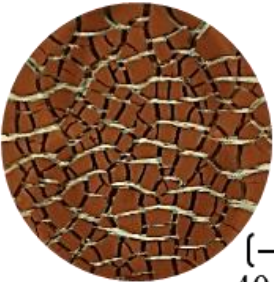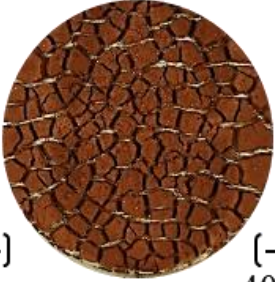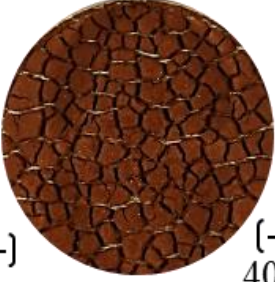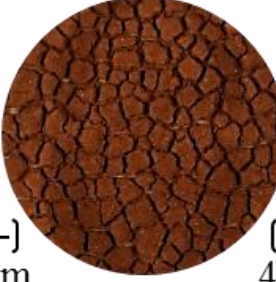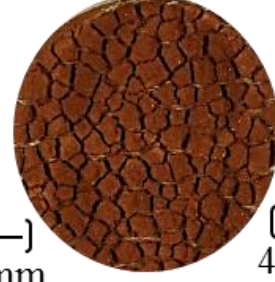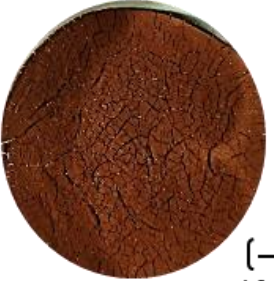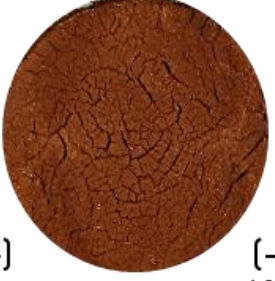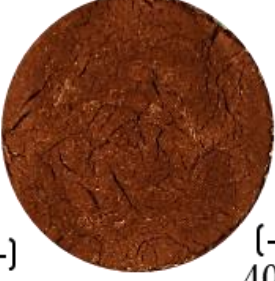
Figure 6.8 Typical desiccation crack patterns of unreinforced and fiber reinforced ($f = 0.5\%$, $l = 12$ mm) samples of 10 mm thickness after each DW cycle
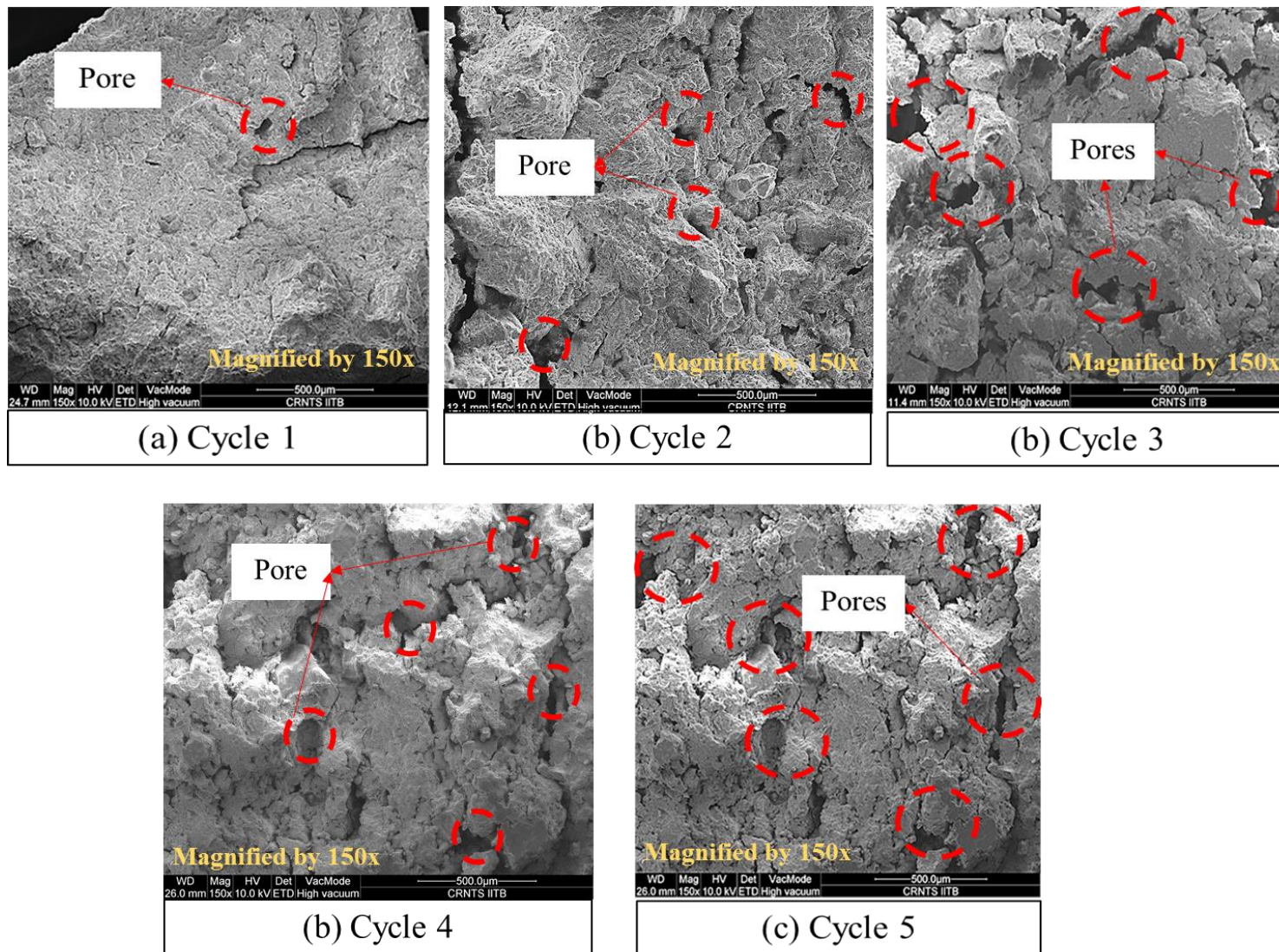
Figure 6.9 SEM images of change in pore structure of unreinforced soil due to increase in DW cycles

In this study, all the considered fiber cut lengths were evenly distributed in the clay matrix during mixing. Figure 6.7 shows the development of average crack opening width, w_{avg} during first drying stage. The crack opening widths provide preferential pathways for flow of liquid through the clay layer. The w_{avg} in unreinforced clay specimens were found to be always more than the fiber-reinforced clay specimens.
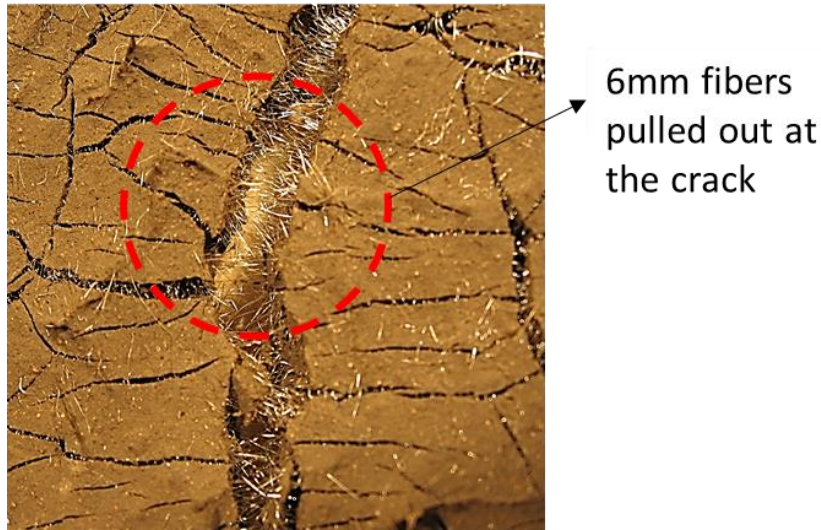
Figure 6.10 Pulling out of 6 mm fibers at the crack during the first cycle

The crack width in unreinforced clay specimens were found to be always more than the fiber-reinforced clay specimens. As can be seen in Figure 6.7, the value of crack width, $c_{w,\ avg}$ for all the fiber-reinforced clay specimens is similar during crack initiation and doubled in the case of fiber length, $l = 6$ mm due to pulling out of fibers. Figure 6.10 shows the pulling out of fibers of cut length, $l = 6$ mm. It is observed that the 6mm fibers get pulled out at the cracks, hence crack widths larger than 16 mm and 18 mm during the first drying cycle are exhibited.

6.6   Closure

In this chapter, the influence of cyclic drying and wetting on the desiccation cracking behaviour of expansive clay reinforced with and without fiber reinforcement was discussed. The unreinforced and fiber reinforced soil specimens were subjected to series of drying and wetting cycles. The process of water evaporation, surface cracks evolution, structure evolution, volume shrinkage and surface temperature behaviour were monitored. The unreinforced soil specimen

lost its complete integrity at the end of three cycles. Whereas, the fiber reinforced soil specimens were still intact as a layer, substantiating the influence of increase in tensile strength due to presence of fibers. This chapter highlights the improved healing property of expansive clay due to the presence of fibers, strength reduction due to cyclic drying and wetting.

LEFT BLANK INTENTIONALLY

Chapter 7

UNDERSTANDING DESICCATION CRACKING BEHAVIOUR OF FIBER-REINFORCED EXPANSIVE CLAY USING DISTRIBUTED FIBER OPTIC SENSING (DOFS)

7.1　Introduction

The most common technique for studying desiccation cracking of soil is the digital image analysis (DIA), due to maintenance of undisturbed specimen conditions, accuracy, and expediency. Researchers have developed and used various techniques for studying desiccation cracking of soil, such as, customized movable boundary containers, measurement probes,

2D/3D laser scanner and pouring very fine sand in the cracks (Peron et al. 2009; Sanchez et al. 2013).

Distributed optical fiber sensors (DOFS) have been a popular geotechnical structural health monitoring technology since a decade(Leung et al. 2015). A sensor is formed by first measuring and storing the Rayleigh backscatter signature of the optical fiber at an ambient state and named as the baseline condition. A change in the strain from the baseline condition results in the shift in the spectrum of light scattered in the fiber. These changes can be measured and calibrated to determine the local strain and/or temperature in the fiber. A digital acquisition system linked to the optical fiber sensors records the behaviour of the structure. With the technological advancements, the DOFS have been used in for maintenance and monitoring of structures like soil nails, soil anchors, pavements, geotextiles, pipelines, piles, retaining walls, tunnels, slopes, and embankments (Zhu et al. 2015). The optical fibers are sensitive to measure change in strain and temperature of the system.

In this chapter, DOFS has been utilized to understand the desiccation cracking behaviour of unreinforced and polypropylene-fiber reinforced expansive soil. To the best of author's knowledge, this is the first report on results of using DOFS for studying desiccation cracking of soil. The strain measured from the DOFS is analysed to study the crack initiation and crack propagation in unreinforced soil specimens. The strain measured in fiber-reinforced soil specimens are compared to that of unreinforced specimens and discussed in subsequent sections. Also, particle image velocimetry (PIV) technique was used to measure the strains developed on the top surface of the specimen during drying, which aided in extracting meaningful information on movement of soil particles in unreinforced and fiber-reinforced soil.

7.2   Working principle of DOFS

To measure the changes in reflective characteristics, distributed sensing utilizes three types of measuring systems known as Rayleigh, Raman and Brillouin based systems. This nomenclature is derived, from the frequency of signal that is analysed and the discrete peaks within the electromagnetic spectrum. More specifically, the light scattering in a fiber optic cable contains three spectral parts: (1) Rayleigh scattering which is directly correlated with the wavelength of

the laser source used, (2) Stokes line components which are from photons shifted to longer wavelengths (lower frequency) than the Rayleigh and (3) anti-Stokes line components which are from photons shifted to shorter wavelengths (higher frequency) than the Rayleigh (Figure 7.1).
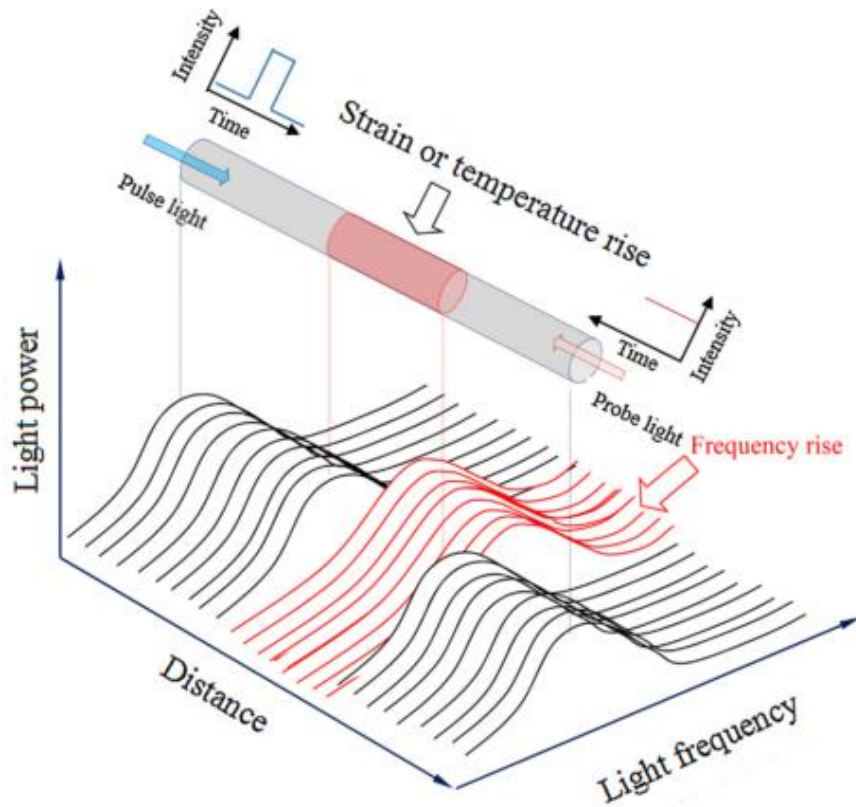
Figure 7.1 Principle of DOFS (After Hong et al. 2015)

Distributed optical fiber sensors (DOFS) have been a popular geotechnical structural health monitoring technology for a decade (Leung et al. 2015). A sensor point is formed by first measuring and storing the Rayleigh backscatter signature of the optical fiber at an ambient state (called the baseline condition).

7.3   Test procedure and program

The fiber length was varied as 6 mm, 12 mm, and 18 mm. The fiber content was maintained 0.5% by dry weight of soil, as it is found to be optimum for fiber reinforced expansive clay as discussed in Chapter 5. Table 7.1 represents the test program for the present study.

Table 7.1 Test program for the desiccation cracking tests equipped with DOFS

Test No.	Test legend	Specimen type	l(mm)	f (%)
1	UR1	UR	-	-
2	FR1	FR	6	0.5
3	FR2	FR	6	0.5
4	FR3	FR	6	0.5
5	FR4	FR	12	0.5
6	FR5	FR	12	0.5
7	FR6	FR	12	0.5
8	FR7	FR	18	0.5
9	FR8	FR	18	0.5
10	FR9	FR	18	0.5

UR- Unreinforced; FR- Fiber reinforced; f- fiber content; l- fiber length

7.3.1 Sample preparation

Mixing method

The desiccation cracking tests were performed in acrylic long rectangular containers to aid parallel cracking. The dimensions of the rectangular mould are 250 X 25 X 20 mm. Two holes of 1 mm diameter were drilled on both side walls of the mould to aid passage of optical fiber. Figure 7.2 shows the arrangement of optical fibers through the soil specimen.

The required quantity of soil was dried, crushed and sieved through 425 µm sieve. The dry soil was mixed with required quantity of fibers of varying cut lengths. The fiber cut length were varied as 6 mm, 12 mm and 18 mm. Water was then gradually added to the dry soil-fiber mix

close to plain soil's liquid limit. The side walls of acrylic rectangular mould were slightly greased with petroleum grease to aid restraint only from the bottom surface during drying. The prepared slurry was then poured into the rectangular moulds till the level of drilled holes with the help of spatula. Then the optical fiber was passed through the drilled holes making a loop at one side as shown in the Figure 7.2.
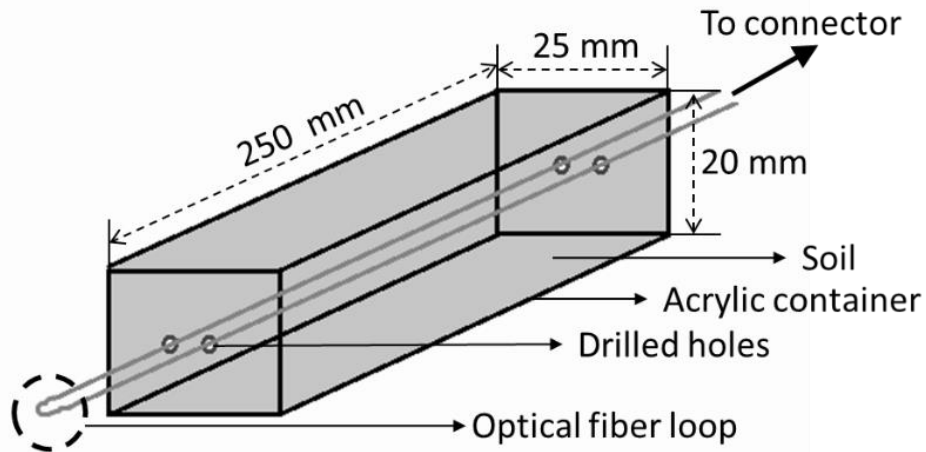
Figure 7.2 Specimen container

This ensured that the optical fiber is laid properly inside the specimen. The remaining slurry was poured in the container till the top of the container, tapped to release any air bubbles, covered with cling wrap, and left for homogenization for at least 24 hours.

7.3.2 Connection of optical fiber with ODiSi

There are two methods of fiber optic splicing, fusion splicing & mechanical splicing. Fusion Splicing Method was used for connecting the optical fiber of specimen with the ODiSI system. Fusion splicing is a junction of two or more optical fibers that have been permanently affixed by welding them together by an electronic arc. The procedure is represented in Figure 7.3, Figure 7.4, and Figure 7.5. Four basic steps to completing a proper fusion splice:

Step 1: Preparing the fiber - Strip the protective coatings, jackets, tubes, strength members, etc. leaving only the bare fiber showing. The main concern here is cleanliness.

Step 2: Cleave the fiber - Using a good fiber cleaver here is essential to a successful fusion splice. The cleaved end must be mirror-smooth and perpendicular to the fiber axis to obtain a proper splice.

Step 3: Fuse the fiber - There are two steps within this step, alignment and heating. Alignment can be manual or automatic depending on what equipment you have. Generally, the higher priced equipment you use, the more accurate the alignment becomes. Once properly aligned the fusion splicer unit then uses an electrical arc to melt the fibers, permanently welding the two fiber ends together.

Step 4: Protect the fiber - Protecting the fiber from bending and tensile forces will ensure the splice not break during normal handling. A typical fusion splice has a tensile strength between 0.5 and 1.5 lbs and will not break during normal handling but it still requires protection from excessive bending and pulling forces. Using heat shrink tubing, silicone gel and/or mechanical crimp protectors will keep the splice protected from outside elements and breakage.
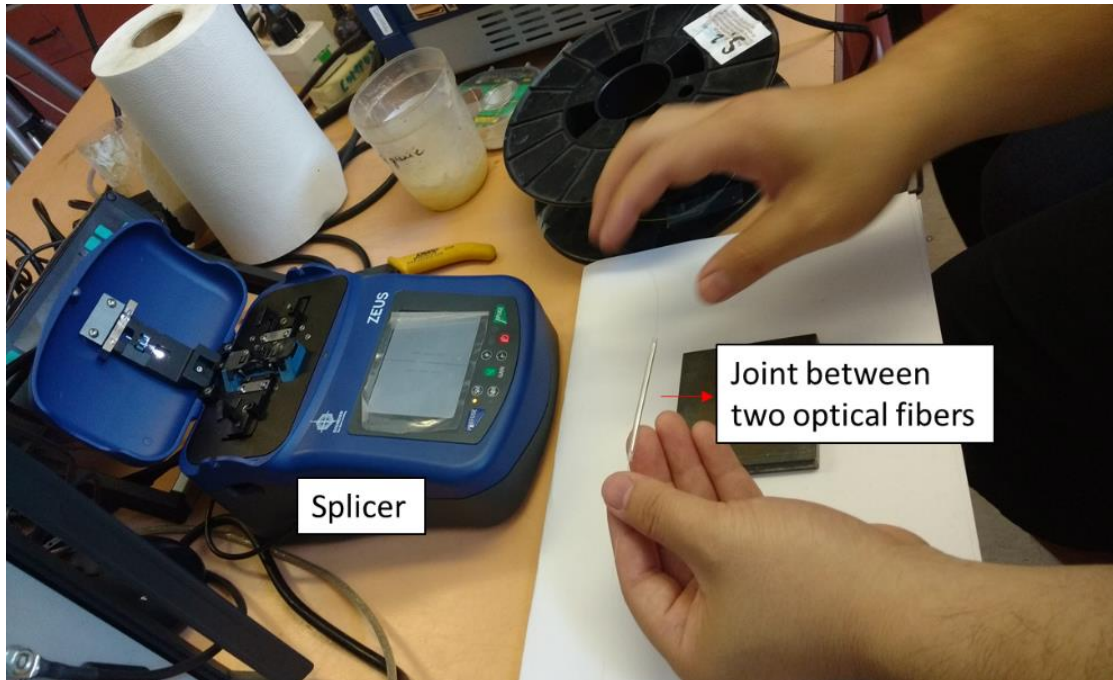
Figure 7.3 Splicer for cleaving of fiber

(a) Removal of top protective layer on optical fiber

(b) Fixing of optical fiber on splicing bracket
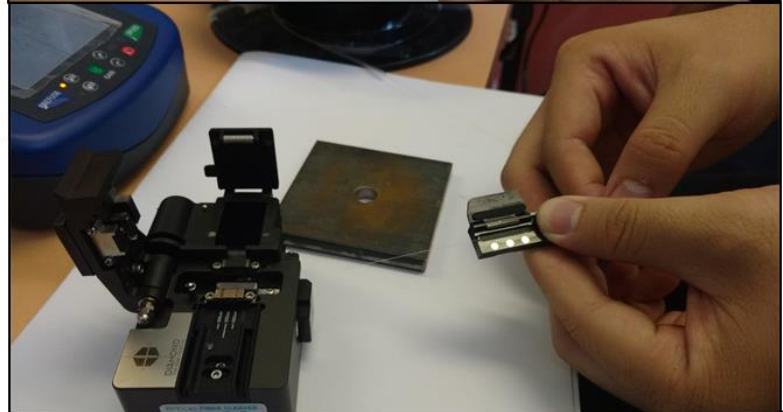
(c) Zoomed image display before fusing

(d) Zoomed image display after fusing

Figure 7.4 Steps for splicing and fusing optical fiber
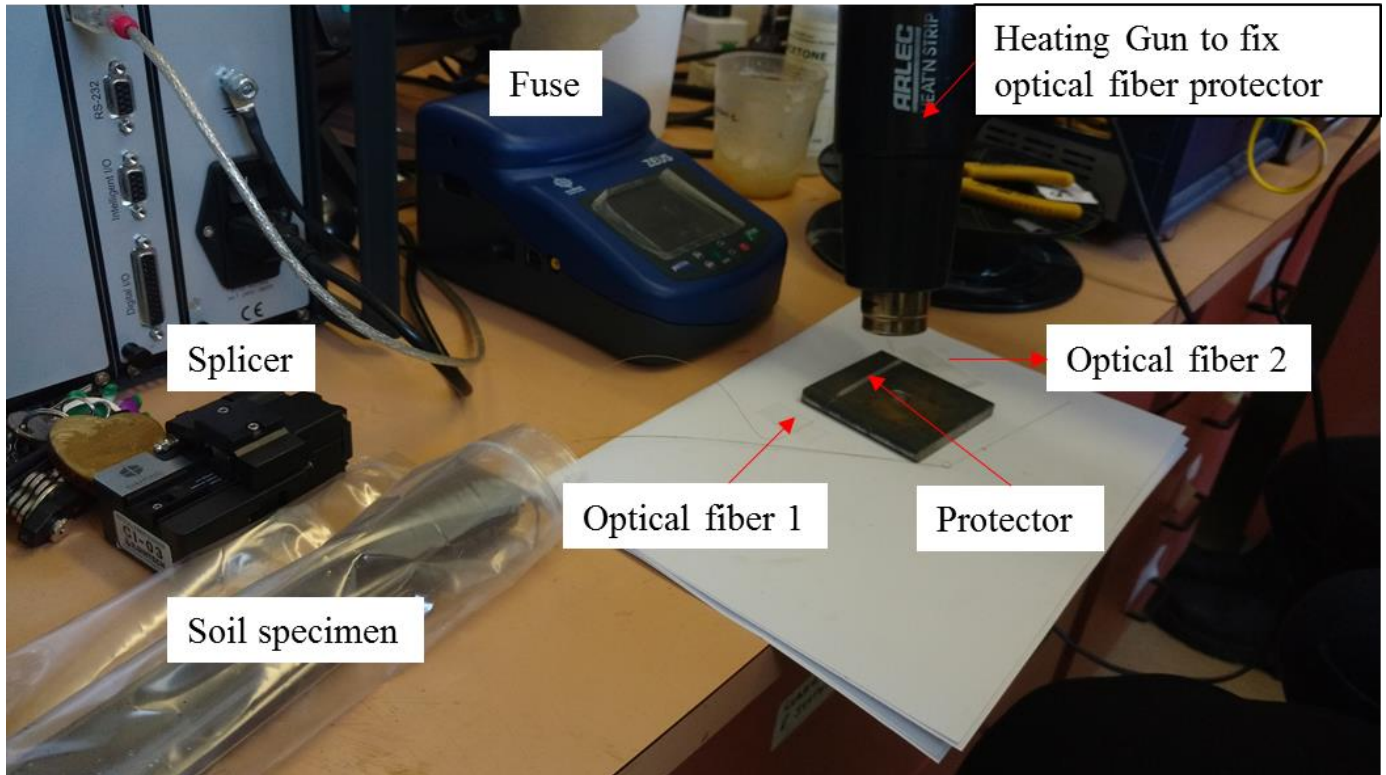
Figure 7.5 Steps for protecting the optical fiber after fusing

Test condition and procedure

The prepared unreinforced and fiber-reinforced soil specimens were kept in the test setup and allowed to desiccate at reasonably constant temperature of 22°C and 40% relative humidity. The tests were performed till the breakage of optical fibers. The specimen container was placed on a weighing balance (accuracy ±0.001g) to continuously log the moisture loss during desiccation.

7.4 Details of Experimental test setup

The test setup consists of an integrated system for monitoring strain measurement using Optical Distributed Sensor Interrogator-B series (ODiSI), monitoring moisture loss data, and DIA system as shown in Figure 7.6. Figure 7.7 shows the photograph of arrangement of ODiSI in test setup.
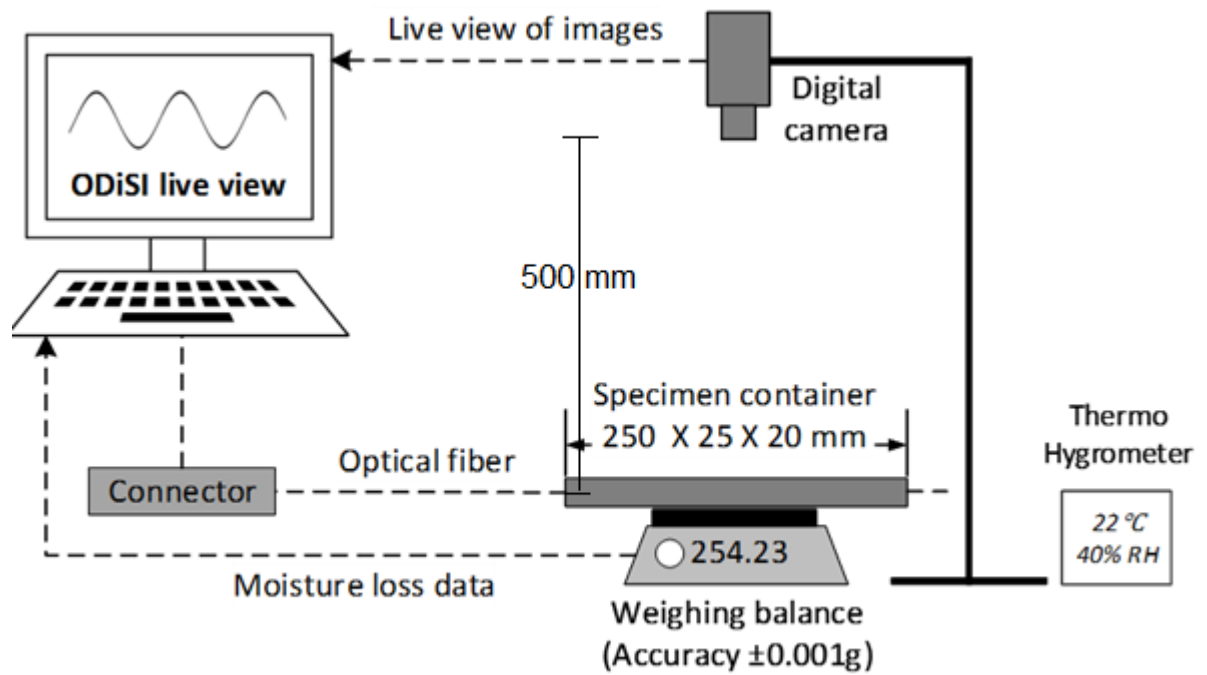
Figure 7.6 Schematic arrangement of test setup
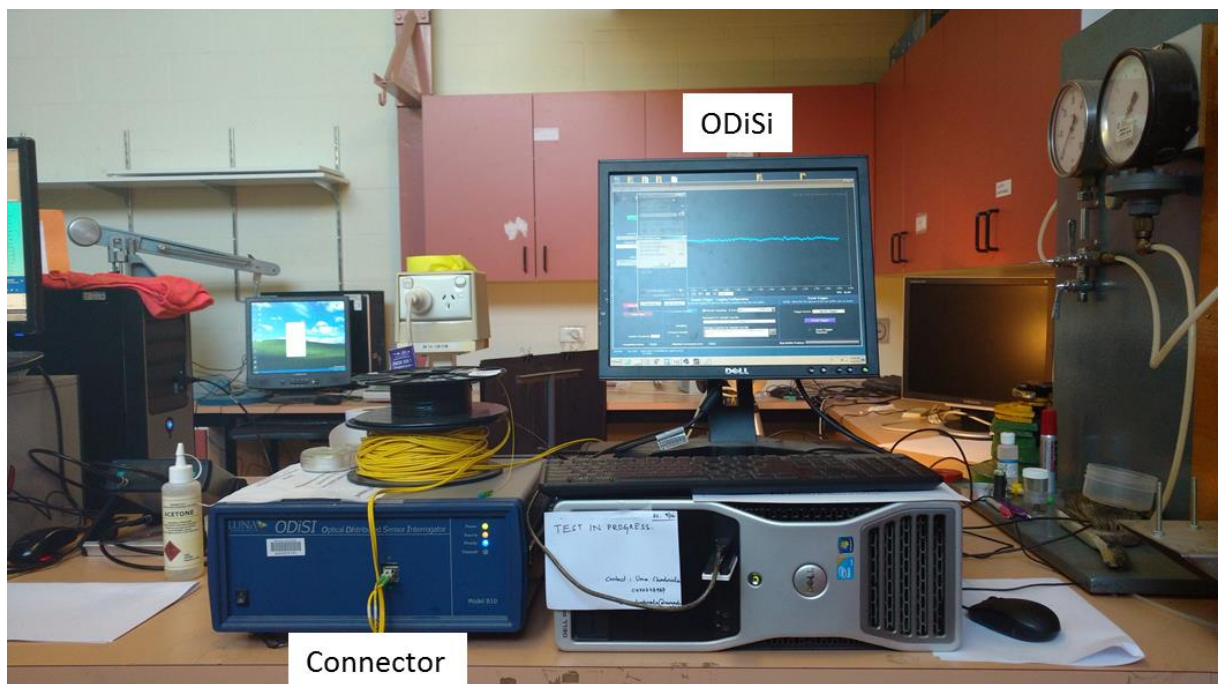
Figure 7.7 Arrangement of ODiSi in test setup

7.4.1 ODiSI

The experiments were conducted using Optical Distributed Sensor Interrogator-B series (ODiSI-B) by Luna Technology. The ODiSI-B utilizes swept-wavelength coherent interferometry to interrogate the optical fiber sensors. The basic components of the optical system include a Tuneable Laser Source (TLS), a Mach-Zender interferometer (with one arm connected to the optical fiber sensor), and a detector (Figure 7.8).
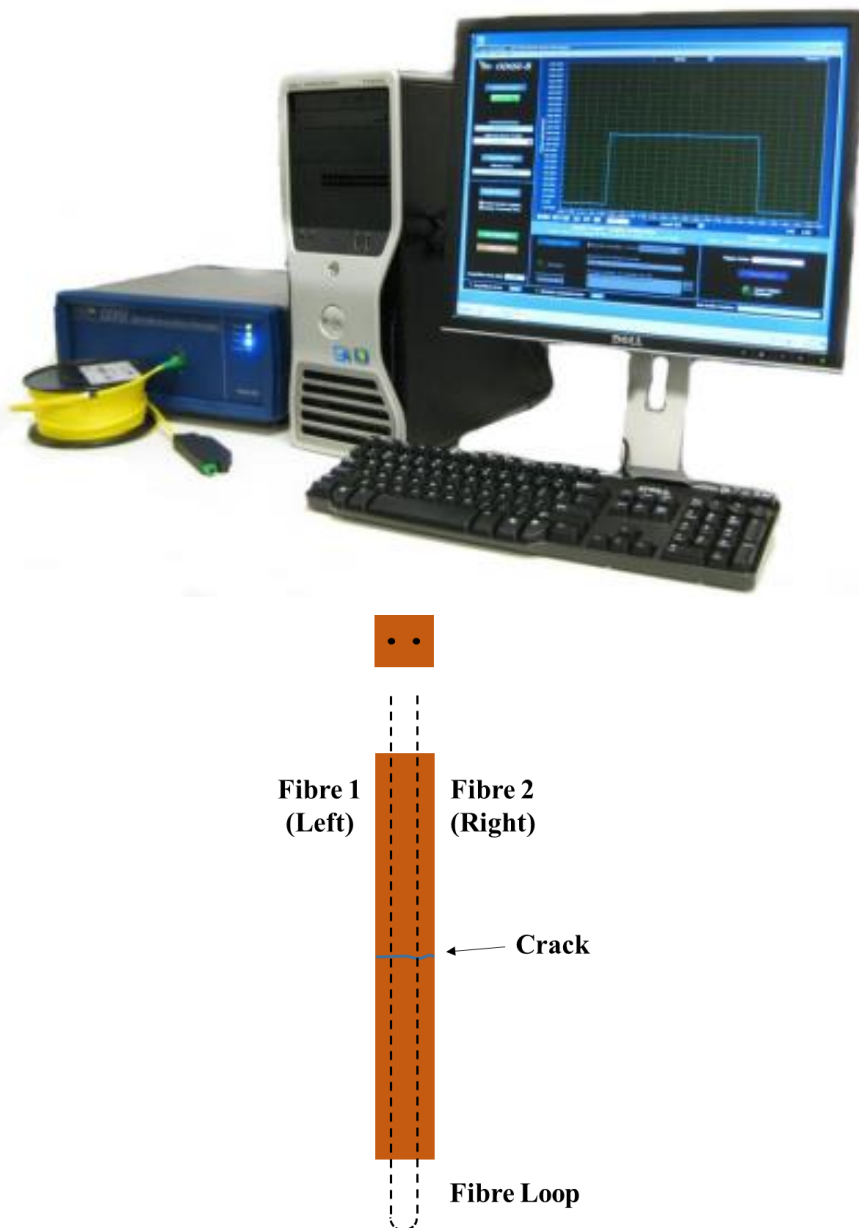
Figure 7.8 ODiSI-B measurement system

A continuous light wave is sent using the laser source. Any physical changes (i.e. local environmental temperature and strain) to the sensor create a measurable change to how light source is scattered from locations along the optical fiber sensor. The optical detector then measures the intensity of the Rayleigh backscattered light as a function of optical frequency.

The data is processed using inverse Fourier transform and thus can be scaled in units of length using the speed of light and the group index of the sensing fiber. The shift in the spectrum of the scattered light is linearly proportion to both strain and temperature as shown in the following:

$$\frac{\Delta v}{v} = K_T T + K_\varepsilon \varepsilon \qquad\qquad (7.1)$$

where v, K_T and $K\varepsilon$ are the frequency, temperature, and strain calibration constants, respectively. This technique results in distributed strain measurements with $1\mu\varepsilon$ resolution or temperature measurements with a 0.1°C resolution. This sensor has a spatial resolution of 5 mm, a maximum measuring length of 10 m and a temporal resolution of 0.01 s (data acquisition rate of 100 Hz).

Test screenshot

The screenshot of the test screen during various stages of the experiment are shown in this section. The ODiSI-B software was used to capture the laser values from the optical fiber. The software will them display a graph of the sensor data's amplitude response. Figure 7.9 shows the screenshot of the software at the beginning of the test. As there is no shrinkage in the soil specimen, no undulations can be seen in the line graph of strain values.

As the specimen undergoes desiccation, the compressive strains start developing in the soil. Small compression strain values can be seen in the test screenshot in Figure 7.10. Further, as the soil desiccates and eventually crack forms, a dip in the compressive strain values are seen, as shown in Figure 7.11.
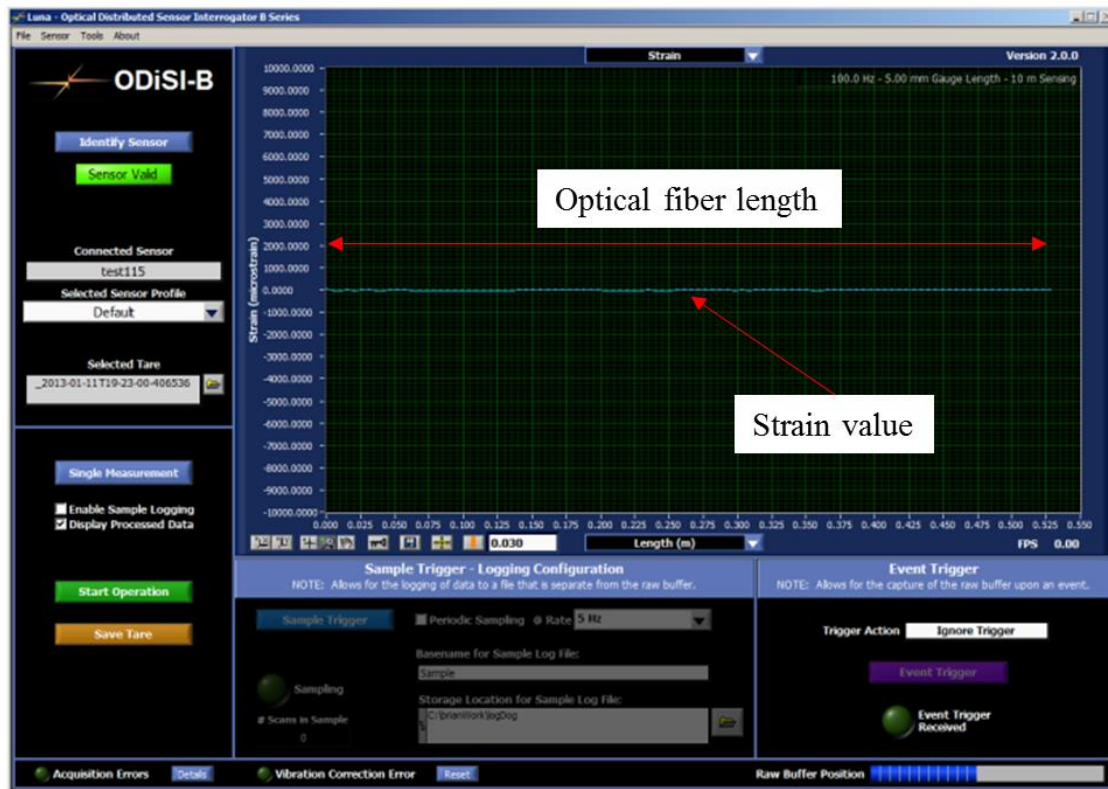
Figure 7. 9 ODiSI-B Sensor Configuration Graph Screen when no strain is developed in the soil

Figure 7.10 ODiSI-B Sensor Configuration Graph Screen when compressive strain is developed in the soil
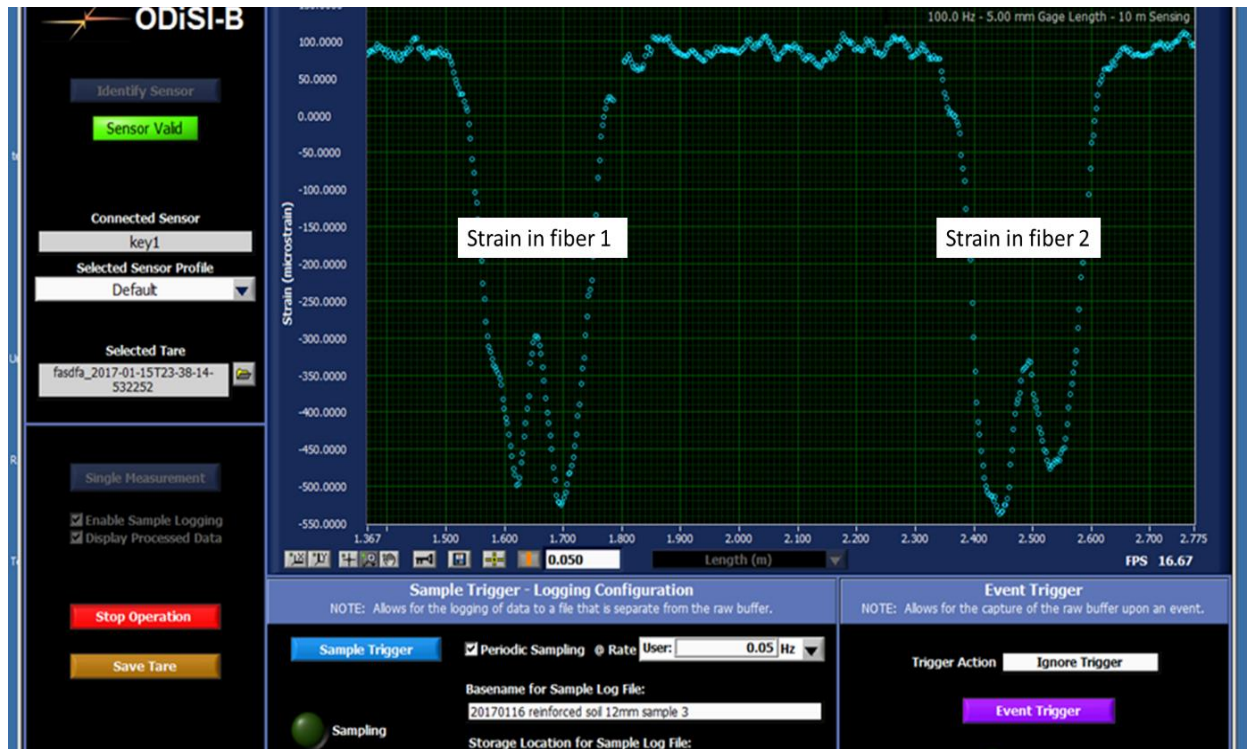
Figure 7.11 ODiSI-B Sensor Configuration Graph Screen when crack is formed in the middle of the specimen

7.4.2 Optical data acquisition system

Reinforcing fibers hold the soil mass against cracking and maintain the soil mass integrity (Viswanadham et al. 2011; Qiang et al. 2014). Observing the movement of soil body during drying could provide us valuable evidence on effect of fiber reinforcement on desiccation cracking of soil. Therefore, sequential images of drying specimen were captured using a digital camera enabled with remote shooting from computer.

PIV analysis was carried out in an image analysis module for MATLAB, GeoPIV_RG (Stanier et al. 2016). Fine white sand was randomly sprinkled on the top surface of the specimen to provide acceptable texture for PIV analysis. Also, accurate target markers were placed to facilitate PIV analysis (White et al. 2005). A secondary camera was also placed on the side of specimen to capture vertical shrinkage in specimen.

7.5   Results and discussion

The strain values obtained from the DOFS were processed through Fourier transform, filtered of the unnecessary noise data and analysed in MATLAB software. The measured strain values are expressed as microstrain (μƐ). The strain values from the DOFS and the displacement vectors obtained from the particle image velocimetry analysis using GeoPIV are presented in this section.

7.5.1 Strain measurement using DOFS

The strength property of soil changes with the decrease of moisture content. The soil specimen experiences considerable longitudinal shrinkage due to greasing of side walls despite predominantly full restraint conditions from the bottom. During desiccation, the soil undergoes both tension and compression due to partial restraint conditions. Initially, the shrinkage causes development of compression and the tension due to basal restraint leads to cracking. The development of compression and tension in soil specimen during desiccation is discussed in this section.

Unreinforced soil specimen

Figure 7.12 shows the development of strain in optical fiber in first 8 hours of drying. Interestingly, first the specimen experiences very low tensile strain (~200μƐ) and slowly develops compressive strain. In the earlier stages of desiccation, it is observed that the soil specimen experiences no horizontal shrinkage and slight vertical shrinkage. The top surface of the soil specimen experiences the large displacement, since initially, moisture loss takes place only from the top surface.
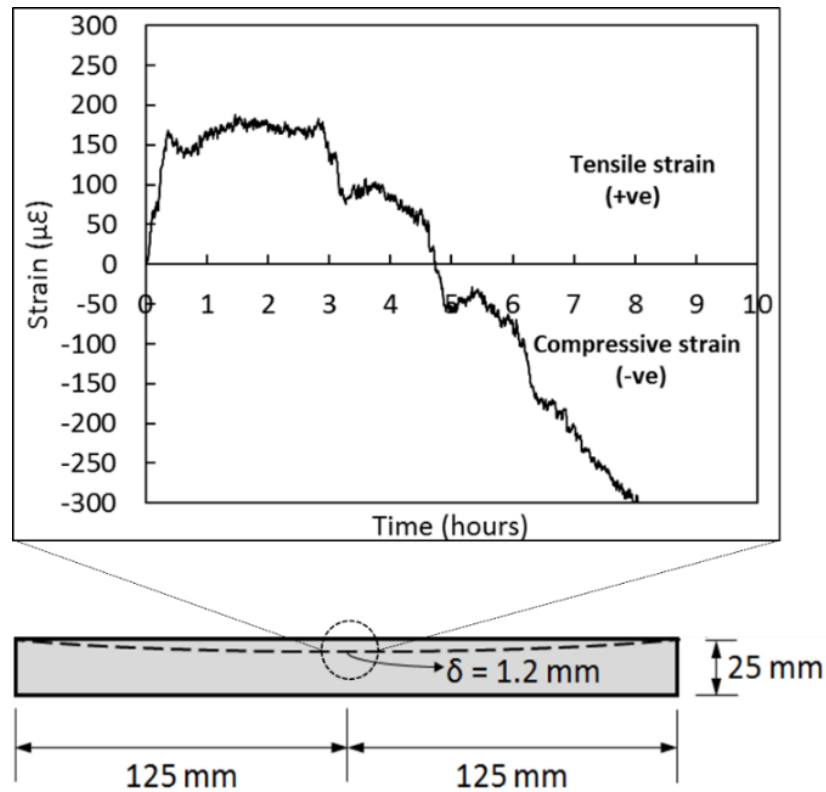
Figure 7.12 Strain profile in first 8 hours of drying for unreinforced soil specimen at the mid of the specimen

The images from side view of desiccating specimen reveal a vertical shrinkage of 1.2 mm (average) at the mid of the specimen (L = 125 mm) after first two hours of drying. During this process, a significant load on the optical fiber reduced leading to development of tensile strain. Upon further desiccation, the specimen reached the stage of isotropic shrinkage leading to development of compressive strain in soil.

Figure 7.13 shows the strain profile along the length of specimen during the test duration for unreinforced soil. A stage reaches where the tensile stresses developed due to the restraint from the bottom surface during compression exceeds the tensile strength of soil. Now, the compressive strain due to soil shrinkage drops abruptly due to increased tension in soil that leads to crack formation. Thereafter, the separated sections shrink independently, and the compressive strain increases accordingly.

A cracking stage was reached when the tensile stresses exceeded the tensile strength of the soil. The partial restraint from the clay-mould interface allows soils to shrink and compressive strain to build up within the soil; however, due to the partial nature of restraints, full shrinkage strains are not allowed be mobilized and this leads development of tensile stresses. As cracking

happens in the middle, the compressive strain drops progressively due to tensile strains that occur near the crack. This is reflected within the optical fiber as a progressive reduction in compressive strain.

Fiber-reinforced soil specimen

Figure 7.14 shows the strain profile of soil reinforced with fiber length $l = 12$ mm when subjected to drying. The plastic fibers prevent the major cracking of the specimen in the middle, and several microcracks form as reflected by local reductions compressive strain profile along with relatively small reduction at the middle. These microcracks act as multiple regions of stress release and hold the soil mass together. The crack initiation does not necessarily take place at the mid-span of the specimen and was observed at many random locations as local perturbations of the compressive strain profile. It appears that the locations of crack initiation are associated with the miniature flaws/openings that are created at the fiber-soil interfaces.

As observed in Figure 7.14, the compressive strain profiles of fiber-reinforced soil specimens show small potential microcracks at which the compressive strain spikes and dips. However, large spikes that are similar to those in Figure 7.13 are not seen, which indicates that the tensile stress that developed was released across a major part of the specimen due to fibers.

(a) Strain contour for unreinforced soil

−1800 με

−300 με

−3000 με

(b) Strains for unreinforced soil

Crack

0 hr
2 hrs
10 hrs
20 hrs
30 hrs
40 hrs
50 hrs

Contour:
Strain (με)

(c) Strain development in unreinforced soil

0 hr

10 hrs

20 hrs

30 hrs

40 hrs

50 hrs
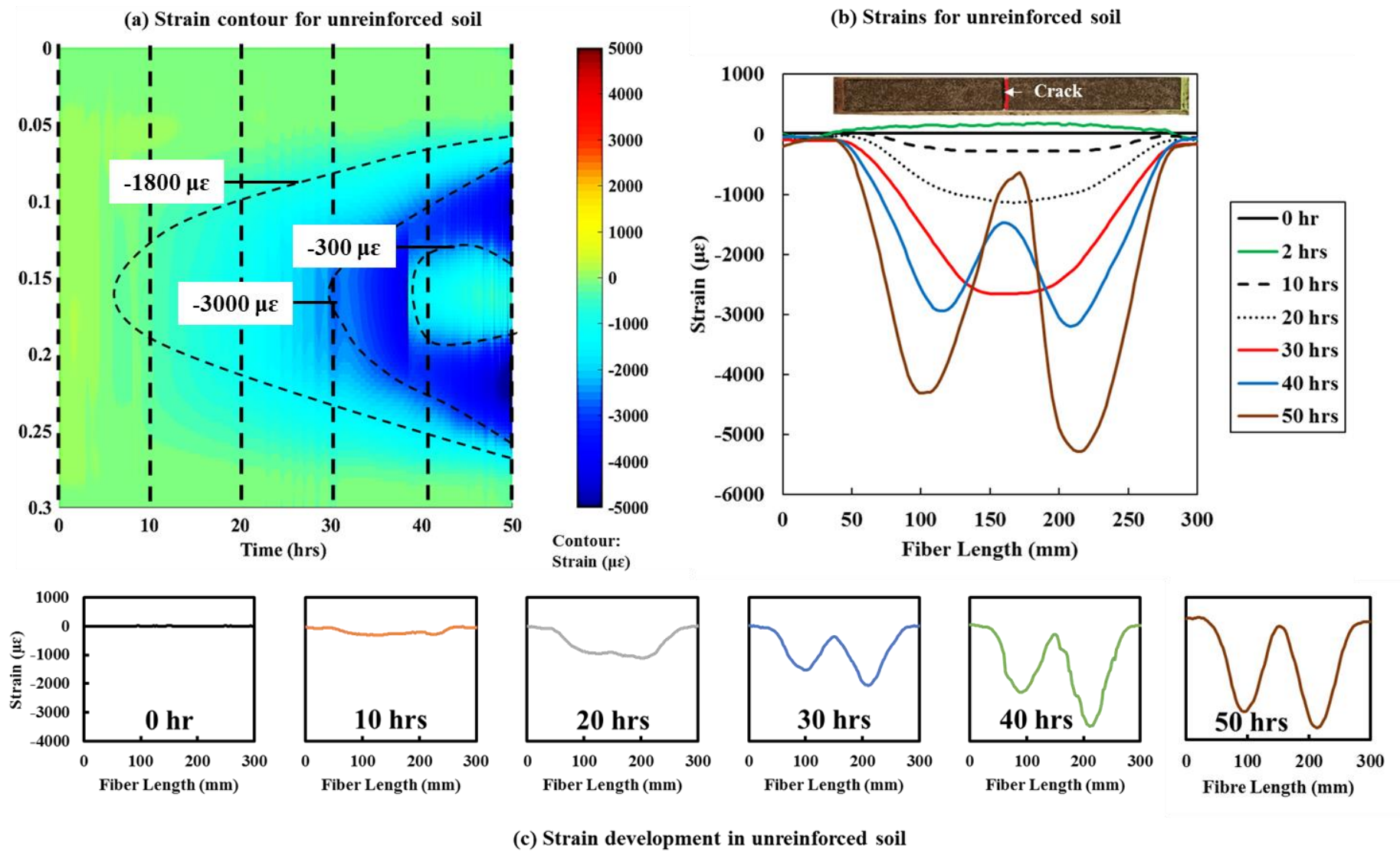
Figure 7.13 Strain profile development in unreinforced soil specimen

213

(a) Strain contour for reinforced soil ($f = 0.5\%, l = 12$ mm)

(b) Strains for reinforced soil ($f = 0.5\%, l = 12$ mm)

(c) Strain development in reinforced soil ($f = 0.5\%, l = 12$ mm)
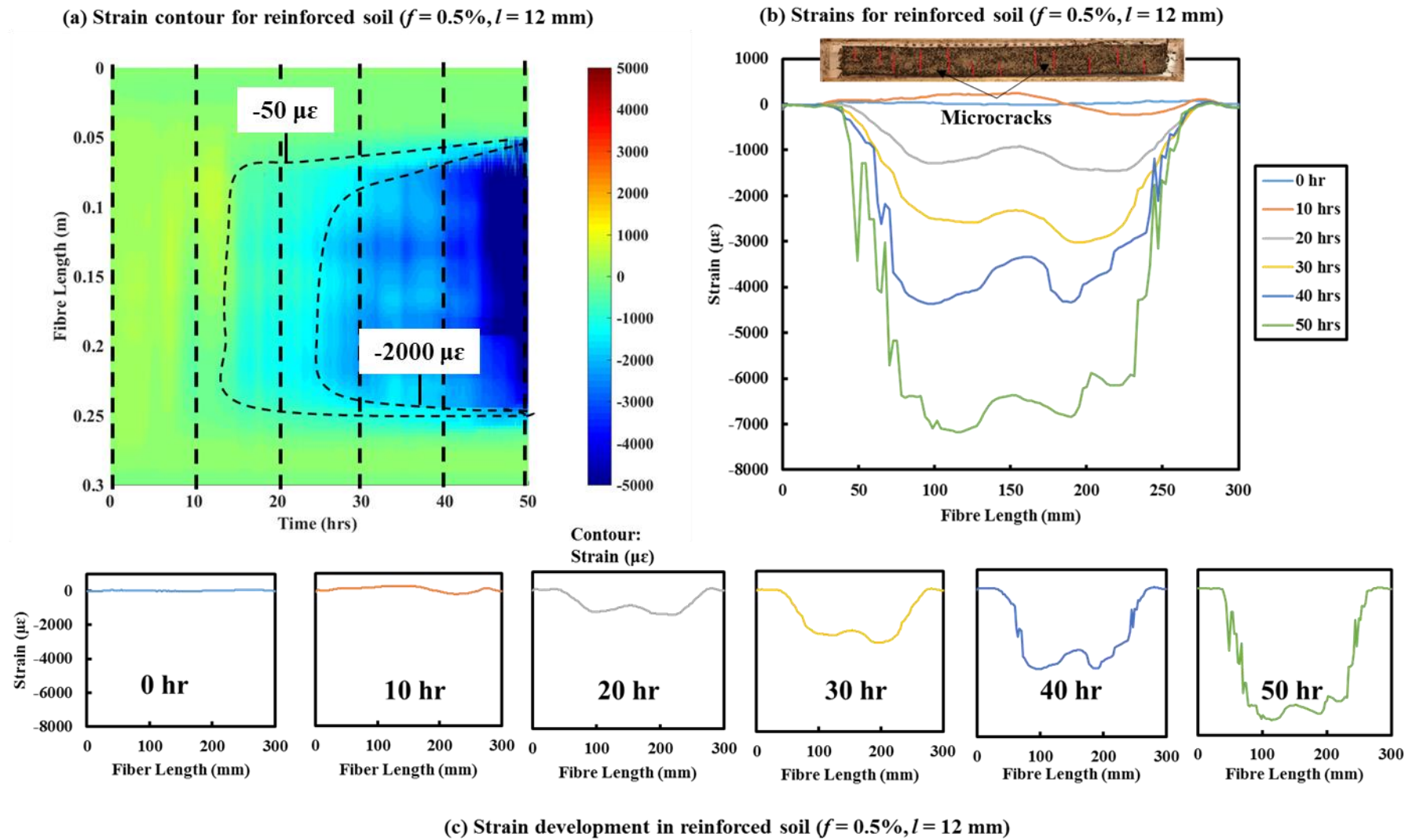
Figure 7.14 Strain profile development in fiber-reinforced soil specimen ($l = 12$mm)

7.5.2 Displacement vector fields using image analysis

PIV technique was employed to study the strain localization and displacement fields in the material after crack formation in unreinforced and fiber-reinforced specimen. The displacement vectors are plotted for given sequence of images from the input command in the software. The output gives the vectoral representation of the displacement vectors and the contour plots of displacements as well. Figure 7.15 shows the displacement vectors in the proximity of the formed crack in unreinforced and fiber-reinforced soil specimen. The soil specimen experiences significant amount of longitudinal strains during desiccation. The displacement vectors before crack initiation indicate movement of soil from sides towards the mid of the specimen. In unreinforced soil specimen, the displacement vectors in the separated soil mass are uniform and move away from the formed crack as the crack widens. Whereas, the displacement vectors in fiber-reinforced soil specimen move in longitudinal direction even after crack formation. The fibers do not allow the crack to widen and the separated soil mass is held intact by the fibers.
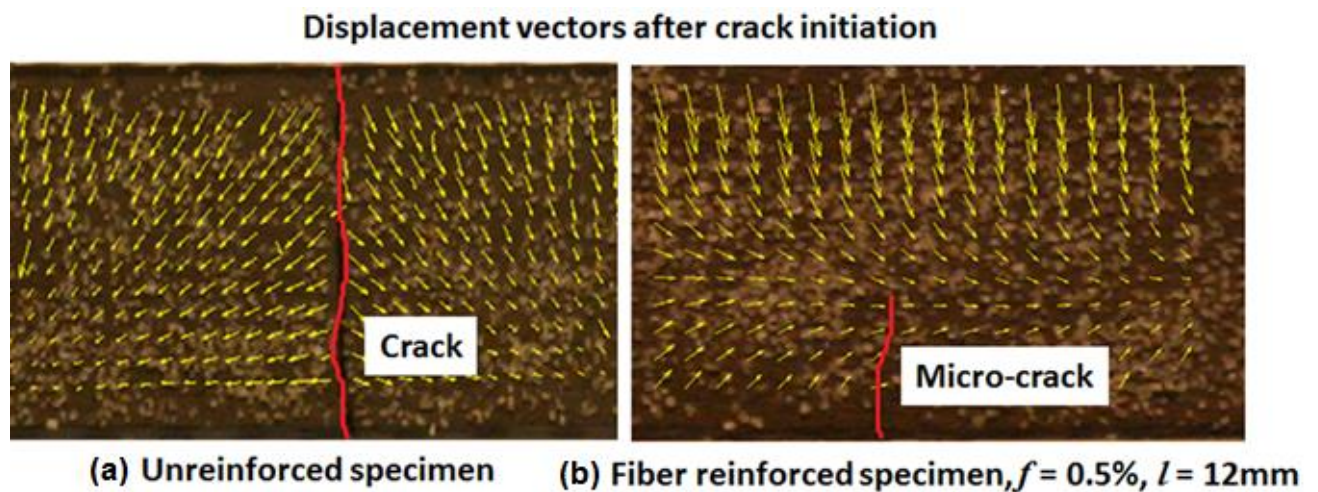
Figure 7.15 Displacement vectors developed during crack formation in unreinforced and fiber reinforced soil specimens

7.5.3 Effect of fiber length

The length of fiber offers surface area for bonding with clay. This leads to increased tensile strength of clay and better resistance to desiccation cracking. Uniform distribution of fibers is of paramount importance to maintain homogeneity and is dependent on fiber length and fiber content. In this study, all the considered fiber cut lengths were evenly distributed in the clay matrix during mixing. Fiber length was varied as 6 mm, 12 mm, and 18 mm. Figure 7. 16 and Figure 7.17 shows the strain profile of soil reinforced with fiber length l = 6mm, 12mm and 18mm when subjected to drying.

The displacement vectors before crack initiation show the movement of soil from the side edges of the mould towards the mid-section of the specimen, generating compressive strains as shown by the fiber. In the unreinforced soil specimen after cracking, the displacement vectors in the separated soil mass are uniform and opposite directions from the crack as it widens; whereas, after cracking, the displacement vectors in fiber-reinforced soil specimen move in predominantly in the same longitudinal direction even after the formation of the crack. It is evident that the fibers do not allow the cracks to widen, and the soil mass is mostly held intact by the fibers.

The tensile strain profile of unreinforced and fiber reinforced soil specimen indicate an increase in the overall tensile strength of soil due to fiber reinforcement. The compressive strain in unreinforced soil specimen attains a peak value before crack formation. Whereas, the compressive strain in fiber-reinforced soil specimens is smoother with small fluctuations due to micro-cracks. This is to be noted that, as the location of crack formation is random in fiber-reinforced soil, the compressive strain value in Figure 7.18 does not indicate the maximum strain developed in the fiber-reinforced specimen during first 24 hours. The specimen reinforced with l = 6 mm experience both random microcracks and wide macro crack at the mid length of the specimen. The crack initiation and crack propagation in specimen reinforced with l = 6 mm was similar to that of unreinforced soil specimen. The 6 mm fiber length was found to be "too short" and failed to restrain the desiccation cracking of soil.

The longer length of the fibers offers an increased surface area for bonding with clay. This leads to increased tensile strength in the clay and better resistance to desiccation cracking. Uniform

distribution of fibers is important in maintaining the homogeneity and is dependent on the length of the fiber and the fiber content. In this study, it was ensured that fibers regardless of their lengths were evenly distributed in the clay matrix during mixing. The fiber length (l) was varied as 6 mm, 12 mm, and 18 mm. Figure 7.18 shows the variation in the strain profile of the unreinforced and all of the fiber-reinforced soil specimens at the mid-length of the specimens during the initial 24 hours of drying. The initial tensile strain profiles indicate that the tensile strains developed during initial desiccation becomes higher as the fiber length increases.
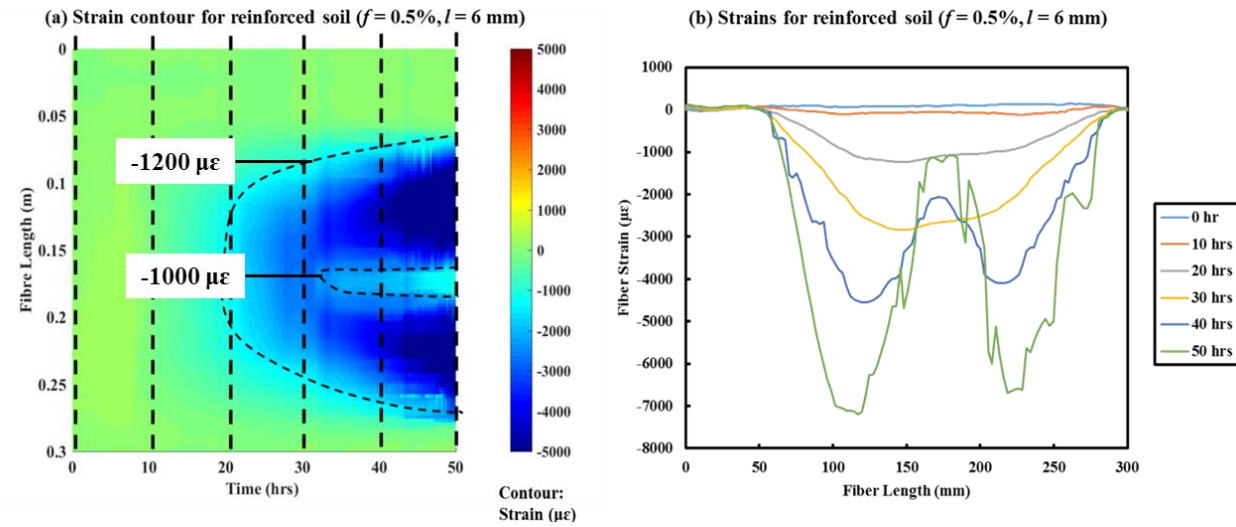
Figure 7. 16 Strain profile development in fiber-reinforced soil specimen (l = 6 mm)
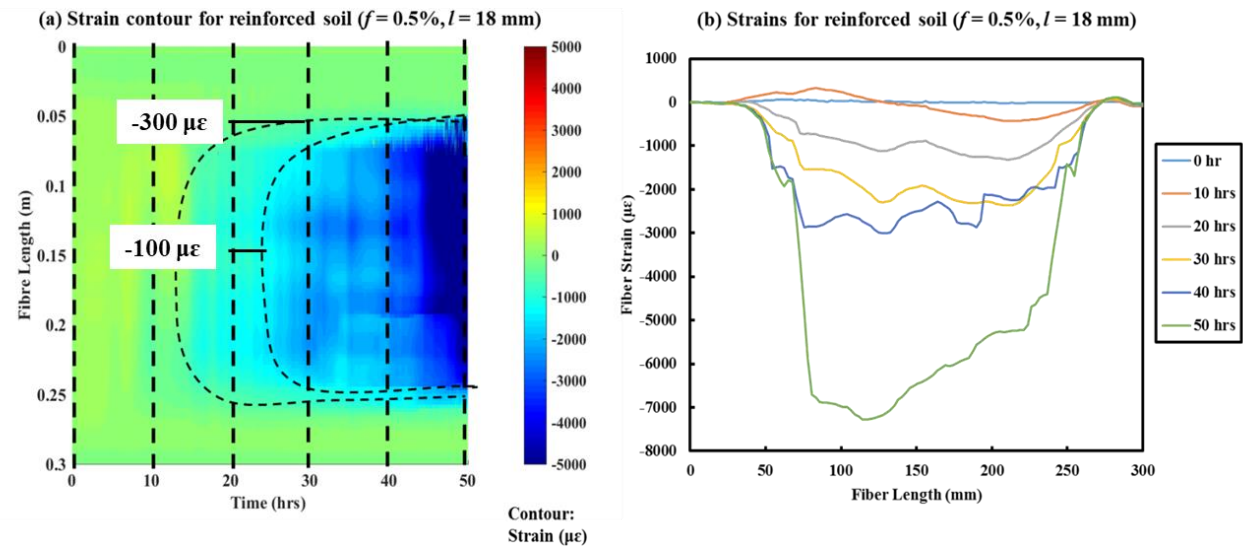
Figure 7.17 Strain profile development in fiber-reinforced soil specimen (l = 18mm)

218
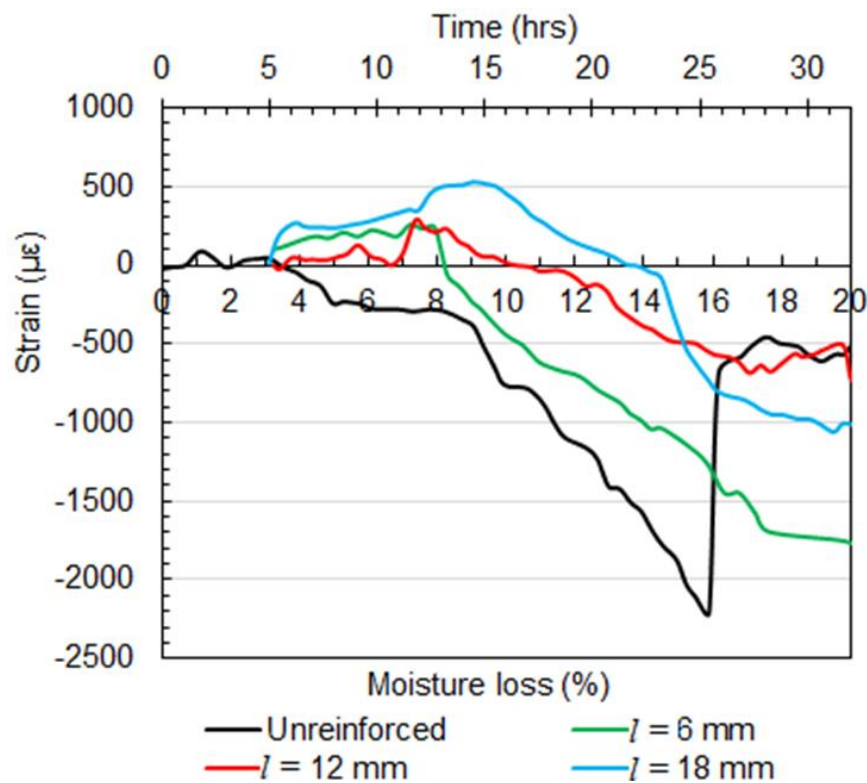
Figure 7.18 Strain profile at the middle of unreinforced and fiber reinforced soil at the mid-length of the specimen (compression positive)

Furthermore, the onset of isotropic shrinkage (i.e., the transition from tensile to compressive strains) is delayed as the fiber length increases. It is not clear why this happens at this stage. The compressive strain in the unreinforced soil specimen attains a peak value before crack formation (at 30 hours) and, in comparison, the compressive strain profiles in the fiber-reinforced soil specimens indicate that microcracks started to occur earlier (26 hours) and they progressed across the specimen upon further desiccation. The specimen reinforced with $l = 6$ mm experienced both random microcracks and major crack at the mid-length of the specimen. The crack initiation and crack propagation in this specimen were closer to those of the unreinforced soil specimen. Hence, it can be argued that the fiber length of 6 mm was found to be "too short" and failed to restrain the desiccation cracking of the soil. This is represented in Figure 7.19. The cracked unreinforced specimen shrank further to produce a 2nd crack summarizes the compressive strain that is required for the formation of the major cracks and microcracks in unreinforced and fiber-reinforced soil specimens.

It can be reported that the strains required for the formation of the first and second cracks in the unreinforced specimen are ~2500 µε and ~4500 µε respectively. On average, the soil specimens that are reinforced with l = 12 mm and l = 18 mm experience microcrack formation at a similar range of strains of about ~3200 µε. However, soil specimens that are reinforced with l = 18 mm require a maximum strain of ~4200 µε for the formation of microcracks.
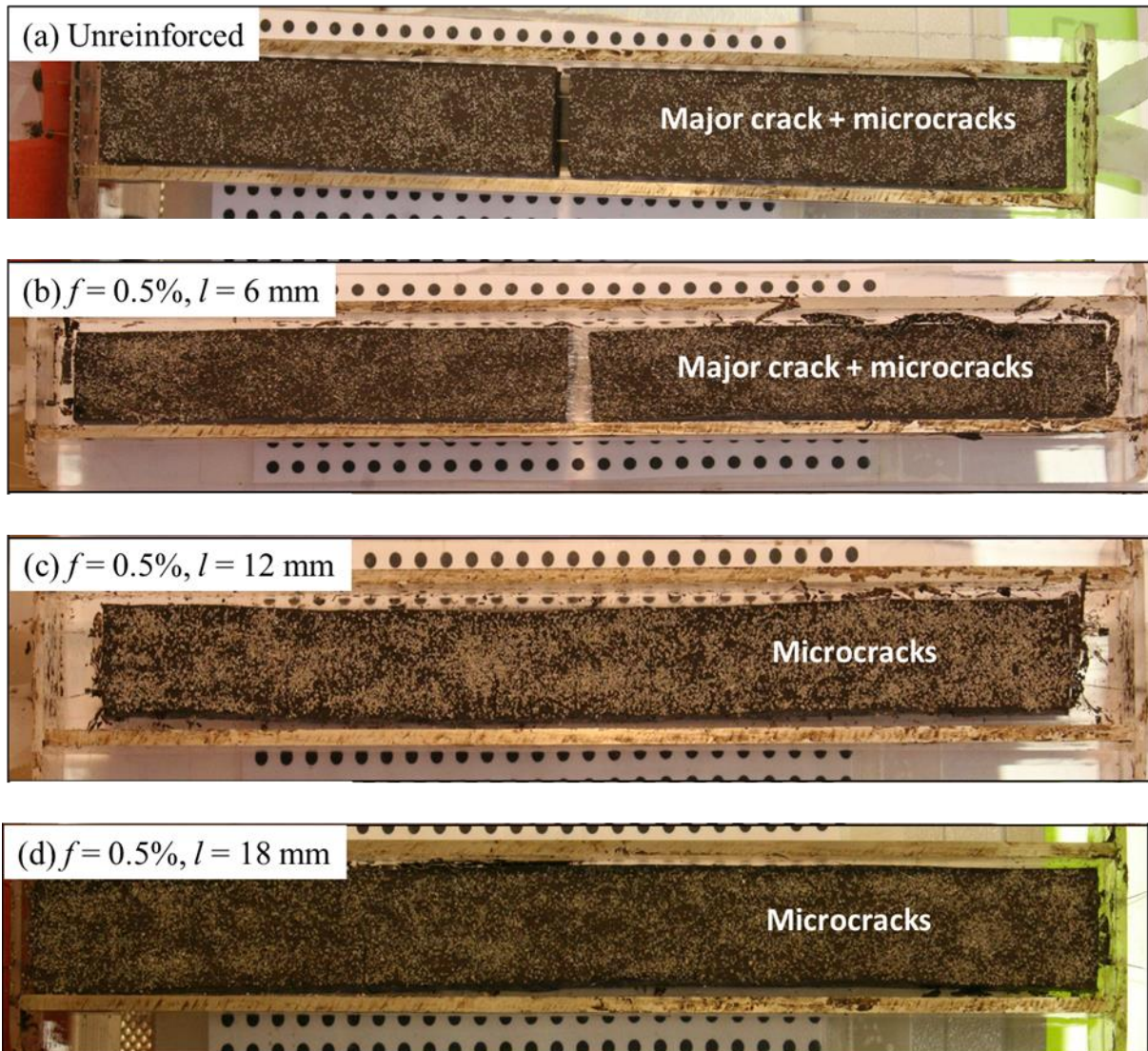
Figure 7.19 Specimens after desiccation cracking tests
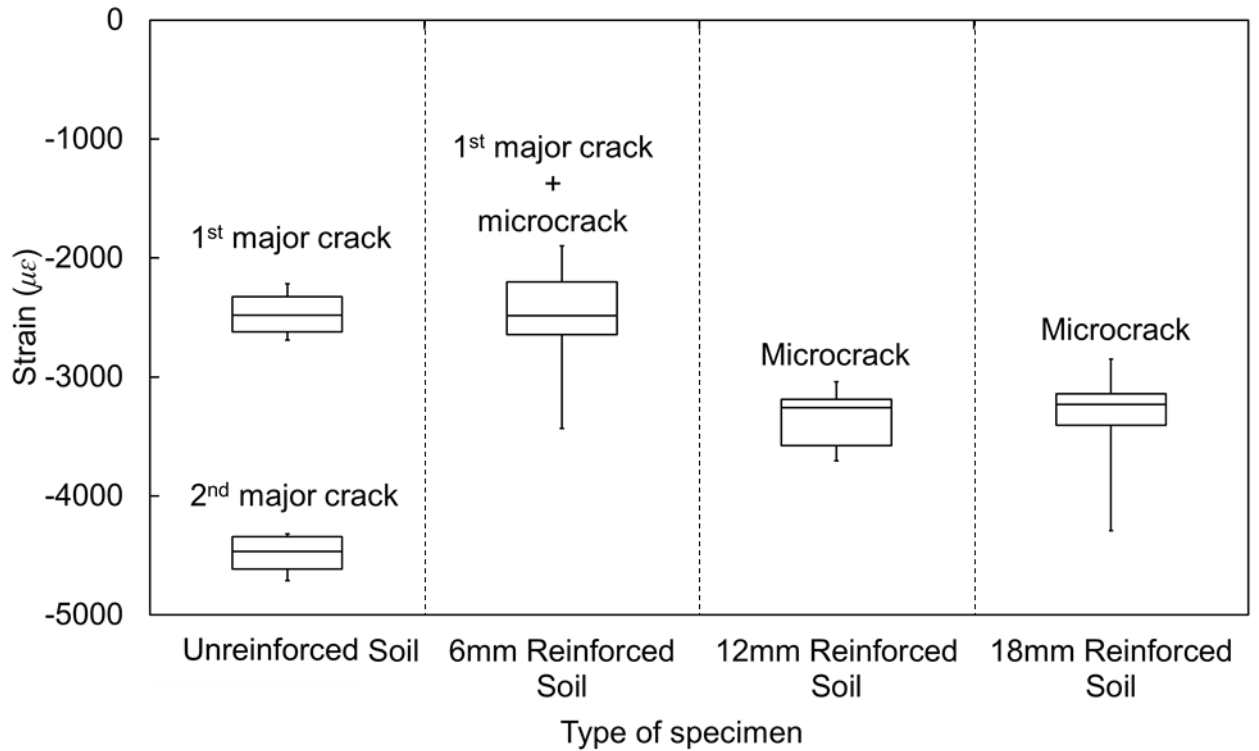
Figure 7.20 Summary of compressive strains developed in all types of soil specimen under consideration

The cracked unreinforced specimen shrinks further to produce secondary cracks. Figure 7.20 summarizes the compressive strain required for 1st and 2nd crack formation in unreinforced and fiber-reinforced soil specimens. It is worthwhile to note that the strain required for the 1st crack is ~2500 µε and ~2000 µε for the 2nd crack. On an average, the soil specimens reinforced with $l = 12$ mm and $l = 18$ mm experience micro-crack formation at similar range of strains, i.e., ~3200µε. However, soil specimens reinforced with $l = 18$ mm require maximum strain of ~4200µε for micro-crack formation.

7.6 Closure

Desiccation cracking is a persistent issue in infrastructure associated with fine grained soils. Reinforcement of soil with discrete randomly distributed fibers helps in reducing the extent of desiccation cracking. Understanding of desiccation cracking of unreinforced and polypropylene fiber-reinforced soil was attempted in this study using distributed optical fiber sensing. The

unreinforced and fiber reinforced soil specimens were instrumented with single mode optical fibers to record the strain development in the soil matrix during shrinkage. The study reveals that the reinforcing fibers certainly help in restraining desiccation cracking of soil. However, fiber length plays a crucial role in its performance. The particle image velocimetry technique was applied to study the surficial strain profiles during the shrinkage of the soil. The displacement vectors generated for the unreinforced and fiber reinforced soil specimens were compared to get interesting information about the difference in the behaviour of shrinkage, crack initiation and crack propagation.

LEFT BLANK INTENTIONALLY

Chapter 8

CENTRIFUGE MODEL TESTS ON DESICCATION CRACKING OF UNREINFORCED AND FIBER REINFORCED CLAY

8.1 Introduction

This chapter presents the centrifuge tests performed on clay layers subjected to desiccation cracking. A small beam centrifuge facility was used in this study. Centrifuge modelling technique provides an excellent tool for the authorisation, particularly in terms of confirming the crack-formation mechanism. This chapter deals with the details of centrifuge model test setup for inducing desiccation cracking in a clay layer. The desiccation cracking behaviour of unreinforced and fiber reinforced clay layer was observed inside a centrifuge in the developed test package with the help of digital camera and the results were analysed with the help of digital image analysis and particle image velocimetry technique.

8.2   Details of developed model test package

The details of small beam centrifuge equipment used in the present study are described in detail in Chapter 3. The model test package used for conducting desiccation cracking tests of unreinforced and fiber reinforced soil specimens includes:

- An acrylic container for holding the soil specimen,

- Heating system for inducing desiccation cracking in the soil specimen at high gravities,

- Image acquisition system for recording the sequential desiccation cracking of the soil specimen.

In this study, consolidated soil specimens were used for carrying out the desiccation cracking tests inside centrifuge at varying gravity levels. Figure 8.1 shows the plan and elevation of the developed test setup.

Acrylic container

A clear acrylic container having external dimensions 140 mm and 140 mm and depth 60 mm was used for conducting centrifuge tests. Even though the system involves heating, acrylic was chosen, as it is light weight and will be helpful is seeing the crack patterns from the side walls. The back, bottom and rear walls were pasted watertight with the help of concentrated chloroform and fastened with 25.4 mm steel Allen screws. A thin layer of white petroleum grease was applied to reduce the friction and adhesion between the inner walls of the container and soil layers. This will help in reducing the boundary effects.

Figure 8.2 shows the schematic representation of the model test package.

High density geofoam was used as a packing material in the acrylic container to hold the soil specimen in right place at high gravities. High density geofoam was chosen, so that no water is absorbed by the foam. The permanent markers were placed on the geofoam.
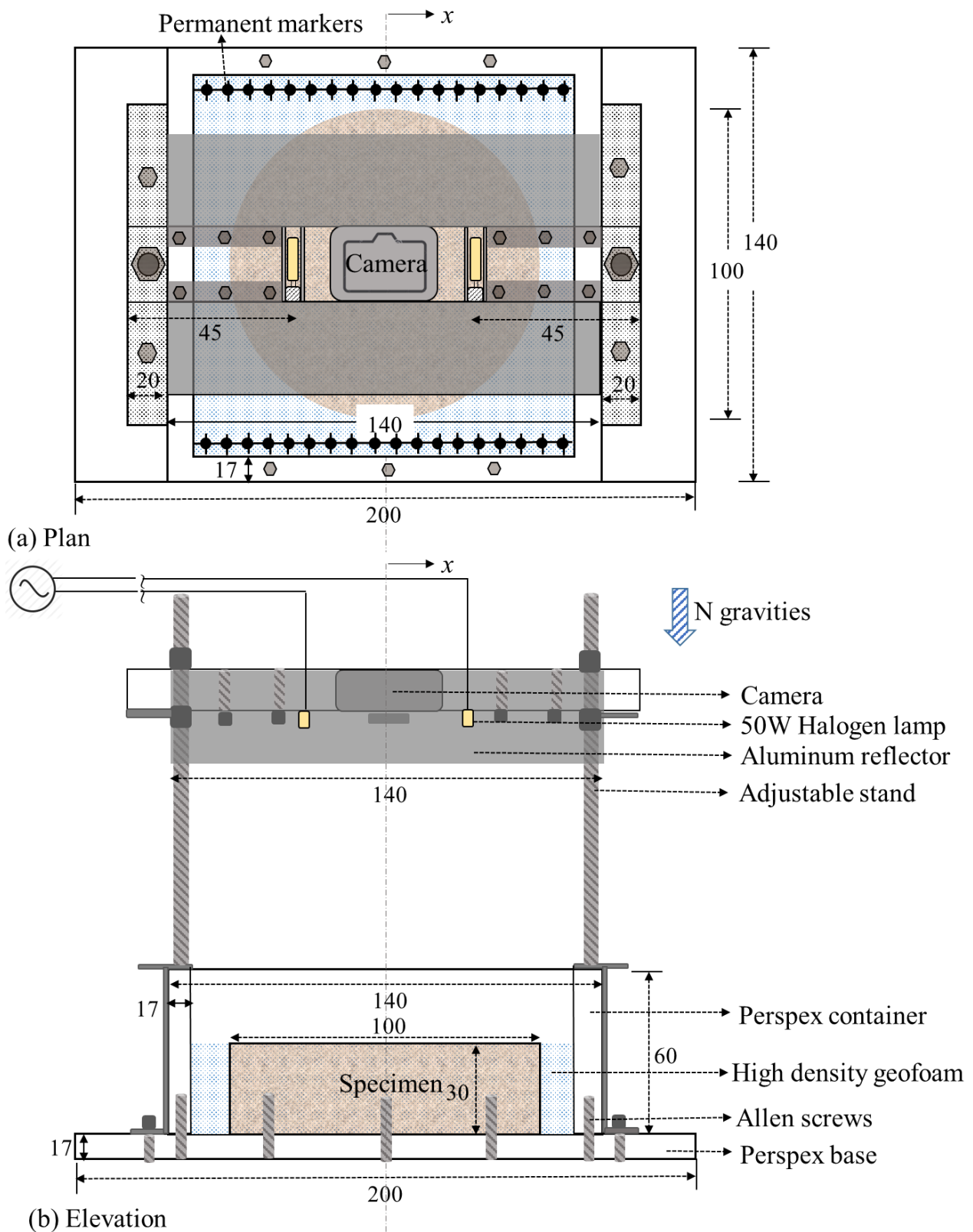
Figure 8.1 Schematic details of test setup used for centrifuge testing (a) Top view, (b) Front elevation (All dimensions are in mm)
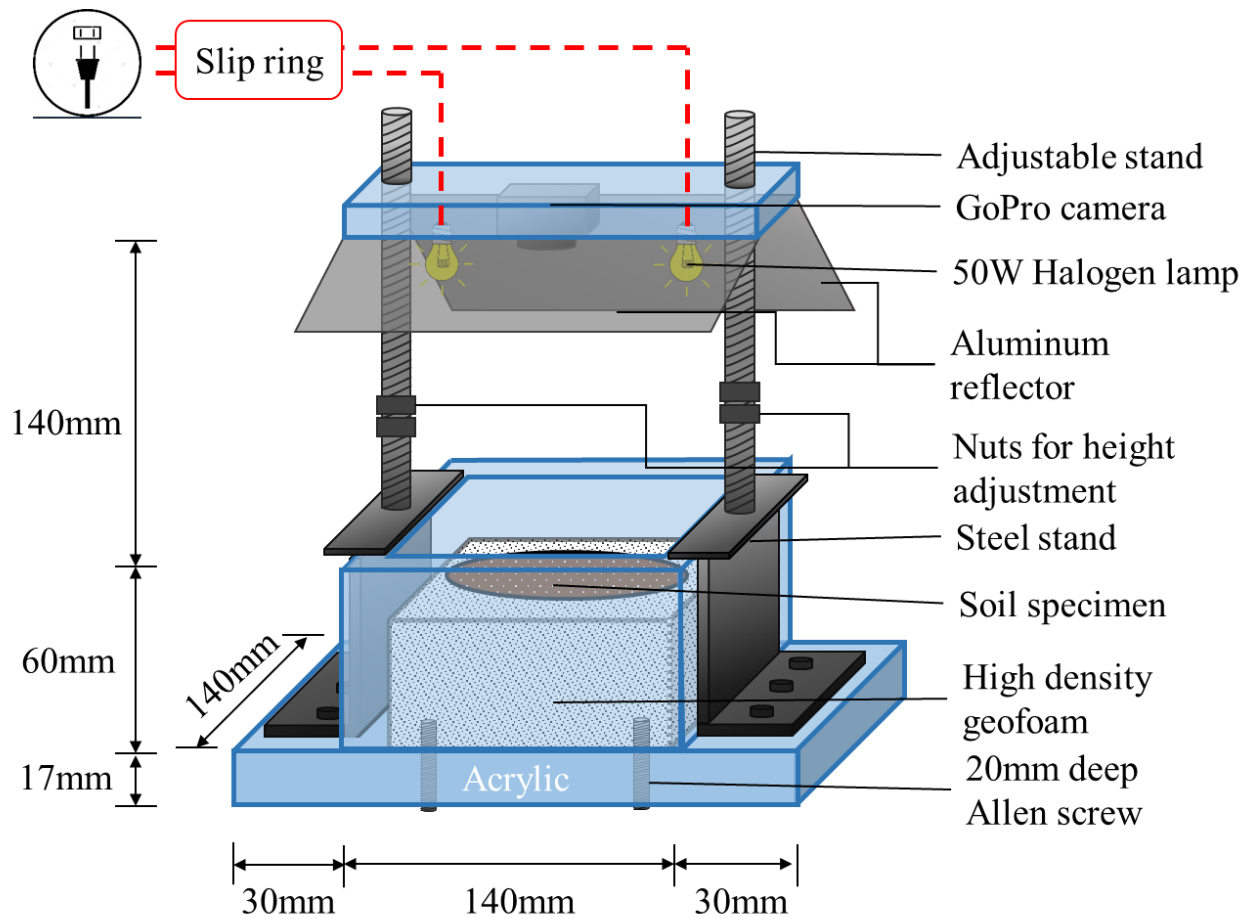
Figure 8.2 Schematic setup of the acrylic container and heating assembly for the present study

Heating system

The heating system consists of two 50 W miniature Tungsten halogen lamps, holder for halogen lamps, aluminium light reflector and stand for holding the lighting assembly with adjustable height. The halogen lamps were held tight with the electric connection with the help of ceramic lamp holders. Slipring assembly was used for supplying electricity to the halogen lamps. The acrylic holder was lined with neoprene rubber to make the assembly heat proof and not affect the digital camera with the heat. The heating system with the lamps and holder arrangement are shown in Figure 8.3.
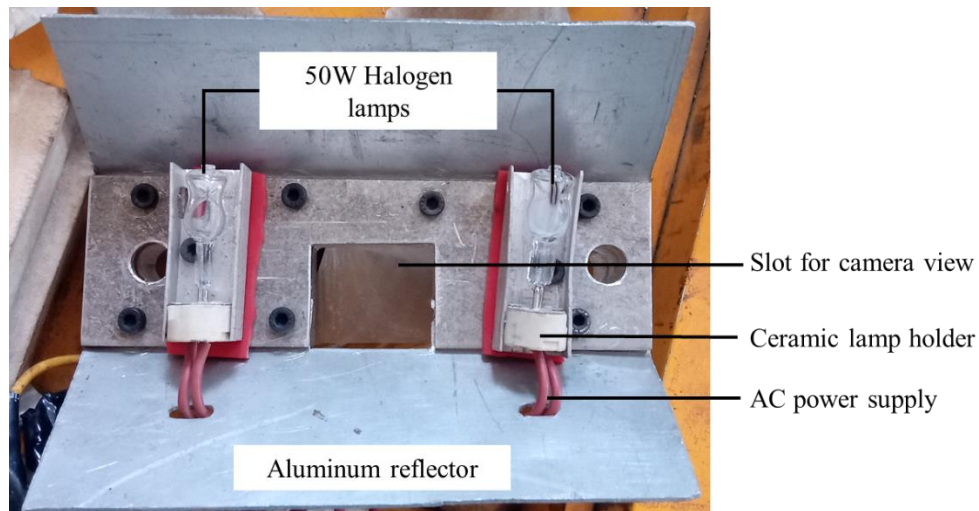
Figure 8.3 Heating system in the centrifuge model test package

Figure 8.4 Perspective view of the test setup mounted onto swinging basket of the centrifuge

Image acquisition system

As discussed in Chapter 3, section 3.3.4, a digital camera was utilized to capture high-resolution pictures at high gravities. Digital camera with the acrylic holding stand has been proof-tested up to 108g. Figure 8.4 shows the actual photograph of the test setup inside the centrifuge basket.

8.3   Test procedure and program

The acrylic container and adjustable stand were assembled together. Sample preparation was accomplished in different stages and is described herein. Oven dried clay was crushed and passed through 425μ IS sieve. Required quantities of dry clay and fibers were mixed to get a homogeneous mixture. Water was slowly added to the clay-fiber mix and mixed with the help of spatula to form a uniform mix. Adequate care was taken to avoid accumulation of fibers. The clay-fiber slurry was covered and left for homogenization for 24 hours. The slurry was poured inside 100 mm consolidation rings. The sample was consolidated under increased applied loading in steps till 180 kPa. The specimen thickness was maintained as 30 mm for 18 tests and 25 mm for 2 tests. The procedure adopted during centrifuge testing is shown in Figure 8.5.
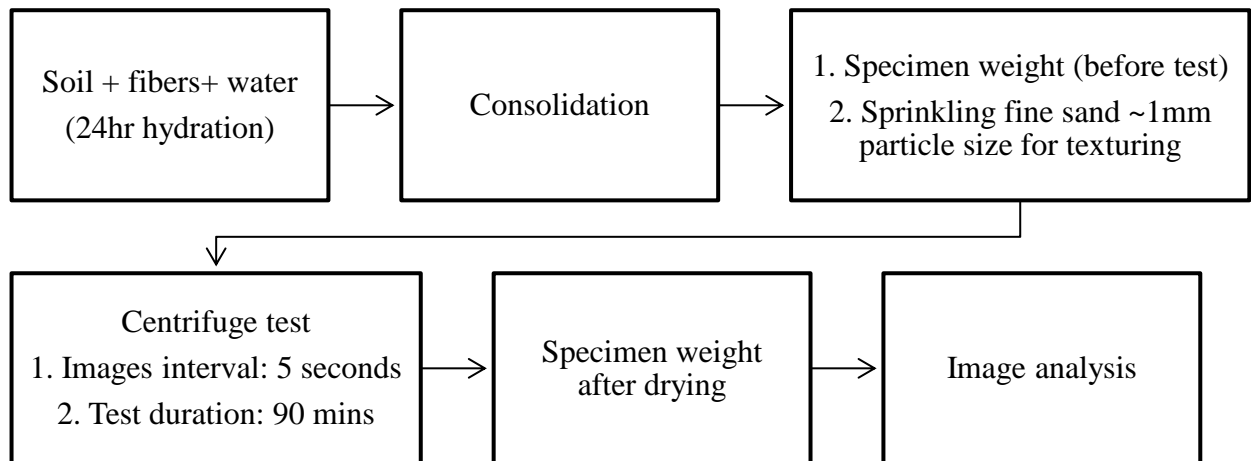
Figure 8.5 Procedure adopted in the study for the centrifuge tests

Figure 8.6 shows the consolidation ring of 100 mm internal diameter designed for preparing specimens for centrifuge experiments. The specimens for all tests were prepared at a water content close to their respective liquid limits, according to section 4.4.1. After leaving the prepared slurry for homogenization, the consolidation ring was kept in a consolidation apparatus. Figure 8.7 shows the consolidation apparatus used to prepare the specimens. To facilitate uniform moisture content distribution and to avoid any in-flight perturbances, the specimens were consolidated till they reached water content close to their respective consistency index of 0.75. The consolidated specimen was carefully extracted from the ring. The depth of specimen was maintained as 30 mm. The specimen was carefully trimmed if the height was not 30 mm. To facilitate seeding during PIV analysis the specimen surface was sprinkled with white sand as shown in Figure 8.8. In this study, the sand used was Indian Standard sand, commercially known as Ennore sand of Grade II. The sand is greyish white in colour, D_{50} of sand is 0.57 mm and classified as poorly graded medium to fine sand, as per Unified Soil Classification System (USCS) (Dave and Dasaka 2013). The specimen with seeding was placed inside model container and packed with high density geofoam to ensure that the specimen does not change its position at high gravities.

As the process of desiccation cracking is slow, happening over large amounts of time, this process is far more efficient than conventional video files. As natural sand has its own texture and colour, when light and shadows are captured by the camera, tracking of particles is somewhat simple (White et al. 2003). However, in the case of clay, the soil grain size is much smaller and more uniform, causing a problem for the PIV tracking patches. To overcome this problem, dyed sand, painted patterns or coloured woodchips are randomly scattered onto the exposed layer of the clay to give the camera a reference stochastic texture pattern. A calibration sheet or points in the form of round black dots over white backgrounds are also necessary. The points are obtained from a Mylar^{TM} sheet (sheet containing round dots which are precisely measured to a known distance) by photocopying it and cut and pasted neatly over the new calibration sheet or soil sample (Figure 8.9). The new calibration points are placed where visible in the photo frame so post-processing can be completed. The images are then calibrated in MATLAB to correct any imperfections in the camera positioning, radial and tangential lens distortion, and refraction (Shannon 2013). Permanent markers of size 3 mm and spacing 6 mm was placed adjacent to the specimen. The marker grid is certified by Max Levy Autograph, Inc., and is accurate within ±0.02mm corner to corner and dot size is accurate to ± 0.013mm or 0.43% error. Dot to dot spacing is ±0.0085mm or 0.14% error (White et al. 2003).
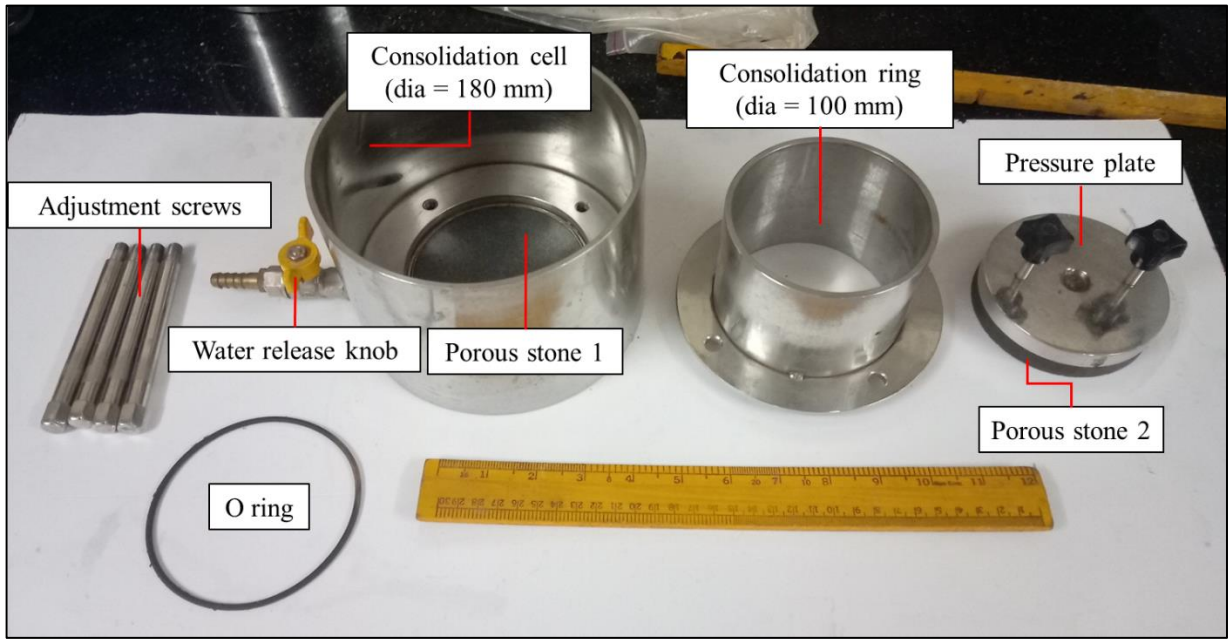
Figure 8.6 Consolidation ring for preparing soil specimens for centrifuge experiments
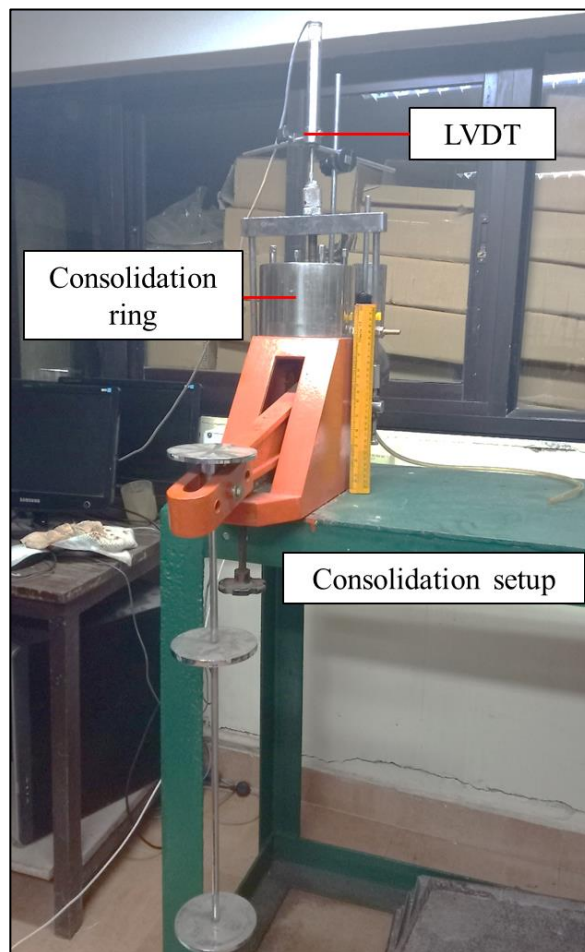
Figure 8.7 Consolidation setup for preparing soil specimens for centrifuge experiments
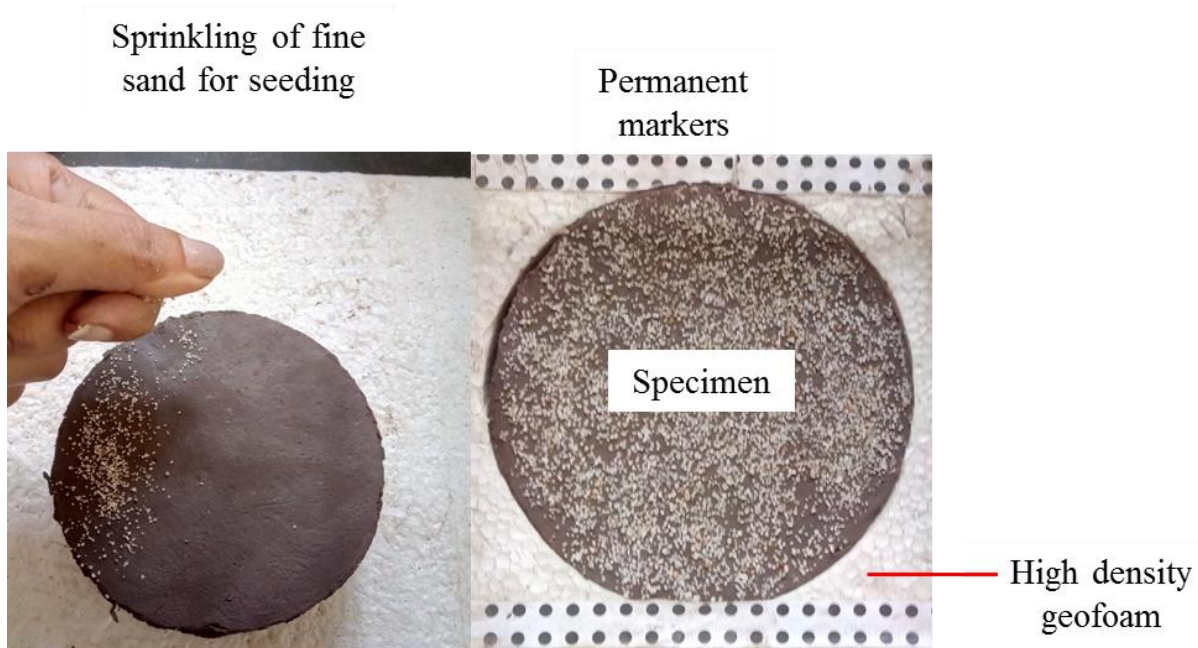
Figure 8.8 Specimen preparation for PIV
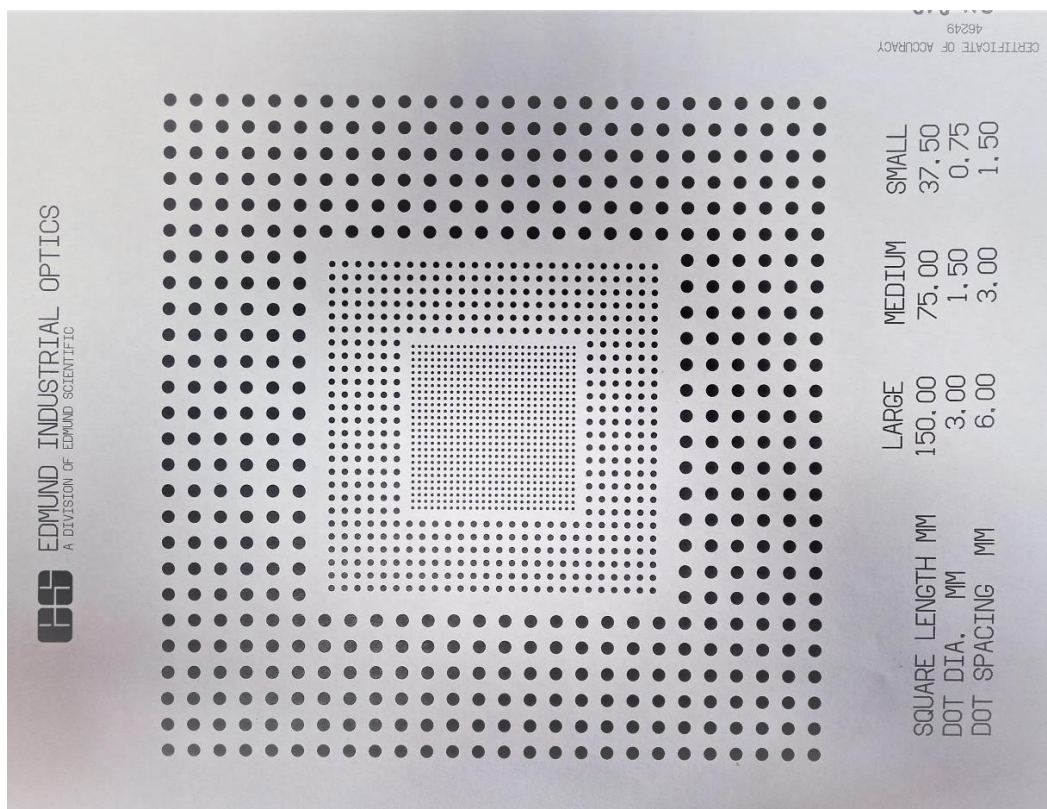
Figure 8.9 Mylar^{TM} sheet used as permanent marker in the present study

Test Program

The tests were performed on unreinforced and fiber-reinforced clay specimens. Three types of geofibers were used in the centrifuge model study, namely polypropylene fibers (PP), polyester fibers (PET) and polypropylene tape (PP-T) fibers. The properties of the geofibers have been discussed in section 4.3.

In total, twenty (20) tests were carried out to understand desiccation cracking behavior of soil. Four (4) 1g tests, namely UR1, FR1, FR5, and FR9 were conducted for all the unreinforced and fiber reinforced soil combinations, so that time scale factor could be checked. The centrifuge tests were conducted at three different gravity levels as shown in Table 8.1, by maintaining corresponding angular velocity revolutions per minute (RPM), so that respective gravities were maintained within the specimen. The centrifuge was allowed to reach the desired angular velocity, before switching on the halogen lamps, powered through the slipring. Each test was carried out for 180 minutes. The camera was set with an interval times to capture images every 5 seconds. In many centrifuge modelling applications, it is difficult to verify the experimental results against the actual field scale phenomenon. The approach to repeat a test at two different scales, a technique known as "modelling of models". If the same phenomenon is observed at the two different scales (i.e., at different gravities, and representing same prototype thickness) then it is assumed that the modelling provides an accurate representation of the prototype phenomenon. Centrifuge model tests FR7, FR13 and FR14 were conducted for studying the influence of fiber type on the desiccation cracking of expansive clay.

Unreinforced clay layer (Series A): Desiccation cracking of unreinforced (UR) clay layer was studied to understand the performance of designed model test package and desiccation cracking inside a centrifuge at high gravities. The influence of thickness of clay layer was studied by considering 5 different clay thicknesses. These were varied by varying the gravity level, and the prototype thickness was varied as 30 mm, 1.77 m, 2.46 m, 3.24 m, and 2.46 m.

Fiber reinforced clay layer (Series B): Desiccation cracking behavior of fiber reinforced clay layer was studied by varying the fiber length with varying prototype thicknesses. The clay was reinforced with polypropylene fibers of varying length. The fiber length was varied as 6 mm, 12 mm and 30 mm. The series are categorized as B1 for $l = 6$ mm, B2 for $l = 12$ mm and B3 for $l = 30$ mm.

Table 8.1Test program for the centrifuge tests in the present study

Test	Test legend	N	Thickness of specimen	Specimen type	Fiber type	f (%)	l (mm)	Series
1	UR1	1	30 mm	UR	-[b]	-[b]	-[b]	A
2	UR2	59	30 mm [1.77 m] [a]	UR	-[b]	-[b]	-[b]	A
3	UR3	82	30 mm [2.46 m]	UR	-[b]	-[b]	-[b]	A
4	UR4	108	30 mm [3.24 m]	UR	-[b]	-[b]	-[b]	A
5	UR5	98.4	25 mm [2.46 m]	UR	-[b]	-[b]	-[b]	A
6	FR1	1	30 mm	FR	PP	0.5	6	B1
7	FR2	59	30 mm [1.77 m]	FR	PP	0.5	6	B1
8	FR3	82	30 mm [2.46 m]	FR	PP	0.5	6	B1
9	FR4	108	30 mm [3.24 m]	FR	PP	0.5	6	B1
10	FR5	1	30 mm	FR	PP	0.5	12	B2
11	FR6	59	30 mm [1.77 m]	FR	PP	0.5	12	B2
12	FR7	82	30 mm [2.46 m]	FR	PP	0.5	12	B2, C
13	FR8	108	30 mm [3.24 m]	FR	PP	0.5	12	B2
14	FR9	1	30 mm	FR	PP	0.5	30	B3
15	FR10	59	30 mm [1.77 m]	FR	PP	0.5	30	B3
16	FR11	82	30 mm [2.46 m]	FR	PP	0.5	30	B3
17	FR12	108	30 mm [3.24 m]	FR	PP	0.5	30	B3
18	FR13	82	30 mm [2.46 m]	FR	PET	0.5	12	C
19	FR14	82	30 mm [2.46 m]	FR	PP-T	0.5	12	C
20	FR15	98.4	25 mm [2.46 m]	FR	PP	0.5	12	B2

UR- Unreinforced; FR- Fiber reinforced; PP- Polypropylene fibers; PET- Polyester fibers; PP-T- Polypropylene tape fibers; f- fiber content; l- fiber length; [a] prototype dimensions within the parenthesis; [b] not relevant/not used.

Influence of type of fiber (Series C): The influence of type of fiber type was studied by varying the material of the fiber used. The fiber type was varied as Polypropylene, Polyester, and Polypropylene-tape. The length of fiber was maintained consistent as $l = 12$ mm. The prototype thickness was maintained as 2.46 m.

8.4   Method of analysis of centrifuge test results

At various stages of cracking, photographs were captured and were later used for analysis and strain computation. The desiccation cracking of unreinforced and fiber-reinforced specimens was studied based on analyzing the images of the front view of the specimen captured at different cracking stages during centrifuge tests, moisture content measurements before and after the test, surface temperature measurements and post-test observations. The image analysis was done using two softwares, i.e. ImageJ and GeoPIV_RG. ImageJ was used for computing the linear and areal measurements. The procedure for measurement is discussed in section 5.4.1. PIV analysis was performed in GeoPIV_RG and the procedure discussed in section 7.5.2 was followed.

8.4.1 Post-test observations

The post-test observations involved measurement of surface temperature, water content and depth of crack in the desiccated specimens.

Surface temperature, θ_s

Desiccation, shrinkage and then cracking on soil surface occur due to water loss by evaporation, this phenomenon seems to be temperature-dependent. The temperature of the surface, θ_s of the specimen was measured with the help of infrared thermometer for a trial test at the interval of every 30 minutes for an unreinforced specimen during 1g and Ng tests. During the Ng tests, the

equipment was stopped every 30 minutes and readings were taken. The temperature was measured at radially varying locations on the surface of the specimen. The locations of surface temperature measurements are shown in Figure 8.10. The measurements were done with the help of digital infrared thermometer MT-4, Cetpar, India. The thermometer is capable of measuring temperature ranges from -32 °C to 550 °C with an accuracy of $\pm$ (2% + 2°C). The average of the measure surface temperatures was then plotted with time as plotted in Figure 8.11.

It can be seen that the surface temperatures, θ_s during 1g tests are higher than that of the Ng tests. It is assumed that the air turbulence due to movement of centrifuge baskets helps in cooling down of the surface temperature, hence the surface temperature is assumed to be $\pm$ 10 degree Celsius from the measured value. Also, since no facility was available to measure the surface temperature during the flight, the surface temperature was assumed to cool down till the equipment reached 0 RPM.
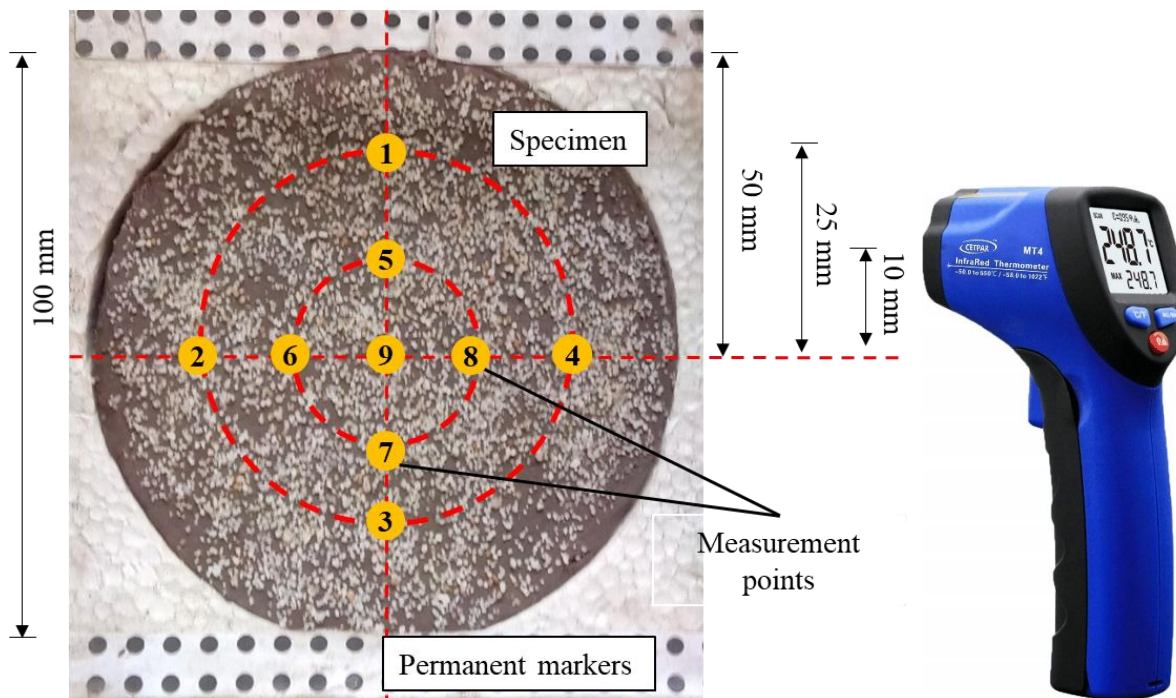
Figure 8.10 Points for the measurement of surface temperature using infrared thermometer
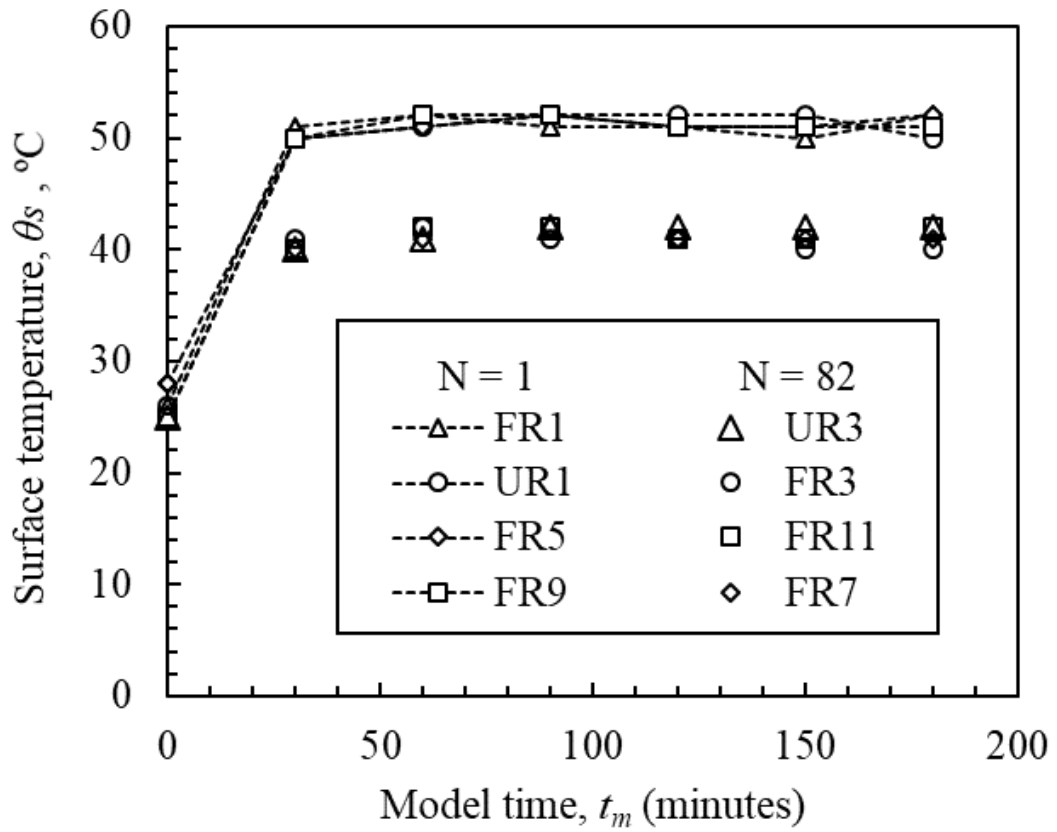
Figure 8.11 Surface temperature as measured by infrared thermometer

Water content

The tested specimens were extruded, and post-test observations were done. The samples for water contents were extruded from top, middle and bottom sections of the specimen to measure the average moisture loss from the specimen. The evaporation rate from the top layers of the specimens is found to be greater than that of the layers beneath it. The moisture lost from the specimen after the test is found to be higher in top layers than the lower layers. This can be attributed to the drying from top and differential suction levels developed through the thickness of clay layer. Figure 8.12 shows the cutting of specimen for water content measurement. Average moisture lost during the centrifuge tests is defined as the change in moisture content of the specimen before the test and after the test is performed. It is expressed in percentage. The moisture loss is measured for all the specimens under consideration. Figure 8.13 shows the average moisture lost in the unreinforced specimen with change in prototype dimensions.

Table 8. 2 Summary of moisture content loss in specimens of prototype thickness of 2.46 m

Test No.	Test Legend	N	Thickness of specimen (mm)	f (%)	l (mm)	$w\%$ (Before)	$w\%$ (After)		Moisture loss (%)
3	UR3	82	30 mm [2.46 m]	_b _b _b _b	_b _b _b _b	63	Average Top Middle Bottom	39 20 48 49	22
12	FR3	82	30 mm [2.46 m]	0.5	6	64	Average Top Middle Bottom	44 37 47 49	20
8	FR7	82	30 mm [2.46 m]	0.5	12	61	Average Top Middle Bottom	43 35 44 49	18
16	FR11	82	30 mm [2.46 m]	0.5	30	65	Average Top Middle Bottom	49 48 47 53	16
18	FR13	82	30 mm [2.46 m]	0.5	12	65	Average Top Middle Bottom	49 48 47 53	16
19	FR14	82	30 mm [2.46 m]	0.5	12	65	Average Top Middle Bottom	49 48 47 53	16

UR- Unreinforced; FR- Fiber reinforced; f- fiber content; l- fiber length; [a] prototype dimensions within the parenthesis; [b] not relevant/not used.

Figure 8.12 Cutting of specimen for measuring moisture content
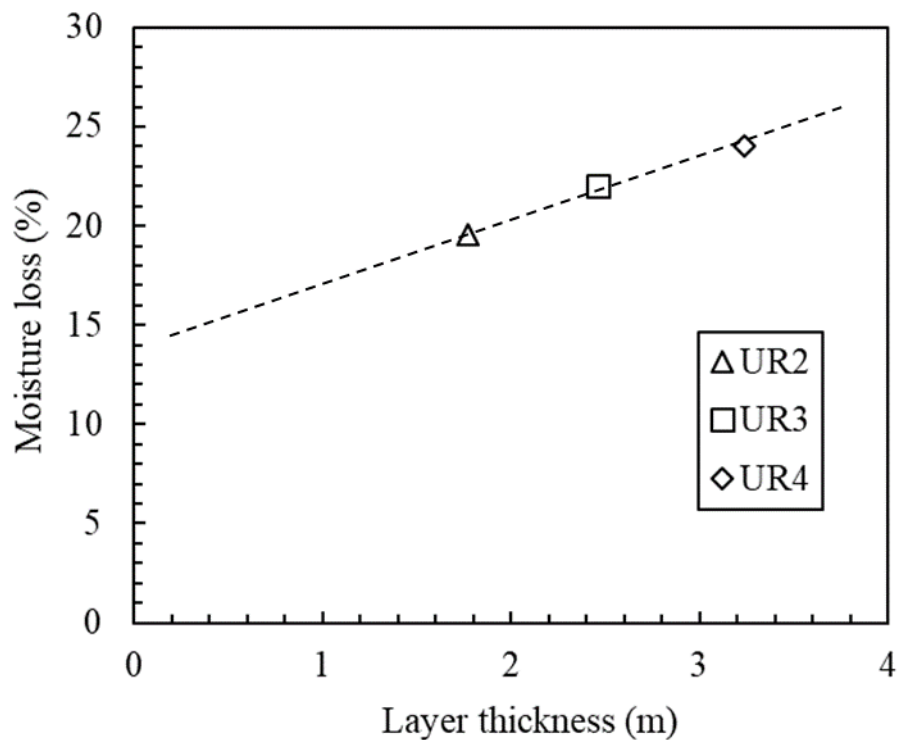
Figure 8.13 Variation of average moisture content loss in unreinforced clay layers with varying prototype dimensions

Depth of crack

The depth of crack was measured with the help of the thin needle arrangement in Vernier calipers, as shown in Figure 8.14. Extremely narrow cracks were measured with the help of thin needles. It was remarked that invariably, the depth of crack in case of unreinforced specimens always went throughout the specimen.
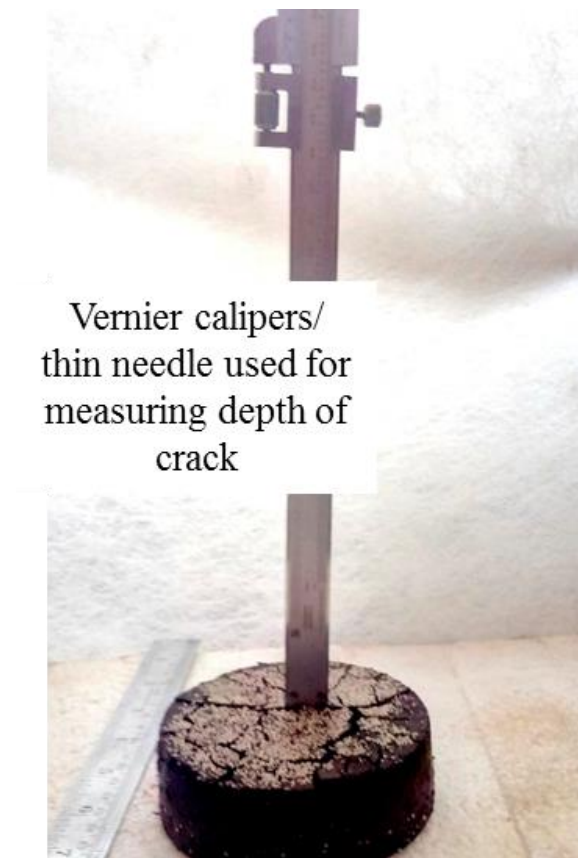
Figure 8.14 Measurement of depth of crack with Vernier calipers

It is seen that the depth of crack measured significantly reduced in case of fiber reinforced soil specimen. The crack depth reduced by about 200% from unreinforced to fiber reinforced soil specimens. However, not much variation is seen when the length of fiber is changed. The fibers reinforced with fiber length $l = 6$ mm show minimum crack depth, then $l = 12$ mm and then specimens reinforced with $l = 30$ mm. The distribution of fibers is uniform in case of longer length of fibers, ensuring uniform reinforcement of soil throughout the specimen. This could be attributed to the larger depths of cracks in fiber reinforced soil specimens with longer lengths of fibers.

8.4.2 Digital image analysis

Image analysis is a process by which meaningful information or measurements can be extracted from digital images, typically by computer algorithms. It is a technique in which the quantitative

data from specimens is obtained by segmenting an image into pixels based on its color (RGB), density or texture. Image analysis is a powerful tool to measure data in desiccating specimens, as placement of other measurement devices is deemed more invasive. The process of digital image analysis (DIA) involves image acquisition, image pre-processing and measurement. The crack feature measurements that were done using the DIA are shown in Figure 8.15.
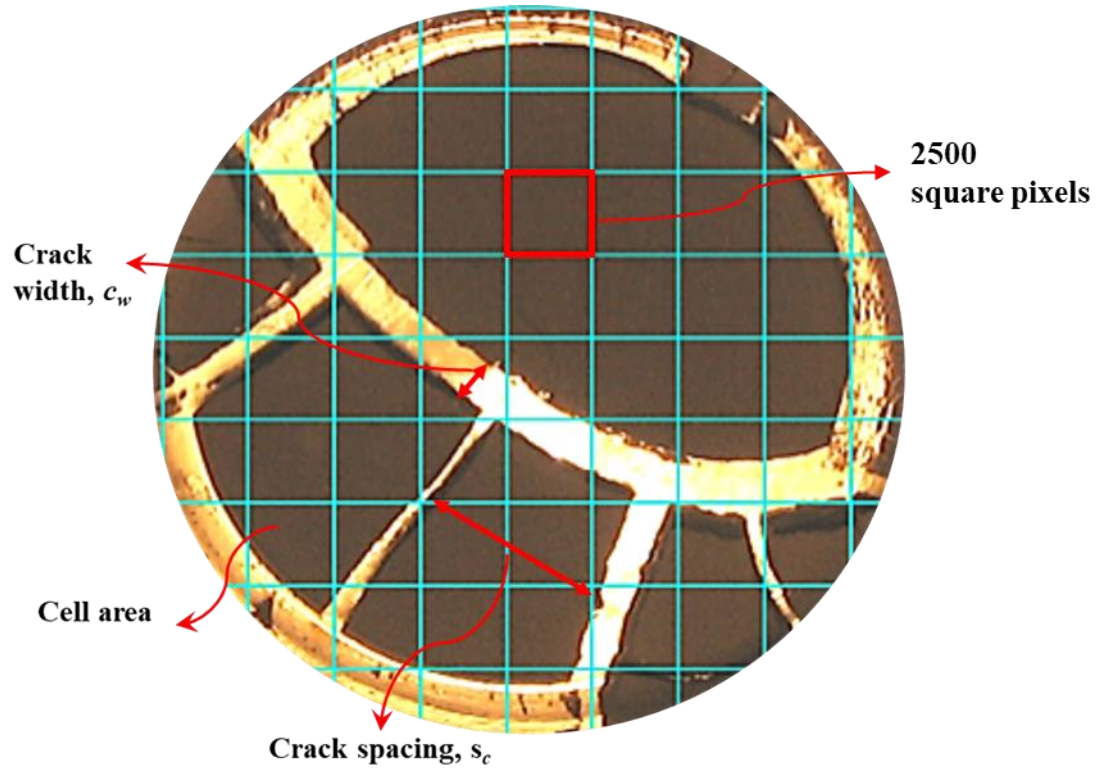
Figure 8.15 Crack feature measurements done during image analysis

The images were captured with a digital camera Hero 4, manufactured by GoPro, USA. The details and specifications of the camera are discussed in section 3.3.4. Two image analysis softwares were utilized during the present investigation: GeoPIV_RG and ImageJ. ImageJ (Abràmoff et al. 2014) was extensively used by Lakshmikantha et al. 2012 to characterize the statistical features of crack patterns in drying soils. The crack measurements like crack width, crack spacing, and crack intensity factor (CIF) was measured with ImageJ using the set permanent markers to set the scale during crack measurements. The average shrinkage strain after the test was computed manually in ImageJ as shown in section 5.4.1. The average of the shrinkage strain values computed throughout the specimen were considered.

8.4.3 Particle Image Velocimetry (PIV) technique

In a typical PIV analysis, the reference/initial image from the series of images is chosen to select the region of interest (RoI) within the initial image. This RoI is meshed into patches/subsets of customized size. The image analysis code/software are used for the analysis of these images. Geo PIV (White et al. 2003), Mat PIV (Sveen and Cowen 2004), PIV lab (Thielicke and Stamhuis 2014) and Open PIV(Taylor et al. 2010) are few among them. Most of the PIV algorithms require a reference image and a region of interest to be defined at the beginning of the analysis. The RoI is divided into subsets of required size and any subset is then analyzed in all the target images successively. In order to improve the accuracy of this process, several neighboring subsets are also included in the calculation. Interpolation of the cross-correlation of the subset corresponding to the correlation peak along with several of its neighboring subsets can drastically enhance the measurement of displacement resolution. For the current study the algorithm used is referred as GeoPIV_RG, an updated version of GeoPIV program (White et al. 2003).The captured images were sequentially analyzed using an open source MATLAB based image processing software GeoPIV_RG. The major steps involved in the analysis are:

a) Image series data input

The fundamental operation of GeoPIV is to track the texture (i.e. the spatial variation of brightness) within a predefined mesh in an image of soil through a series of images. A mesh consists of square patches is defined in the reference image (usually the first image of a series of image). Then the program compares the texture of those patches with a second image. Each patch from the reference image is compared with a larger area in the second image in order to find the best match for the patch terms of texture. The location at which the highest correlation is found indicates the displacement of that patch (or the soil element) relative to the reference image

b) Selection of region of interest (RoI)

A region of interest is the pixel range in which the PIV analysis is performed. A rectangular RoI is selected for the series of input images such that the major shrinkage and cracking takes place in the selected region.

c) Selection of appropriate seed correlation coefficient by trial and error

The RoI had a mesh size of 50 x 50 pixels as shown in Figure 8.16. The most suitable patch size for an application was chosen by running several trials. The larger the patch size, the higher the accuracy but the lesser the information within a given area. Patch sizes varying from 10 x 10 pixels to 40 x 40 pixels were used get the optimum output minimising wild vectors (patches that lose their track on texture).
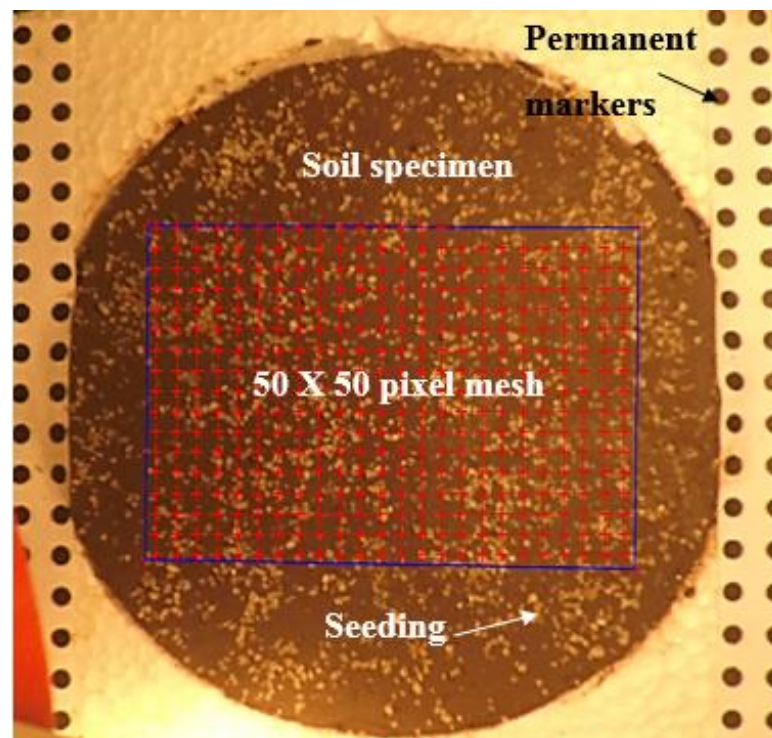
Figure 8.16 Selection of region of interest and mesh size for PIV analysis

d) Calculate displacement of seed subset (pixels)

Displacements and strains were calculated to an acceptable accuracy. It was challenging to measure the strains in desiccating soils without disturbing the cracking process. Placing strain gauges or any other similar equipment on the soil could affect the location of crack initiation.

e) Delete wild vectors (if any)

Due to grain rearrangement, because these lead to a reduction in the subset correlation and cause erroneous displacements to be estimated (known as "wild" vectors), as shown in Figure 8.17.

f) Plot displacement vectors

The displacement vectors are plotted for given sequence of images from the input command in the software. The output gives the vectoral representation of the displacement vectors and the contour plots of displacements as well. Figure 8.18 shows the output plot from the software GeoPIV_RG.

Before deletion   After delection
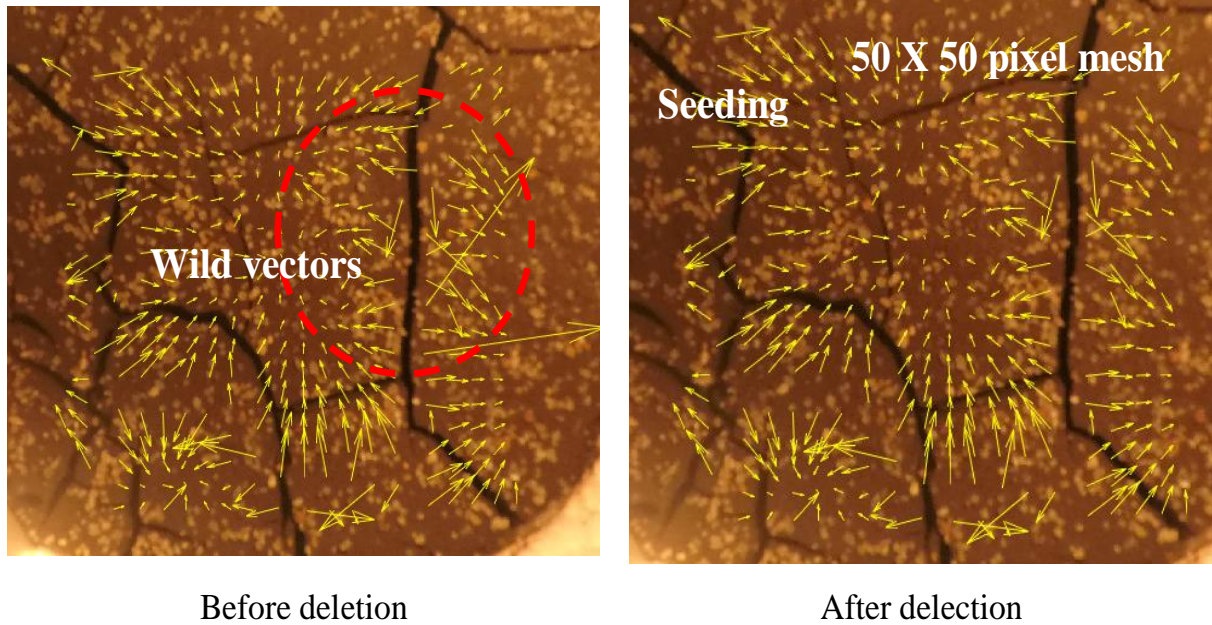
Figure 8.17 Deletion of unnecessary wild vectors in the software

g) *Strain computation from the displacements*

Strains are computed in MATLAB by Delaunay triangulation. It is a triangulation in which every circumcircle of a triangle is an empty circle. The blue triangles are valid and used during strain compute. The red triangles are invalid and ignored during strain computation. Figure 8.19 shows the mesh triangle generated for the strain computation. Various types of strains can be computed in the software, that being, total linear strain, major (most-compressive) principal total strain, minor (least-compressive) principal total strain, maximum total shear strain, anticlockwise rotation of major (i.e. most compressive) principal total strain (degrees), total volumetric strain, total logarithmic strain, incremental volumetric strain.

h) *Plot strains for the image sequence*

The desired computed strains for the input image sequence were plotted as contour maps.

Figure 8. 20 shows images of crack propagation in unreinforced soil UR3 with elapsed model time in minutes. The prototype thickness of the clay layer is 2.46 m. The theoretical prototype time is mentioned in the parentheses. Accordingly, the PIV analysis was performed on image series of test UR3 and the strain outputs with elapsed time have been tabulated in
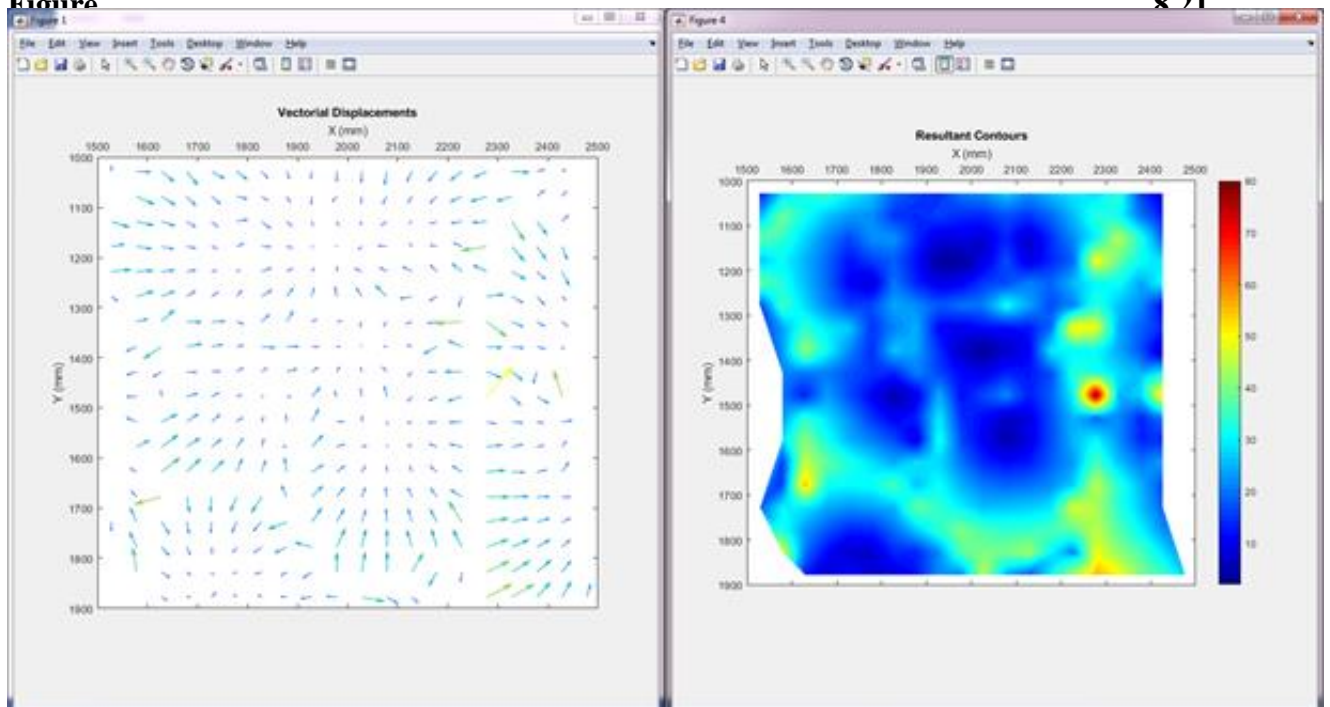
Figure 8.21

Figure 8.18 Displacement vectors between any two images
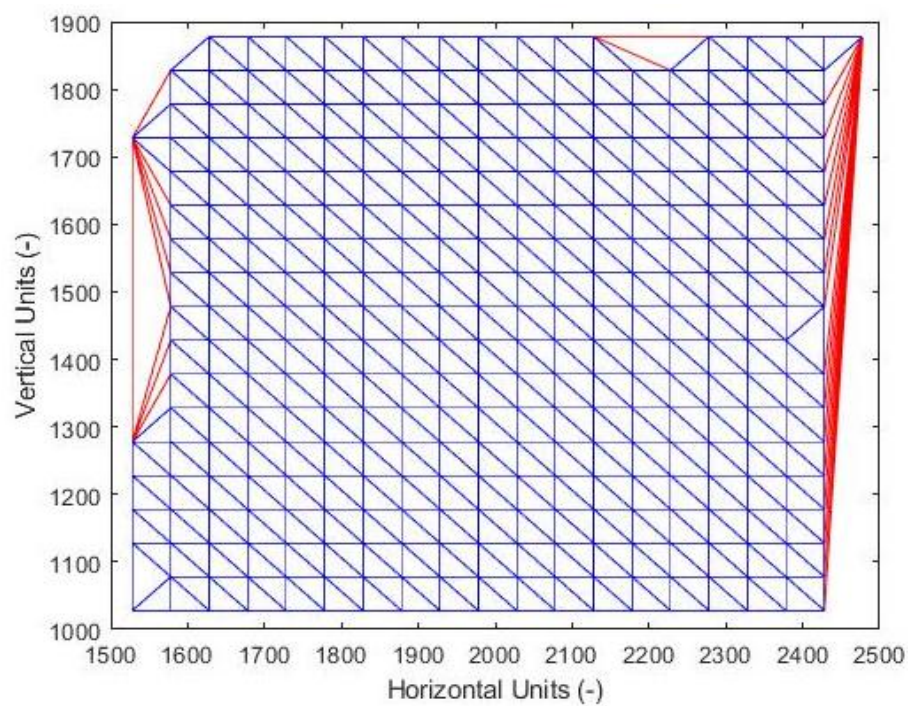
Figure 8.19 Mesh triangles used for strain computation

Unreinforced (UR3, N=82)
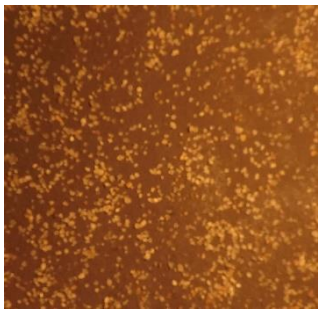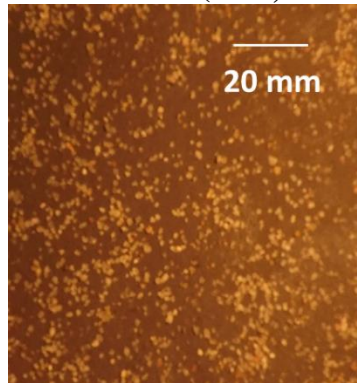
20 mm

(a) 0 min [0 days]   (b) 5 min [23 days]   (c) 10 min [47 days]   (d) 15 min [70 days]

(e) 20 min [93 days]   (f)25 min [117 days]   (g)30 min [140 days]   (h)35 min [163 days]

(i) 40 min [187 days]   (j)45 min [210 days]   (k)50 min [233 days]   (l)55 min [257 days]

(m)60 min[280 days]   (n)65 min [304 days]   (o)70 min [327 days]   (p)75 min [350 days]

246

(q)80 min [374 days]   (r)85 min [397 days]   (s)90 min [420 days]   (t)95 min [444 days]

(u)100 min[467days]   (v)105 min[490 days]   (w)110 min[514 days]   (x)115 min [537 days]

(y)120 min [560 days]   (z)125 min [584 days]   (aa)130 min [607 days]   (ab)135 min [630 days]

(ac)140 min[654 days]   (ad)145 min[677 days]   (ae)150 min [700 days]   (af)155 min [724 days]

(ag)160 min[747 days]   (ah)165 min[770 days]   (ai)170 min [794 days]   (aj)175 min [817 days]

Figure 8. 20 Propagation of crack in unreinforced soil specimen UR3 with model time elapsed (prototype time in parentheses)

Unreinforced (UR3, N=82)
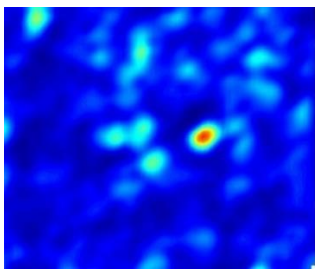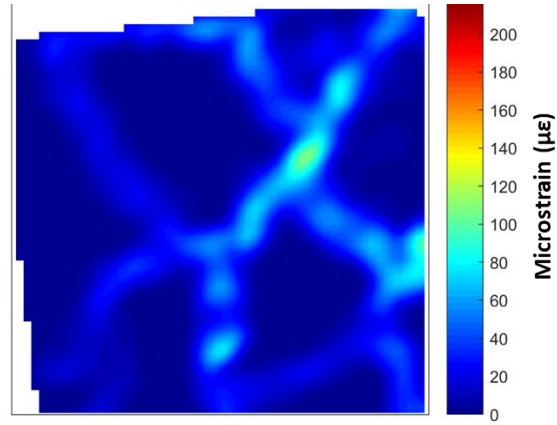
(a) 0 min [0 days]   (b) 5 min [23 days]   (c) 10 min [47 days]   (d) 15 min [70 days]
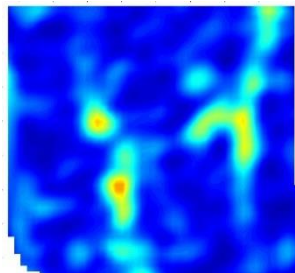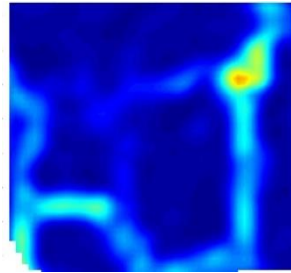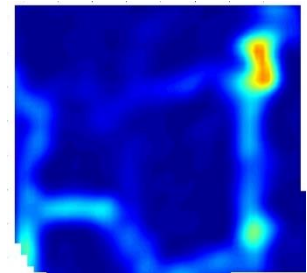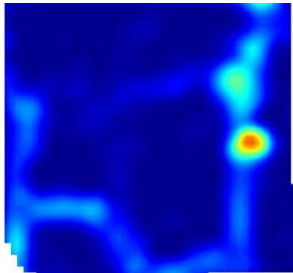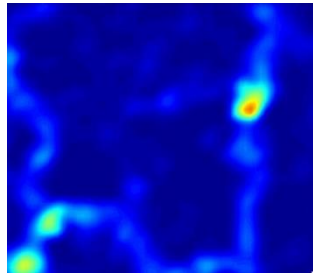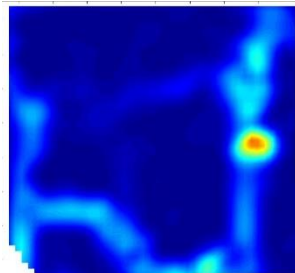
(e) 20 min [93 days]   (f)25 min [117 days]   (g)30 min [140 days]   (h)35 min [163 days]

(i) 40 min [187 days]   (j)45 min [210 days]   (k)50 min [233 days]   (l)55 min [257 days]

(m)60 min[280 days]   (n)65 min [304 days]   (o)70 min [327 days]   (p)75 min [350 days]

(q)80 min [374 days]   (r)85 min [397 days]   (s)90 min [420 days]   (t)95 min [444 days]

(u)100 min[467days]   (v)105 min[490 days]   (w)110 min[514 days]   (x)115 min [537 days]

(y)120 min [560 days]   (z)125 min [584 days]   (aa)130 min [607 days]   (ab)135 min [630 days]

(ac)140 min[654 days]   (ad)145 min[677 days]   (ae)150 min [700 days]   (af)155 min [724 days]
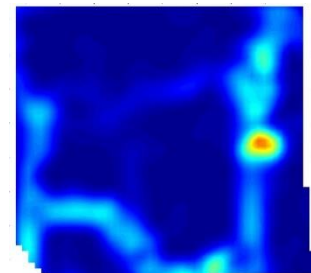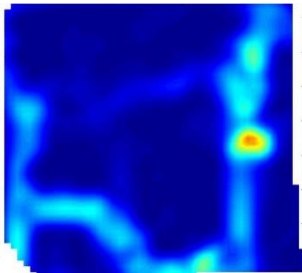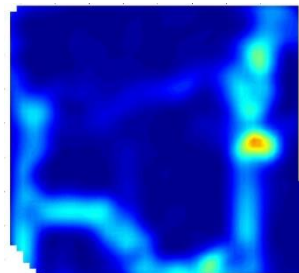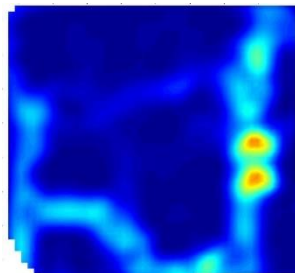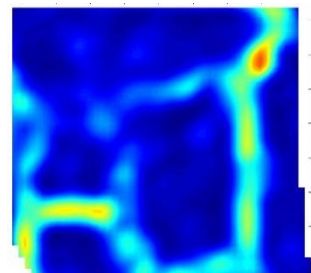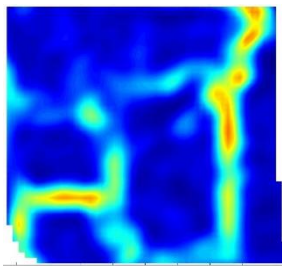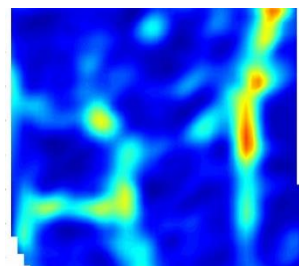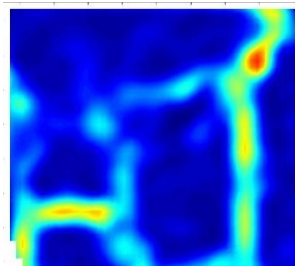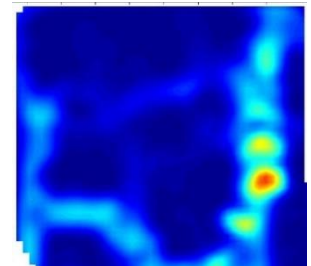
(ag)160 min[747 days]   (ah)165 min[770 days]   (ai)170 min [794 days]   (aj)175 min [817 days]
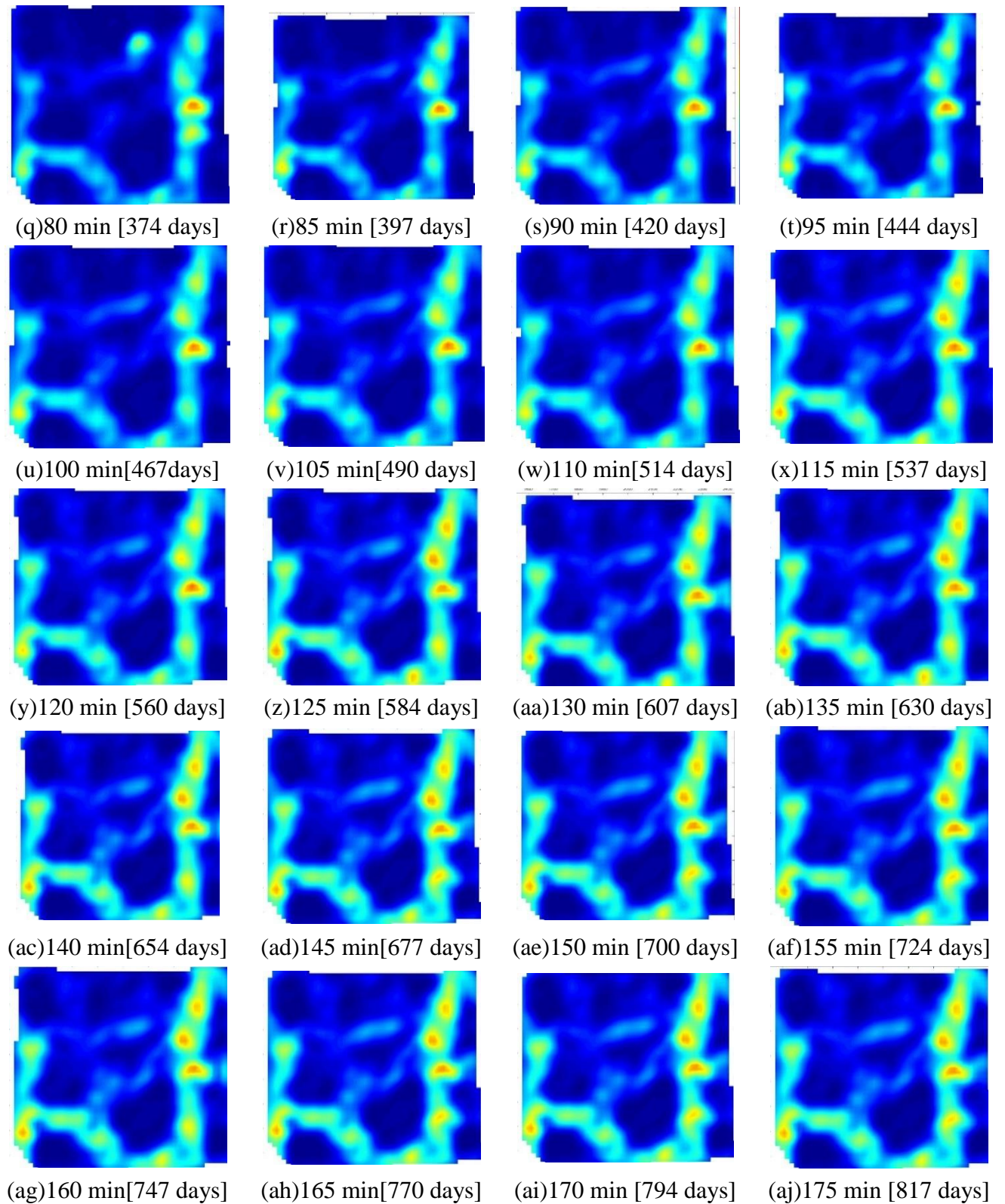
Figure 8.21 Strains output of input image series of unreinforced soil specimens UR3

8.5   Results and discussion

In this section the results from centrifuge tests [Series A, Series B, Series C] are discussed, that being, the crack width, crack spacing, crack depth, crack intensity factor, time of crack initiation and strain profile for unreinforced and fiber reinforced soil. The performance of developed test setup at varying gravity levels, influence of fiber reinforcement, thickness of clay layer, fiber length and fiber type on different crack feature measurements has been discussed. The average shrinkage strain, ε_{avg} is computed manually n the software ImageJ. Table 8. 3 summarizes the results from the centrifuge model tests.

8.5.1 Performance of developed system at varying gravity levels

The performance of developed desiccation cracking setup and validation of derived scaling laws was performed by adopting "modelling of models" for the given set of experiments. It is based on the concept that a scale model of a geotechnical system at N gravities should have a similar behaviour as the prototype under normal gravity. This implies, then, that more than one model of the same prototype can be constructed using different scale factors N_1, N_2, etc., and, as long as the tests are performed at the appropriately scaled gravity level, the results should all be similar. That is, the behaviour of a model at N_1g should be similar to that of a model at N_2g, and so on. Prototype thickness of 2.46m was simulated for unreinforced and fiber reinforced specimen of l = 6 mm by maintaining g-levels of 82g and 98.4g for specimen thicknesses of 30mm and 25mm respectively (Figure 8.22).

Theoretically, modelling of models can be represented in a plot of clay layer thickness versus gravity level on a log-log scale. The model specimen thicknesses (d_m [mm]) at different g-levels are plotted in Figure 8.23 along with theoretical prototype thicknesses (d_p [mm]) at various gravity levels (N).

Table 8. 3 Summary of results from the centrifuge model tests

Test No.	Test Legend	N	Fiber type	f %	l (mm)	[a] Thickness of specimen	*Time of crack initiation t_i	[#]Normalized crack width c_w/d	[#]Normalized crack spacing s_c/d	[#]Normalized crack depth d_c/d
1	UR1	1	-[b]	-[b]	-[b]	30 mm	54 min	0.066	0.440	0.50
2	UR2	59	-[b]	-[b]	-[b]	30 mm [1.77 m]	5 min [12 days]	0.057	0.434	1.00
3	UR3	82	-[b]	-[b]	-[b]	30 mm [2.46 m]	5 min [23 days]	0.077	0.403	1.00
4	UR4	108	-[b]	-[b]	-[b]	30 mm [3.24 m]	3 min [24 days]	0.076	0.475	1.00
5	UR5	98.4	-[b]	-[b]	-[b]	25 mm [2.46 m]	4 min [27 days]	0.079	0.670	1.00
6	FR1	1	PP	0.5	6	30 mm	75 min	0.026	0.186	0.10
7	FR2	59	PP	0.5	6	30 mm [1.77 m]	6 min [15 days]	0.033	0.175	0.13
8	FR3	82	PP	0.5	6	30 mm [2.46 m]	5 min [23 days]	0.035	0.161	0.13
9	FR4	108	PP	0.5	6	30 mm [3.24 m]	4 min [32 days]	0.034	0.170	0.17
10	FR5	1	PP	0.5	12	30 mm	60 min	0.022	0.220	0.27

11	FR6	59	PP	0.5	12	30 mm [1.77 m]	6 min [15 days]	0.026	0.227	0.20
12	FR7	82	PP	0.5	12	30 mm [2.46 m]	6 min [28 days]	0.034	0.233	0.23
13	FR8	108	PP	0.5	12	30 mm [3.24 m]	5 min [41 days]	0.030	0.215	0.20
14	FR9	1	PP	0.5	30	30 mm	60 min	0.024	0.265	0.40
15	FR10	59	PP	0.5	30	30 mm [1.77 m]	5 min [12 days]	0.038	0.273	0.33
16	FR11	82	PP	0.5	30	30 mm [2.46 m]	4 min [19 days]	0.029	0.253	0.27
17	FR12	108	PP	0.5	30	30 mm [3.24 m]	2 min [16 days]	0.033	0.267	0.30
18	FR13	82	PET	0.5	12	30 mm [2.46 m]	3 min [14 days]	0.021	0.227	0.27
19	FR14	82	PP-T	0.5	12	30 mm [2.46 m]	4 min [19 days]	0.049	0.225	0.23
20	FR15	98.4	PP	0.5	12	30 mm [2.46 m]	5 min [34 days]	0.034	0.250	0.24

UR- Unreinforced; FR- Fiber reinforced; PP- Polypropylene fibers; PET- Polyester fibers; PP-T- Polypropylene tape fibers; f- fiber content; l- fiber length; [a] prototype dimensions within the parenthesis; [b] not relevant/not used; *time in prototype dimensions in parenthesis; [#]Average value throughout the specimen

(a) Test UR3, FR7

c_e ↓ 82 g c_e

Specimen

$d_m = 30$ mm

Prototype layer thickness
$d_p = 2.46$m

(b) Test UR5, FR15

c_e ↓ 98.4 g c_e

Specimen

$d_m = 25$ mm

Prototype layer thickness
$d_p = 2.46$m
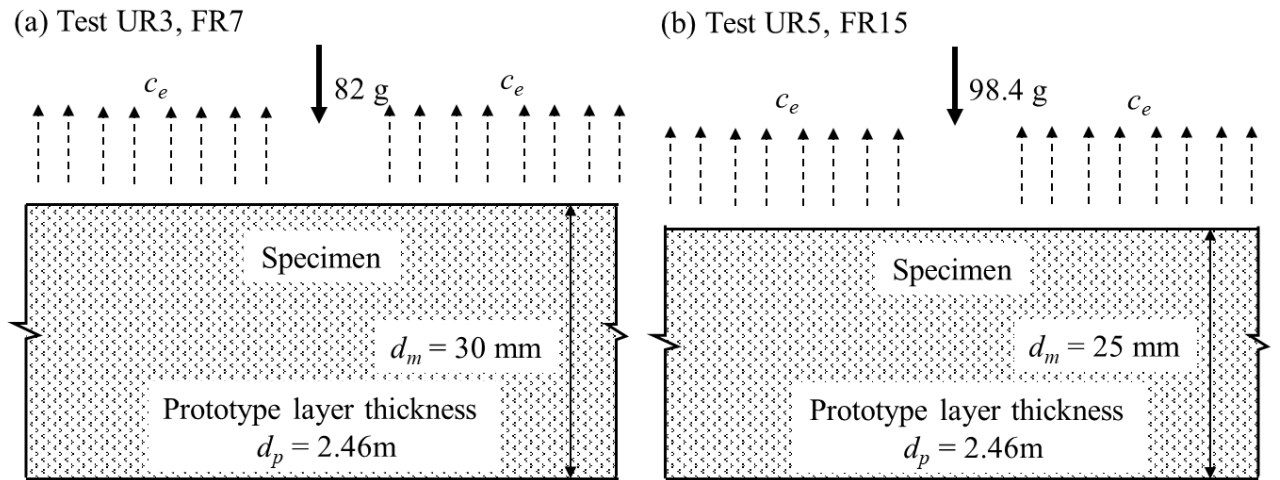
Figure 8.22 Concept of modelling of models for the experimental validation tests conducted (a) UR3, FR7, (b) UR5, FR15

Clay layer thickness (mm)

1   10   100   1000   10000

1

$d_p = 2.46$m

$d_m = 25$mm $d_m = 30$mm

10

N [N: g level]

N = 82

100

UR3, FR7
UR5, FR15

N = 98.4

Modelling of models
$d_p = N\, d_m$

1000

10000
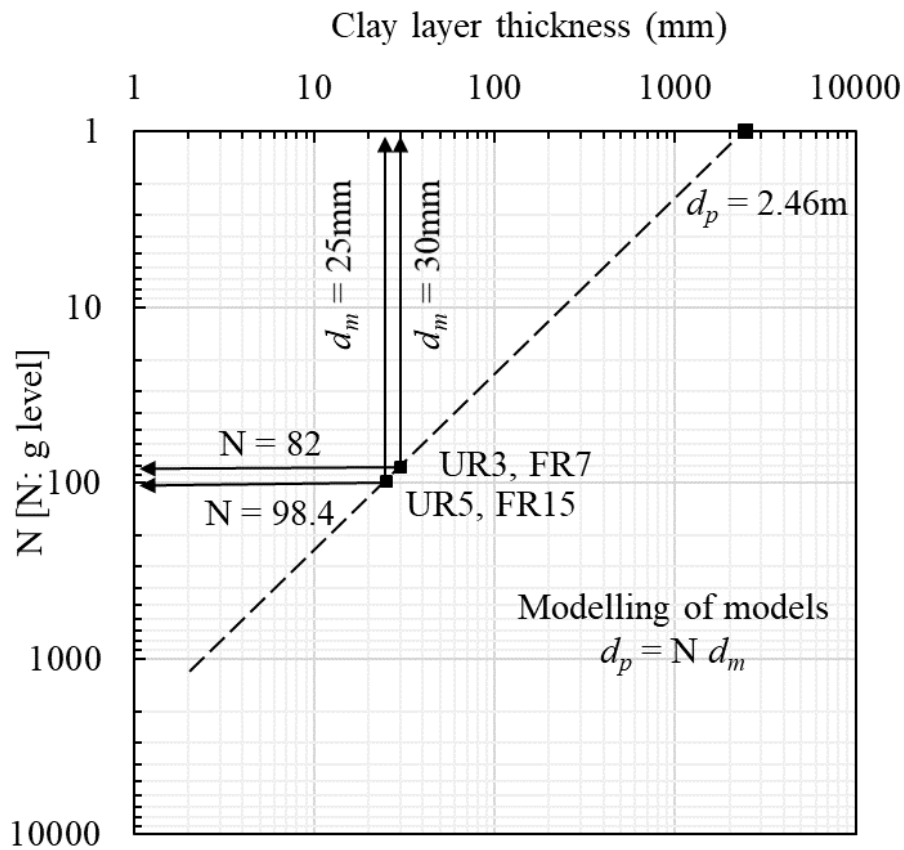
Figure 8.23 Modelling of model thicknesses from test UR3, UR5, FR7, FR15

253

In order to validate the control system of the desiccation cracking setup against the scaling laws related to time, a range of prototype thicknesses (varying from 1.77 m to 3.24 m) was simulated in centrifuge at g-levels of 59g, 82g and 108g. The recorded model time of crack initiation (t_{im} min) for test UR3, UR5, FR7 and FR15 were plotted against their corresponding gravity level on a log-log scale, along with the corresponding theoretical prototype time of crack initiation (t_{ip} min). Figure 8.24 represents the validation of scaling law related to time at high gravities using the modelling of models approach. It can be opined that the resultant plots obtained by connecting the model and prototype values represent a set of parallel straight lines inclined at an angle of 45° to the horizontal, i.e. 1V: 1H inclination. Therefore, the time scale factor of $1/N^2$ is validated.

	N	t_{im} (min)	t_{ip} (days)
UR3	82	5	23
UR5	98.4	4	27
FR7	82	6	28
FR15	98.4	5	34
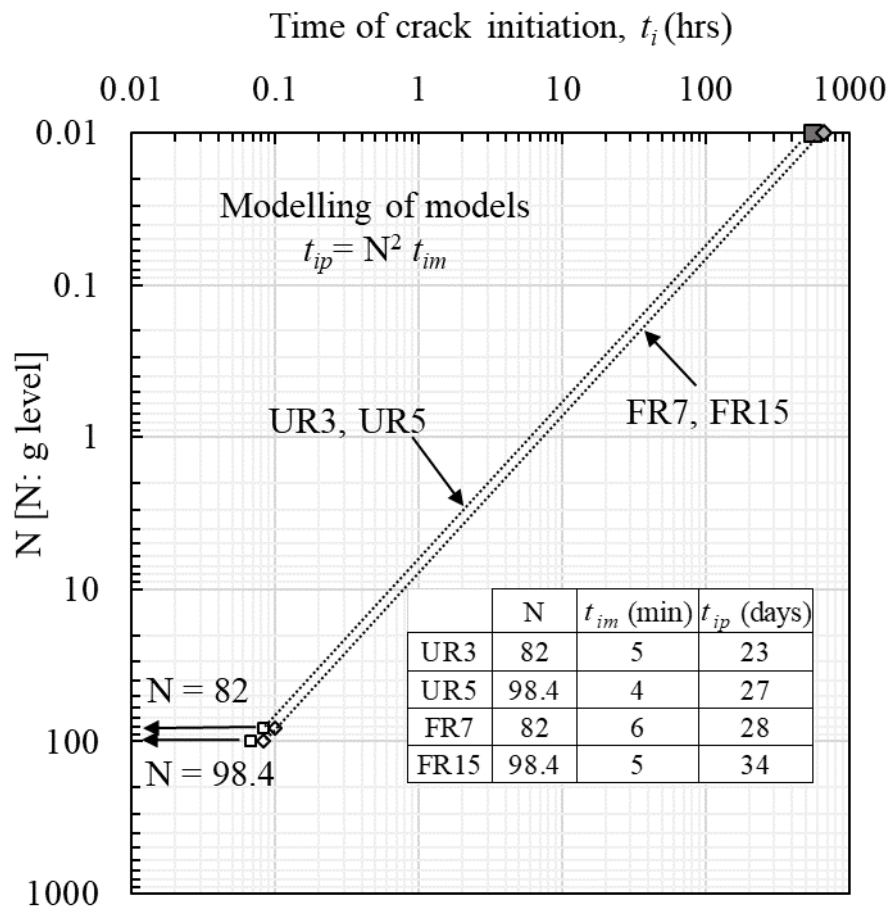
Figure 8.24 Validation of scaling law related to time at high gravities

Even though the plot has a 1V: 1H inclination, we can see that since the variation in the time of crack initiation is very less, the points in the plot are very close. Therefore, a greater number of tests with large variation in specimen thicknesses could be attempted to have a better validation plot of the scaling law for time of crack initiation.

Figure 8.25 presents the variation of normalized crack width, c_w/d with time for unreinforced layer of prototype thickness, $d_p = 2.46$ m [Test: UR3 and UR5]. The propagation of crack width with time for different model thicknesses is measured to be almost same. The crack width increases with increase in time (model and prototype). Thereby substantiating that the clay layer represents the same prototype thickness.

Similarly, Figure 8.26 presents the variation of normalized crack width, c_w/d with time for fiber-reinforced layer of prototype thickness, $d_p = 2.46$ m [Test: FR7 and FR15]. The propagation of crack width with time for different model thicknesses is also measured to be almost the same. The crack width increases with increase in time (model and prototype).

As the soil desiccates, the number of cracks increase, thereby reducing the spacing between cracks (Figure 8.27). Figure 8.28 presents the variation of normalized crack spacing, s_c/d with time for unreinforced layer of prototype thickness, $d_p = 2.46$ m [Test: UR3 and UR5]. Here, the crack spacing after crack initiation has been considered, and it decreases with increase in the intensity of cracking of specimen. The propagation of crack spacing with time for different model thicknesses ($d_m = 30$ mm, 25mm) is measured to be almost same. Thereby substantiating that the clay layer represents same prototype thickness.

Similarly, the variation of normalized crack width for fiber reinforced clay layer of prototype thickness, $d_p = 2.46$ m [Test: FR7 and FR15] is presented in Figure 8.29. As the propagation of crack spacing is almost similar for the two specimens, it can be opined that the specimens represent the same prototype thickness, thereby proving that the test setup performs in agreement with the modelling of models.
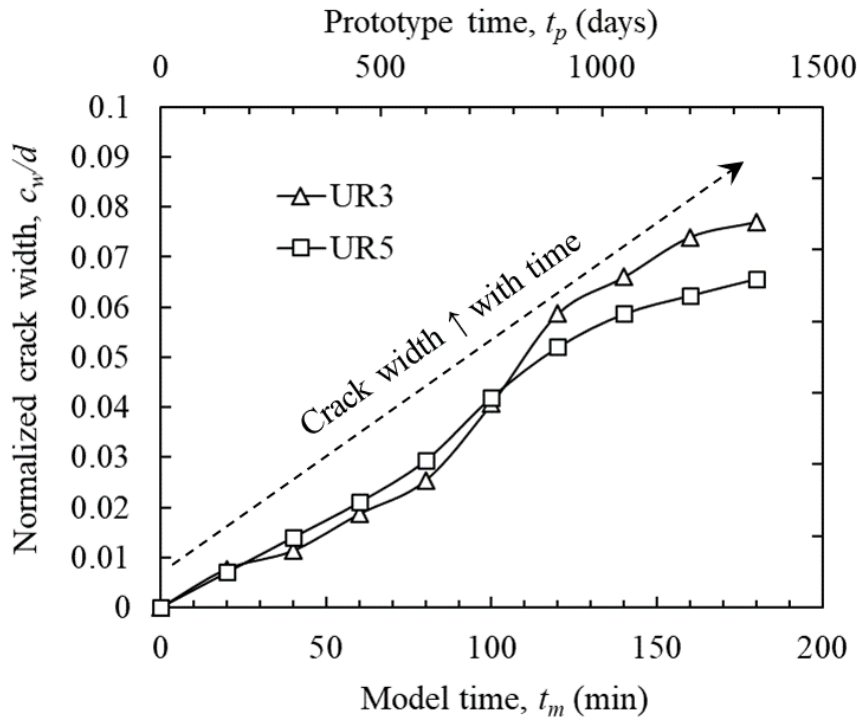
Figure 8.25 Variation of normalized crack width, c_w/d with time for unreinforced layer of prototype thickness, d_p = 2.46 m [Test: UR3, UR5]
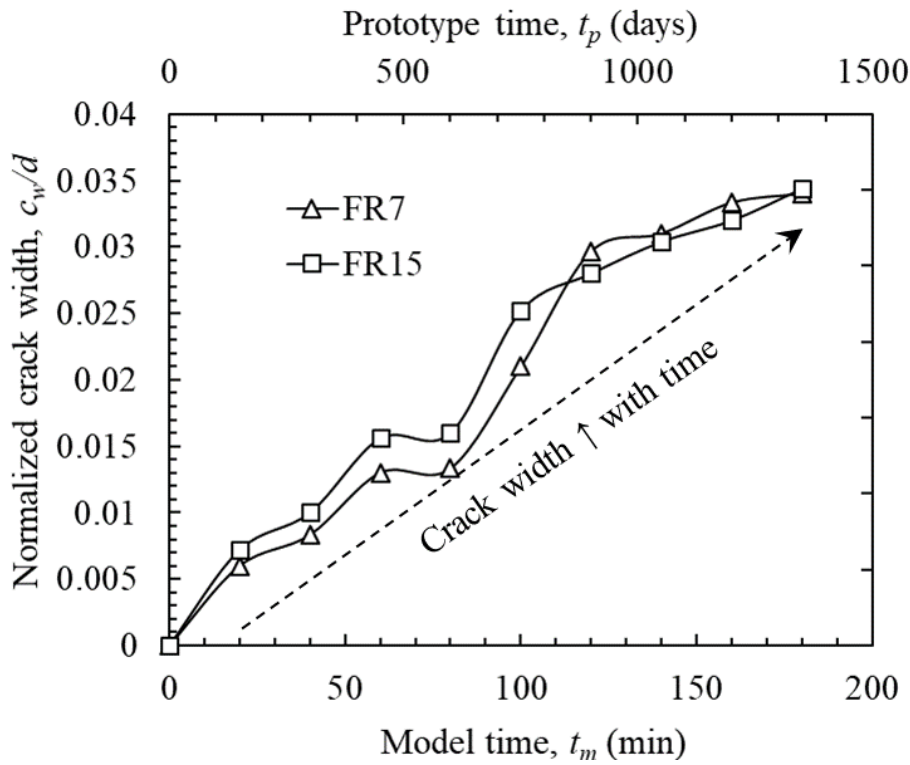
Figure 8.26 Variation of normalized crack width, c_w/d with time for fiber -reinforced layer of prototype thickness, d_p = 2.46 m [Test: FR7, FR15]

(a) Section XX, t_m = 20 min

(b) Section XX, t_m = 50 min

(c) Section XX, t_m = 80 min

(a) t_m = 20 min

(b) t_m = 50 min

(c) t_m = 80 min
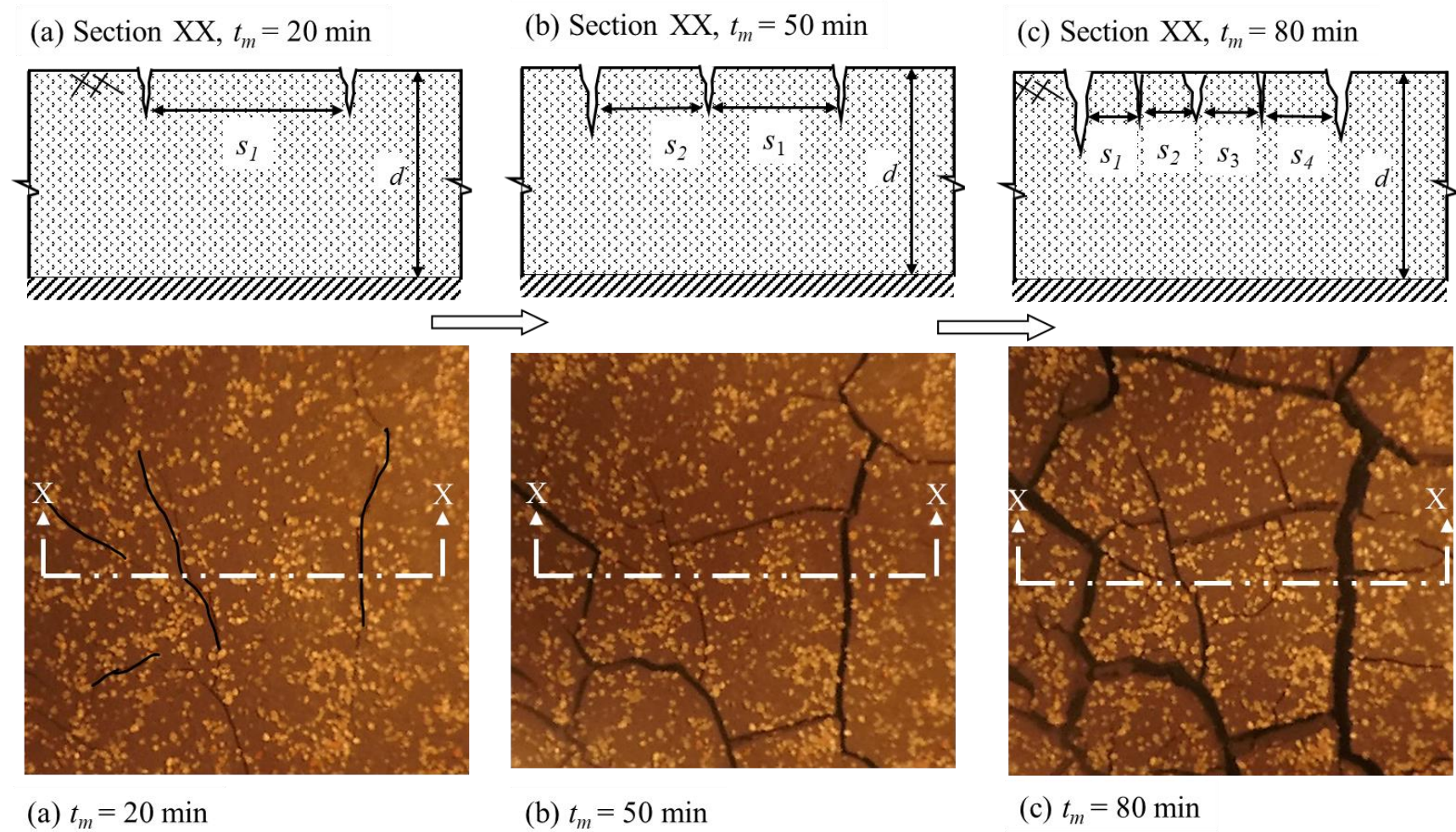
Figure 8.27 Schematic representation of reduction of average crack spacing with model time [Test : UR3]

257
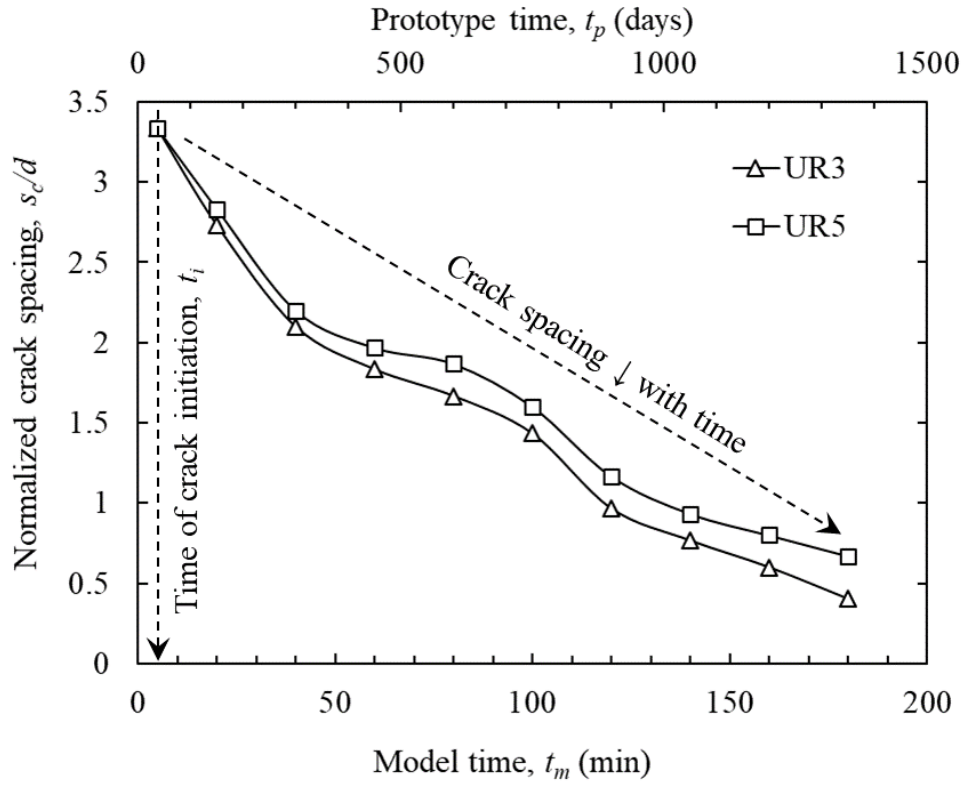
Figure 8.28 Variation of normalized crack spacing, s_c/d with time for unreinforced clay layer of prototype thickness, d_p = 2.46 m [Test: UR3, UR5]
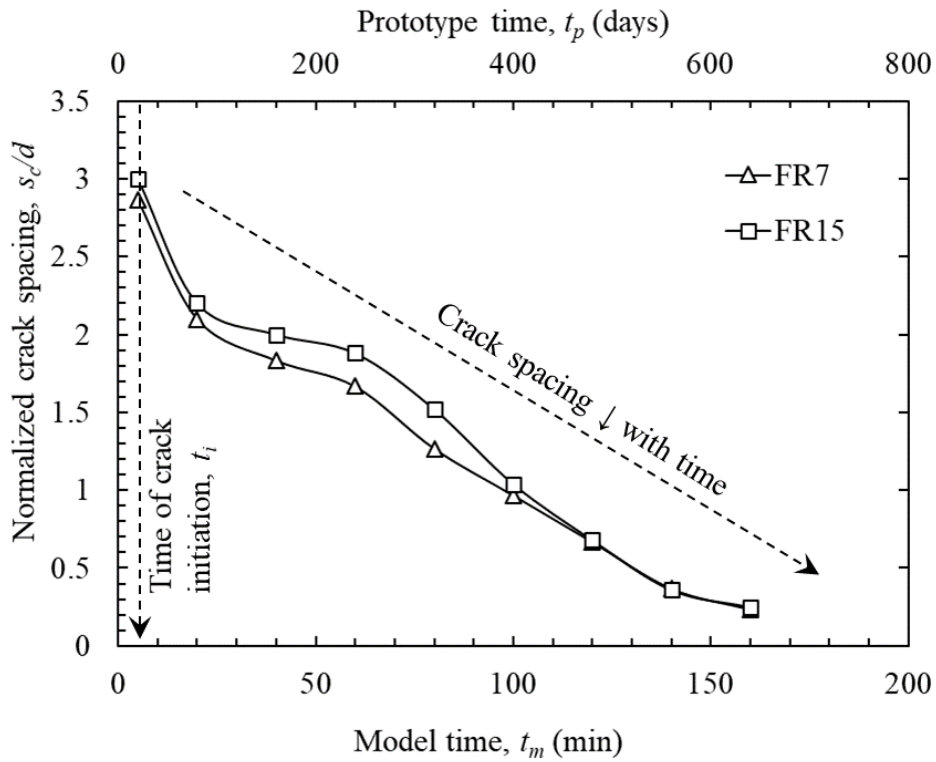
Figure 8.29 Variation of normalized crack spacing, s_c/d with time for fiber-reinforced clay layer of prototype thickness, d_p = 2.46 m [Test: FR7, FR15]

8.5.2 Influence of fiber reinforcement

The performance of unreinforced clay layer [Series A] was studied by conducting a series of centrifuge model tests which were aimed to measure the crack features of unreinforced clay layers of varying thicknesses. Test series B was conducted to study the desiccation cracking behaviour of fiber reinforced clay layer with varying fiber length and varying prototype thicknesses. The fiber length was varied as 6 mm [test B1], 12 mm [test B2] and 30 mm [test B3]. In this section the results from test series A were compared to that of series B in terms of crack morphology, crack feature measurements and post-test observations.

Crack morphology

The morphology of the cracks in unreinforced and fiber-reinforced soil specimens were different. When subjected to desiccation under nearly controlled environmental conditions, typical uniform, long, and thick cracks were observed in the expansive soil without any fibers (unreinforced). The wide cracks formed in unreinforced soil specimens can be termed as major cracks. The major cracks separate the cells formed after cracking, which may act as a potential pathway for the fluids to pass through the layer.

However, the cracks in the case of fiber-reinforced soil, were non-uniform, smaller, jagged, and tortuous. The width of the cracks reduced drastically, resulting in an increase in the number of fine cracks. These fine cracks could be termed as minor cracks. Minor cracks act as points of release of developed tensile stresses in the specimen during desiccation cracking. Due to the presence of fibers, even after cracking, the cells are held intact. Figure 8.30 represents the crack morphology and pattern at the end of the tests UR3, FR3 (l = 6 mm), FR7 (l = 12 mm) and FR11(l = 30 mm). Unreinforced specimens cracked throughout the layer depth in all the cases at higher gravity levels (Figure 8.31). The cracked soil mass could be easily moved, as presented in Figure 8.17. Although there is a drastic change due to fiber reinforcement (Figure 8.30), the crack morphology is not affected significantly due to the change in fiber length. Figure 8.32 shows the variation in the normalized depth of crack for unreinforced and fiber-reinforced clay layers of varying thicknesses. There is a 60-80% decrease in the depth of crack due to presence of fibers in the clay.
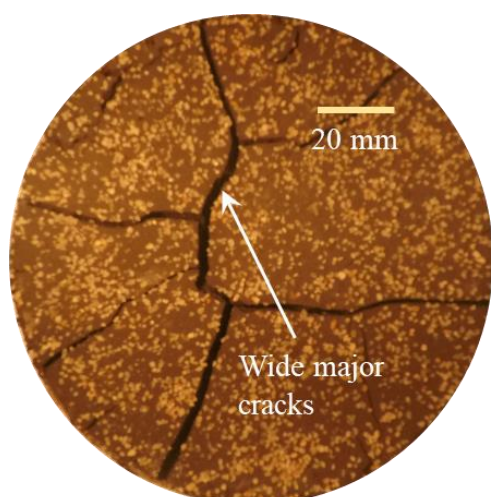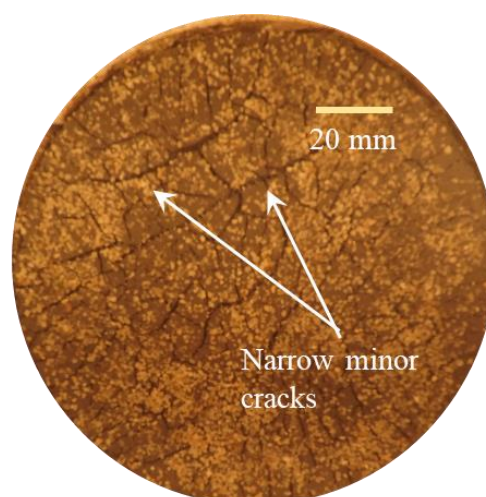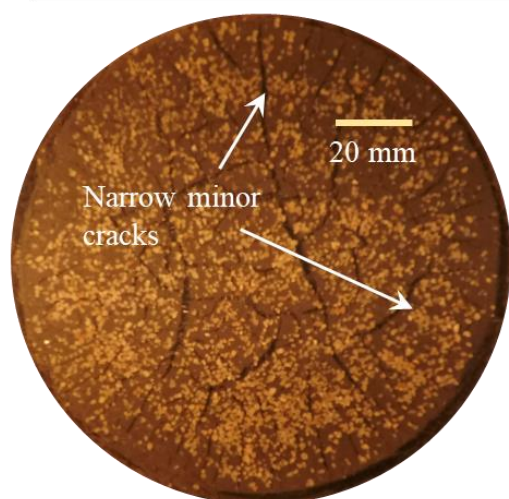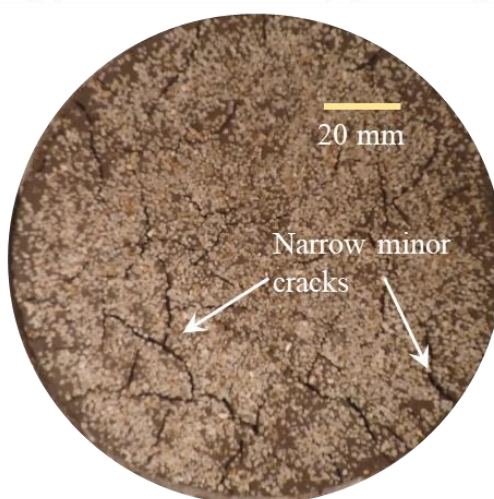
Figure 8.30 Crack morphology at the end of the centrifuge test (a) UR3, (b) FR3, (c) FR7 (d) FR11

The depth of crack is defined as the vertical extent to which the crack is pass through the thickness of specimen. The permeability of compacted soil barriers depends on the intensity and depth of crack. Moore and Ali (1982) observed that the overall infiltration of water through a fractured compacted clay layer is more dependent on the depth of the crack than the intensity of cracking. A numerical study on a fractured clay soil undergoing infiltration was used to state that the depth, intensity and frequency of cracking must be considered to estimate the overall infiltration and performance of the clay layer.

Table 8. 4 Summary of centrifuge test results on unreinforced clay layer [Series - A]

Parameters	Test legend				
	UR1	UR2	UR3	UR4	UR5
[a] **Thickness of specimen**	30 mm	30 mm [1.77 m]	30 mm [2.46 m]	30 mm [3.24 m]	25 mm [2.46 m]
*** Time of crack initiation, t_i**	54 min	5 min [12 days]	5 min [23 days]	3 min [24 days]	4 min [27 days]
Cracking pattern	Wide, shallow	Wide, deep	Wide, deep	Wide, deep	Wide, deep
[#] **Normalized crack width, c_w/d**	0.066	0.057	0.077	0.076	0.079
[#] **Normalized crack spacing, s_c/d**	0.44	0.434	0.403	0.475	0.67
[#] **Normalized crack depth, d_c/d**	0.5	1	1	1	1
CIF (%)	12	30	35	38	36
[c] **Average shrinkage strain, ε_{avg} (%)**	15.23	19.29	18.56	19.32	20.01

UR- Unreinforced; [a] prototype dimensions within the parenthesis; [b] not relevant/not used; *time in prototype dimensions in parenthesis; CIF-Crack intensity factor; [c] computed manually by ImageJ; [#] Average value throughout the specimen

Cracked soil chunks
free to move
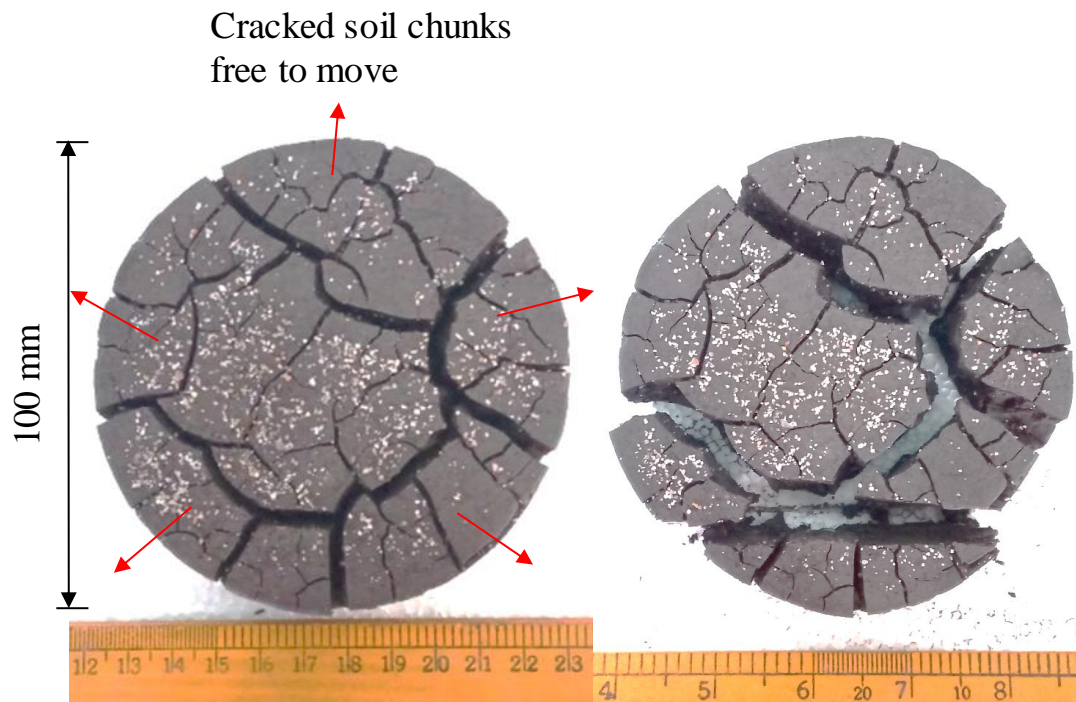
Figure 8.31 Unreinforced soil specimen after the test UR3
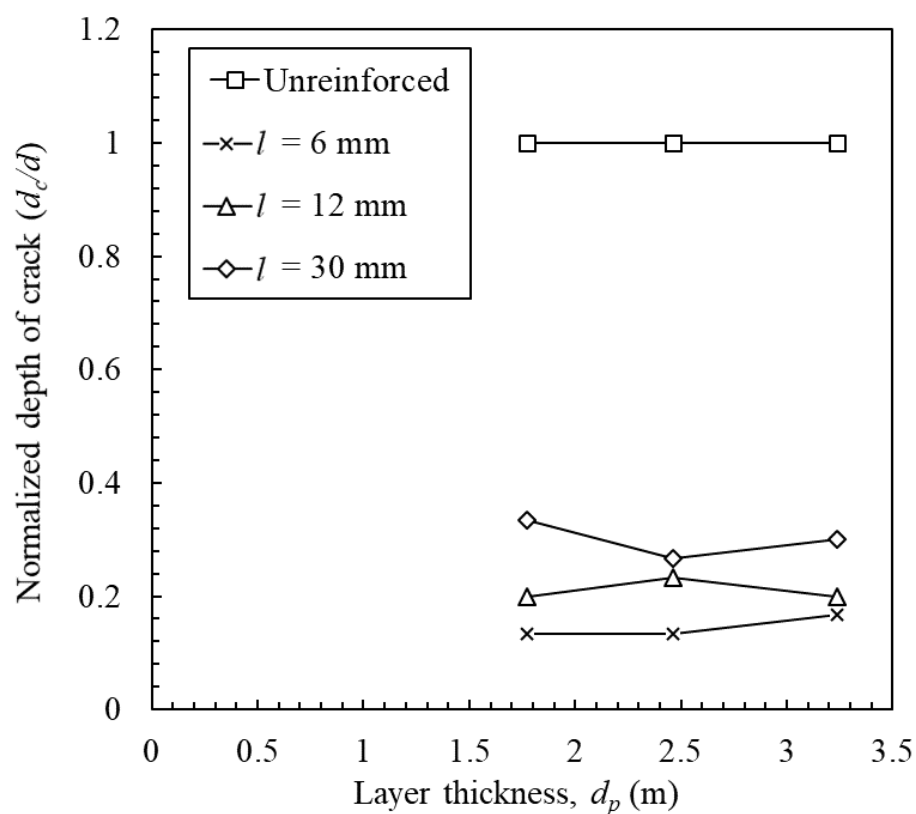
Figure 8.32 Normalized depth of crack for unreinforced and fiber-reinforced clay layers

of varying thicknesses

Figure 8.31 Unreinforced soil specimen after the test. Unreinforced clay specimens cracked throughout their depths, and the soil chunks were free to be moved after cracking, emphasizing the failure of clay layer.

(a) Top view

2 mm

100 mm

Prototype thickness, d_p=2.46 m

(b) Side view
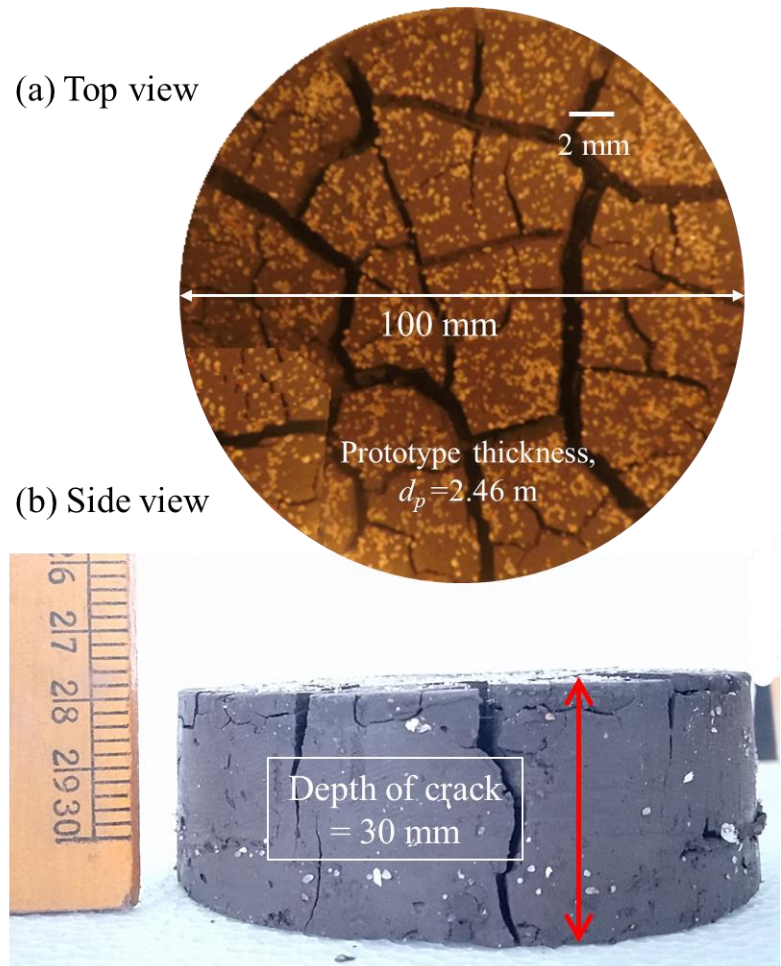
Depth of crack = 30 mm

Figure 8.33 Depth of crack in unreinforced soil specimen (UR3)

At the field, measuring crack depth is an approximate method due to the irregular shape and complex geometry (Yesiller et al. 2000). The depth, width and spacing of cracks are not uniform throughout the area. Generally, the highest depths and widths are recorded. However, according to the filed data, the typical crack depths in unreinforced clay layers in landfill lines extend from 1.0 to 1.3 m or extend up to entire depth.

In a situation where the depth and intensity of cracking both are very high, the worst infiltration of leachate through the compacted clay layer is observed.

Crack intensity factor (CIF)

The crack intensity factor (Miller et al. 1998) was computed for unreinforced and fiber reinforced soil specimens by dividing the area of cracks to the total initial area of the specimen. The CIF was computed for each specimen at the end of the test and plotted in Figure 8.34. In this study, the area of cracks was computed by converting the RGB image to binary image and thereby calculating the area of total region that got converted into black. Clearly, the CIF is found to be highest in unreinforced specimens for all the considered prototype thicknesses. The intensity of cracking is reduced by 59-67% in fiber reinforced specimens than in unreinforced specimens.
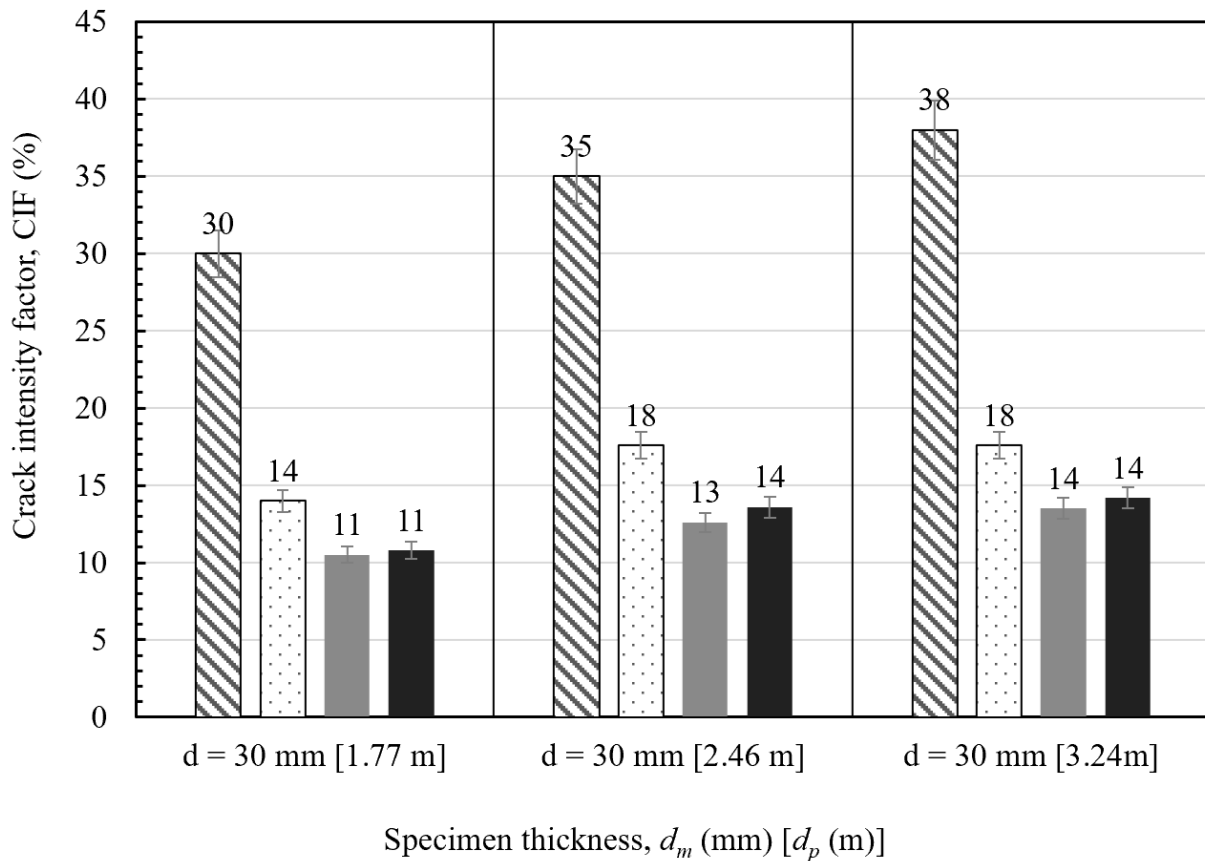
Figure 8.34 Crack intensity factor for unreinforced [Series A] and fiber reinforced soil specimens [Series B1, B2, B3] for varying prototype thicknesses [1.77m, 2.46 m, 3.24 m]

Permeability

It is clear from the permeability values derived from the consolidation tests of unreinforced and fiber reinforced soils, that the permeability of clay increases due to addition of fibers before undergoing desiccation cracking.

264

However, to understand effective permeability values of the unreinforced and fiber reinforced clay layers after undergoing desiccation cracking, a simplified seepage model has been used given by Mundell 1985. This model on the permeability of a desiccated clay layer is based on Darcy's law. Considering a clay layer (either unreinforced or fiber reinforced) of thickness d_p which has undergone desiccation cracking is shown in Figure 8.35.
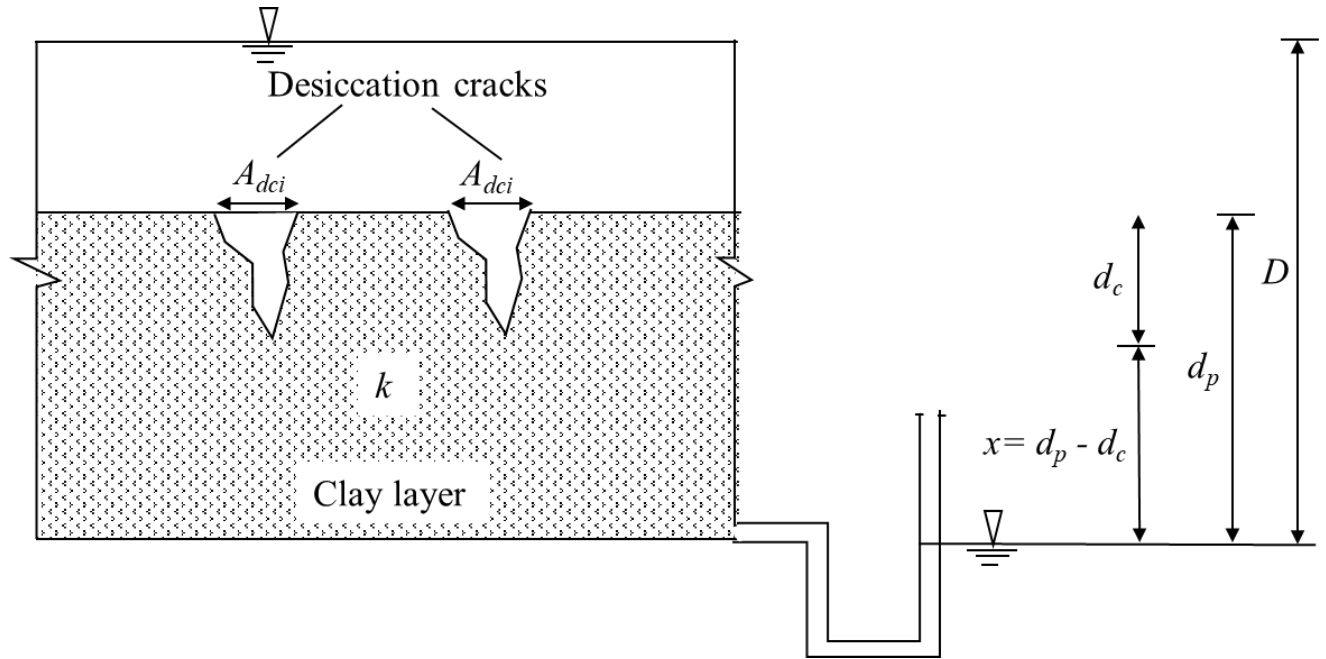
Figure 8.35 Seepage model through a clay layer with desiccation cracks

From the model, it can be seen that

$$Q_c = k_c I A_c = k_c \frac{D}{d_p} A_c \tag{8.1}$$

$$Q_{dc} = k_c I A_{dc} = k_c \frac{D}{x} A_{dc} \tag{8.2}$$

$$Q_t = k_e I A_t \tag{8.3}$$

$$Q_t = Q_c + Q_{dc} \tag{8.4}$$

$$A_t = A_c + A_{dc} \tag{8.5}$$

$$CIF = \frac{A_{dc}}{A_t} \tag{8.6}$$

Where, k_c is the permeability of intact clay (unreinforced or fiber-reinforced) layer, k_e is the equivalent permeability of the clay layer, A_t, A_c, A_{dc} are the total area of clay layer, total area of the intact clay layer, total area of cracked area, respectively. Q_t, Q_c, Q_{dc} are the seepage through total clay layer, seepage through intact clay layer, seepage through desiccation cracks,

respectively. And, *I* is the hydraulic gradient and CIF is the crack intensity factor of the corresponding clay (unreinforced or fiber reinforced) layer. Setting equations 8.3, 8.4 equal to each other, substituting, and solving yields the following equation for the permeability of the clay layer:

$$k_e = k_c \left[1 - CIF + CIF \left(\frac{d_p}{d_p - d_c} \right) \right] \tag{8.7}$$

Considering the permeability values estimated in 4.4.2, and the measured CIF and depth of crack d_c values for clay layers of prototype thickness d_p, a plot of ratio of equivalent permeability of desiccated clay layer and permeability of intact clay (unreinforced or fiber-reinforced) layer, k_e / k_c and uncracked depth *x* can be plotted as shown in Figure 8.36.
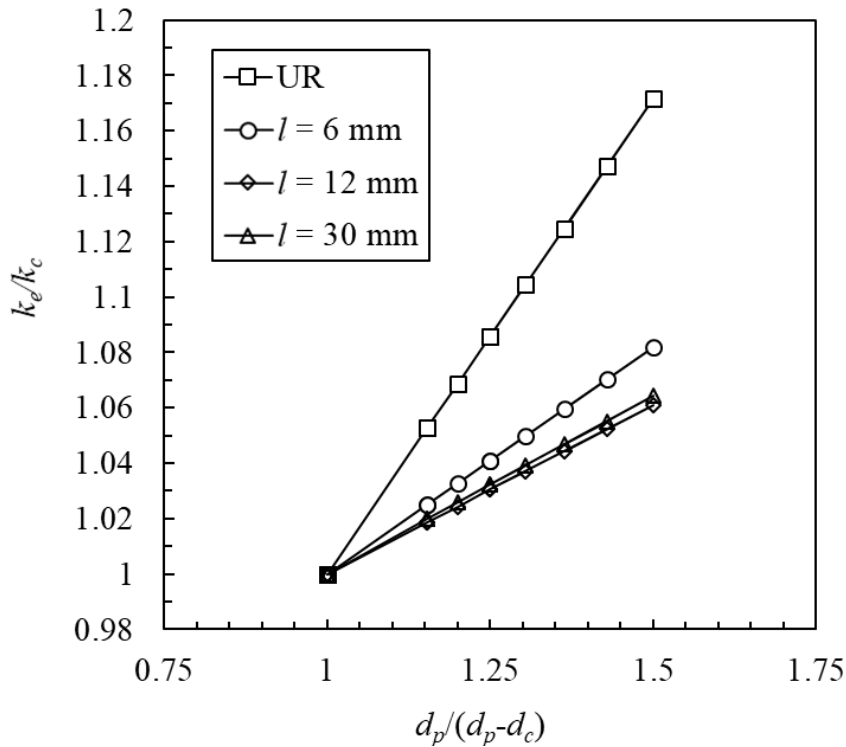
Figure 8.36 Effect of desiccation crack quantity and thickness on equivalent permeability of unreinforced and fiber-reinforced clay layer

It presents the effect of desiccation crack quantity and thickness on equivalent permeability of cracked unreinforced and fiber-reinforced clay layer. As shown in the figure, the equivalent permeability of cracked unreinforced clay layer is always higher than that of the cracked fiber-reinforced clay layer. This substantiates the fact that fiber reinforcement is efficient in reducing the permeability of a clay layer by reducing the intensity of cracking.

PIV analysis for unreinforced and fiber reinforced clay layer

PIV analysis was used on the images of unreinforced and fiber reinforced clay specimens undergoing desiccation cracking to determine the volumetric strains. Thusyanthan et al. (2007) used PIV in the tensile cracking in clays. The procedure explained in section 8.4.3 was followed. Figure 8.38 - Figure 8. 39 show the displacement vectors and volumetric strains in unreinforced (Test: UR3, UR4 and UR5) soil specimens at an interval of 60 minutes. Figure 8. 40Figure 8. 42 show the displacement vectors and volumetric strains in specimens reinforced with fiber length $l = 6$ mm (Test: FR2, FR3 and FR4) at an interval of 60 minutes. Similarly, Figure 8. 43-Figure 8. 45 and Figure 8. 46 Figure 8. 48 show the displacement vectors and volumetric strains in specimens reinforced with fiber length $l = 12$ mm (Test: FR6, FR7 and FR8) and fiber length $l = 30$ mm (Test: FR10, FR11 and FR12), respectively. The command for generation of volumetric strain is used in plotting the strains, as it gives the nearest possible values to the shrinkage strain of the soil. However, the depth of the specimen is ignored in the computation. The displacement vectors were overlapped on the strain contour plot to make the plot more comprehensive. In both cases, the soil specimens experience a significant amount of strains during desiccation.

In the unreinforced soil specimen after cracking, the displacement vectors in the separated soil mass are uniform and opposite directions from the crack as it widens; whereas, after cracking, the displacement vectors in fiber-reinforced soil specimen move in predominantly in the same direction even after the formation of the crack. It is evident that the fibers do not allow the cracks to widen, and the soil mass is mostly held intact by the fibers. As the soil shrinks, compressive strains (positive volumetric strain, $\varepsilon_{vol)}$) are seen to be developed in the soil specimen. As the crack appears, the tension strain (negative volumetric strain, $\varepsilon_{vol)}$) seems to develop at the cracks, and the rest of separated soil mass continues to shrink. Also, the strain levels are found to be higher in the case of unreinforced specimen. It means, the vector displacements of particles are higher in the unreinforced specimen. The displacement vectors before crack initiation indicate movement of soil from sides towards the mid of the specimen.

In unreinforced soil specimen, the displacement vectors in the separated soil mass are uniform and move away from the formed crack as the crack widens. Whereas the displacement vectors in fiber-reinforced soil specimen move in longitudinal direction even after crack formation. The fibers do not allow the crack to widen and the separated soil mass is held intact by the fibers.

(a) Volumetric strain after 60 mins (%)   (b) Volumetric strain after 120 mins (%)   (c) Volumetric strain after 180 mins (%)
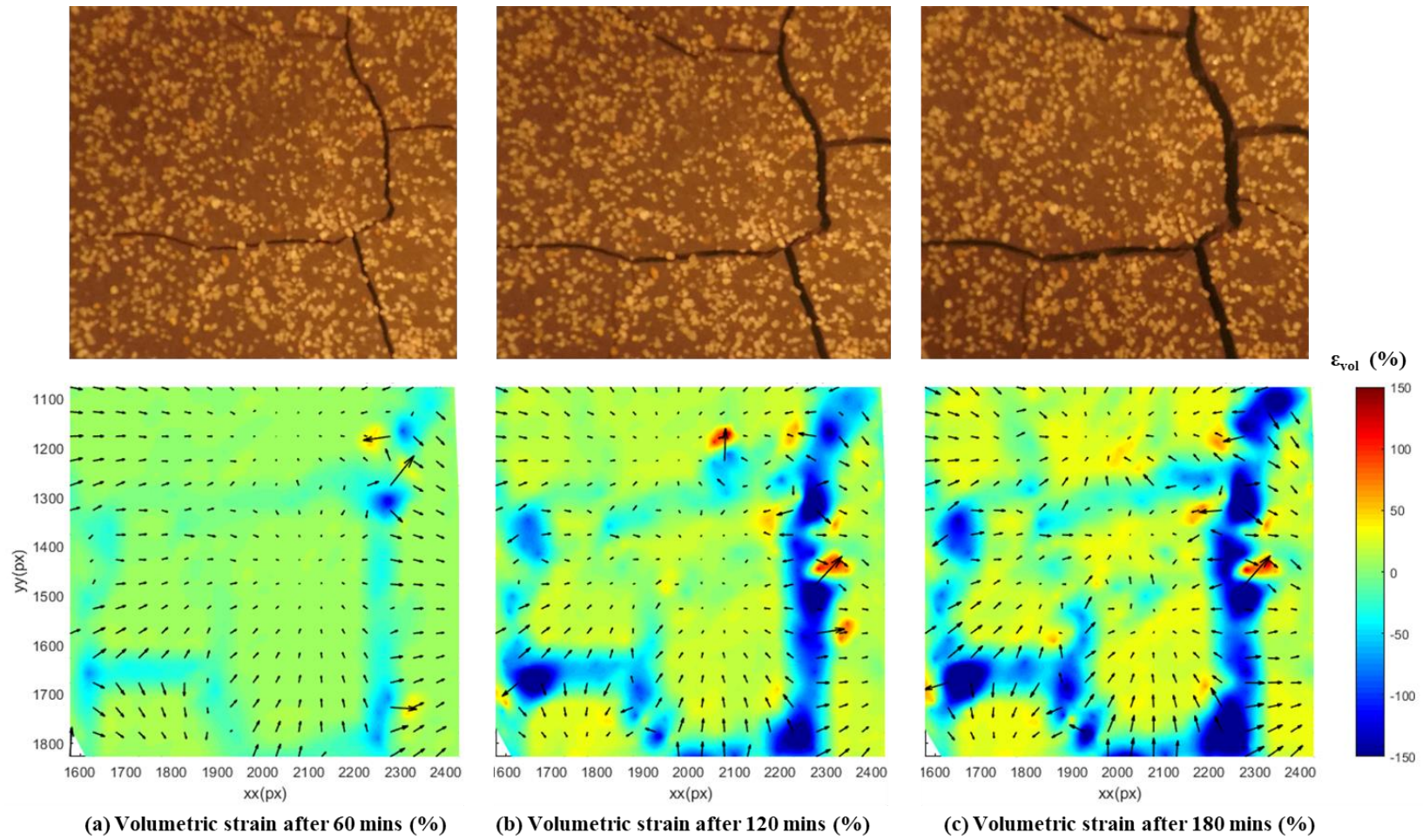
Figure 8. 37 Strain propagation for unreinforced soil specimen UR2, prototype dimensions 1.77 m

(a) Volumetric strain after 60 mins (%)   (b) Volumetric strain after 120 mins (%)   (c) Volumetric strain after 180 mins (%)
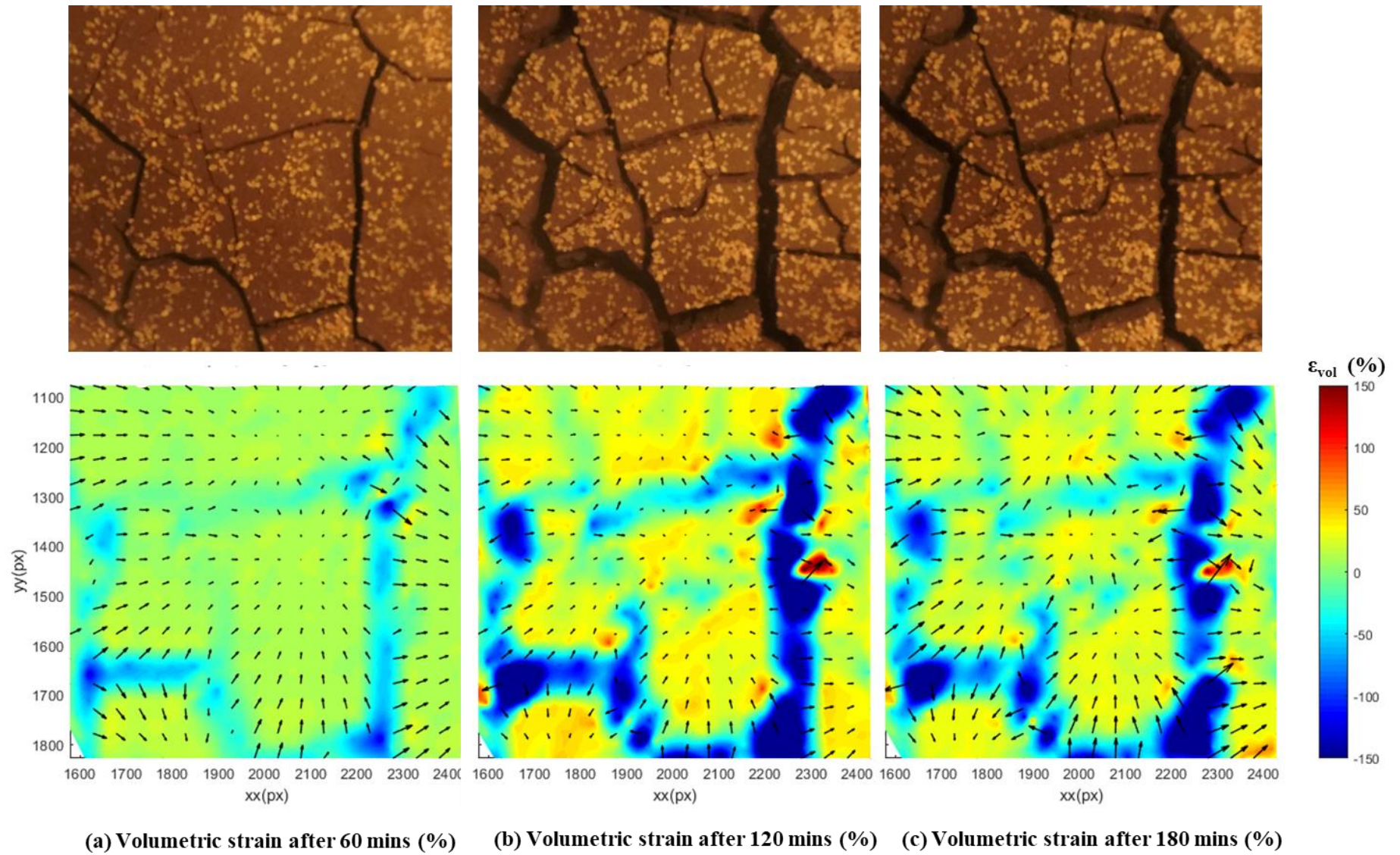
Figure 8.38 Strain propagation for unreinforced soil specimen UR3, prototype dimensions 2.46 m

269

(a) Volumetric strain after 60 mins (%)   (b) Volumetric strain after 120 mins (%)   (c) Volumetric strain after 180 mins (%)
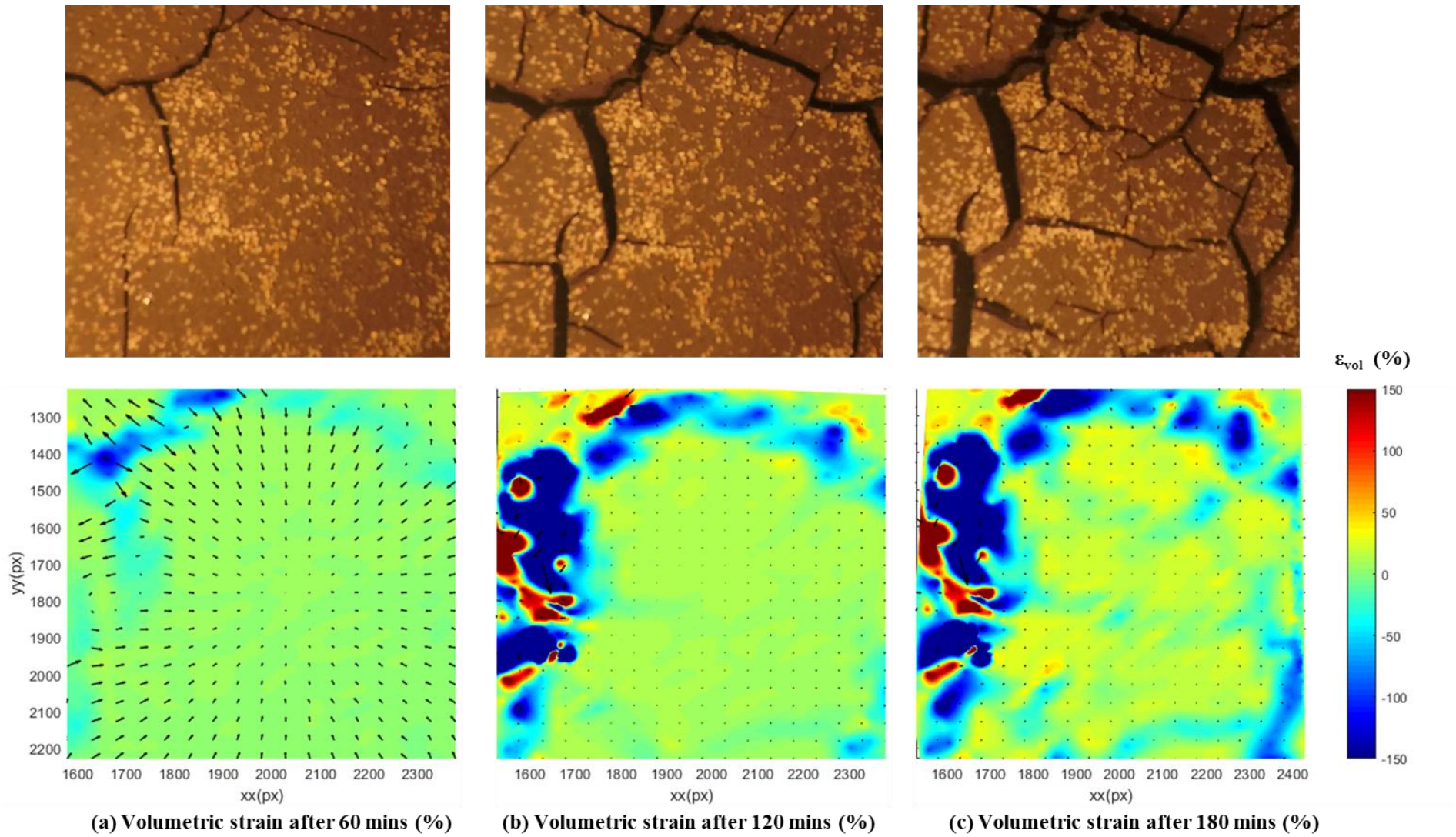
Figure 8. 39 Strain propagation for unreinforced soil specimen UR3, prototype dimensions 3.24 m

(a) Volumetric strain after 60 mins (%)   **(b) Volumetric strain after 120 mins (%)**   **(c) Volumetric strain after 180 mins (%)**
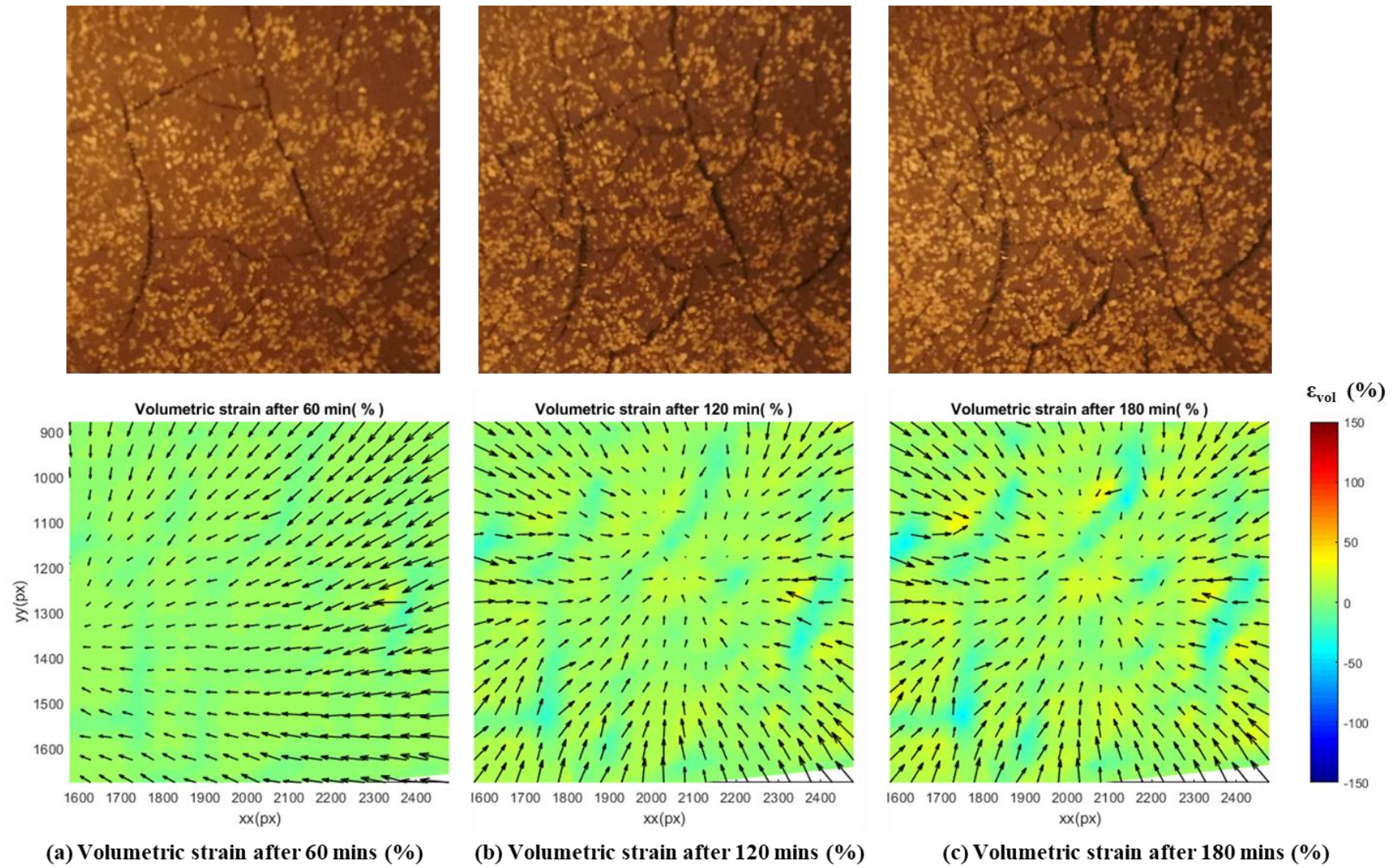
Figure 8. 40 Strain propagation for reinforced soil specimen FR2, prototype dimensions 1.77 m

271

(a) Volumetric strain after 60 mins (%) (b) Volumetric strain after 120 mins (%) (c) Volumetric strain after 180 mins (%)
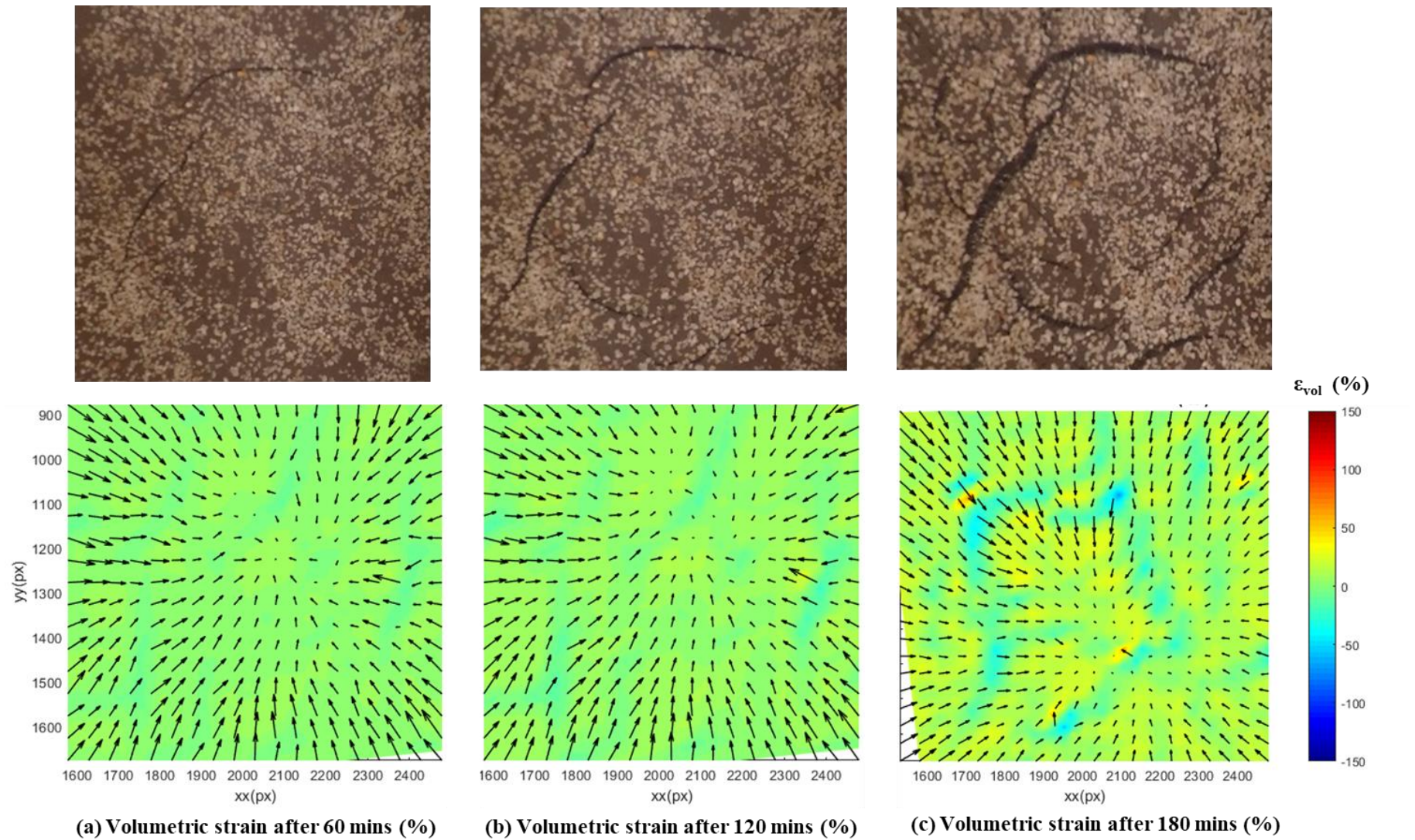
Figure 8. 41 Strain propagation for reinforced soil specimen FR3, prototype dimensions 2.46 m

272
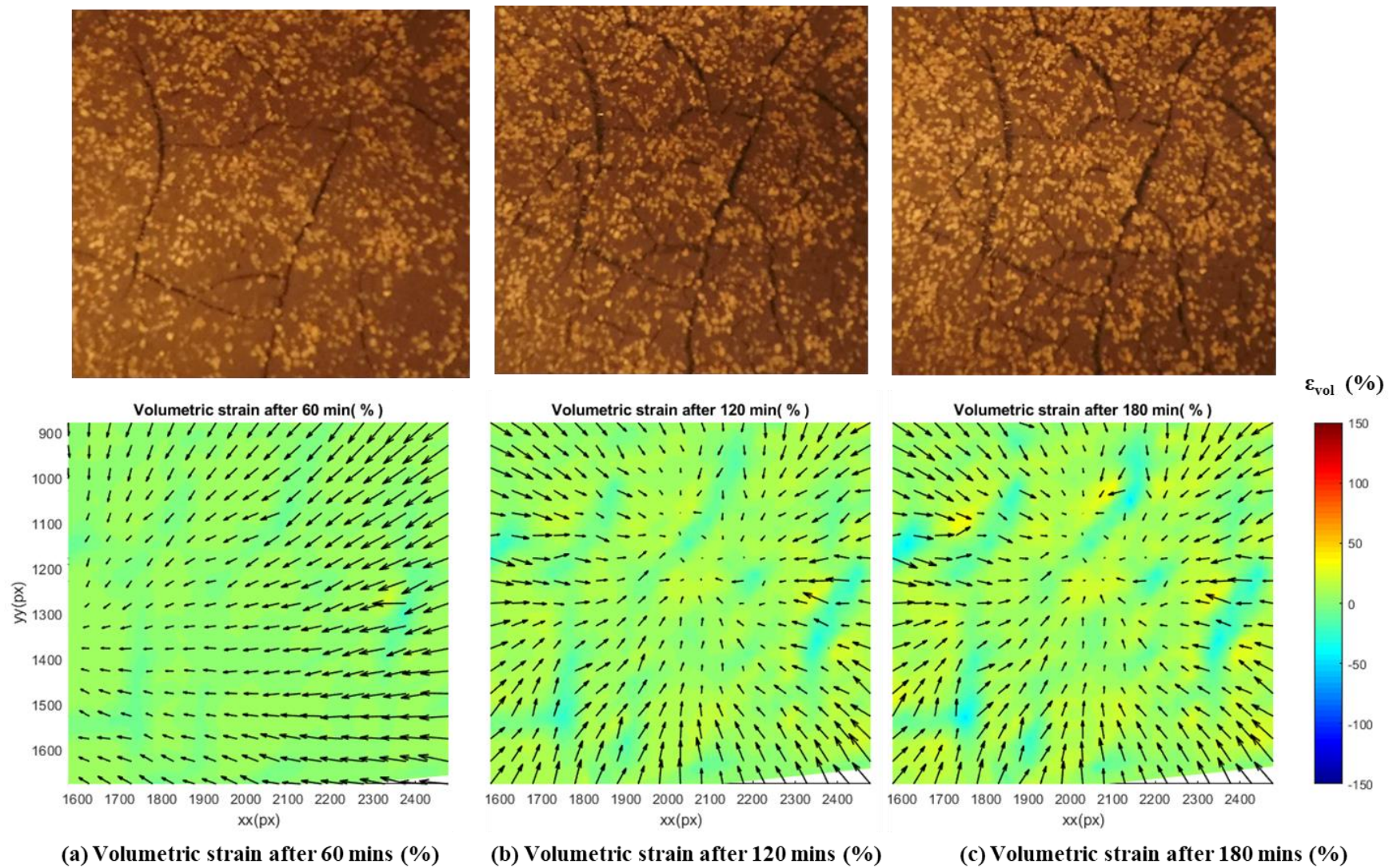
Figure 8. 42 Strain propagation for reinforced soil specimen FR4, prototype dimensions 3.24 m

(a) Volumetric strain after 60 mins (%)   (b) Volumetric strain after 120 mins (%)   (c) Volumetric strain after 180 mins (%)
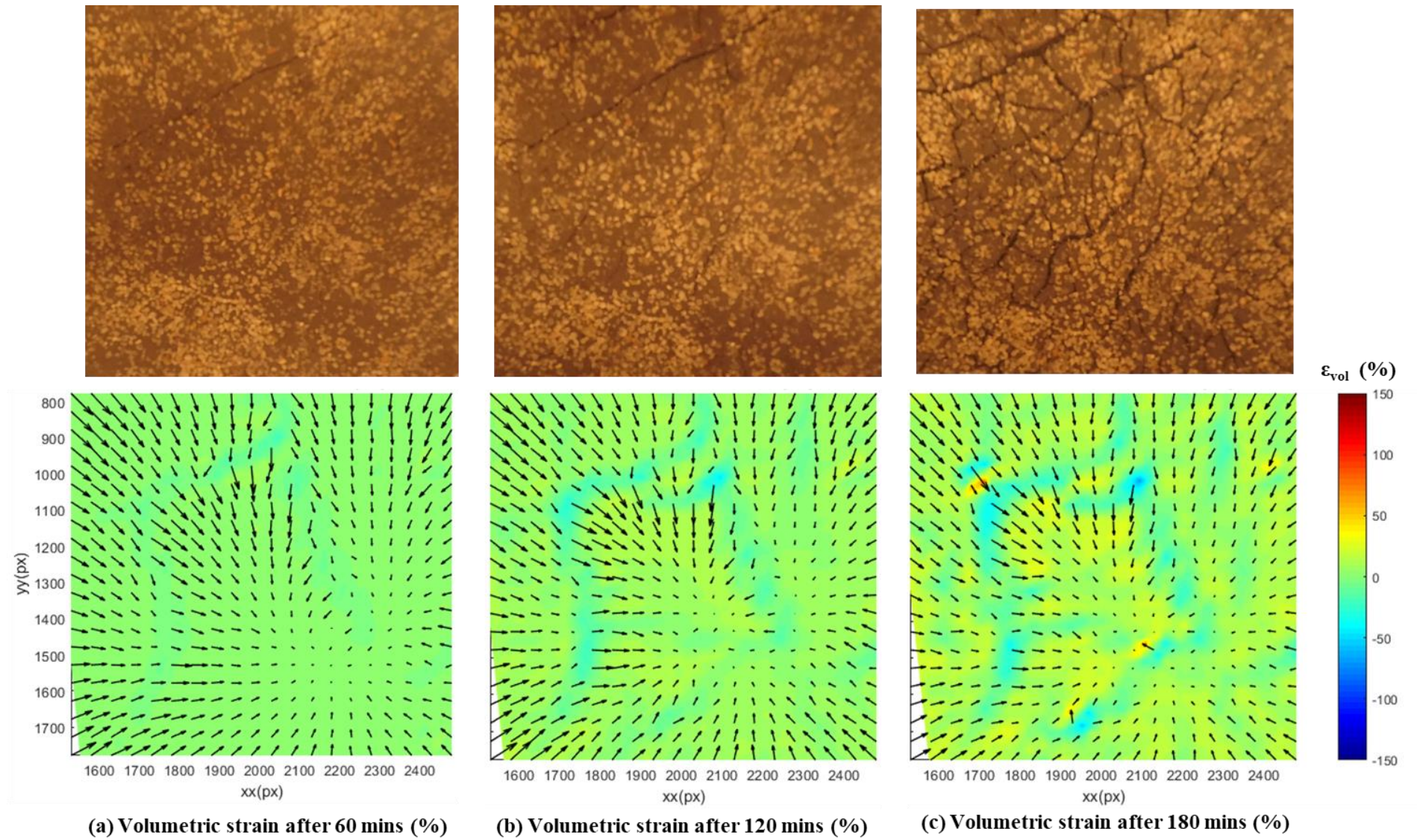
Figure 8. 43 Strain propagation for reinforced soil specimen FR6, prototype dimensions 1.77 m

(a) Volumetric strain after 60 mins (%)　　(b) Volumetric strain after 120 mins (%)　　(c) Volumetric strain after 180 mins (%)
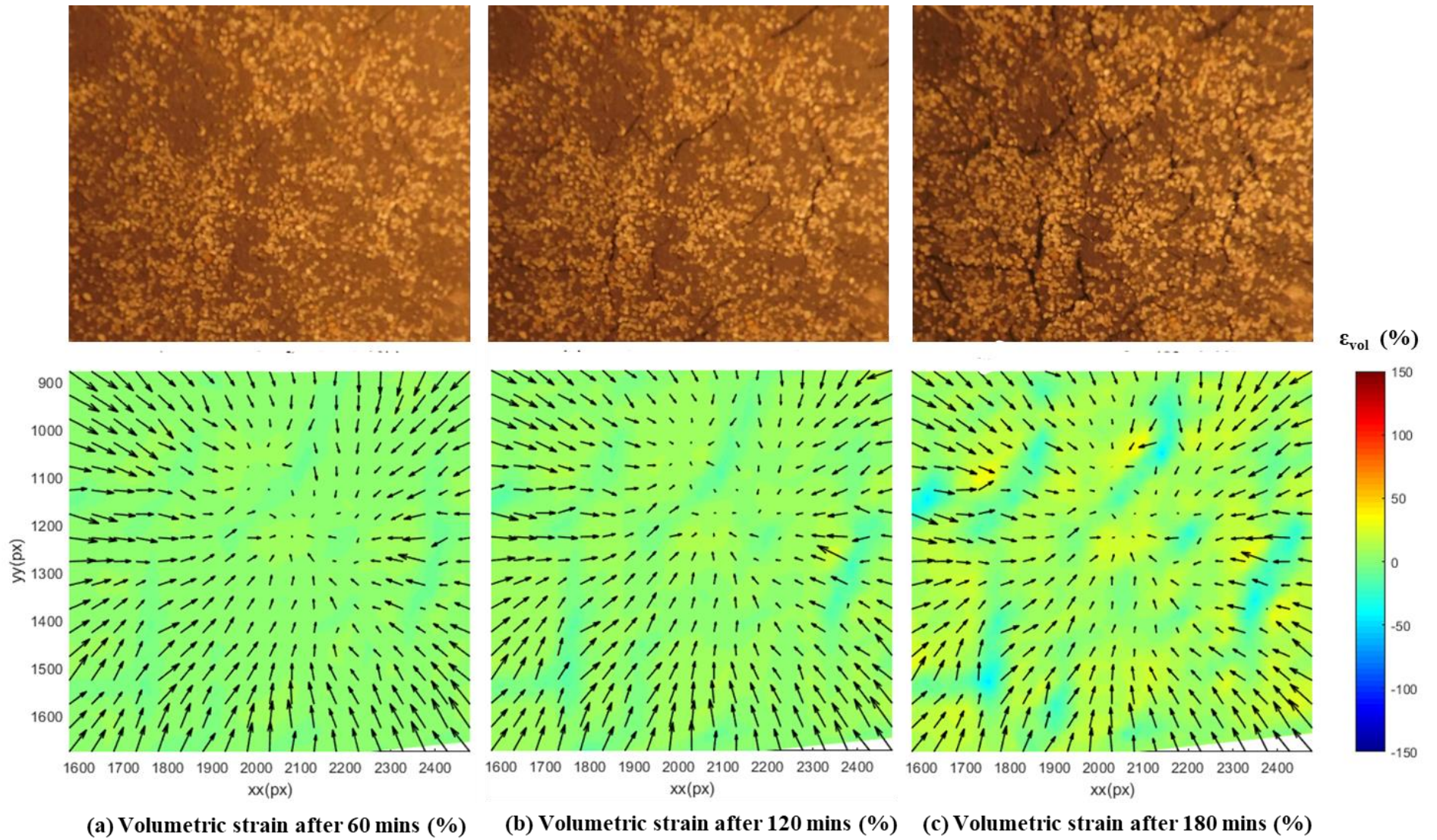
Figure 8.44 Strain propagation for reinforced soil specimen FR7, prototype dimensions 2.46 m

(a) Volumetric strain after 60 mins (%)   **(b) Volumetric strain after 120 mins (%)**   **(c) Volumetric strain after 180 mins (%)**
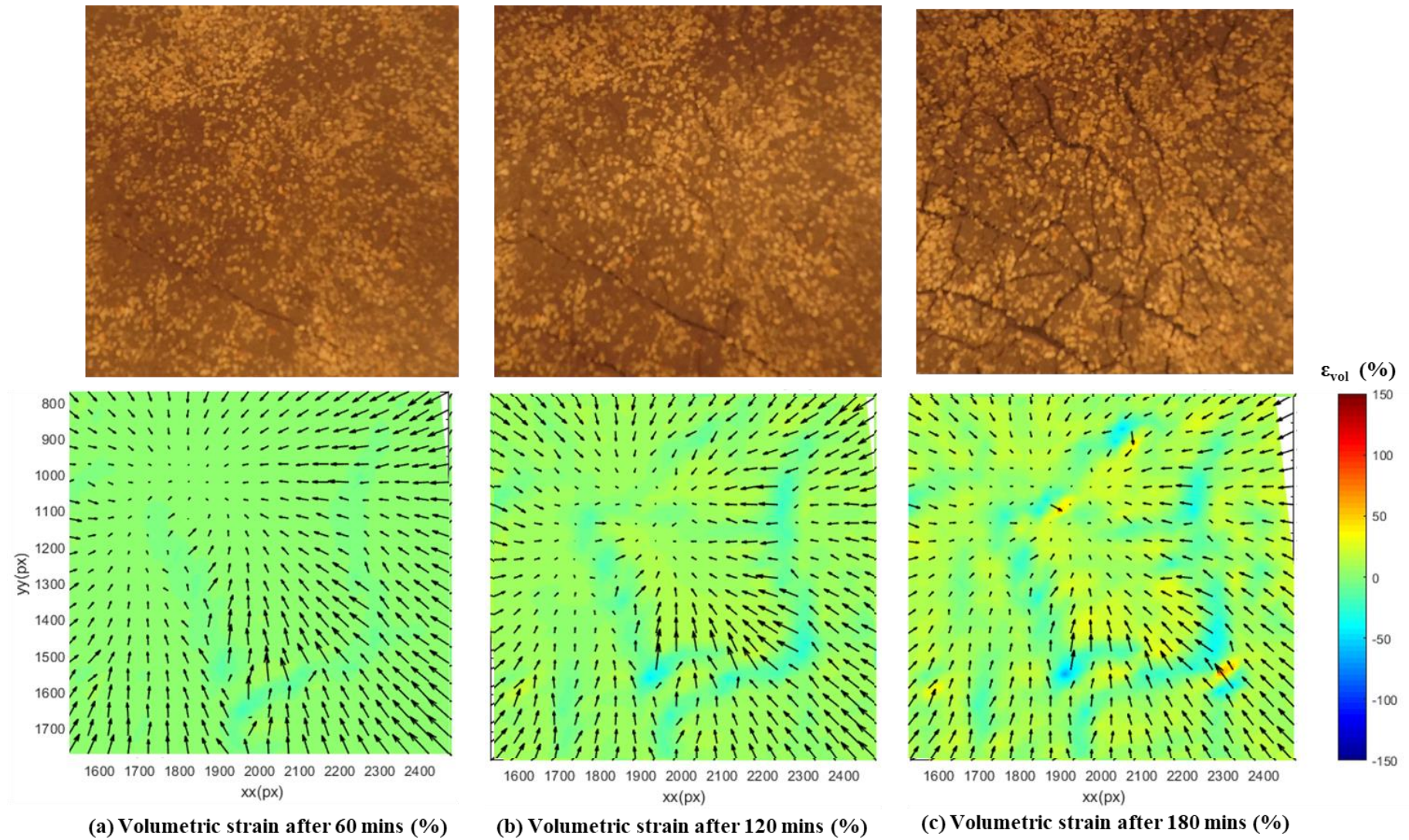
Figure 8. 45 Strain propagation for reinforced soil specimen FR8, prototype dimensions 3.24 m

(a) Volumetric strain after 60 mins (%)   (b) Volumetric strain after 120 mins (%)   (c) Volumetric strain after 180 mins (%)
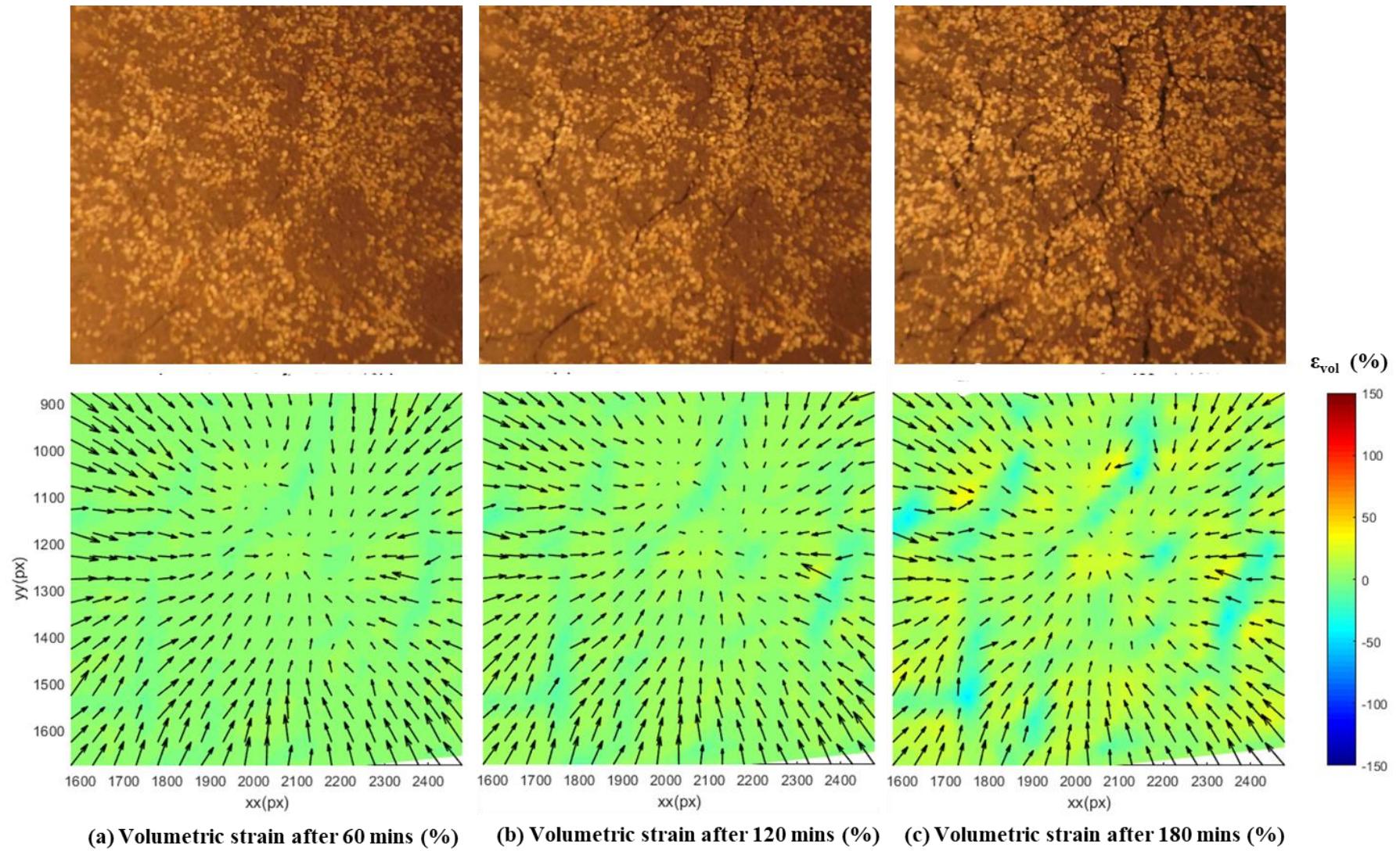
Figure 8. 46 Strain propagation for reinforced soil specimen FR10, prototype dimensions 1.77 m
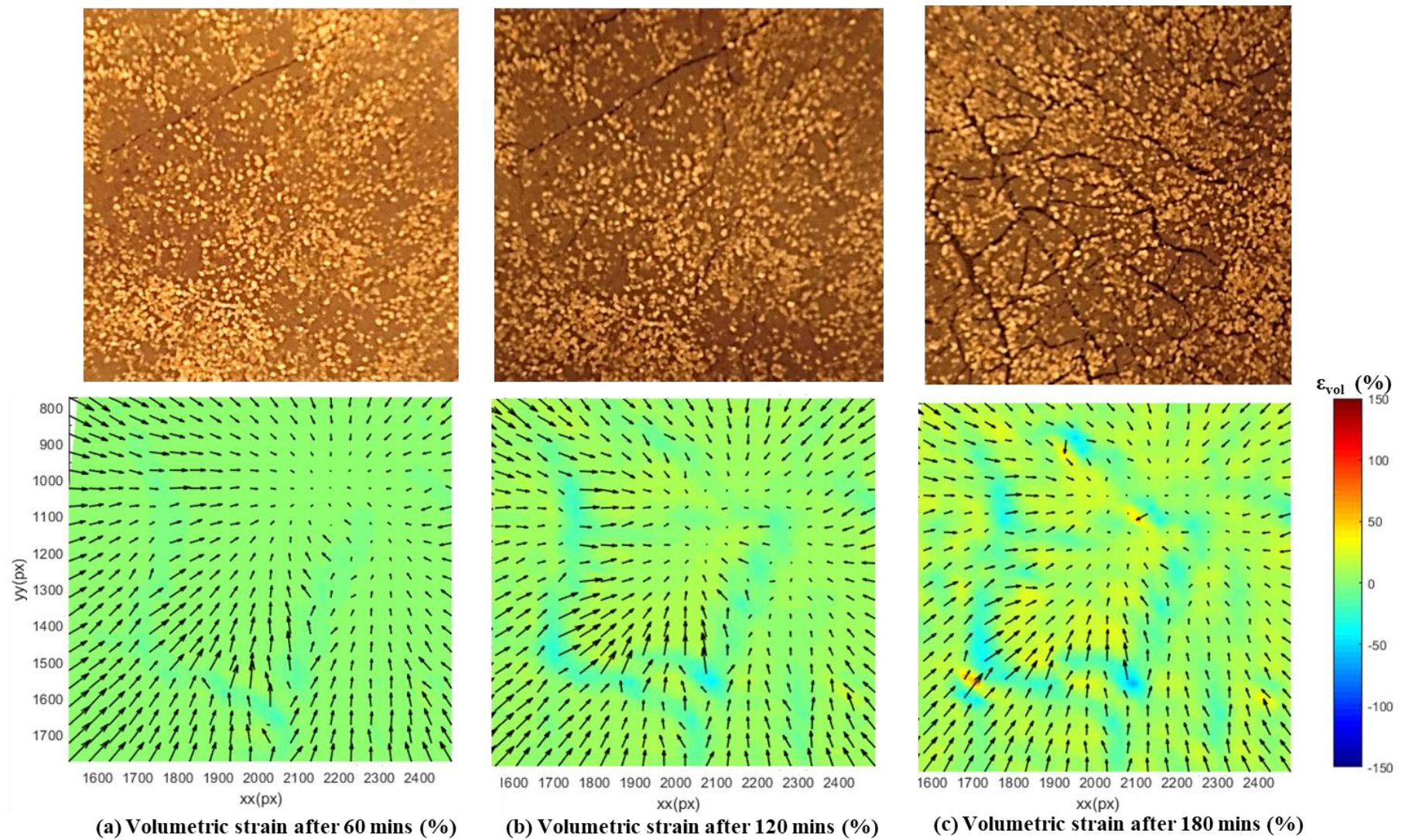
Figure 8. 47 Strain propagation for reinforced soil specimen FR11, prototype dimensions 2.46 m

278

(a) Volumetric strain after 60 mins (%)   (b) Volumetric strain after 120 mins (%)   (c) Volumetric strain after 180 mins (%)
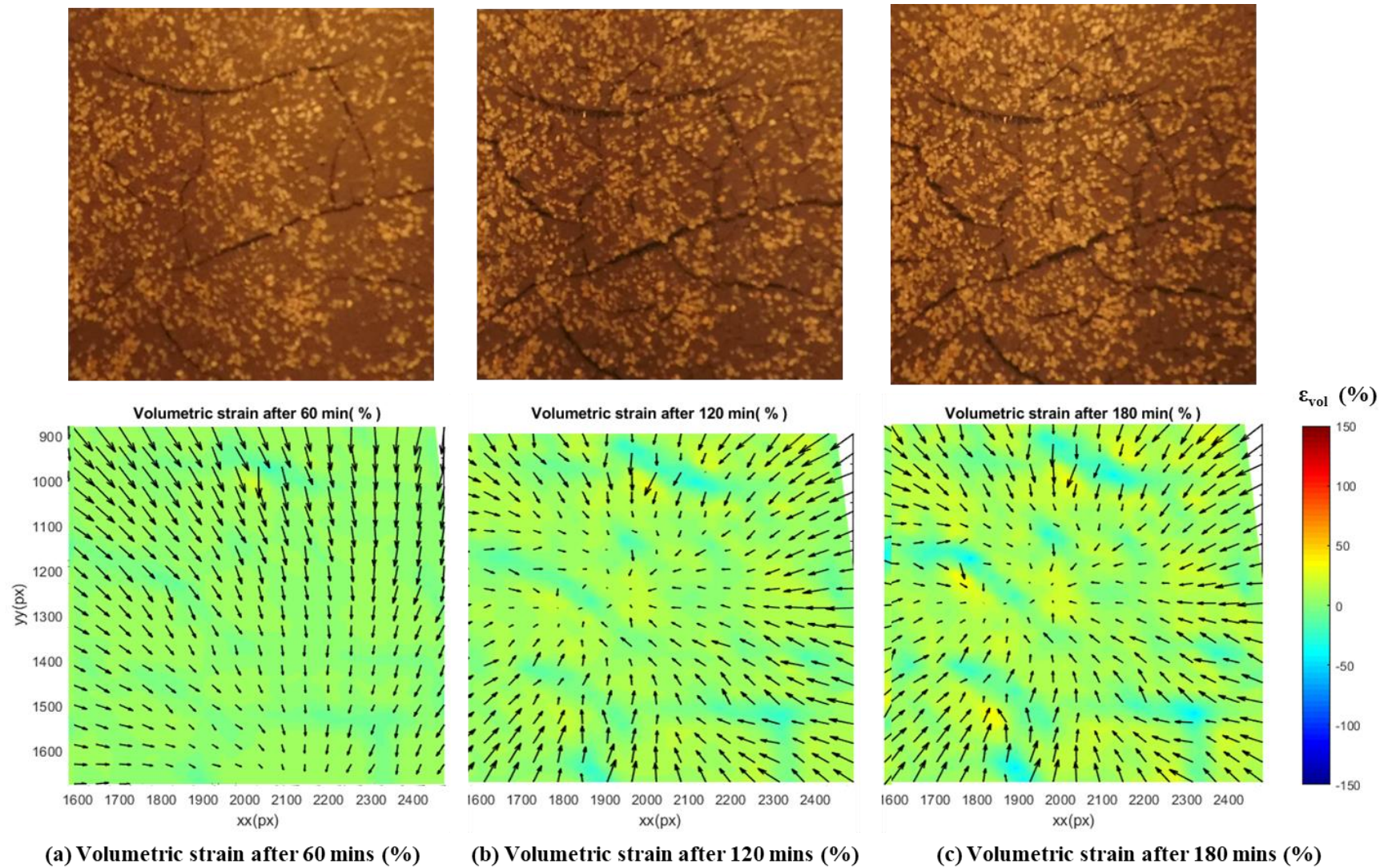
Figure 8. 48 Strain propagation for reinforced soil specimen FR12, prototype dimensions 2.46 m

8.5.3 Influence of thickness of soil layer

In order to study the influence of thickness of soil layer on the desiccation cracking behaviour of unreinforced and fiber reinforced clay layers, prototype thickness, d_p was varied as 1.77 m (Test UR2, FR2, FR6, FR10), 2.46 m (Test UR3, FR3, FR7, FR11) and 3.24 m (Test UR4, FR4, FR8, FR12).

Cracking pattern: Figure 8.49 and Figure 8.50 present the desiccation cracking patterns for unreinforced and fiber reinforced soil specimens with varying prototype thicknesses.
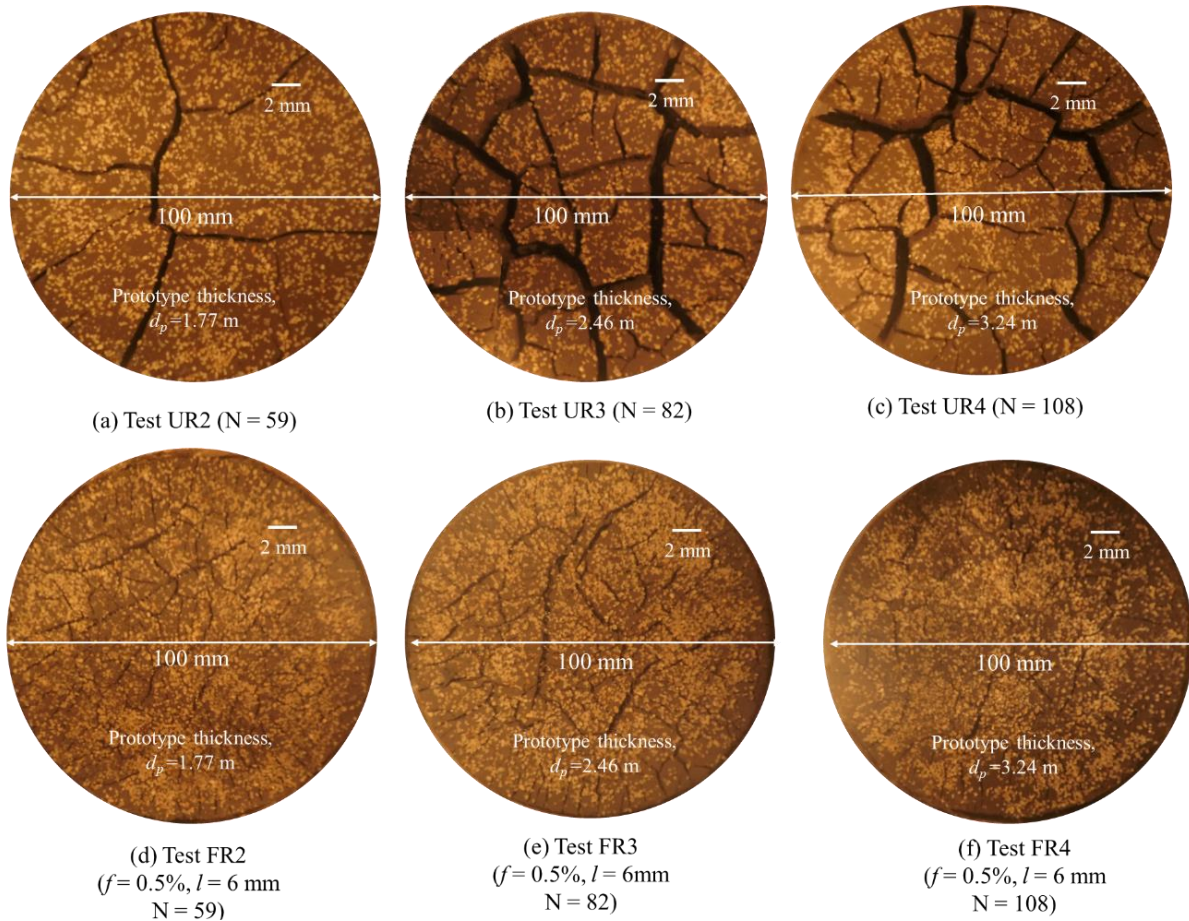
Figure 8.49 Desiccation cracking pattern for unreinforced and fiber reinforced soil specimens with varying prototype thicknesses for tests (a) UR2, (b) UR3, (c) UR4, (d) FR2, (e) FR3, (f) FR4

280
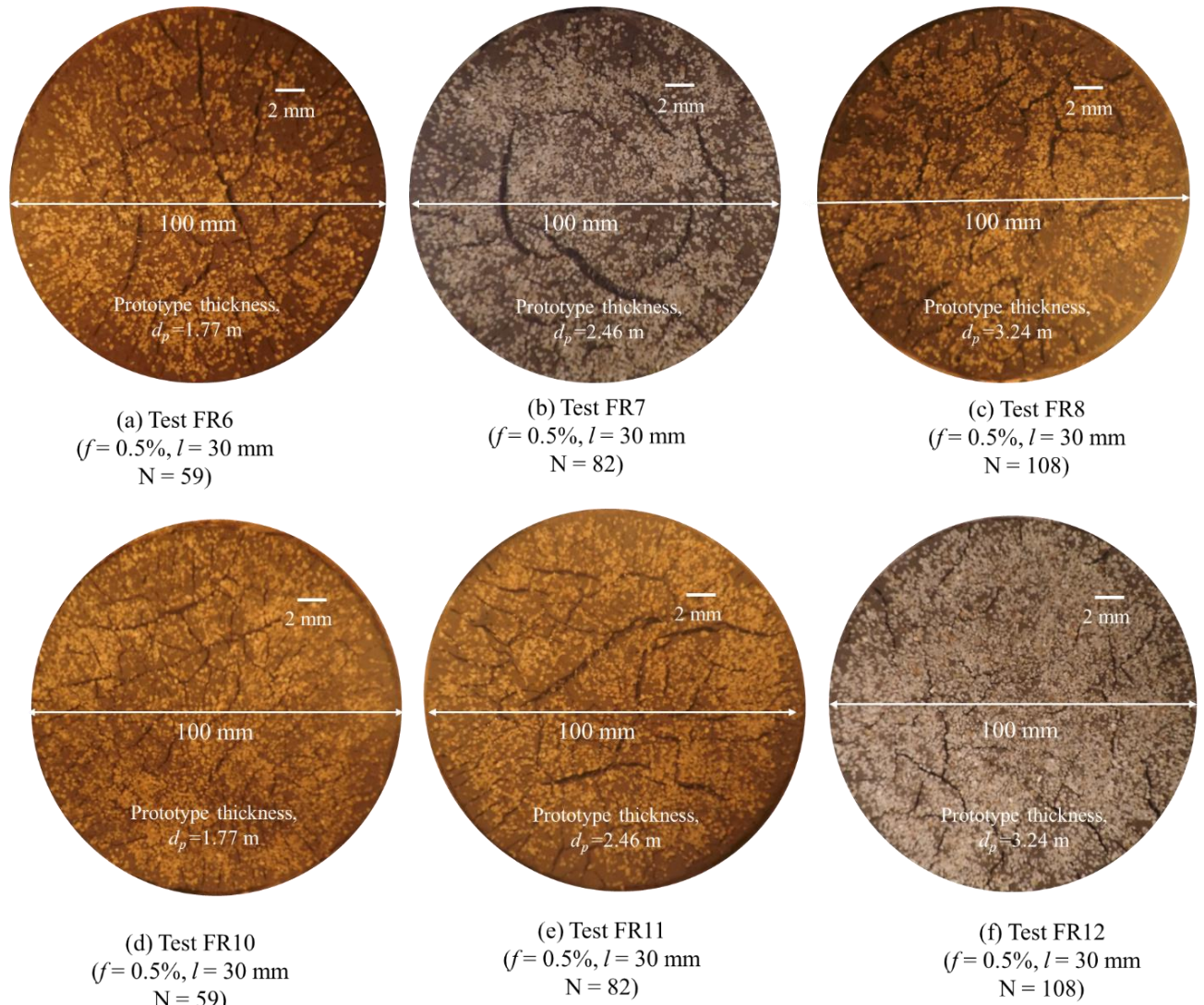
Figure 8.50 Desiccation cracking pattern for fiber reinforced soil specimens with varying prototype thicknesses for tests (a) FR6, (b) FR7, (c) FR8, (d) FR10, (e) FR11, (f) FR12

Figure 8.51 suggests that the moisture loss from the specimen at the end of the test is higher for specimens with larger thicknesses.

The crack patterns for unreinforced soil specimens were found to become more intense and wider with an increase in the clay layer thickness. In thicker clay layers, an internal restraint condition starts to develop as the top surface begins to desiccate. As the soil desiccates, this internal restraint leads to development of higher tensile stresses in the layer, thereby causing wider and more penetrating cracking patterns throughout the depth of specimen. Whereas, the cracking patterns are found not to be significantly dependent on the change in clay layer thickness for fiber reinforced specimens as shown in Figure 8.49 and Figure 8.50.
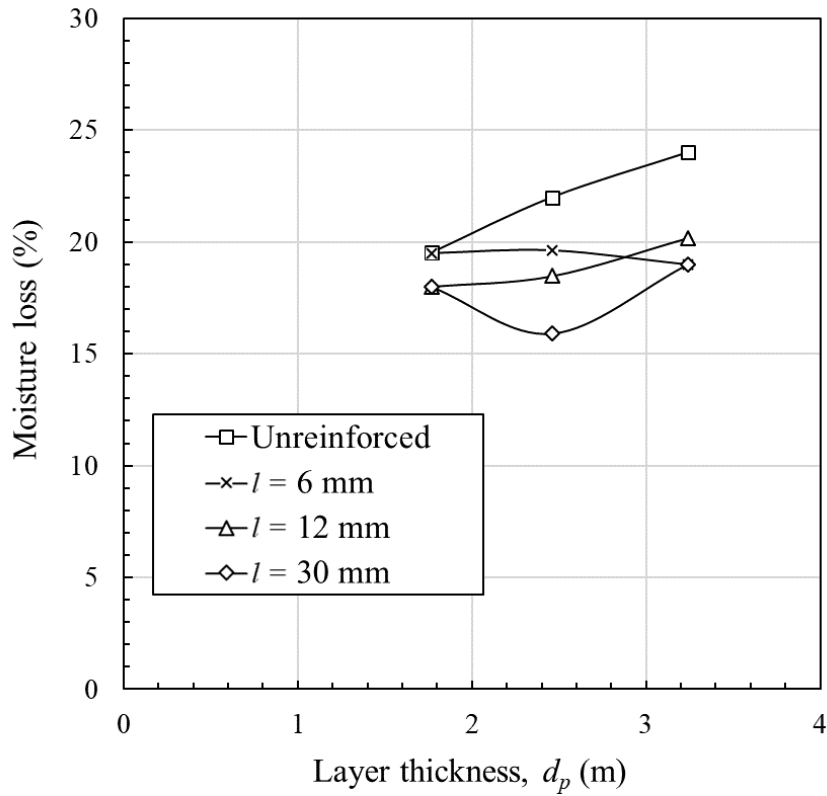
Figure 8.51 Variation of moisture loss at the end of the test for different clay layer thickness of unreinforced and fiber reinforced specimens

It can be argued that the tensile stresses developed in the clay layer due to internal restraint get released as minor cracks on the top layer. The fibers prevent further penetration and propagation of cracks vertically and horizontally, respectively.

Crack feature measurements: The crack feature measurements were assessed and compared for specimens with varying clay layer thicknesses keeping other parameters constant like specimen type (UR of FR), fiber type (PP, PET or PP-T), fiber length ($l = 6$ mm, 12mm or 30 mm) and fiber content ($f = 0.5\%$). Figure 8.52 presents the variation of normalized crack width (c_w/d) for different varying specimen thicknesses for unreinforced and fiber reinforced specimens. As can be seen from the images, the values of normalized crack width (c_w/d) also demonstrate that the crack width increases with increase in the layer thickness for unreinforced specimens.
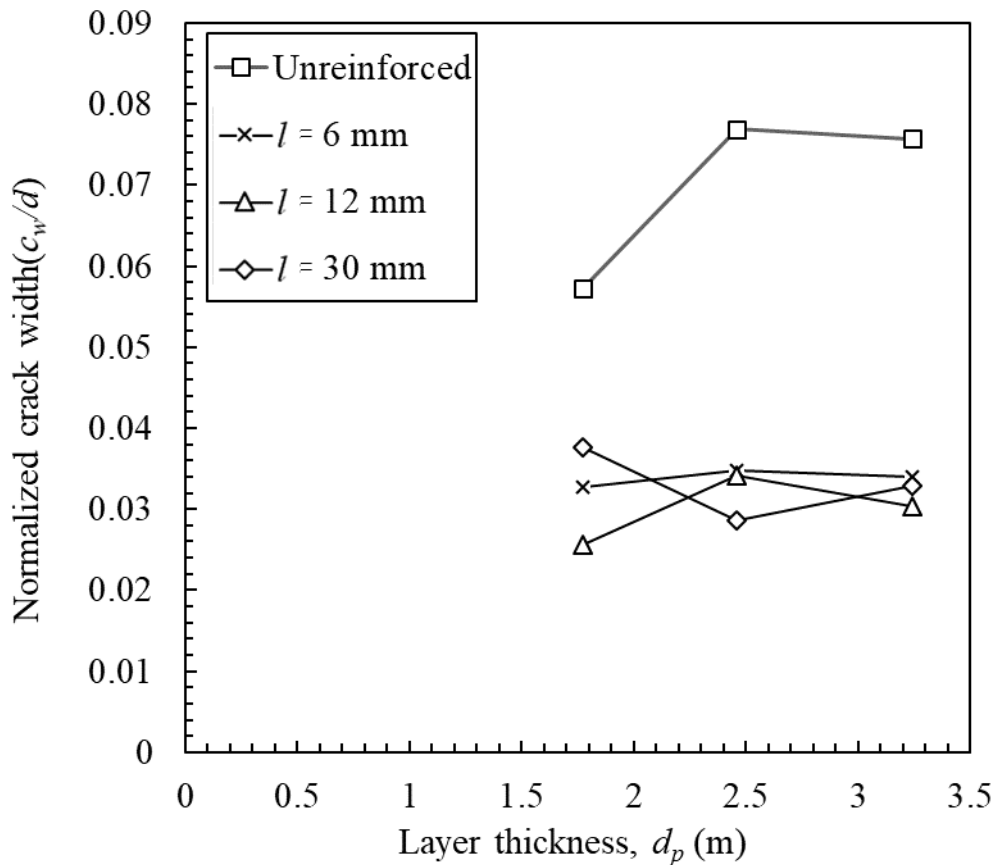
Figure 8.52 Variation of normalized crack width (c_w/d) for different varying specimen thicknesses for unreinforced and fiber reinforced specimens

In the 1g tests conducted in section 6.5.1, it was observed that the crack width increases with increases in specimen thickness for unreinforced and fiber reinforced specimens as well (clay layer thickness = 5mm, 10 mm, 15 mm). However, in the centrifuge tests, the crack width values seem to be independent of thickness of clay layer specimen, showing that the clay layer thickness doesn't affect the crack width for layer thicknesses as high as 1.77 m to 3.24 m. Figure 8.53 shows the variation of time of crack initiation for unreinforced clay layers of varying thicknesses. The time of crack initiation increases with increase in clay layer thickness.

Similar behaviour is observed in fiber reinforced soil specimens, that the time of crack initiation increases with increase in clay layer thickness. Figure 8.54, Figure 8. 55 and Figure 8. 56 show the variation of time of crack initiation for fiber-reinforced clay layers of varying thicknesses, reinforced with fibers of length l = 6 mm,12 mm and 30 mm, respectively. Typically, the time of crack initiation increases with increase in the clay layer thickness.
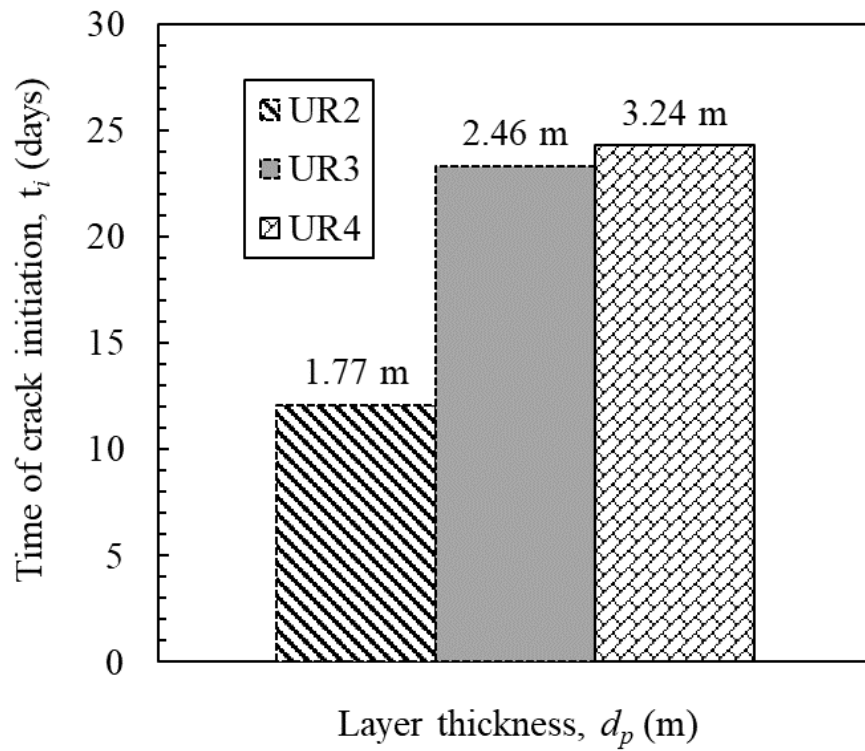
Figure 8.53 Time of crack initiation for unreinforced clay layers of varying thickness [Test: UR2, UR3, UR4]
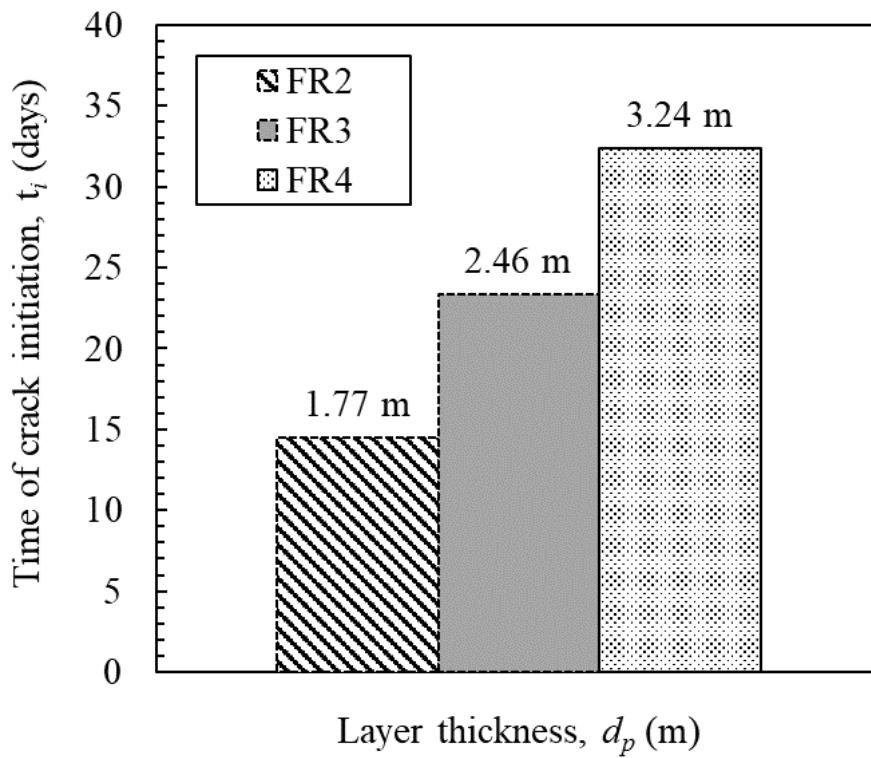
Figure 8.54 Time of crack initiation for fiber-reinforced clay layers ($l = 6$ mm) of varying thickness [Test: FR2, FR3, FR4]
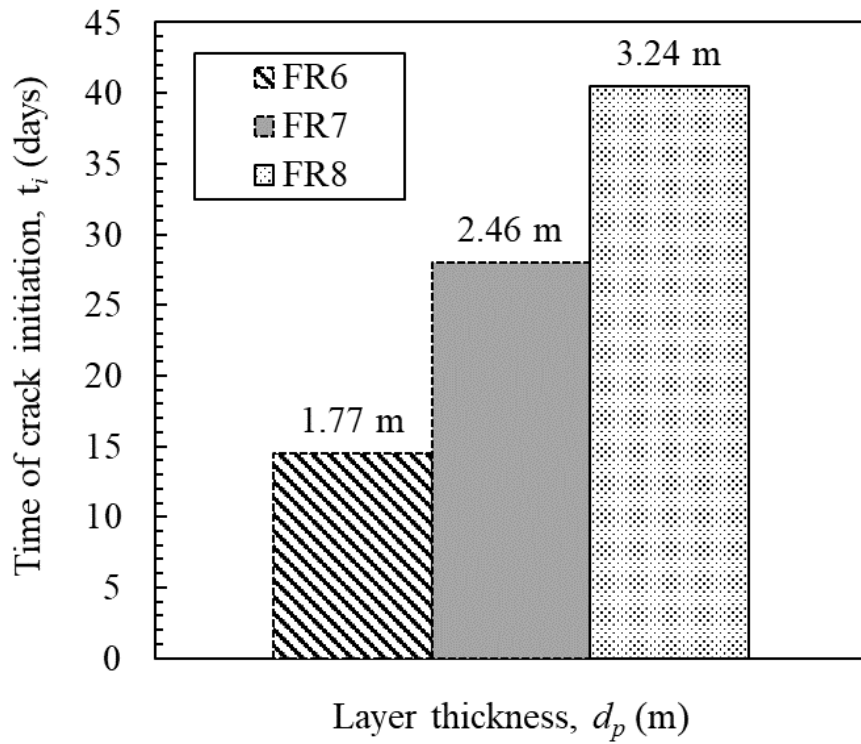
Figure 8. 55 Time of crack initiation for fiber-reinforced clay layers (l = 12 mm) of varying thickness [Test: FR6, FR7, FR8]
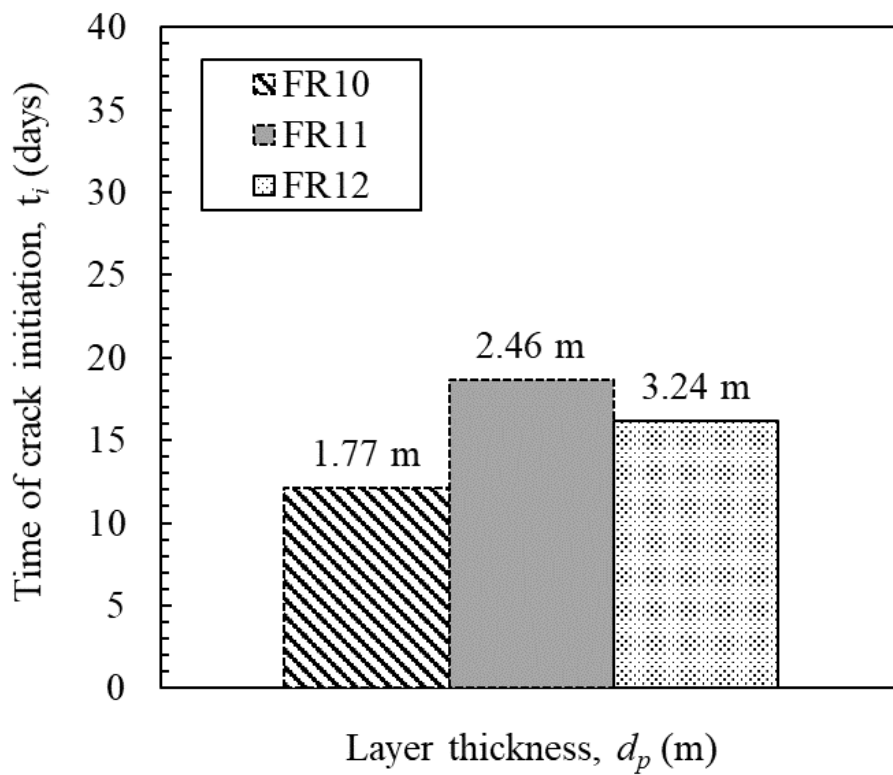
Figure 8. 56 Time of crack initiation for fiber-reinforced clay layers (l = 30 mm) of varying thickness [Test: FR10, FR11, FR12]

Figure 8. 57 Figure 8. 59 represent the variation of normalized crack width, c_w/d with time for unreinforced and fiber reinforced clay layers of varying thicknesses, i.e. $d_p = 1.77$ m, 2.46 m and 3.24 m. the primary ordinate represents the model time, whereas the secondary ordinate represents the time in prototype dimensions. The crack width increases as the crack propagates with due course of time. The normalized crack width, c_w/d of unreinforced clay layers are invariably larger than fiber reinforced clay layers. It is also observed that the crack width reduction, i.e. difference in the crack width of unreinforced and fiber reinforced clay layers is larger in case of thicker clay layers. The reduction in crack widths and maintaining certain stiffness within cracked layers were desirable properties for improved performance of a modified barrier system.
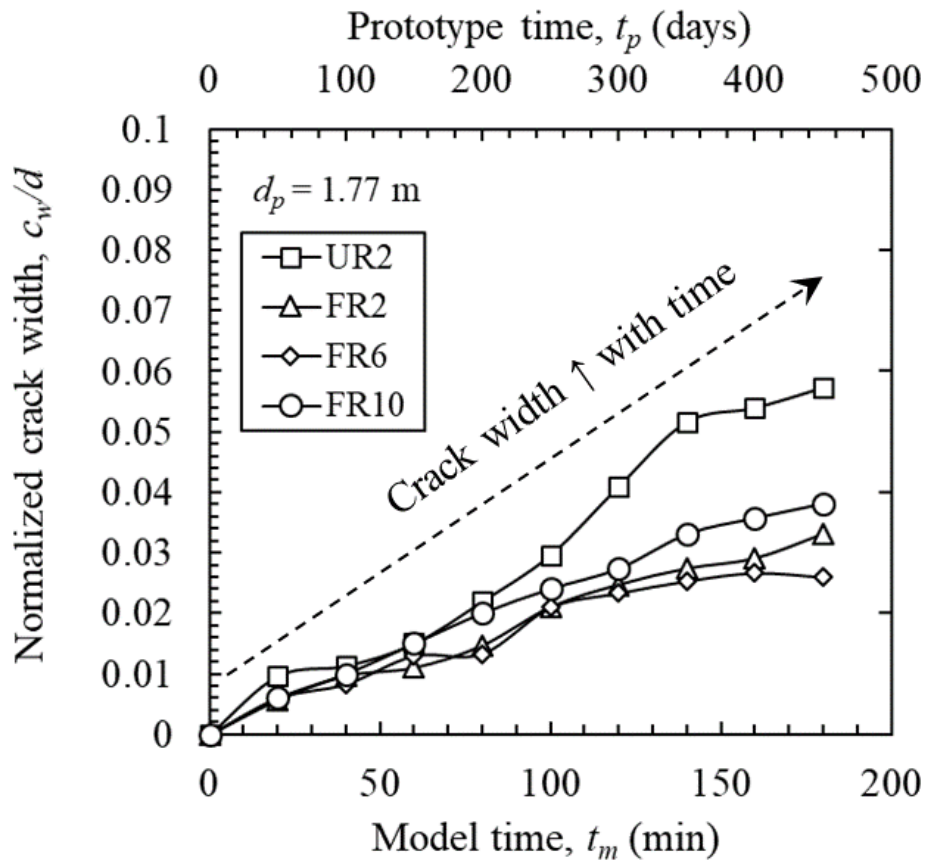
Figure 8. 57 Variation of normalized crack width, c_w/d with time for unreinforced and fiber reinforced clay layers of layer of prototype thickness, $d_p = 1.77$ m

As shown in Figure 8.27, the crack spacing reduces as the cracks propagate in clay specimens. Figure 8. 60 Figure 8. 62 show the variation of normalized crack spacing, s_c/d with model time (prototype time in secondary axis) for unreinforced and fiber reinforced clay layers of varying thicknesses, i.e. $d_p = 1.77$ m, 2.46 m and 3.24 m.
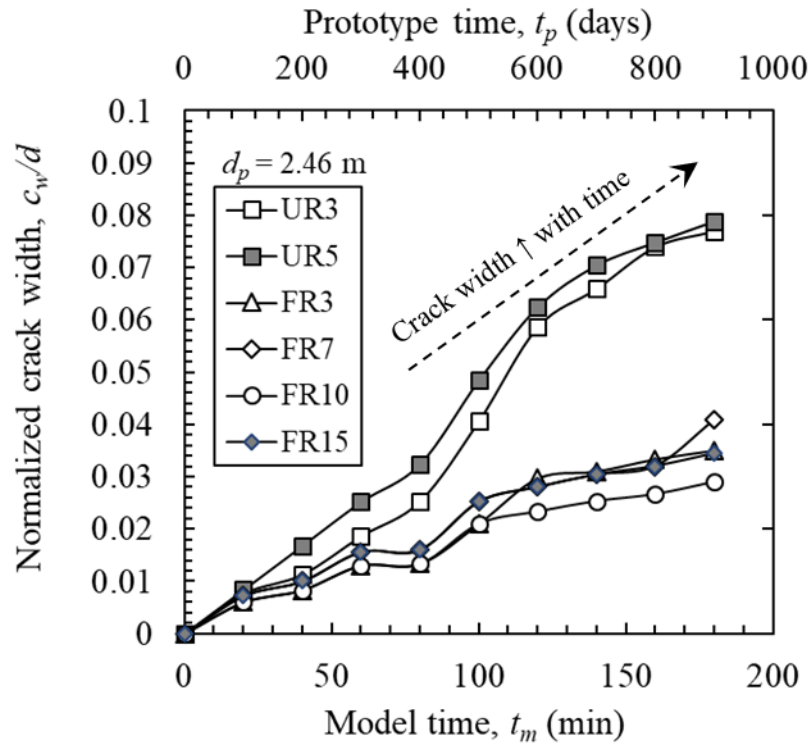
Figure 8. 58 Variation of normalized crack width, *cw/d* with time for unreinforced and fiber reinforced clay layers of layer of prototype thickness, *dp* = 2.46 m
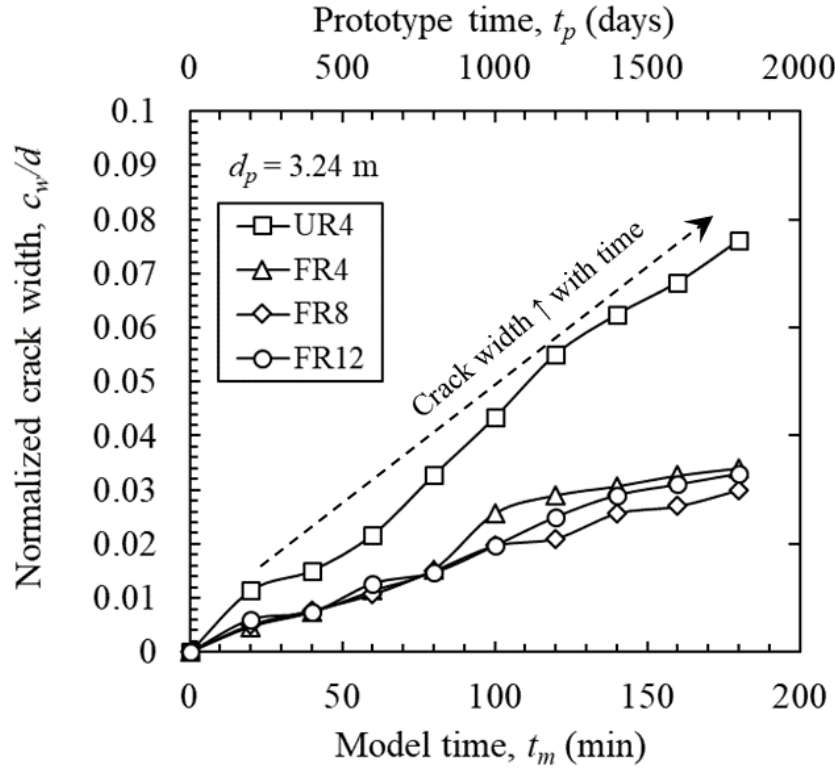
Figure 8. 59 Variation of normalized crack width, *cw/d* with time for unreinforced and fiber reinforced clay layers of layer of prototype thickness, *dp* = 3.24 m
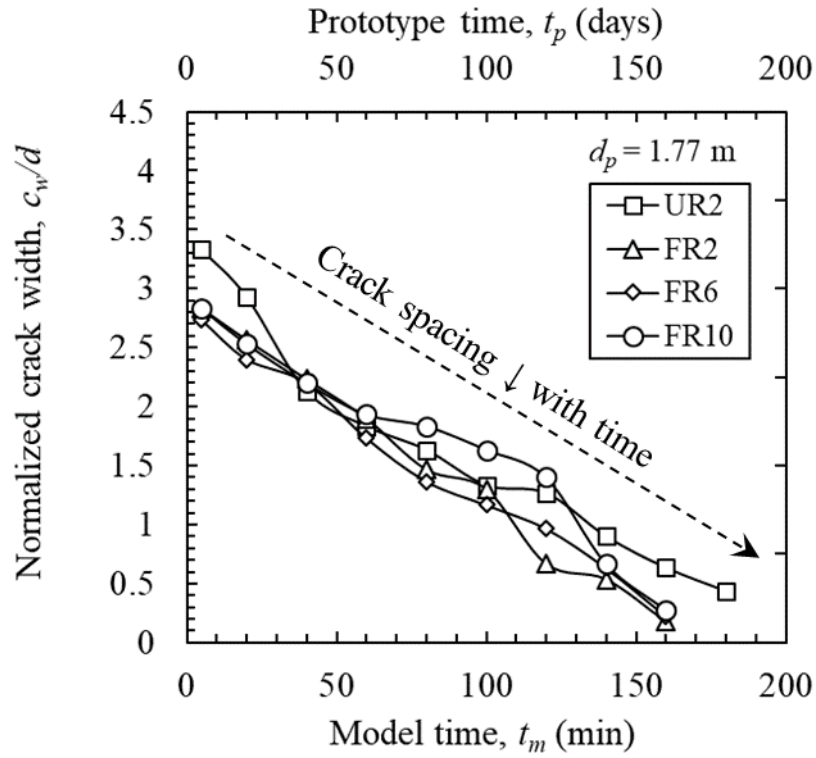
Figure 8. 60 Variation of normalized crack spacing , s_c/d with time for unreinforced and fiber reinforced clay layers of layer of prototype thickness, d_p = 1.77 m
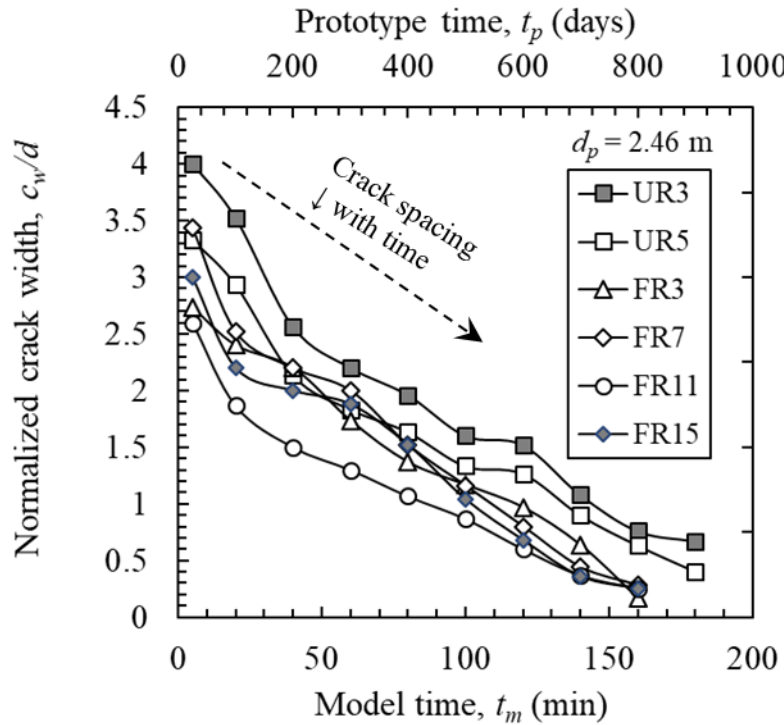
Figure 8. 61 Variation of normalized crack spacing, s_c/d with time for unreinforced and fiber reinforced clay layers of layer of prototype thickness, d_p = 2.46 m
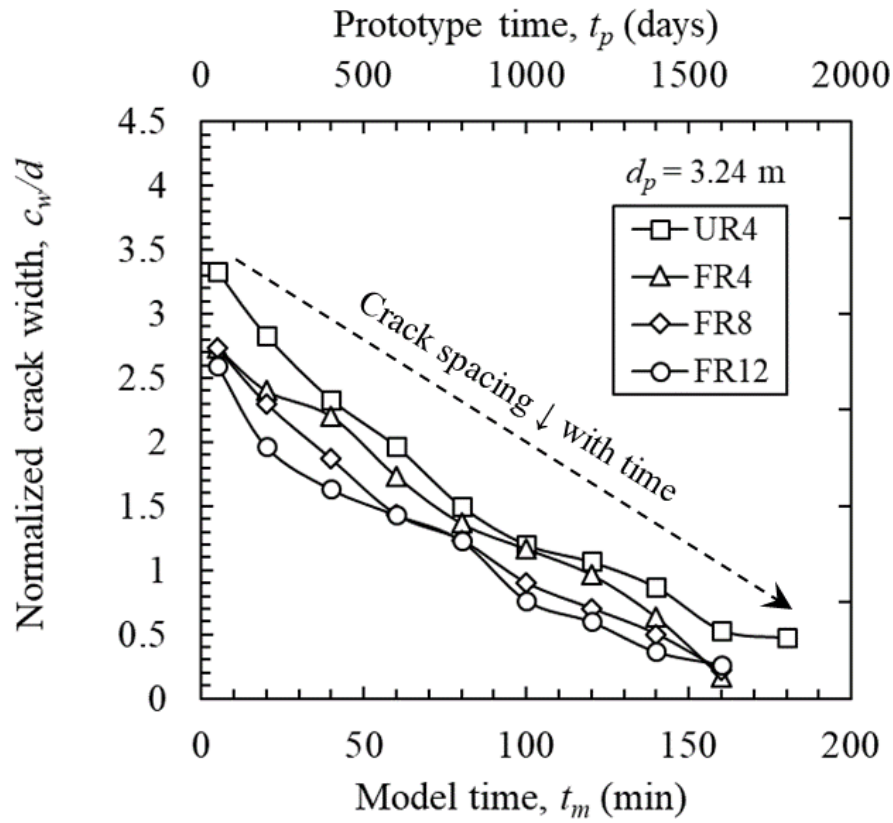
Figure 8. 62 Variation of normalized crack spacing, s_c/d with time for unreinforced and fiber reinforced clay layers of layer of prototype thickness, d_p = 3.24 m

Clay layers reinforced with fiber length l = 12 mm and 18 mm are found to be more effective in reinforcing the clay than fibers of length l = 30 mm. Hence, an optimum fiber length exists for a given fiber content. If the fiber is too long, it gets clogged and the reinforcement benefit is not fully developed. Obviously, for different soils the selection of the fiber length should be adapted and optimized to better interact with soils in the context of decreasing desiccation cracks.

8.5.4 Influence of fiber length [Series-B]

In order to study the influence of fiber length, l on the desiccation cracking behaviour of fiber-reinforced clay, fiber lengths were varied as 6 mm (Series-B1: Test FR2, FR3, FR4), 12 mm (Series-B2: Test FR6, FR7, FR8) and 30 mm (Series- B3: Test FR10, FR11, FR12). The fiber

289

length plays a significant role in the desiccation cracking behaviour of fiber reinforced clay, as discussed in sections 5.6.4, 6.5.3 and 7.5.3. The fiber length directly affects evaporation rate and suction profile of a clay layer undergoing desiccation. Figure 8.63 gives variation of moisture loss from unreinforced and fiber reinforced clay layer of prototype thickness, $d_p =$ 2.46 m. the fiber reinforced soil specimens exhibit higher moisture retention capacity due to the presence of fibers. Figure 8.63 gives the variation in moisture loss in the specimen with varying fiber lengths. For a given clay layer thickness, the moisture loss from the layer decreases with increase in the fiber length. This behaviour is also reflected in the consistency limits of fiber reinforced soil. The liquid limit is found to be increasing with an increase in fiber length and fiber content, owing to increased moisture retention in the soil-fiber interface and micro-pores generated due to entangled fibers. Figure 8.64 Depth of crack at the end of test for fiber reinforced soil specimens with prototype thickness of 1.77 m. Short and narrow cracks ran vertically through the specimen. Although the cracks were present throughout the depth, they were not continuous, ensuring better integrity in the clay layer. Figure 8.66 shows that the crack depth is found to be minimum with fiber length $l = 6$ mm and maximum with fiber length, $l =$ 30 mm.
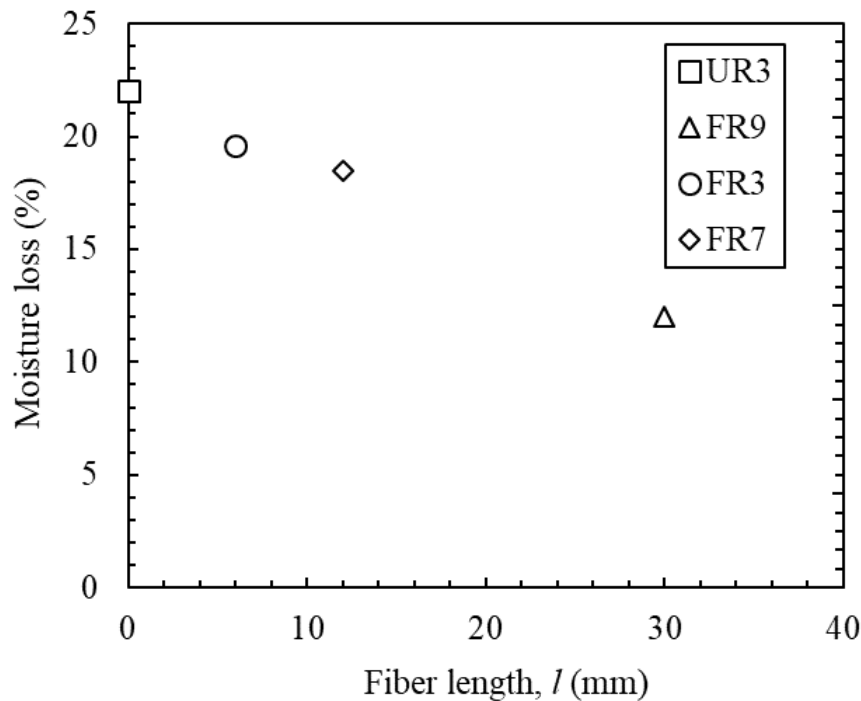
Figure 8.63 Average moisture loss in the specimen with varying fiber lengths
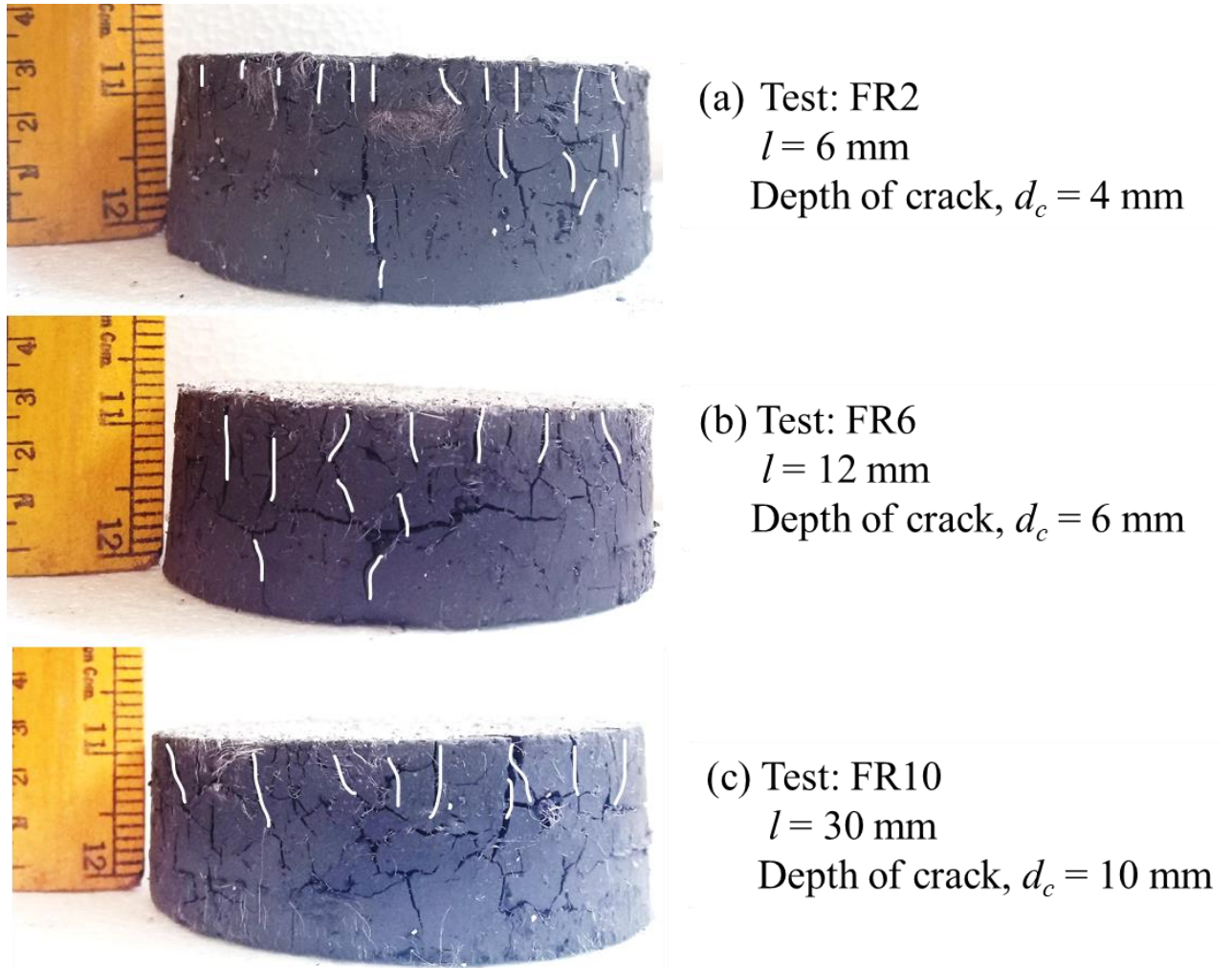
(a) Test: FR2
   $l = 6$ mm
   Depth of crack, $d_c = 4$ mm

(b) Test: FR6
   $l = 12$ mm
   Depth of crack, $d_c = 6$ mm

(c) Test: FR10
   $l = 30$ mm
   Depth of crack, $d_c = 10$ mm

Figure 8.64 Depth of crack at the end of test for fiber reinforced soil specimens with prototype thickness of 1.77 m [Test: FR2, FR6, FR10]

Figure 8. 65- Figure 8. 67 give the variation of normalized depth of crack for fiber reinforced clay specimens of 1.77 m, 2.46 and 3.24 m prototype thicknesses. Figure 8.68 gives the normalized crack spacing for fiber reinforced soil specimens reinforced with varying fiber lengths [Series-B]. The presence of fiber reinforcement inclusions reduces the crack spacing. However, it increases with increase in fiber length.
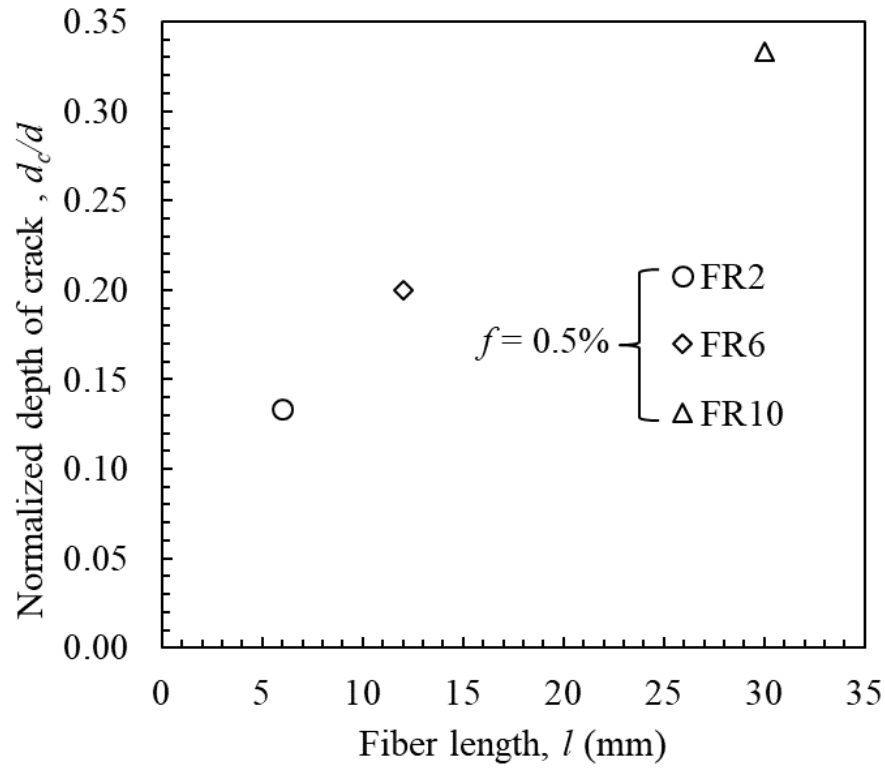
Figure 8. 65 Variation of normalized depth of crack for fiber reinforced clay specimens of 1.77 m prototype thickness
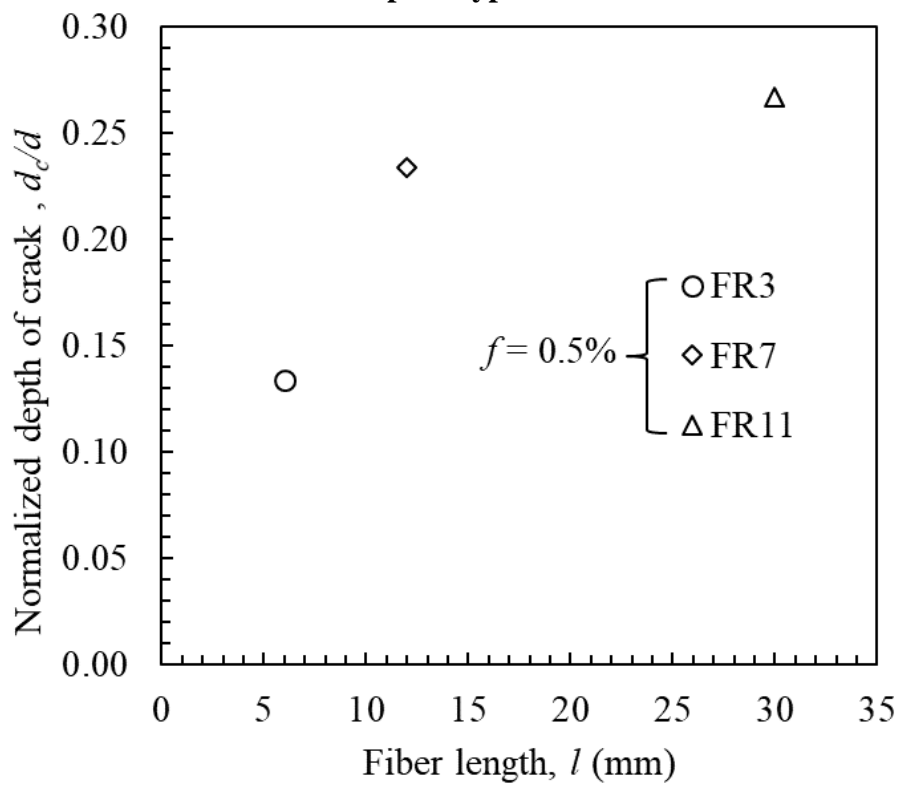
Figure 8.66 Variation of normalized depth of crack for fiber reinforced clay specimens of 2.46 m prototype thickness
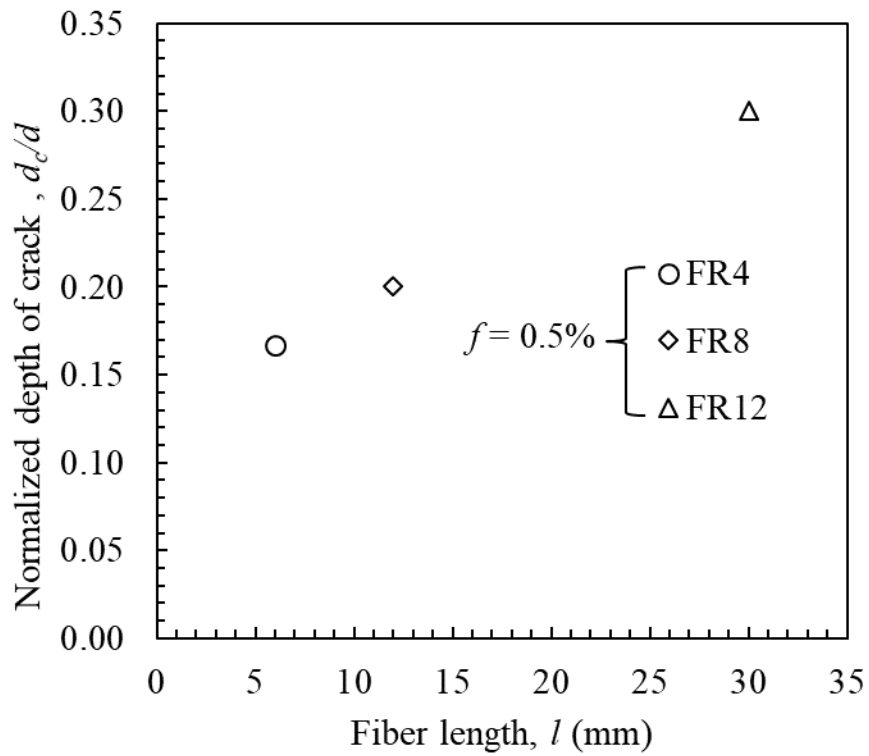
Figure 8. 67 Variation of normalized depth of crack for fiber reinforced clay specimens of 3.24 m prototype thickness
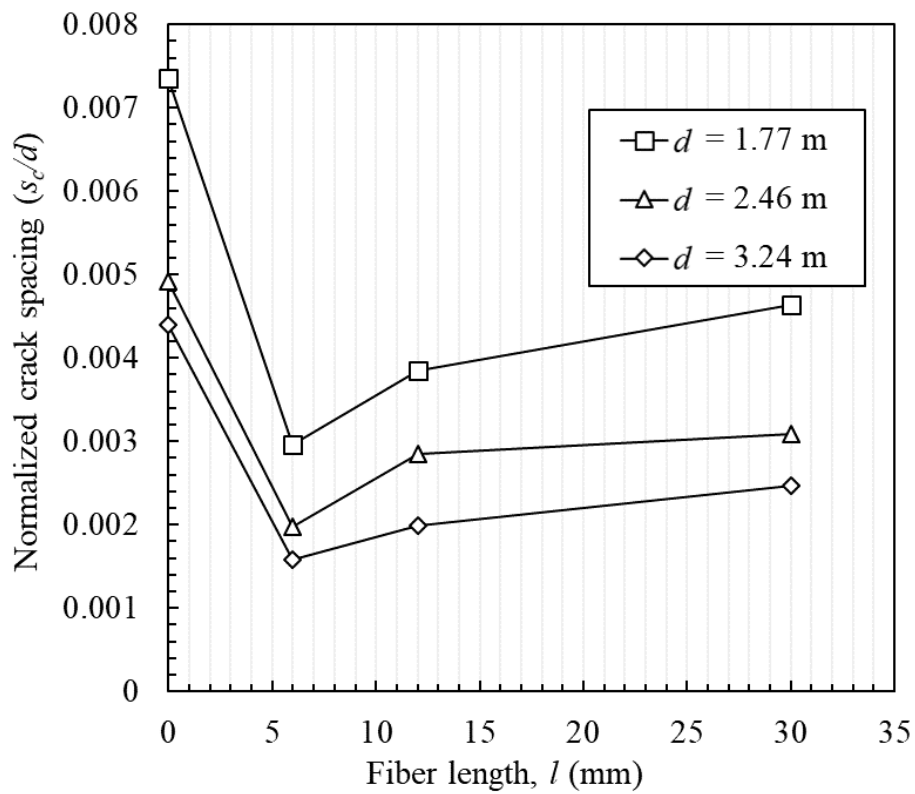
Figure 8.68 Normalized crack spacing for fiber reinforced soil specimens [Series-B]

Table 8.5 Summary of centrifuge test results on fiber-reinforced clay layer of fiber length l = 6 mm [Series – B1]

Parameters	Test legend			
	FR1	FR2	FR3	FR4
[a] **Thickness of specimen**	30 mm	30 mm [1.77 m]	30 mm [2.46 m]	30 mm [3.24 m]
Fiber type-length	PP-6 mm	PP-6 mm	PP-6 mm	PP-6 mm
*****Time of crack initiation, t_i**	75 min	6 min [15 days]	5 min [23 days]	4 min [32 days]
Cracking pattern	Narrow, shallow	Narrow, shallow	Narrow, shallow	Narrow, shallow
[#]**Normalized crack width, c_w/d**	0.033	0.035	0.034	0.076
[#]**Normalized crack spacing, s_c/d**	0.175	0.161	0.17	0.475
[#]**Normalized crack depth, d_c/d**	0.13	0.13	0.17	1
CIF (%)	10.2	14	17.6	17.6
CRR (%)	15.00	53.33	49.71	53.68
[c]**Average shrinkage strain, ε_{avg} (%)**	12.43	12.9	13.56	13.55

UR- Unreinforced; [a] prototype dimensions within the parenthesis; [b] not relevant/not used; *time in prototype dimensions in parenthesis; CIF- Crack intensity factor; CRR- Crack reduction ratio; c Computed manually in ImageJ; [#]Average value throughout the specimen

Table 8.6 Summary of centrifuge test results on fiber-reinforced clay layer of fiber length $l = 12$ mm [Series – B2]

Parameters	Test legend				
	FR5	FR6	FR7	FR8	FR15
[a] **Thickness of specimen**	30 mm	30 mm [1.77 m]	30 mm [2.46 m]	30 mm [3.24 m]	25 mm [2.46 m]
Fiber type-length	PP-12 mm	PP-12 mm	PP-12 mm	PP-12 mm	PP-12 mm
*****Time of crack initiation, t_i**	60 min	6 min [15 days]	6 min [28 days]	5 min [41 days]	5 min [34 days]
Cracking pattern	Narrow, shallow	Narrow, shallow	Narrow, shallow	Narrow, shallow	Narrow, shallow
[#]**Normalized crack width, c_w/d**	0.026	0.034	0.03	0.076	0.034
[#]**Normalized crack spacing, s_c/d**	0.227	0.233	0.215	0.475	0.25
[#]**Normalized crack depth, d_c/d**	0.2	0.23	0.2	1	0.24
CIF (%)	9.6	10.5	12.6	13.5	13
CRR (%)	20	65	64	64.47	63.89
[c]**Average shrinkage strain, ε_{avg} (%)**	13.43	12.45	13.22	12.78	13.65

UR- Unreinforced; [a] prototype dimensions within the parenthesis; [b] not relevant/not used; *time in prototype dimensions in parenthesis; CIF- Crack intensity factor; CRR- Crack reduction ratio; [c] Computed manually in ImageJ; [#]Average value throughout the specimen

Table 8. 7 Summary of centrifuge test results on fiber-reinforced clay layer of fiber length $l = 30$ mm [Series – B3]

Parameters	Test legend			
	FR9	**FR10**	**FR11**	**FR12**
[a] **Thickness of specimen**	30 mm	30 mm [1.77 m]	30 mm [2.46 m]	30 mm [3.24 m]
Fiber type-length	PP-30 mm	PP-30 mm	PP-30 mm	PP-30 mm
*Time of crack initiation, t_i	60 min	5 min [12 days]	4 min [19 days]	2 min [16 days]
Cracking pattern	Narrow, shallow	Medium, shallow	Medium, shallow	Medium, shallow
[#]**Normalized crack width, c_w/d**	0.024	0.038	0.029	0.033
[#]**Normalized crack spacing, s_c/d**	0.265	0.273	0.253	0.267
[#]**Normalized crack depth, d_c/d**	0.4	0.3	0.27	0.30
CIF (%)	9.4	10.8	13.6	14.2
CRR (%)	21.66	64	61.14	62.63
[c]**Average shrinkage strain, ε_{avg} (%)**	15.43	14.9	14.78	14.59

UR- Unreinforced; [a] prototype dimensions within the parenthesis; [b] not relevant/not used; *time in prototype dimensions in parenthesis; CIF- Crack intensity factor; CRR- Crack reduction ratio; [c] Computed manually in ImageJ; [#]Average value throughout the specimen

The typical crack spacing values for a field clay layer with depth of crack of 4 m is about 1m (Morris et al. 1992). The crack spacing is better understood as a dimensionless parameter of (s_c/d), where d is thickness of specimen. The ratio of average of all final spacing values to the corresponding depth of specimen at the end of the test is defined as (s_c/d). The effect of fiber content and fiber length on the crack spacing at 1g conditions have been discussed in section 5.5. The s_c/d reduces with addition of fibers. For a given soil and basal conditions, the crack spacing decreases with increase in the specimen depth. Similar observations can be made from the normalized crack spacing (s_c/d) versus fiber length, l plot in Figure 8.68.

The crack spacing decreases with increase in clay layer thickness. However, for a given layer thickness, the crack spacing increases with the increase in fiber length. This increase in crack spacing is due to non-uniform mixing and distribution of longer fibers in the clay matrix. Though, it is worth noting that the crack spacing in fiber reinforced specimens never exceeds the crack spacing of unreinforced soil specimen for a given clay layer thickness.

8.5.5 Influence of fiber type [Series-C]

To study the influence of fiber type on the desiccation cracking behaviour of fiber reinforced clay, a short series of tests was conducted and grouped as series-C. the type of geofibers were varied as PP, PET and PP-T fibers. The clay was reinforced with PP (Test: FR7), PET (Test: FR13) and PP-T (Test: FR14) fibers while keeping other parameters like fiber length ($l = 12$ mm), fiber content ($f = 0.5\%$) and clay layer thickness ($d_p = 2.46$ m) constant in all the tests. The specimen preparation procedure was followed as discussed in section 8.3.

The variation of crack intensity factor (CIF) for fiber reinforced clay layers of prototype thickness of 2.46 m with different types of fibers is shown in Figure 8.69. The reinforcing fibers help in restraining the desiccation cracking by proving a bond between the cracked soil mass and that is proportional to area of reinforcement. It is observed that the finer fibers perform better in restraining desiccation cracking, by proving uniform distribution over larger area under reinforcement. The CIF of specimens reinforced with PP and PET fibers was similar (~12.5%), as the cross-sectional area of these fibers was similar (~ 40µm).

Table 8. 8 Summary of centrifuge test results on fiber-reinforced clay layer of varying fiber type [Series – C]

Parameters	Test legend		
	FR7	**FR13**	**FR14**
[a] **Thickness of specimen**	30 mm [2.46 m]	30 mm [2.46 m]	30 mm [2.46 m]
Fiber type-length	PP-12 mm	PET-12 mm	PP-T-12 mm
*****Time of crack initiation, t_i**	6 min [28 days]	3 min [14 days]	4 min [19 days]
Cracking pattern	Narrow, shallow	Medium, shallow	Medium, shallow
Normalized crack width, c_w/d	0.03	0.021	0.049
Normalized crack spacing, s_c/d	0.215	0.227	0.225
Normalized crack depth, d_c/d	0.2	0.27	0.23
CIF (%)	12.6	12.2	20.2
CRR (%)	64	65.14	42.29
#Average shrinkage strain, ε_{avg} (%)	13.22	15.1	18.82

UR- Unreinforced; [a] prototype dimensions within the parenthesis; [b] not relevant/not used; *time in prototype dimensions in parenthesis; CIF-Crack intensity factor; CRR- Crack reduction ratio; # Computed manually in ImageJ
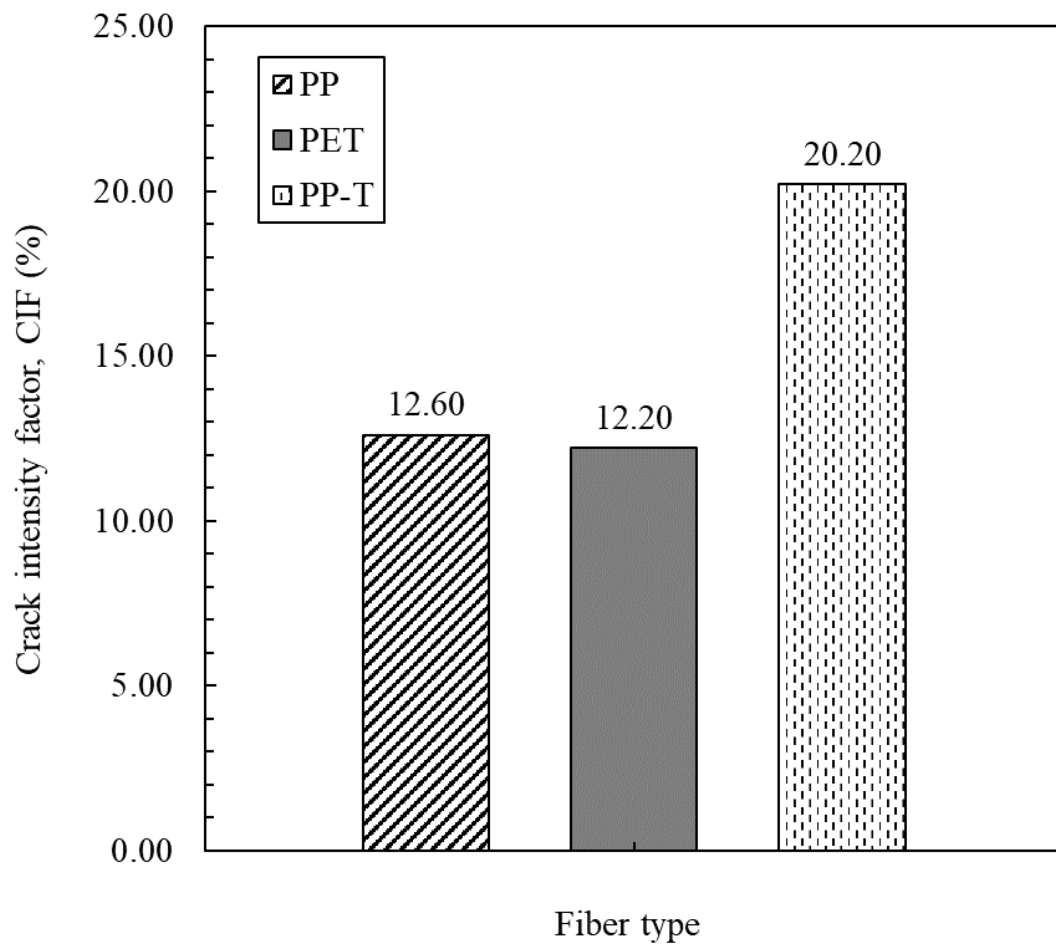
Figure 8.69 Crack intensity factor for clay layers reinforced with different fiber type
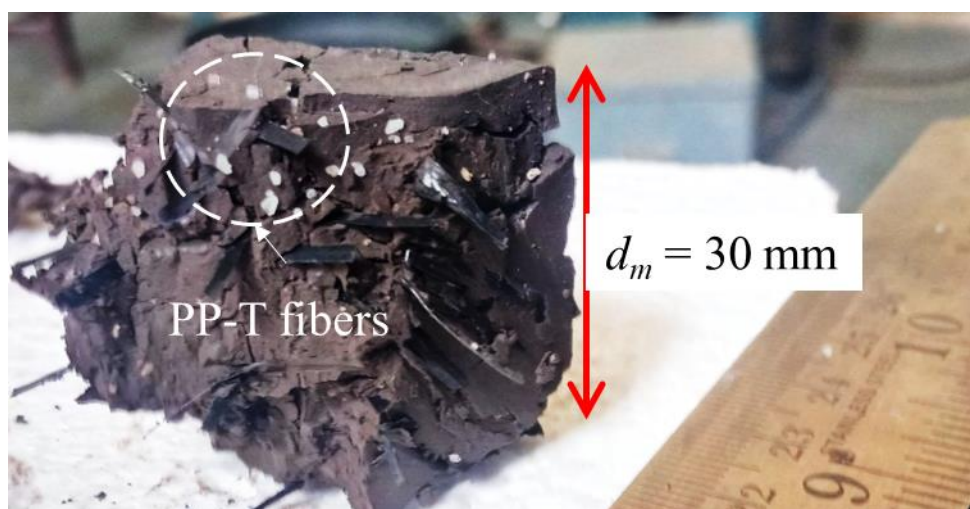
Figure 8.70 Cross section of cracked specimen reinforced with PP-T fibers [Test: FR14]

The specimens reinforced with PP-T fibers (thickness = 2 mm) exhibited higher crack intensity of 20.2%. As the fibers are relatively thicker than the PP and PET fibers, PP-T fibers have lower volume distribution of fibers in a given cross section area, owing to poor reinforcement and higher crack intensity (Figure 8.70).

The normalized crack width (c_w/d) and the crack patterns at the end of the test for series-C are shown in Figure 8.71. As discussed above, the specimens reinforced with PP (Test: FR7) and PET (Test: FR13) exhibited narrow and fiber cracking, with model crack widths, c_w of 1.02 mm and 0.64 mm respectively. The crack patterns in specimens reinforced with PP-T (Test: FR14) were similar to that of unreinforced specimens, with model crack widths, c_w of 1.46 mm.
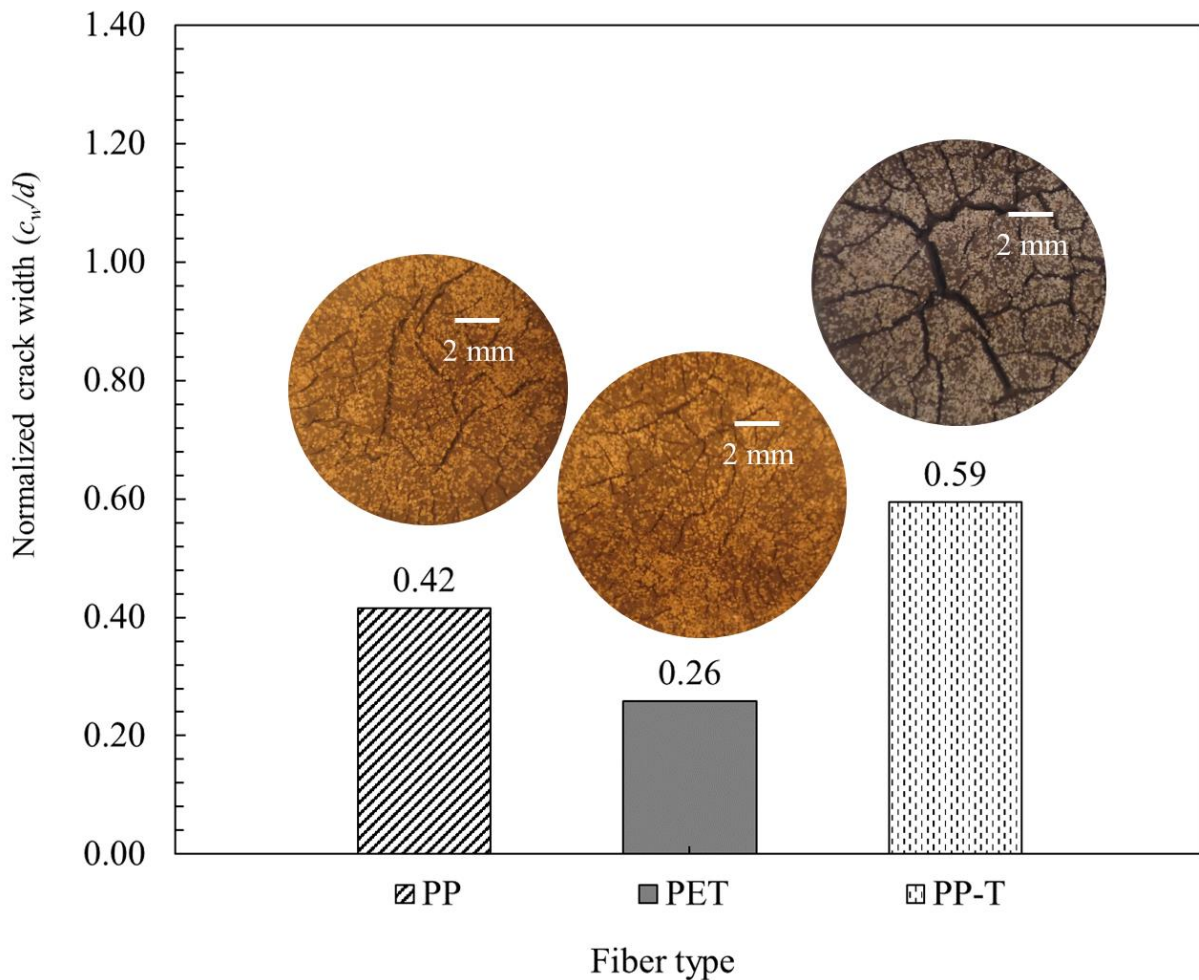
Figure 8.71 Variation of normalized crack width (c_w/d) for fiber reinforced soil specimens reinforced with varying fiber type [Series-C]

From this series of test, PP fibers were found to be most effective in restraining desiccation cracking, due to better distribution in clay matrix. Also, PP being lighter in weight than PET

fibers (Specific gravity, G_s of PP = 0.91, Specific gravity, G_s of PET = 1.35), more volume of fibers are found in a given mass of fibers, leading to better reinforcement of clay matrix. Further, it can also be attributed to the triangular cross-section of the PP and PET fibers (Section 4.3) which facilitated improved interlocking between the soil particles compared to the PP-T fibers with a flat surface and rectangular cross-section. This was found in good agreement with the observations and measurements in the desiccation cracking tests.

8.6   Closure

In total, twenty tests were carried out to understand desiccation cracking behavior of soil. Four (4) 1g tests, were conducted for all the unreinforced and fiber reinforced soil combinations to check the working of the test setup. This chapter deals with the details of centrifuge model test setup for inducing desiccation cracking in a clay layer. It presents the centrifuge model test package, model preparation and testing procedure. In total 16 centrifuge tests were conducted in the present study to examine the performance of unreinforced and fiber reinforced clay layers when subjected to desiccation cracking. The influence of fiber reinforcement, influence of specimen thickness, influence of fiber-length and influence of fiber type was studied in the tests. The clay barriers with no fiber reinforcement were found to exhibit the highest amount of cracking upon desiccation. The unreinforced soil specimens were found to experience full wide and full depth cracking and found to lose the integrity. The crack intensity and crack widths were found to increase for increase in the thickness of clay layer. The performance of clay layers reinforced with fibers was found to be superior to corresponding unreinforced clay layers of same thickness. The fiber reinforced clay layers maintained relatively low intensity of cracks and narrow crack widths. The depths of crack were also observed to restraint only till middle of the specimen for most of the fiber reinforced soil specimens. This indicates the influence of fibers in maintain the integrity if the clay layer during cracking. The influence of fiber length was studied and fiber reinforced soil specimens reinforced with shorter fiber lengths were found to be more efficient in restraining desiccation cracking due to better mixing and uniform distribution throughout the specimen. The polypropylene fibers were found to be best in retraining desiccation cracking when compared to polyester fibers and polypropylene tape fibers.

Chapter 9

SUMMARY AND CONCLUSIONS

9.1 Summary

The engineering properties of expansive clay may be improved or modified by suitable additives, for usage as a sustainable material in construction. Clay-rich soils having low hydraulic conductivity are used in waste containment systems like landfill liners and covers. Since expansive clays have a high clay content and low hydraulic conductivity (in the order of 1×10^{-9} m/s,) they can potentially be used as an impervious barrier material in landfill lining systems. However, due to their shrink-swell nature, they have a tendency of severe desiccation cracking leading to distress in impervious barriers of landfill lining systems. Desiccation cracking alters the long-term sealing effect of impervious barrier layers in landfill lining systems to generate leachate, which may eventually contaminate the soil and groundwater. The hydraulic conductivity of the clay layer increases as much as by an order of three due to

cracking, because the cracks act as drainage paths for water infiltration. Various methods such as moisture barriers and chemical stabilization have been attempted in the past to mitigate desiccation cracking of clay barriers. Other methods of reducing desiccation cracking involve the usage of surface moisture barriers, compaction control, surcharge loading and thermal methods.

Original use of the fiber reinforcement involved the natural use of plant roots or the use of available fibers such as sisal, straw, coconut fiber, coir and the like in order to increase the shear strength and stability of slopes. The most common type of synthetic fibers are polypropylene, polyester, polyethylene, glass, steel and polyvinyl alcohol fibers. Fiber reinforcement technique has recently attracted increasing attention in several geotechnical applications. The main advantage of discrete reinforcement of soil with fibers over conventional geosynthetic sheet reinforcement is the absence of a single potential plane of failure. However, the systematic knowledge pertaining to the use of fiber reinforcement technique, emphasizing the influence of fiber type, fiber content and fiber length on the desiccation cracking and tensile strength-strain characteristics of the soil; and to restrain desiccation cracking is limited. Hence, in the present study an attempt was made to evaluate the influence of fiber reinforcement on the desiccation cracking behaviour and tensile strength-strain characteristics of the unreinforced and fiber reinforced expansive clay through laboratory and centrifuge tests.

The natural expansive clay called black cotton soil was used in the study. The soil was selected such that it exhibits considerable expansive and shrinkage nature when subjected to moisture variations. The soil was characterised for its physical, chemical, mineralogical properties and classified as CH type of clay according to USCS. Synthetic model geofibers were selected as polypropylene (PP), polyester (PET) and polypropylene tape (PP-T) fibers. The geofibers were characterised for their physical, mechanical and chemical properties. The properties of expansive clay -fiber blends were evaluated by conducting in total nineteen (19) consistency limit tests liquid limit, plastic limit, shrinkage limit and ten (10) consolidation tests. Permeability of clay-fiber blend was deduced from the consolidation tests. The influence of PP fiber length on the permeability of expansive clay was studied by varying the fiber lengths as 6 mm, 12 mm and 30 mm.

In total ten (10) desiccation cracking tests were performed in the laboratory test setup prepared for subjecting desiccation cracking on specimens. The fiber reinforced clay samples were subjected to desiccation cracking at constant temperature and relative humidity. The specimens

were constantly heated with the help of halogen lamps placed at constant height over the specimens. The change in moisture and propagation of cracks was continuously monitored with the help of weighing balance and digital camera, respectively. In order to study the influence of fiber reinforcement of desiccation cracking behaviour of expansive clay, the fiber length was varied as 0.25%, 0.5% and 0.75% and the fiber length was varied as 15 mm,30 mm and 50 mm. Specimens were prepared by mixing dry soil with required amount of PET fibers and adding water close to liquid limit to the soil-fiber mix. Digital image analysis was used to evaluate the results and it was found that the fiber reinforcement significantly altered the desiccation cracking of expansive clay. The crack intensity reduced with increase in fiber content, however reduced for very high fiber contents and reduced with increase in fiber length. From the present study, an optimum fiber content of 0.5% and fiber length of 15 mm was concluded.

As the soil at field conditions in subjected to seasonal moisture variations, the effect of cyclic drying-wetting of fiber reinforced soil was studied. This was done by subjecting the desiccated specimen to wetting, and then drying the wet specimen again. This process of drying and wetting was repeated on PP fiber reinforced specimens and compared to that of unreinforced specimens. In total, twelve (12) tests were performed to study the effect of cyclic drying wetting on the desiccation cracking behaviour. The effect of specimen thickness was also studied by varying the specimen thickness as 5 mm,10 mm and 15 mm. The fiber length was varied as 6 mm,12 mm and 18 mm, whereby keeping the fiber content constant. The results were recorded by digital image acquisition system and evaluated to assess the efficiency of fibers in healing of cracks in expansive clay. The severity of cracking was found to increase with increase in number of drying-wetting cycles, however, it found to get stabilize after 3 cycles. The fiber reinforced soil specimens showed better sealing of cracks during the wetting cycle when compared to unreinforced specimens.

Tension cracking is very common and important phenomenon in the case of clay layers. In this study, sixteen (16) direct tensile tests were conducted to examine the influence of discrete and randomly distributed fibers in improving the tensile strength-strain characteristics of the clay layers with an objective to evaluate the influence of water content, fiber content and fiber length. The PP fiber lengths were varied as 12 mm, 30 mm and 50 mm, fiber content as 0.25%, 0.35%,0.5%,0.65%, and 0.75% and water content as 45%,40%, 35% and 30%. It was observed that as the fiber content is increased keeping fiber length as constant and also as fiber length is

increased keeping fiber content as constant, there is an increase in peak tensile strength. The longer fibers are found to have significant influence in increasing peak tensile strength.

Reinforcement of soil with discrete randomly distributed fibers helps in reducing the extent of desiccation cracking. Understanding of desiccation cracking of unreinforced and polypropylene fiber-reinforced soil was attempted in this study using distributed optical fiber sensing (DOFS) at Monash University, Australia. Single optical fiber was laid through linear shrinkage mould containing the unreinforced and fiber reinforced soil specimen. the change in the strain in soil was recorded through the optical fibers. The study reveals that the compressive strains due to shrinkage of soil develop as the drying progresses, and as the crack appears the specimen experiences tensile strains at the crack. Fiber length plays a crucial role in its performance. Particle image velocimetry was used to deduce interesting information on the movement of soil particles during shrinkage.

For better understanding of desiccation cracking behaviour of fiber reinforced expansive clay, robust physical modelling is needed. Therefore, desiccation cracking of expansive clay was modelled in a 0.5m radius small centrifuge facility at IIT Bombay, India. Considering the practical difficulties and time delay in performing full-scale model tests and also the limitations of reduced scale model tests for simulating stress dependant phenomenon, centrifuge model tests were used to study the desiccation cracking behaviour of clay layers with varying thicknesses by varying the gravity levels as 59, 82 and 108 gravities. The scale factors and modelling considerations for desiccation cracking were established. An in-flight desiccation cracking system including heating system, lighting assembly, image acquisition system and specimen container was designed and fabricated. In the present study, twenty (20) centrifuge tests were performed on unreinforced and fiber reinforced clay specimens. The influence of specimen thickness, influence of fiber reinforcement, influence of fiber length and influence of fiber type was studied. The tests were groups as series A, series B and series C. The series A was mainly aimed to evaluate the effect of desiccation cracking of unreinforced clay layers and to study the performance of designed system by modelling of models technique. Series B was aimed at studying the influence of fiber length. This was done by varying the PP fiber length as 6 mm,12 mm and 30 mm. The influence of fiber type was evaluated in series C by varying fiber type as P, PET and PP-T fiber, keeping the fiber length and specimen thickness constant. The results were analysed and evaluated using digital image analysis and particle image velocimetry technique.

9.2 Conclusions

Based on the analysis and interpretation of laboratory desiccation tests, cyclic drying-wetting of fiber reinforced clay, direct tensile strength tests, desiccation tests with DOFS system and centrifuge tests, the following major conclusions can be drawn:

9.2.1 Based on desiccation cracking tests of unreinforced and fiber-reinforced expansive clay

A series of desiccation tests were performed on expansive clay with and without polyester fibers. The following conclusions can be made from the present study that investigated the desiccation cracking behaviour of polyester fiber inclusions in expansive soil:

- A significant change in the cracking pattern of expansive clay is observed due to the presence of fibers. While wide crack widths and long cracks are formed in unreinforced soil, the addition of fibers controlled the crack width opening, the cracked area, and the propagation of cracks through the bridging action of fibers. The fibers decreased the connectivity of crack networks.

- The crack intensity and shrinkage strain for fiber-reinforced soil were found to be substantially less than those of unreinforced soil. However, fiber length and fiber content plays an important role in reinforcement. The effect of fibers at longer lengths of fibers at higher fiber contents was found to be insignificant. The distribution of fibers throughout the clay mass was found to be uniform in soil specimen that were reinforced with fibers of length 15 mm and 30 mm.

- The image processing technique was found to be effective in quantifying the crack feature measurements and providing useful information. Undoubtedly, fiber inclusion helps in crack reduction due to the increased tensile strength of the clay mass. In this study, 66% crack reduction was achieved from the range of fiber lengths and fiber contents used. Crack features such as crack width, crack spacing, and cell area became narrower with the addition of fibers.

- Maximum crack reduction of fiber reinforced clay was found to be for fiber length 15 mm at 0.5% fiber content. More comprehensive study on the use of a mixture of short and long fiber lengths is needed in order to address barriers that are subjected to different ranges of tensile stresses and strains.

- The SEM images reveal that the fibers hold a separated soil mass at a micro level. The interaction between the fibers and the soil is entirely due to adhesion. The clay particles adhere to the irregular trilobal cross section of the polyester fiber, which provides better interfacial strength. This shows that fiber reinforcement can be considered as an efficient method to restrain desiccation cracking of clay barriers that are used in waste containment systems.

- This study was undertaken by preparing the soil and fibers at dry state and then mixing them to almost slurry state. This process is strictly applicable to certain field scenarios such as slurry walls, mine tailings etc. So further work is necessary to study soils that are compacted close to compaction optimum water contents as applicable to field compacted clay liners.

- Through tensile tests performed on unreinforced soil reached a peak tensile stress and then rapidly decreased as the specimen cracked and further movement of the mould take place which shows a brittle behaviour. But the soil specimens containing fibers reached higher peak tensile stress and then gradually lost strength as the fibers were pulled out of the soil with an increase in strain, showing a ductile nature.

9.2.2 Based on cyclic drying-wetting of unreinforced and fiber-reinforced expansive clay

Desiccation and cracking behaviour of clay layers reinforced with and without fibers from a slurry state upon three drying-wetting (DW) cycles were investigated through laboratory experiments. The process of water evaporation, surface cracks evolution, structure evolution, volume shrinkage and surface temperature behaviour were monitored. The geometric characteristics of crack pattern after each cycle were quantitatively analysed by image processing. The following conclusions can be drawn:

- The results from the first drying were dominated by smooth crack networks in case of unreinforced soil sample and reinforced soil samples. The unreinforced soil samples exhibit complete separation at the cracks.

- During the inundation of clay layer with water, the poured water resulted in rapid healing of the desiccation cracks formed in the previous drying. A typical aggregated structure was developed and significantly intensified the specimen heterogeneity; moreover, the second wetting path led to significant rearrangement of clay particles and modification of the pore network; these processes are generally irreversible and drastically influence the desiccation cracking behaviour during the subsequent drying path. In case of small fiber lengths of 6 mm, the fibers were found to get separated from the clay mass and float on the top.

- After the second drying cycle, since the specimen homogeneity decreased, the cracks were more irregular and jagged than that observed after the first drying cycle. The average crack width reduced by 33.3% from first to second cycle in case of unreinforced specimens of thickness 15 mm. The bonds between the formed aggregates were broken quickly in the third wetting path and no new micro-cracks were induced.

- The unreinforced soil specimen lost its complete integrity at the end of three cycles with a CIF of 42%. Whereas, the fiber reinforced soil specimens were still intact as a layer with a CIF of 15–20%, substantiating the influence of increase in tensile strength due to presence of fibers.

- SEM images reveal the porous structure formed due to the cyclic drying and wetting of the soil. The severity in cracking increases with increase in drying-wetting cycles and was observed to reach to a stable structure after 3 cycles. Fibers hold on to the soil even at the end of five cycles. This shows that fiber reinforcement can be considered as an efficient method to restrain desiccation cracking of clay layers that are used in waste containment systems.

9.2.3 Based on investigation of desiccation cracking of expansive clay using distributed fiber optic sensing (DOFS)

Desiccation cracking is a persistent issue in infrastructure associated with fine grained soils. Reinforcement of soil with discrete randomly distributed fibers helps in reducing the extent of desiccation cracking. Understanding of desiccation cracking of unreinforced and polypropylene fiber-reinforced soil was attempted in this study using distributed optical fiber sensing (DOFS).

The study reveals that the reinforcing fibers certainly help in restraining desiccation cracking of soil. However, fiber length plays a crucial role in its performance. Based on the desiccation cracking tests, the strain from DOFS, and the displacement vectors from PIV, the following conclusions can be drawn:

- The compressive strain that is developed in unreinforced soil specimen increases with loss of moisture, and the soil specimen experiences a progressive reduction in compressive strain with formation and progression of cracking. It is interesting to note that during the cracking entire soil specimen is experiencing compressive strains. However, the cracking appears to happen since tensile stresses develop within soil due to mobilized compressive strain is less than the free shrinkage strain due to partial restraints.

- The compressive strain profile that develops in the fiber-reinforced soil specimen is less undulated than that in the unreinforced soil specimen due to the formation of micro-cracks. In fiber reinforced specimens, the tensile stresses developed due to partial restrains are released across the major part of the specimen in the form of microcracks. Therefore, the compressive strain profiles of fiber-reinforced soil specimens show small spikes and dips due to unlike unreinforced specimens.

- The displacement vectors after PIV analysis show that the crack widens in unreinforced soil specimens after the initiation of the crack, whereas in fiber-reinforced soil specimens, the widening of the crack is restrained and controlled. The displacement vectors after crack formation in fiber reinforced specimens indicate that the fibers do not allow the microcracks to widen, thereby maintaining the integrity of soil specimen.

- Fibers of length, $l = 6$ mm, were found to be too short to restrain desiccation cracking and were pulled out across the width of the crack. Soil specimens that were reinforced

with a fiber length $l = 18$ mm were found to possess the highest compressive strain (~4200 $\mu\varepsilon$) before cracking and demonstrated delay in cracking.

9.2.4 Based on centrifuge test results on desiccation cracking of unreinforced and fiber reinforced clay

In the present study the response of fiber reinforcement on desiccation cracking of clay was studied using centrifuge modelling technique. An attempt has been made to ascertain the influence of fiber reinforcement, thickness of the clay barrier, and fiber length and fiber type in the performance of clay reinforced with distributed fibers. Based on the desiccation cracking tests inside centrifuge, the strain and displacement vectors from PIV, the following conclusions can be drawn:

- Scale factors and modelling considerations for centrifuge modelling of the phenomenon of desiccation cracking of unreinforced and fiber-reinforced clay layers were verified and the use of centrifuge modelling technique for studying desiccation behaviour of clay is demonstrated adequately. The linear dimensions of the crack feature measurements (width, spacing and depth) are to be reduced by 1/N times that of corresponding prototype values. The deduced scaling considerations imply that fiber dimensions need to be identical in a centrifuge model and prototype and can be treated as discrete inclusions, analogues to other admixtures such as lime and cement.

- By adopting the modelling of models technique, it was established that the time of crack initiation for a model clay layer at high gravities was found to be $1/N^2$ times the time of crack initiation at the field.

- In all the centrifuge tests performed, unreinforced clay layers invariably experienced wide and full depth cracking and found to lose integrity when subjected desiccation cracking, indicating the need for evolving at strengthening measures. Fiber reinforcement reduced the intensity of cracking considerably. The fiber length was varied as, $l = 6$ mm, 12 mm and 30 mm. Effect of fiber length play a crucial role and the fiber length of 12 mm was found to be the best in prevention of desiccation cracking

of clay. For the same prototype thickness, d_p of 2.46 m, unreinforced clay layer demonstrated normalized crack width 54%-62% greater than that of reinforced clay layers. Whereas, the normalized depth of crack reduced by 77%-83% in fiber reinforced clay layers than that of unreinforced clay layers.

- The specimen thickness significantly influences the crack feature measurement of clay layers. The normalized crack width, c_w/d for unreinforced clay layers of prototype thickness, d_p 1.77 m, 2.46 m and 3.24 m was 0.057, 0.076 and 0.077, representing the corresponding CIF values of 30%, 35% and 38% respectively. An increase in clay layer thickness, d_p from 1.77 m to 2.46 m, delays the time of crack initiation for specimens reinforced with fibers of length, l = 6 mm, 12 mm and 30 mm by 53%, 85% and 58%, respectively.

- The magnitude of average shrinkage strain, ε_{avg} values at the end of the test corresponding to unreinforced clay layers of d_p = 1.77 m, 2.46 m and 3.24 m were in the range of 18% - 19% and always found to be higher than that of the respective fiber reinforced clay layers, i.e. 13% - 14% for l = 6 mm, 12% - 13% for l = 12 mm and 14% - 16% for l = 30 mm.

- The CIF and CRR values for PP, PET and PP-T fiber reinforced clay layers of thickness, d_p = 2.46 m were found to be 12.6% and 64%, 12.2% and 65.14% and 20.2% and 42.29%, respectively. The PP fibers were found to be superior in restraining desiccation cracking in the present study. Although, the PET fibers performed almost like that of the polypropylene fibers. The PP-T fibers were found to be inefficient in arresting the desiccation cracks due to their rectangular cross section and larger thickness.

Based on the laboratory desiccation cracking test analysis and interpretation of tensile tests, and centrifuge tests on unreinforced and fiber reinforced clay layers, it can be concluded that a fiber content of 0.50% and fiber length 12 mm can be considered as optimum combination for restraining desiccation cracking. In geotechnical application where low permeability is the only concern, the suggested optimum combination of fiber content and short fibers can be used. However, in geotechnical applications where tensile strength is a concern, longer lengths of fibers i.e. l = 50 mm at a fiber content of 0.5% might be considered.

9.3 Major research contributions

Following are major contributions from the present study:

- The study demonstrates the use of different types of geofibers in restraining desiccation cracking of expansive clay

- The desiccation cracking behaviour of unreinforced and fiber reinforced expansive clay was performed by setting up a laboratory scale experimental setup to induce desiccation cracking in soil specimens at relatively constant environmental conditions.

- The effect of cyclic drying and wetting on the desiccation cracking behaviour was studied in the laboratory setup. The healing property of fiber reinforced expansive clay are addressed. Use of SEM for understanding of pore distribution in specimens subjected to various drying and wetting cycles is also attempted.

- An optimum combination of fiber content and fiber length of geofibers is suggested based on the laboratory desiccation cracking tests. The tensile strength improvement of the expansive clay due to presence of geofiber inclusions in explored by performing direct tensile strength tests on unreinforced and fiber reinforced soil specimens.

- The study demonstrates the use of distributed optical fiber system in assessing the strains in soil specimens undergoing shrinkage and desiccation cracking.

9.4 Limitations

- Understanding of desiccation cracking of expansive clay using distributed optical fiber sensing was performed on small linear shrinkage specimens. It may be interesting to evaluate the strains in the large clay specimens.

- At field, Adequate care needs to be taken while mixing the fibers with soil to ensure uniform distribution. Although uniform distribution is possible for smaller fiber length, uniform distribution of longer fiber lengths is difficult to maintain.

9.5   Scope for future work

- The influence of synthetic fibers like polypropylene and polyester desiccation cracking of expansive clay was studied using laboratory and centrifuge model tests. However, the effect of natural fibers on the desiccation cracking was not performed in this study.
- The influence of geofiber type was studied by conducting permeability tests and centrifuge model tests. But the influence of fiber type in improving the tensile strength of the soil was not studied through direct tensile tests extensively.
- The moisture content, suction and temperature inside soil body were not studied during the desiccation cracking centrifuge tests on clay layers subjected to desiccation cracking.
- It will be interesting to study the desiccation cracking characteristics of the expansive clay when they are doped with appropriate chemicals such as Nanomaterials, minerals, and surfactants) along with geofibers under different environmental conditions.

REFERENCES

Abduljauwad, S. N. (1993). "Treatment of Calcareous Expansive Clays." *ASCE, Geotechnical Special Publication No. 36*, K. D. Sharp, ed., Dallas, Texas, United States, 100–115.

Abedine, A. Z. El, and Robinson, G. H. (1971). "A study on cracking in some vertisols of the Sudan." *Geoderma*, 5(1), 229–241.

Abràmoff, M. D., Magalhães, P. J., and Ram, S. J. (2014). "Image Processing with ImageJ." *Biophotonics International*, 11(7), 36–42.

Abu-Hejleh, A., N., and Znidarcic, D. (1995). "Desiccation theory for soft cohesive soils." *Journal of Geotechnical Engineering, ASCE*, 121(6), 493–502.

Al-Rawas, G. (2006). "Classification of expansive soils A case study from the Arabian Gulf." *Expansive Soils: Recent Advances in Characterization and Treatment*, A. A. Al-Rawas and M. F. A. Goosen, eds., Taylor & Francis Group, London, UK, 2–9.

Albrecht, B. A., and Benson, C. H. (2001). "Effect of desiccation on the compacted natural clays." *Journal of Geotechnical and Geoenvironmental Engineering*, 127(1), 67–75.

Allan, M. L., and Kukacka, L. E. (1995). "Strangth and durability of polypropylene fiber reinforced grout." *Cement and Concrete Research*, 25(3), 511–521.

Allen, J. R. L. (1982). *Sedimentary structures : their character and physical basis. Volume 1.* Elsevier Scientific.

Alonso, E. E., Romero, E., Hoffmann, C., and Garcia-Escudero, E. (2005). "Expansive bentonite-sand mixtures in cyclic controlled-suction drying and wetting." *Engineering Geology*, 81(3), 213–226.

Araki, H., Koseki, J., and Sato, T. (2016). "Tensile strength of compacted rammed earth materials." *Soils and Foundations*, 56(2), 189–204.

ASTM D 422. (2007). "Standard Test Method for Particle-Size Analysis of Soils." *ASTM International, West Conshohocken, PA*, 1(1), 1–8.

ASTM D1577-07. (2018). "Standard Test Methods for Linear Density of Textile Fibers." *ASTM International, West Conshohocken, PA*, 1(Reapproved), 1–10.

ASTM D3822-14. (2014). "Standard Test Method for Tensile Properties of Single Textile Fibers." *ASTM International, West Conshohocken, PA*, 1(June), 1–10.

ASTM D427. (2004). "Standard Test Method for Shrinkage Factors of Soils by the Mercury Method." *ASTM International, West Conshohocken, PA*, 1(1), 1–6.

ASTM D4318, and ASTM. (2017). "Standard Test Methods for Liquid Limit, Plastic Limit, and Plasticity Index of Soils." *ASTM International, West Conshohocken, PA*, 1(1), 1–14.

ASTM D5550 − 14. (2014). "Standard Test Method for Specific Gravity of Soil Solids by Gas Pycnometer." *ASTM International, West Conshohocken, PA*, 1(1), 1–4.

ASTM D698. (2012). "Standard test methods for laboratory compaction characteristics of soil using standard effort." *ASTM International, West Conshohocken, PA*, 1(1), 1–13.

Ayad, R., Konrad, J., and Soulie, M. (1997). "Desiccation of a sensitive clay : application of the model CRACK." *Canadian Geotechnical Journal*, 34(1), 943–951.

Bhadriraju, V., Puppala, A. J., Enayatpour, S., and Pathivada, S. (2005). "Digital imaging to evaluate shrinkage strain potentials of fiber reinforced expansive soils." *GeoFrontiers 2005, Geotechnical Special Publication No. 138*, P. W. Mayne, E. Rathje, J. DeJong, A. Rechenmacher, J. Yamamuro, S. Sharma, and C. Willson, eds., ASCE, Austin, 2251–

2262.

Birle, E., Heyer, D., and Vogt, N. (2008). "Influence of the initial water content and dry density on the soil–water retention curve and the shrinkage behavior of a compacted clay." *Acta Geotechnica*, 3(3), 191–200.

Buckingham, E. (1914). "On Physically Similar Systems; Illustrations of the Use of Dimensional Equations." *Physical Review*, American Physical Society, 4(4), 345–376.

Butterfield, R. (1999). "Dimensional analysis for geotechnical engineers." *Géotechnique*, Thomas Telford Ltd, 49(3), 357–366.

Chaduvula, U., Viswanadham, B. V. S., and Kodikara, J. (2016). "A study on desiccation cracking behavior of polyester fiber-reinforced expansive clay." *Applied Clay Science*, Elsevier, 142(1), 1–10.

Chen, F. H. (1988). *Foundations on expansive soils*. (ELSEVIER, ed.), Elsevier;Distributors for the U.S. and Canada Elsevier Science Pub. Co., Amsterdam- Oxford- New York- Tokyo.

Chico, R. J. (1964). "Playa Mud Cracks: Regular and King Size." *USA LImited War Laboratory*, Geological Society of America, 306–308.

Cho, S. E. E., and Lee, S. R. R. (2001). "Instability of unsaturated soil slopes due to infiltration." *Computers and Geotechnics*, Elsevier, 28(3), 185–208.

Colina, H., and Roux, S. (2000). "Experimental model of cracking induced by drying shrinkage." *The European Physical Journal E*, 1(1), 189–194.

Corte, A., and Higashi, A. (1964). *Experimental research on Desiccation Cracks in Soil*. U.S. Army Snow, Ice and Permafrost Establishment.

Costa, S., Kodikara, J., and B.Shannon. (2013). "Salient factors controlling desiccation cracking of clay in laboratory experiments." *Geotechnique*, 63(1), 18–29.

Costa, S., Kodikara, J., Barbour, S. L., and Fredlund, D. G. (2018). "Theoretical analysis of desiccation crack spacing of a thin, long soil layer." *Acta Geotechnica*, Springer Berlin Heidelberg, 13(1), 39–49.

Daniel, D. E., and Wu, Y.-K. (1993). "Compacted clay liners and covers for arid sites." *Journal of Geotechnical Engineering, ASCE*, 119(2), 223–237.

Dave, T. N., and Dasaka, S. M. (2013). "In-house calibration of pressure transducers and effect of material thickness." *Gemomechanics and Engineering*, 5(1), 1–15.

Diambra, A., Russell, A. R., Ibraim, E., and Muir Wood, D. (2007). "Determination of fibre orientation distribution in reinforced sands." *Géotechnique*, 57(7), 623–628.

Divya, P. V., Viswanadham, B. V. S., and Gourc, J. P. (2014). "Evaluation of Tensile Strength-Strain Characteristics of Fiber-Reinforced Soil through Laboratory Tests." *Journal of Materials in Civil Engineering, ASCE*, 26(1), 14–23.

Divya, P. V. (2012). "Studies on the Behaviour of Geofiber-Reinforced Clay Barriers of Landfill Covers." Indian Institute of Technology Bombay.

El-Halim, A. A. A. (2017). "Image processing technique to assess the use of sugarcane pith to mitigate clayey soil cracks: Laboratory experiment." *Soil and Tillage Research*, Elsevier B.V., 169(1), 138–145.

Elias, E. A., Salih, F. M., Salih, A. A., and Alaily, F. (2001). "Selected morphological characteristics of soils from Gezira Vertisols , with particular reference to cracking." *International Agrophysics, Polish Academy of sciences*, 15, 79–86.

Estabragh, A. R., Namdar, P., and Javadi, A. A. (2012). "Behavior of cement-stabilized clay reinforced with nylon fiber." *Geosynthetics International*, 19(1), 85–92.

Freilich, B. J., Kuhn, J. A., and Zornberg, J. G. (2008). "Desiccation of Fiber-Reinforced Highly Plastic Clays." *GeoAmericas 2008, The first Pan American Geosynthetics Conference & Exhibition, 2-5 March 2008, Cancun, Mexico*, R. Bathurst and E. M. Palmeira, eds., International Geosynthetics Society, 232–241.

Frost, J. D., and Han, J. (1999). "Behavior of interfaces between fiber-reinforced polymers and sand." *Journal of Geotechnical and Geoenvironmental Engineering, ASCE*, 125(8), 633–640.

Habel, W. R., and Krebber, K. (2011). "Fiber-optic sensor applications in civil and geotechnical engineering." *Photonic Sensors*, University of Electronic Science and Technology of

China, 1(3), 268–280.

Haines, W. B. (1923). "The volume-changes associated with variations of water content in soil." *The Journal of Agricultural Science*, Cambridge University Press, 13(03), 296.

Hannant, D. J., Branch, J., and Mulheron, M. (1999). "Equipment for tensile testing of fresh concrete." *Magazine of Concrete Research*, Thomas Telford Ltd , 51(4), 263–267.

Harianto, T. (2014). "Design criteria of soil-fiber mixtures as a material for landfill cover barrier system." *Lowland Technology International*, 16(1), 1–8.

Harianto, T., Hayashi, S., Du, Y.-J., and Suetsugu, D. (2008). "Effects of Fiber Additives on the Desiccation Crack Behavior of the Compacted Akaboku Soil as A Material for Landfill Cover Barrier." *Water, Air, and Soil Pollut*, 194, 141–149.

Harris, R. C. (2004). "Giant desiccation cracks in Arizona." *Arizona Geological Survey, AZGS*, 34(2), 1–3.

Hasegawa, H., and Ikeuti, M. (1966). "On the Tensile Strength Test of Disturbed Soils." *Rheology and Soil Mechanics / Rhéologie et Mécanique des Sols*, Springer Berlin Heidelberg, Heidelberg, 405–412.

He, J., Wang, Y., Li, Y., and Ruan, X. (2015). "Effects of leachate infiltration and desiccation cracks on hydraulic conductivity of compacted clay." *Water Science and Engineering*, Elsevier Ltd, 8(2), 151–157.

Herrera, M. C., Lizcano, A., and Santamarina, J. C. (2007). "Colombian volcanic ash soils." *Characterization and Engineering Properties of Natural Soils.*, T. S. Tan, K. K. Phoon, D. W. Hight, and S. Leroueil, eds., London: Taylor and Francis, 2385–2409.

Holmes, D. M., Vasant Kumar, R., and Clegg, W. J. (2006). "Cracking during lateral drying of alumina suspensions." *Journal of the American Ceramic Society*, 89(6), 1908–1913.

Hu, L., Peron, H., Hueckel, T., and Laloui, L. (2006). "Numerical and phenomenological study of desiccation of soil." *GeoShanghai 2006, Geotechnical Special Publication No.148, ASCE*, N. Lu, L. R. Hoyos, and L. Reddi, eds., 166–173.

Idso, S. S., Reginato, R. J., Jackson, R. D., Kimball, B. A., and Nakayama, F. S. (1974). "The

three stages of dryinf of a field soil." *Soil Science Society of America Proceedings*, 38(5), 831–837.

Isbell, R. F. (1992). "A brief history of national soil classification in australia since the 1920's." *Australian Journal of Soil Research*, 30(6), 817–824.

Julina, M., and Thyagaraj, T. (2018). "Quantification of desiccation cracks using X-ray tomography for tracing shrinkage path of compacted expansive soil." *Acta Geotechnica*, 4(1), 1–22.

Kalkan, E. (2009). "Influence of silica fume on the desiccation cracks of compacted clayey soils." *Applied Clay Science*, 43(3–4), 296–302.

Katti, R. K. (1978). "Search for Solutions to Problems in Black Cotton Soils." *First IGS Annual Lecture*, Indian Geotechnical Society, Delhi, 1–58.

Kenney, T., Lau, D., and Ofoegbu, G. (1984). "Permeability of compacted granular materials." *Canadian Geotechnical Journal*, 21(1), 726–729.

Kindle, E. M. (1917). "Some factors affecting the development of mud-cracks." *The Journal of Geology*, 25(2), 135–144.

Kindle, E. M. (1923). "Notes on Mud Crack and Ripple Mark in Recent Calcareous Sediments." *The Journal of Geology*, 31(2), 138–145.

Kleppe, J. H., and Olson, R. E. (1985). *Desiccation Cracking of Soil Barriers*. *Hydraulic Barriers in Soil and Rock, ASTM STP 874*, (A. I. Johnson, R. K. Frobel, N. J. Cavalli, and C. B. Pettersson, eds.), American Society for Testing and Materials, Philadelphia.

Kodikara, J., Barbour, S. L., and Fredlund, D. G. (1999). "Changes in clay structure and behavior due to wetting and drying." *Proceedings 8th Australia New Zealand Conference on Geomechanics: Consolidating Knowledge, Australian Geomechanics Society*, N. D. Vitharana and R. Colman, eds., Hobart, Tasmania, 179–186.

Kodikara, J., Barbour, S. L., and Fredlund, D. G. (2000). "Desiccation cracking of soil layers." *Proceedings of the Asian Conference in Unsaturated Soils, UNSAT ASIA 2000, Singapore*, H. Rahardjo, D. G. Toll, and E. C. Leong, eds., Balkema, 693–698.

Kodikara, J. K., Barbour, S. L., and Fredlund, D. G. (2002). "Structure Development in Surficial Heavy Clay Soils: A Synthesis of Mechanisms." *Australian Geomechanics*, 37(3), 25–40.

Kodikara, J. K., and Choi, X. (2006). "A simplified analytical model for desiccation cracking of clay layers in laboratory tests." *Unsaturated soils 2006, ASCE, Geotechnical Special Publication No.147*, G. A. Miller, C. E. Zapata, S. L. Houston, and D. G. Fredlund, eds., 2558–2569.

Kodikara, J., Nahlawi, H., and Bouazza, A. (2004). "Modelling of curling in desiccating clay." *Canadian Geotechnical Journal*, 41(3), 560–566.

Konrad, J. M., and Ayad, R. (1997). "An idealized framework for the analysis of cohesive soils undergoing desiccation." *Canadian Geotechnical Journal*, 34(1), 477–488.

Koyluoglu, U. (1993). "Soil mechanics for unsaturated soils." *Soil Dynamics and Earthquake Engineering*, Wiley, 12(7), 449–450.

Kunert, H. G., Marquez, A. A., Fazzini, P., and Otegui, J. L. (2016). "Failures and integrity of pipelines subjected to soil movements." *Handbook of Materials Failure Analysis with Case Studies from the Oil and Gas Industry*, 105–122.

Lachenbruch, A. H. (1962). "Mechanics of Thermal Contraction Cracks and Ice-Wedge Polygons in Permafrost." *Geological Society of America Special Papers*, 70(1), 1–66.

Lakshmikantha, M. R., Prat, P. C., and Ledesma, A. (2012). "Experimental evidence of size effect in soil cracking." *Canadian Geotechnical Journal*, 49(3), 264–284.

Langhaar, H. L. (1951). *Dimensional analysis and theory of models*. *John Wiley, New York*.

Leavell, D. A., and Peters, J. F. (1987). *Uniaxial tensile test for soil*. Washington, DC.

Leung, C. K. Y., Wan, K. T., Inaudi, D., Bao, X., Habel, W., Zhou, Z., Ou, J., Ghandehari, M., Wu, H. C., and Imai, M. (2015). "Review: optical fiber sensors for civil engineering applications." *Materials and Structures*, 48(4), 871–906.

Leung, M., and Vipulanandan, C. (1995). "Treating Contaminated, Cracked and Permeable Field Clay with Grouts." *Geoenvironment 2000 Characterization, Containment, Remediation, and Performance in Environmental Geotechnics*, Y. B. Acar and D. E.

Daniel, eds., 829–843.

Maher, M. H., and Gray, D. H. (1990). "Static response of sands reinforced with randomly distributed fibers." *Journal of Geotechnical Engineering, ASCE*, 116(11), 1661–1677.

McCleskey, L. K., Puppala, A. J., Dronamraju, S. V., and Perrin, L. (2008). "Remedial Measures Planned to Prevent Surficial Failures." *GeoEdmonton'08: A Heritage of Innovation*, D. Martin and R. Skirrow, eds., Canadian Geotechnical Society.

Mesbah, A., Morel, J. C., Walker, P., and Ghavami, K. (2004). "Development of a Direct Tensile Test for Compacted Earth Blocks Reinforced with Natural Fibers." *Journal of Materials in Civil Engineering, ASCE*, 16(1), 95–98.

Mijares, R. G., and Khire, M. V. (2010). "Soil water characteristic curves of compacted clay subjected to multiple wetting and drying cycles." *GeoFlorida 2010: Advances in analysis, modelling and design, ASCE, Geotechnical Special Publication No.199*, D. O. Fratt, A. J. Puppala, and B. Muhunthan, eds., 400–409.

Miller, C. J., Asce, M., and Rifai, S. (2004). "Fiber Reinforcement for Waste Containment Soil Liners." *Journal of Environmental Engineering*, 130(8), 891–895.

Miller, C. J., Mi, H., and Yesiller, N. (1998). "Experimental analysis of desiccation crack propagation in clay liners." *Journal of the American water resources association*, 34(3), 677–686.

Moore, C. A., and Ali, E. M. (1982). "Permeability of cracked clay liners." *8th Annual Research Symposium on Land Disposal of Hazardous Waste, U.S. Environmental Protection Agency*, Municipal Environment Research Laboratory, Cincinnati, 174–178.

Morris, P. H., Graham, J., and Williams, D. J. (1992). "Cracking in drying soils." *Canadian Geotechnical Journal*, 29(2), 263–277.

Mundell, J. A. (1985). "Discussion of ' Predicting Hydraulic Conductivity of Clay Liners ' by David E. Daniel (February, 1984)." *Journal of Geotechnical Engineering, ASCE*, 111(12), 1459–1464.

Nag, S., Sinha, S., Sadhukhan, S., Dutta, T., and Tarafdar, S. (2010). "Crack patterns in desiccating clay-polymer mixtures with varying composition." *Journal of physics.*

Condensed matter : an Institute of Physics journal, 22(1), 015402.

Nahlawi, H., Chakrabarti, S., and Kodikara, J. (2004). "A Direct Tensile Strength Testing Method for Unsaturated Geomaterials." *Geotechnical Testing Journal, ASTM*, 27(4), 1–6.

Nahlawi, H., and Kodikara, J. K. (2006). "Laboratory experiments on desiccation cracking of thin soil layers." *Geotechnical and Geological Engineering*, 24(6), 1641–1664.

Nelson, J. D., Chao, K. C., Overton, D. D., and Nelson, E. J. (2015). *Foundation Engineering For Expansive Soils*.

Nelson, J. D., and Miller, D. J. (1992). *Expansive soils : problems and practice in foundation and pavement engineering*. J. Wiley.

Netravali, A. N., Krstic, R., Crouse, J. L., and Richmond, L. E. (1993). "Chemical Stability of Polyester Fibers and Geotextiles Without and Under Stress." *Geosynthetic Soil Reinforcement Testing Procedures*, (S. C. J. Cheng, ed.), Philadelphia, ASTM STP 1, 207–217.

O'Callaghan, J. F., and Loveday, J. (1973). "Quantitative Measurement of Soil Cracking Patterns." *Pattern Recognition Pergamon press*, 5(1), 83–98.

Olgun, M. (2013). "Effects of polypropylene fiber inclusion on the strength and volume change characteristics of cement-fly ash stabilized clay soil." *Geosynthetics International*, 20(4), 263–275.

Peron, H., Hueckel, T., Laloui, L., and Hu, L. B. (2009). "Fundamentals of desiccation cracking of fine-grained soils: experimental characterisation and mechanisms identification." *Canadian Geotechnical Journal*, 46(10), 1177–1201.

Peters, A., and Durner, W. (2008). "Simplified evaporation method for determining soil hydraulic properties." *Journal of Hydrology*, 356(1–2), 147–162.

Plé, O., and Lê, T. N. H. (2012). "Effect of polypropylene fiber-reinforcement on the mechanical behavior of silty clay." *Geotextiles and Geomembranes*, 32, 111–116.

Puppala, A. J., Manosuthkij, T., Nazarian, S., and Hoyos, L. R. (2011). "Threshold moisture content and matric suction potentials in expansive clays prior to initiation of cracking in

pavements." *Canadian Geotechnical Journal*, 48(1), 519–531.

Qi, C., Weiss, J., and Olek, J. (2003). "Characterization of plastic shrinkage cracking in fiber reinforced concrete using image analysis and a modified Weibull function." *Materials and structures*, 36(1), 386–395.

Qiang, X., Hai-jun, L., Zhen-ze, L., and Lei, L. (2014). "Cracking, water permeability and deformation of compacted clay liners improved by straw fiber." *Engineering Geology*, 178(1), 82–90.

Ramachandran, V. S., Ahmad, F. U., and Jain, L. C. (1959). "The Dark Colour of Black Cotton Soils." *The proceedings of the Indian Academy of Sciences*, 50(1), 314–322.

Rayhani, M. H., Yanful, E. K., and Fakher, A. (2007). "Desiccation-induced cracking and its effect on the hydraulic conductivity of clayey soils from Iran." *Canadian Geotechnical Journal*, 44(3), 276–283.

Ringrose-Voase, a. J., and Sanidad, W. B. (1996). "A method for measuring the development of surface cracks in soils: application to crack development after lowland rice." *Geoderma*, 71(3–4), 245–261.

Rowe, R. K. (2012). "Short- and long-term leakage through composite liners." *Canadian Geotechnical Journal*, 49(2), 141–169.

Safari, E., Jalili Ghazizade, M., Abduli, M. a, and Gatmiri, B. (2014). "Variation of crack intensity factor in three compacted clay liners exposed to annual cycle of atmospheric conditions with and without geotextile cover." *Waste management*, 34(8), 1408–15.

Sanchez, M., Atique, A., Kim, S., Romero, E., and Zielinski, M. (2013). "Exploring desiccation cracks in soils using a 2D profile laser device." *Acta Geotechnica*, 8(6), 583–596.

Satyanarayana, B. (1966). "Swelling Pressure and Related Mechanical Properties of Black Cotton Soils." Indian Institute of Science, Bangalore.

Scherer, G. W. (1990). "Theory of Drying." *Journal of the American Ceramic Society*, Wiley/Blackwell (10.1111), 73(1), 3–14.

Schofield, A. N. (1980). "Cambridge geotechnical centrifuge operations." *Géotechnique*, 30(3),

227–268.

Shannon, B. M. (2013). "Fracture Propagation of Cohesive Soils Under Tensile Loading and Desiccation." Monash University, Australia.

Stanier, S. A., Blaber, J., Take, W. A., and White, D. J. (2016). "Improved image-based deformation measurement for geotechnical applications." *Canadian Geotechnical Journal*, 53(5), 727–739.

Steinberg, M. L. (1998). *Geomembranes and the control of expansive soils in construction*. McGraw-Hill.

Subbarao, G. V., Siddartha, D., Muralikrishna, T., Sailaja, K. S., and Sowmya, T. (2011). "Industrial Wastes in Soil Improvement." *International Scholarly Research Network, ISRN Civil Engineering*, 2011(1), 1–5.

Sveen, J. K., and Cowen, E. A. (2004). "Quantitative imaging techniques and their application to wavy flows." *Advances in Coastal and Ocean Engineering*, 9(1), 1–49.

Tagnit-Hamou, a., Vanhove, Y., and Petrov, N. (2005). "Microstructural analysis of the bond mechanism between polyolefin fibers and cement pastes." *Cement and Concrete Research*, 35(2), 364–370.

Tang, C.-S., Cui, Y.-J., Tang, A.-M., and Shi, B. (2010a). "Experiment evidence on the temperature dependence of desiccation cracking behavior of clayey soils." *Engineering Geology*, 114(3–4), 261–266.

Tang, C.-S., Shi, B., Cui, Y.-J., Liu, C., and Gu, K. (2012). "Desiccation cracking behavior of polypropylene fiber–reinforced clayey soil." *Canadian Geotechnical Journal*, 49(9), 1088–1101.

Tang, C.-S., Shi, B., and Zhao, L.-Z. (2010b). "Interfacial shear strength of fiber reinforced soil." *Geotextiles and Geomembranes*, 28(1), 54–62.

Tang, C.-S., Wang, D.-Y., Cui, Y., Shi, B., and Li, J. (2014). "Tensile Strength of Fiber-Reinforced Soil." *Journal of Materials in Civil Engineering, ASCE*, 28(7), 04016031.

Tang, C., Shi, B., Gao, W., Chen, F., and Cai, Y. (2007). "Strength and mechanical behavior of

short polypropylene fiber reinforced and cement stabilized clayey soil." *Geotextiles and Geomembranes*, 25(3), 194–202.

Tang, C., Shi, B., Liu, C., Gao, L., and Inyang, H. I. (2011). "Experimental Investigation of the Desiccation Cracking Behavior of Soil Layers during Drying." *Journal of Materials in Civil Engineering, ASCE*, 23(6), 873–878.

Tang, C., Shi, B., Liu, C., Zhao, L., and Wang, B. (2008). "Influencing factors of geometrical structure of surface shrinkage cracks in clayey soils." *Engineering Geology*, 101(3–4), 204–217.

Tarafdar, S., Mal, D., Sinha, S., and Middya, T. R. (2006). "Crack Patterns in Laponite Films Dried in Electrostatic Field." *Materials Science*.

Tay, Y. Y., Stewart, D. I., and Cousens, T. W. (2001). "Shrinkage and desiccation cracking in bentonite sand landfill liners." *Engineering Geology*, 60(1), 263–274.

Taylor, D. W. (1948). *Fundamentals of soil mechanics*. Wiley, New York.

Taylor, R. N. (1995). *Centrifuges in modelling: principles and scale effects." Geotechnical Centrifuge Technology*. (R. N. Taylor, ed.), Blackie Academic and Professional, Glasgow, U. K.,.

Taylor, Z. J., Gurka, R., Kopp, G. A., and Liberzon, A. (2010). "Long-Duration Time-Resolved PIV to Study Unsteady Aerodynamics." *IEEE Transactions on Instrumentation and Measurement*, 59(12), 3262–3269.

Thielicke, W., and Stamhuis, E. J. (2014). "PIVlab – Towards User-friendly, Affordable and Accurate Digital Particle Image Velocimetry in MATLAB." *Journal of Open Research Software*, Ubiquity Press, 2(1), 1–10.

Tollenaar, R. N., van Paassen, L. A., and Jommi, C. (2017a). "Observations on the desiccation and cracking of clay layers." *Engineering Geology*, 230(1), 23–31.

Tollenaar, R. N., van Paassen, L. A., and Jommi, C. (2017b). "Small Scale Evaporation Tests on a Clay: Influence of Drying Rate on a Clayey Soil Layer." *Canadian Geotechnical Journal*, 55(8), 437–445.

Towner, G. D. (1987). "The Mechanics of Cracking of Drying Clay." *Journal of Agricultural Engineering Research*, 36(1), 115–124.

Uday, K. V., and Singh, D. N. (2013). "Investigation on Cracking Characteristics of Fine-Grained Soils Under Varied Environmental Conditions." *Drying Technology*, 31(2), 1255–1266.

Velde, B. (1999). "Structure of surface cracks in soil and muds." *Geoderma*, 93(1–2), 101–124.

Viswanadham, B. V. S., Rajesh, S., Divya, P. V., and Gourc, J. P. (2011). "Influence of randomly distributed geofibers on the integrity of clay-based landfill covers : a centrifuge study." *Geosynthetics International*, 18(5), 2555-.

Viswanadham BVS, Phanikumar BR, M. R. (2009). "Swelling behaviour of a geo fibre-reinforced expansive soil." *Geotextiles and Geomembranes*, 27, 73–76.

Wahab, R. M. A. Al, and El-Kedrah, M. A. (1995). "Using Fibers to Reduce Tension Cracks and Shrink/Swell in a Compacted Clay." *Geoenvironment 2000: Characterization, Containment, Remediation, and Performance in Environmental Geotechnics, ASCE Geotechnical Special Publication No.46*, Y. B. Acar and D. E. Daniel, eds., 791–805.

Wang, L. L., Tang, C. S., Shi, B., Cui, Y. J., Zhang, G. Q., and Hilary, I. (2018). "Nucleation and propagation mechanisms of soil desiccation cracks." *Engineering Geology*, 238(3), 27–35.

White, D. J., Take, W. A., and Bolton, M. D. (2003). "Soil deformation measurement using particle image velocimetry (PIV) and photogrammetry." *Geotechnique*, 53(7), 619–631.

White, D., Randolph, M., and Thompson, B. (2005). "An image based deformation measurment system for the geotechcnical centrifuge." *IJPMG- International Journal of Physical Modelling in Geotechniquesing in Geotechniques*, 3(1), 01–12.

Wiggins, J. H., Slosson, J. E., and Krohn, J. (1978). *Natural Hazards: Earthquake, Landslide, Expansive Soils Loss Models*. Redondo Beach, CA: J.H. Wiggins Co.

Win, S. (2006). "Tensile strength of compacted soils subject to wetting and drying." The University of New South Wales.

Witherspoon, P. A., Wang, J. S. Y., Iwai, K., and Gale, J. E. (1980). "Validity of cubic law for fluid flow in a deformable rock fracture." *Water Resources Research*, 16(6), 1016–1024.

Wojnar, L. (1999). *Image Analysis: Applications in Materials Engineering*.

Wong, L., Lim, K., Chiu, W. K., Kodikara, J., and Chowdhury, N. (2016). "Using water hammer to enhance the detection of stiffness changes on an out-of-round pipe with distributed optical-fibre sensing." *Structural Control and Health Monitoring*, e1975(12), 1–10.

Yesiller, N., Miller, C. ., Inci, G., and Yaldo, K. (2000). "Desiccation and cracking behavior of three compacted landfill liner soils." *Engineering Geology*, 57(1–2), 105–121.

Zarzycki, J., Prassas, M., and Phalippou, J. (1982). "Synthesis of glasses from gels: the problem of monolithic gels." *Journal of Materials Science*, Kluwer Academic Publishers, 17(11), 3371–3379.

Zhu, H. H., Shi, B., Yan, J. F., Zhang, J., and Wang, J. (2015). "Investigation of the evolutionary process of a reinforced model slope using a fiber-optic monitoring network." *Engineering Geology*, Elsevier B.V., 186(1), 34–43.

Ziegler, S., Leshchinsky, D., and Ling, H. I. (1998). "Effect of short polymeric fibers on crack development in clays." *Soils and Foundations*, 38(1), 247–253.

LIST OF PUBLICATIONS

International Journals

Published

- Chaduvula, U., Viswanadham, B. V. S., and Kodikara, J. (2016). "A study on desiccation cracking behaviour of polyester fiber-reinforced expansive clay." Applied Clay Science, 142(1), 1–10.

International/national conferences:

- Chaduvula, U, Viswanadham, B.V.S., Kodikara, J. (2016). Desiccation Cracking Behaviour of Geofiber-Reinforced Expansive Clay, Proc. GeoChicago 2016, Sustainability and Resiliency in Geotechnical Engineering. ASCE, Geotechnical Special Publication No. 271, A. De, K.R. Reddy, N. Yesiller, D. Zekkos, A. Farid (Eds.), 368-377.

- Chaduvula, U., Manogaran, I., Viswanadham, B. V. S., and Kodikara, J. (2017). "Some Studies on Desiccation Cracking of Fiber-Reinforced Expansive Clay Subjected to Drying and Wetting Cycles." *PanAm Unsaturated Soils 2017: Swell-Shrink and Tropical Soils*, ASCE, R. H. Laureano, M. John S., H. Sandra L., and L. William J., (Eds.), Dallas, Texas, 361–370.

- Indupriya, M., Chaduvula, U., Viswanadham, B.V.S. (2016). Studies on desiccation cracking behaviour of geofiber reinforced clay, Proceedings of Indian Geotechnical Conference 2016 (IGC-2016), Indian Institute of Technology Madras, Chennai, Paper No. 527, 1-4 (CD ROM Copy)

Under preparation

- Chaduvula, U., Wong L., Shannon B., Viswanadham, B. V. S., and Kodikara, J.," Understanding desiccation cracking behaviour of polypropylene fiber-reinforced expansive clay using distributed fiber optic sensing". (For possible publication in Acta Geotechnica, Springer).

- Chaduvula U., Palsapure A., Viswanadham, B. V. S., and Kodikara J., "Effect of Fiber-Reinforcement on Liquid Limit of Expansive Soil". (For possible publication in Indian Geotechnical Journal, Springer).

- Chaduvula U., Viswanadham, B. V. S., and Kodikara J. "Centrifuge Model Studies on Desiccation Cracking of Fiber-Reinforced Expansive Clay". (For possible publication in International Journal of Physical Modelling in Geotechnics, ICE).

ANNEXURES

LEFT BLANK INTENTIONALLY

A1.   Specific Gravity measurement
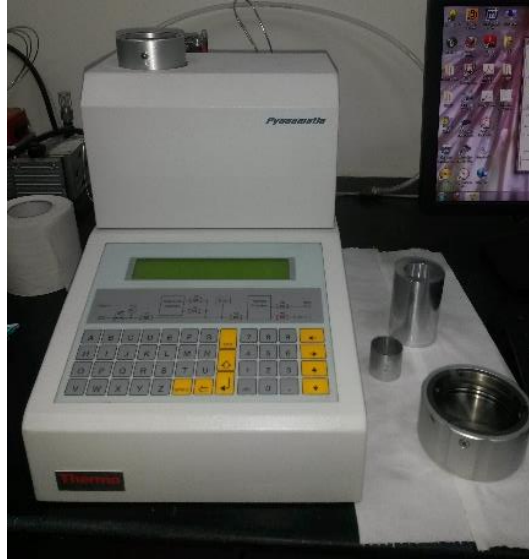
Figure A1.1 Helium Gas Pycnometer used for determination of specific gravity of soil and fiber mix by He-gas pycnometer (Pycnomatic ATC at IIT Bombay)

Figure A1.1 shows the Pycnomatic ATC facility available at Chemical Engineering Department, IIT Bombay. Specific gravity measurement for soil and fiber mix cannot be measured accurately conventional pycnometer with water as ingressing fluid. The properties of fibers may vary after boiling of mix inside pycnometer. Hence, the density measurement was carried out on Helium Gas Pycometer. For required settings in the instrument, the pore size of soil was measured by SEM images. The sample holder of 25cc capacity was used in the measurement. As the fibers have negligible weight in comparison to soil, no much variation in specific gravity was observed, as shown in Table A1.1.

Table A1.1 Specific gravity as measured by He-gas pycnometer

Soil type	Specific gravity (Gs)
Black cotton soil	2.583
Black cotton soil+0.5% 15mm fiber	2.579

LEFT BLANK INTENTIONALLY

A2. Sample preparation and details of SEM analysis

Details of SEM analysis:

In the present study, SEM analysis was performed for obtaining detailed information on pure soil, fibers and fiber reinforced soil after desiccation test.
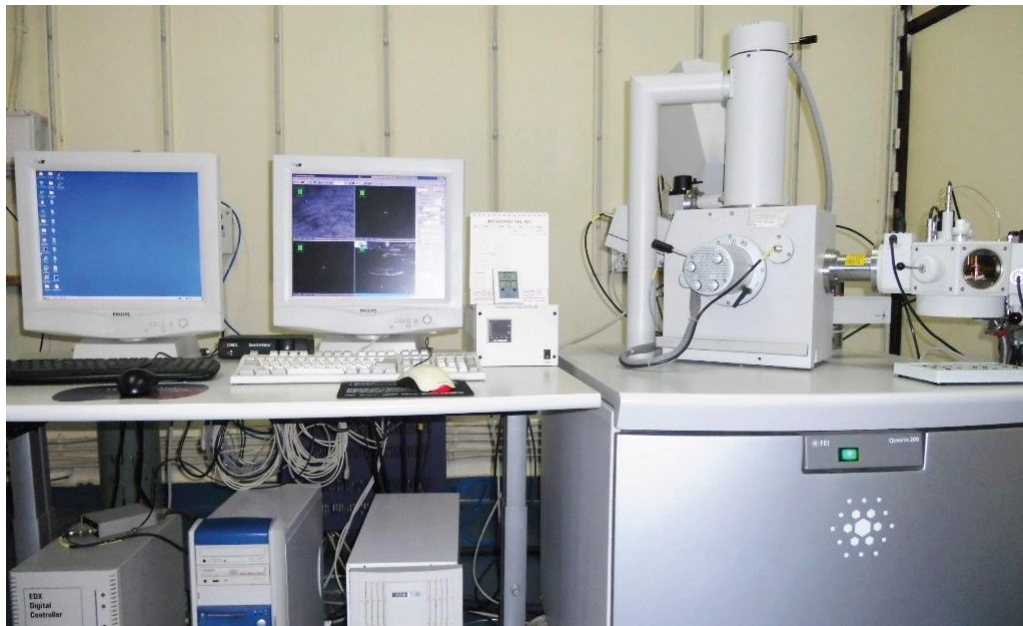
Figure A2.1 SEM equipment used in the present study (SAIF, IIT Bombay)

Samples were extracted carefully without disturbing the tested conditions. SEM analysis helps in knowing soil particles and fiber arrangement in a fiber reinforced soil with different percentage of fibers. Small SEM samples were oven dried in order to avoid the presence of moisture. In SEM, electrons are emitted by electron gun and the specimen must be electrically conductive, at least at the surface. Nonconductive specimens tend to charge when scanned by the electron beam and in that case an ultrathin coating of electrically conductive material such as gold can be applied. In such cases, Environmental SEM is useful especially for non-metallic materials. The equipment used in the present study for SEM analysis is shown in Figure A2.1.

a) Soil sample mounted on a specimen stub

b) Opened sample chamber

c) SEM images obtained
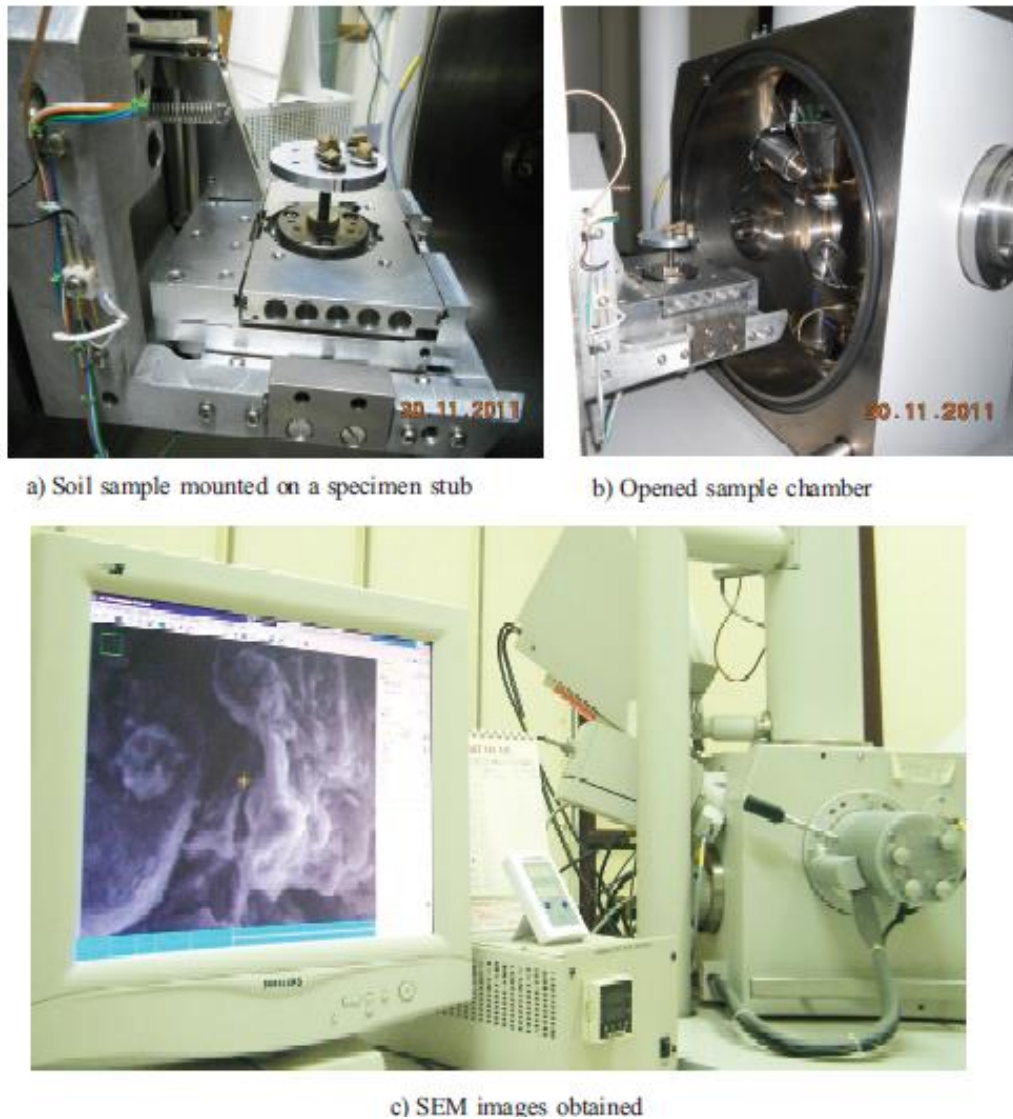
Figure A2.2 Different stages in SEM analysis (SAIF, IIT Bombay)

All samples must also be of an appropriate size to fit in the specimen chamber and are generally mounted rigidly on a specimen holder called a specimen stub. The sample is mounted in the stub in the sample chamber of SEM equipment and SEM images can be obtained as shown in the Figure A2.2.

A3. X-ray fluorescence spectrometer

X-ray Fluorescence analysis is a physical method which directly analyses almost all chemical elements of the periodic system in solids, powders or liquids. These materials may be solids such as glass, ceramics, metal, rocks, coal, plastic or liquids, like petrol, oils, paints, solutions or blood. Model S4 PIONEER BRUKER aXS (Figure A3.1), X-ray fluorescence analysis is a fast, non-destructive and environmentally friendly analysis method with very high accuracy and reproducibility. All elements of the periodic table from Beryllium to Uranium can be measured qualitatively, semi-quantitatively and quantitatively in powders, solids and liquids.

Figure A3.1 Figure X-ray fluorescence spectrometer used in the study at IIT Bombay

X-ray source is generated from Rhodium, used as the standard anode material. The tube and generator are designed for a permanent output of 4 kW. The refracted X-rays are detected by the Scintillation counter and proportional counter and SPECTRA plus Software Package for X-ray Spectrometers Version 1.6 is used for analysing the results.

LEFT BLANK INTENTIONALLY

A4. Calibration curves for load cell and potentiometers used in tensile tests in the laboratory
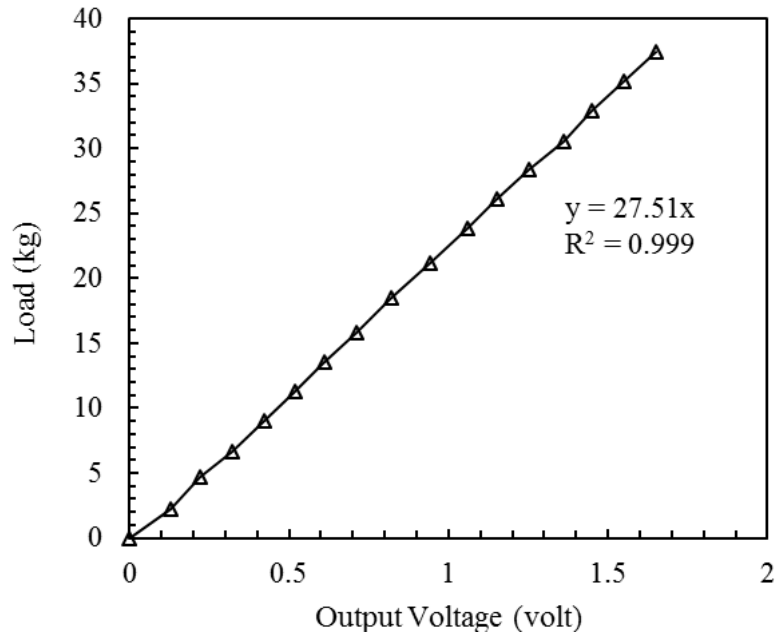
Figure A4.1 Calibration curves for load cell used in the present study

In the figure, the load cell calibration shows: $y = 27.51x$, $R^2 = 0.999$
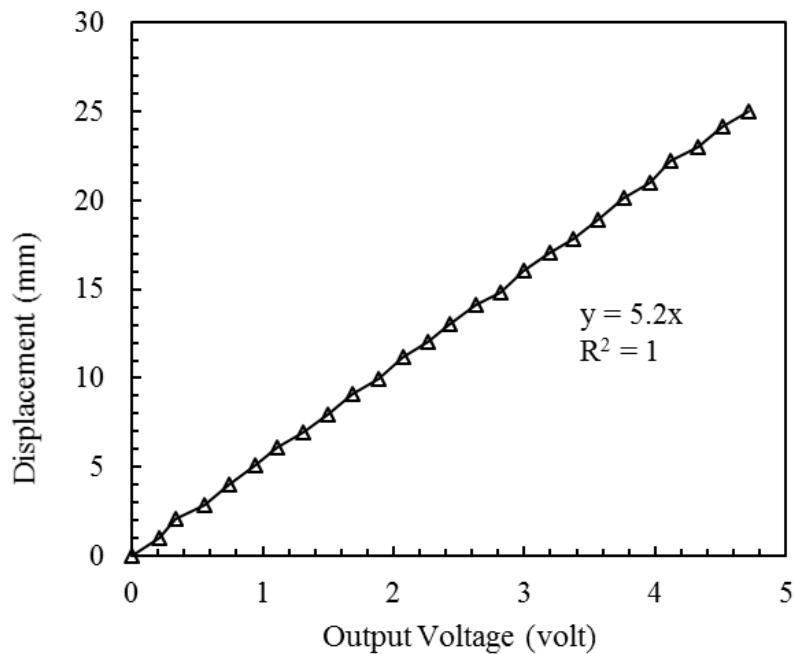
Figure A4.2 Variation of output with displacement [For potentiometer: P2036]

In the figure, the potentiometer calibration shows: $y = 5.2x$, $R^2 = 1$

$$y = 5.20x$$
$$R^2 = 0.999$$
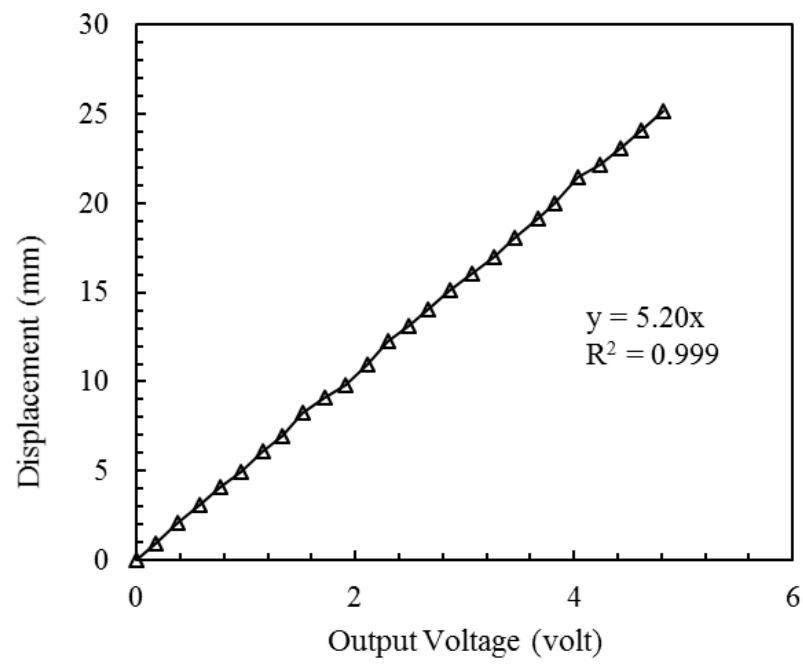
Figure A4.3 Variation of output with displacement [For potentiometer: P3444]

A5. WP4Cchilled mirror dewpoint potentiometer

The WP4C (Figure A5.1) can measure suctions greater than 0.3 MPa and over the air dried theoretical maximum suction of 100 MPa. Samples were consolidated to 100 kPa and left to dry at constant room temperature (22°C) until a predefined moisture content was reached. Samples were tested in the dewpoint potentiometer device at a temperature of 22°C.

Figure A5.1 WP4C dewpoint potentiometer at Monash University, Australia

LEFT BLANK INTENTIONALLY

A6. UMS HYPROP for suction measurement

The UMS HYPROP (Figure A6.1 and Figure A6.2) determines the unsaturated hydraulic conductivity and water retention characteristics of soil samples through laboratory evaporation method (Peters and Durner 2008). Two high pressure tensiometers (<300 kPa range) are placed at two height levels inside the soil sample from the base.
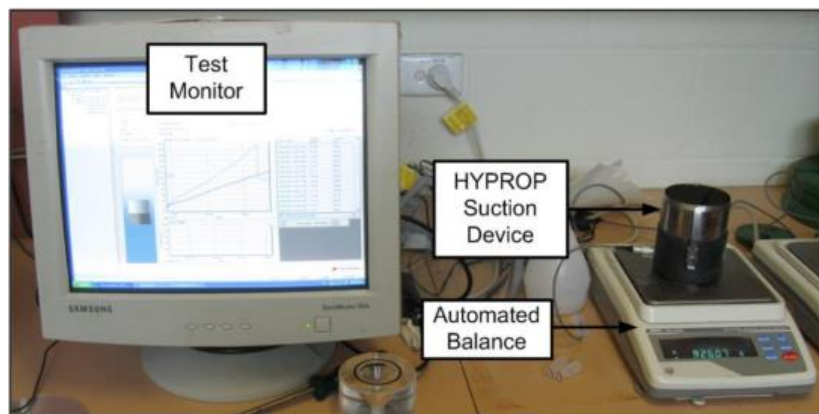
Figure A6.1 UMS HYPROP for suction measurement at Monash University, Australia
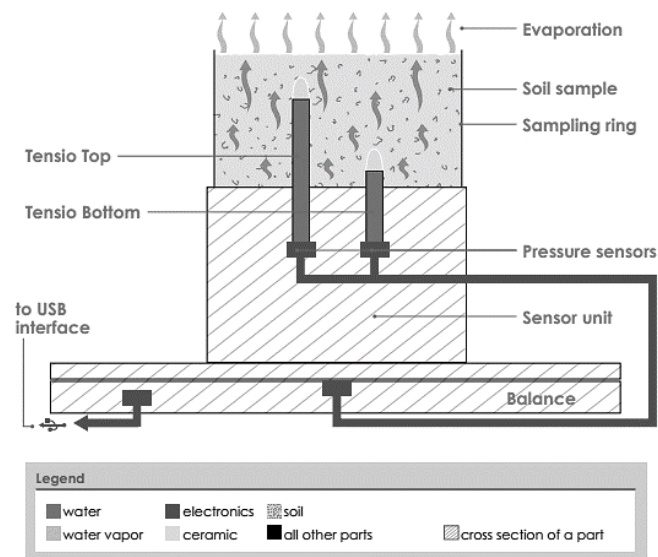
Figure A6.2 Schematic diagram of working mechanism of UMS HYPROP (Source: https://sestar.irb.hr)

LEFT BLANK INTENTIONALLY

ACKNOWLEDGEMENTS